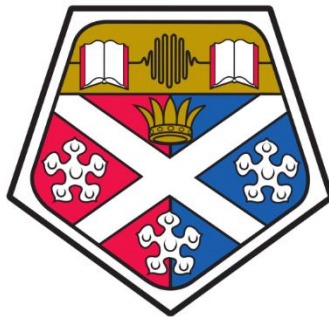


*Development of a DNA Biosensor
to Detect Antimicrobial Resistance*

Adrian Butterworth

Department of Biomedical Engineering
University of Strathclyde



Thesis submitted in partial fulfilment for the degree of
Doctor of Philosophy

2021

'This thesis is the result of the author's original research. It has been composed by the author and has not been previously submitted for examination which has led to the award of a degree.'

'The copyright of this thesis belongs to the author under the terms of the United Kingdom Copyright Acts as qualified by University of Strathclyde Regulation 3.50. Due acknowledgement must always be made of the use of any material contained in, or derived from, this thesis.'

Signed: *A Butterworth*

Date: 31st March 2021

Abstract

Antimicrobial resistance is a growing worldwide healthcare challenge, with increasing resistance rates limiting treatment options for common bacterial infections. Advances in diagnostic procedures can provide treatment options more rapidly, improving patient outcomes and maintaining the efficacy of our current antibiotic stockpiles. In this thesis, the development of a DNA biosensor for antibiotic resistance is detailed. Based on electrochemical techniques, the binding of resistance gene sequences at probe modified electrode surfaces is detected. Different low-cost electrode formats are examined for their suitability as DNA sensing platforms. Detection is based upon the formation of a self-assembled monolayer consisting of blocking and probe molecules, and different methods for forming these layers are also explored. Amplification reactions are designed to enrich the specific DNA target using both polymerase chain reaction and isothermal techniques. Amplicons from these reactions are tested on different carbon and gold electrode substrates, as well as on a low-cost potentiostat system which could provide a cost effective, self-contained diagnostic platform. DNA targets are detected on each of these systems, and performance of the low-cost potentiostat is shown to be comparable to a benchtop potentiostat. A solid-phase amplification reaction is then developed, which is used to attach a horseradish peroxidase enzyme label directly to the DNA amplicon produced at the electrode surface. This process is used to detect cells containing antimicrobial resistance gene sequences from culture medium using a simple heat lysis as preparation. Cultures of resistance bearing *E. coli* are distinguished from blank and *S. aureus* templates using this solid-phase system, with a limit of detection of 319 CFU/mL detected in under one hour. This system shows promise for further development of cost-effective genetic sensing for rapid identification of antimicrobial resistance genes.

Acknowledgements

I would first like to thank my supervisor, Dr Damion Corrigan, for the countless hours of support he provided during my PhD, and for the opportunities he pushed me to take. I have undertaken more experiences than I could have imagined during my time at Strathclyde largely thanks to your enthusiasm and drive.

I would also like to thank Dr Michelle Maclean, Dr Andrew Ward, Dr Ewen Blair and Dr Stuart Hannah for the help and support they have provided throughout the time we have worked together. Thanks too to the entire RC647 and RC375 research groups for being fantastic colleagues and full of banter. I have thoroughly enjoyed working with you all and hope our paths cross again soon!

Thanks to all my co-authors who contributed to the various projects we have published. Your support really helped me find my feet as a researcher and put myself forward into the world of research.

Finally, I would like to thank my fiancée Rebecca for all the support she has given me throughout my PhD. I appreciate all the times we discussed experiments, failures, and successes together, you helped me reach a resolution more often than not. Thanks for also being the best lockdown partner I could have asked for.

Contents

1	Introduction	1
1.1	Microbiology and Antimicrobial Resistance	1
1.1.1	Gram-negative Pathogens	1
1.1.2	Antibiotics and Antimicrobial Resistance	3
1.1.3	Gram-negative Bacteria and Antibiotic Resistance	5
1.1.4	Antibiotic Resistance in Clinically Important Bacteria	11
1.1.5	Strategies Against Antimicrobial Resistance	13
1.2	Biosensors	15
1.2.1	DNA Detection	16
1.2.2	Integrated Protocols for DNA Amplification and Electrochemical Detection	24
1.2.3	Detection of Antimicrobial Resistance using Electrochemical Techniques	26
1.3	Electrochemistry Basics	29
1.3.1	Electrode-Solution Interface	30
1.3.2	Self-Assembled Monolayers and Surface Passivation	32
1.3.3	Electrochemical Tests	34
1.4	Scope of the Thesis	46
2	Developing an Electrochemical Sensor and Amplification System for DNA Detection	48
2.1	Selection and Characterisation of Gold Electrodes for Biosensing	48
2.1.1	Low-Cost Electrodes for Biosensing	48
2.1.2	Electrode Surface Characterisation	50
2.2	Electrode Cleaning and Electrochemical Characterisation of Gold	52
2.2.1	Methods	52
2.2.2	Results & Discussion	53
2.3	DNA Biosensing on Gold Electrodes	56
2.3.1	Methods	56
2.3.2	Results and Discussion	57
2.3.3	Conclusions	65
2.4	Characterisation and Sensing on Carbon Electrodes	65
2.4.1	Methods	66
2.4.2	Results and Discussion	67
2.4.3	Conclusions	74
2.5	Methods for Design & Amplification of a Synthetic DNA Template	74

2.5.1	Selection of Antibiotic Resistance Genes-----	75
2.5.2	Design of an Artificial Plasmid Containing Antibiotic Resistance Genes -----	76
2.5.3	Transformation of Competent <i>E. coli</i> with Plasmid DNA -----	77
2.5.4	Growth and Maintenance of <i>E. coli</i> Cultures -----	78
2.5.5	Production of DNA Targets from a Synthetic Plasmid-----	79
2.6	Conclusions-----	83
3	Electrochemical Detection of Antimicrobial Resistance Genes -----	85
3.1	Detecting a Clinically Relevant AMR Gene Sequence on Gold Electrodes -----	85
3.1.1	Methods-----	85
3.1.2	Results & Discussion-----	86
3.1.3	Conclusions-----	90
3.2	Electrochemical Detection of PCR Product Using a Low Cost Potentiostat-----	91
3.2.1	SimpleStat Design Overview-----	92
3.2.2	Methods-----	94
3.2.3	Results and Discussion-----	95
3.2.4	Conclusions-----	100
3.3	Detecting a Clinically Relevant AMR Gene Sequence on Carbon Electrodes-----	101
3.3.1	Methods-----	101
3.3.2	Results & Discussion-----	105
3.3.3	Conclusions-----	116
3.4	Detection of Amplified AMR Genes: A Return to Gold -----	118
3.4.1	Methods-----	118
3.4.2	Results and Discussion-----	119
3.4.3	Conclusions-----	122
4	Detection of Amplified DNA Using Enzyme Tagged Nucleotides -----	123
4.1	Methods-----	126
4.1.1	Measurement of TMB Redox Responses on Gold SPEs -----	126
4.1.2	Measurement of HRP Oxidation of TMB-----	126
4.1.3	Examining RPA Reaction Efficiency with Low Concentration dNTPs-----	126
4.1.4	Measurement of HRP-dTTP Inclusion into Solid-Phase RPA -----	126
4.1.5	RPA Amplification from <i>E. coli</i> Cultures-----	128
4.1.6	Detection of Plasmid Bearing <i>E. coli</i> Through HRP-dTTP Solid-Phase RPA -	129
4.1.7	Discrimination of Plasmid Bearing and Non-Plasmid Bearing Bacteria -----	129
4.2	Results and Discussion-----	131

4.2.1	Measurement of TMB Redox Responses on Gold SPEs -----	131
4.2.2	Measurement of HRP Oxidation of TMB-----	133
4.2.3	Examining RPA Reaction Efficiency with Low Concentration dNTPs-----	134
4.2.4	Measurement of HRP-dTTP Inclusion into Solid Phase RPA -----	135
4.2.5	RPA Amplification from E. coli Cultures-----	139
4.2.6	Detection of Plasmid Bearing E. coli Through HRP-dTTP Solid-Phase RPA -	140
4.2.7	Discrimination of Plasmid Bearing and Non-Plasmid Bearing Bacteria ----	142
4.3	Conclusions-----	158
5	Conclusions and Future Work-----	161
5.1	Conclusions-----	161
5.2	Future Work-----	166
6	References -----	168

i. Publications and Conference Proceedings

This thesis contains work presented in the following papers:

Butterworth, A., Blues, E., Williamson, P., Cardona, M., Gray, L., Corrigan, D.K., **2019**. *SAM Composition and Electrode Roughness Affect Performance of a DNA Biosensor for Antibiotic Resistance*. *Biosensors* 9, 22. <https://doi.org/10.3390/bios9010022>

Butterworth, A., Corrigan, D., Ward, A.C., **2019**. *Electrochemical detection of oxacillin resistance with SimpleStat: a low cost integrated potentiostat and sensor platform*. *Anal. Methods* 11, 1958–1965. <https://doi.org/10.1039/C9AY00383E>

The following papers were produced in addition to the work presented here:

Akbulut, S.O., Ghorbanpoor, H., İpteç, B.Ö., Butterworth, A., Avcioglu, G., Kozacı, L.D., Topateş, G., Corrigan, D.K., Avci, H., Güzel, F.D., **2020**. *Impedance testing of porous Si3N4 scaffolds for skeletal implant applications*. *SN Appl. Sci.* 2, 823. <https://doi.org/10.1007/s42452-020-2624-4>

Veza, V.J., Butterworth, A., Lasserre, P., Blair, E.O., MacDonald, A., Hannah, S., Rinaldi, C., Hoskisson, P.A., Ward, A.C., Longmuir, A., Setford, S., Farmer, E.C.W., Murphy, M.E., Corrigan, D.K., **2021**. *An electrochemical SARS-CoV-2 biosensor inspired by glucose test strip manufacturing processes*. *Chem. Commun.* <https://doi.org/10.1039/D1CC00936B>

Conference proceedings resulting from this work:

Butterworth, A., **2019**. *Development of a DNA Biosensor to Detect Antibiotic Resistance*, presented at 6th Analytical Biosciences Early Career Researcher Meeting, University of Cambridge, 28-29 March 2019.

Butterworth, A., **2019**. *Development of a DNA Biosensor to Detect Antibiotic Resistance*, presented at Scotland and North of England Electrochemistry Symposium, University of Edinburgh, 9 April 2019.

ii. List of Figures

Figure 1.1 – Example structures of antibiotics of different classes. -----	4
Figure 1.2 – Diagram of how antibiotic resistance can arise within a susceptible population. -----	5
Figure 1.3 – Development of antimicrobial resistance through mutation. -----	8
Figure 1.4 – Schematic of plasmid uptake from the environment. -----	9
Figure 1.5 – Schematic of plasmid transfer through conjugation. -----	10
Figure 1.6 – Schematic of transduction for horizontal gene transfer. -----	10
Figure 1.7 – Diagram of a typical Polymerase Chain Reaction. -----	18
Figure 1.8 – Overview of some common label-based electrochemical methods for DNA detection. -----	21
Figure 1.9 – Overview of some common label-free electrochemical methods for DNA detection. -----	23
Figure 1.10 – Image and schematic for 3-electrode cell for electrochemical measurements. -----	30
Figure 1.11 – Formation of different ion layers at an electrode solution interface. -----	31
Figure 1.12 – Schematic for the formation of a confluent alkanethiol SAM on gold. -----	33
Figure 1.13 – Cyclic voltammetry plots for 2 mM $\text{Fe}(\text{CN})_6^{3-/4-}$ over a gold disc electrode. ---	37
Figure 1.14 – Impedance magnitude of a single point in the Nyquist plot. -----	38
Figure 1.15 – Example EIS response. -----	40
Figure 1.16 – DPV potential waveform (A) and current response (B). -----	41
Figure 1.17 – Example DPV plot for $\text{Fe}(\text{CN})_6^{3-/4-}$. -----	42
Figure 1.18 – SWV potential waveform (A) and example SWV plot (B). -----	43
Figure 1.19 – Schematic of redox species depletion following application of a potential step -----	44
Figure 2.1 – Gold electrodes examined as a potential biosensor platform. -----	50
Figure 2.2 – SEM images of different electrode surfaces -----	51
Figure 2.3 – AFM images of (A) AT SPE and (B) thin-film gold electrode. -----	51
Figure 2.4 – Voltammograms of 0.1M H_2SO_4 cleaning CV for different electrode types. ----	53
Figure 2.5 – Voltammograms of 2mM $\text{Fe}(\text{CN})_6^{3-/4-}$ CV responses of different electrode types after cleaning. -----	55

Figure 2.6 – Nyquist plot of 2mM $\text{Fe}(\text{CN})_6^{3-/4-}$ electrochemical impedance spectroscopy on different electrode types after cleaning.-----	55
Figure 2.7 – Example 2mM $\text{Fe}(\text{CN})_6^{3-/4-}$ impedance response changes on AT screen-printed electrode as SAM formation and DNA detection process progresses. -----	58
Figure 2.8 – Mean electrochemical impedance spectroscopy R_{CT} change for 2mM $\text{Fe}(\text{CN})_6^{3-/4-}$ on polycrystalline gold electrodes following DNA target binding.-----	59
Figure 2.9 – Mean electrochemical impedance spectroscopy R_{CT} change for 2mM $\text{Fe}(\text{CN})_6^{3-/4-}$ on PGEs with and without TCEP pre-reduction of the MCH SAM.-----	60
Figure 2.10 – Mean electrochemical impedance spectroscopy R_{CT} change for 2mM $\text{Fe}(\text{CN})_6^{3-/4-}$ on immersion cleaned AT screen-printed electrodes following DNA target binding.-----	61
Figure 2.11 – Mean electrochemical impedance spectroscopy R_{CT} change for 2mM $\text{Fe}(\text{CN})_6^{3-/4-}$ on CV cleaned AT screen-printed electrodes following DNA target binding.-----	62
Figure 2.12 – Mean electrochemical impedance spectroscopy R_{CT} change for 2mM $\text{Fe}(\text{CN})_6^{3-/4-}$ on BT screen-printed electrodes following DNA target binding. -----	63
Figure 2.13 – Mean electrochemical impedance spectroscopy R_{CT} change for 2mM $\text{Fe}(\text{CN})_6^{3-/4-}$ on thin-film gold electrodes (TFGEs) following DNA target binding. -----	64
Figure 2.14 – Cleaning and electrografting voltammograms for carbon surface preparation on glassy carbon electrodes.-----	68
Figure 2.15 – Example 1mM $\text{Fe}(\text{CN})_6^{3-/4-}$ measurements on glassy carbon electrodes functionalised with DNA probe and blocked with 1% ethanolamine. -----	69
Figure 2.16 – Cleaning and electrografting voltammograms for carbon surface preparation on screen printed carbon electrodes. -----	70
Figure 2.17 –1mM $\text{Fe}(\text{CN})_6^{3-/4-}$ DPVs following surface modification on screen-printed carbon electrodes.-----	71
Figure 2.18 – Mean EIS (ΔR_{CT}) & DPV ($\Delta \text{Peak I}$) signal change on polycrystalline gold and glassy carbon electrodes, functionalised with their respective protocols, when detecting complementary DNA target.-----	72
Figure 2.19 – Example 1mM $\text{Fe}(\text{CN})_6^{3-/4-}$ DPV responses and dose response curve of synthetic DNA target on carbon SPE. -----	73
Figure 2.20 – Diagram of the artificial plasmid created to hold antibiotic resistance gene segments.-----	77

Figure 2.21 – Diagram of a typical RPA reaction showing elongation of one primer. -----	81
Figure 2.22 – Image of 2% agarose gel containing PCR amplicons of different plasmid gene segments (identified at top).-----	82
Figure 2.23 – Image of 2% agarose gel isothermal PCR amplicons of the bla _{OXA-1} gene. ----	83
Figure 3.1 – Mean electrochemical impedance spectroscopy R _{CT} change for 2mM Fe(CN) ₆ ^{3-/4-} on different electrode types, modified with 6-mercapto-1-hexanol (MCH) or 6-mercapto-1-propanol (MCP), in response to PCR amplicon binding. -----	87
Figure 3.2 – PCR amplicon detection and sequence specificity testing on PGEs. -----	89
Figure 3.3 – PCR amplicon detection on TFGEs.-----	90
Figure 3.4 – SimpleStat PCB and circuit diagram. -----	93
Figure 3.5 – Voltammetric characterisation of SimpleStat on-board gold electrodes using 2mM Fe(CN) ₆ ^{3-/4-} .-----	95
Figure 3.6 – Further characterisation of SimpleStat on-board electrodes. -----	96
Figure 3.7 – Detection of PCR amplicon on SimpleStat on-board gold electrodes.-----	97
Figure 3.8 – Atypical Fe(CN) ₆ ^{3-/4-} CV responses on SimpleStat on-board electrodes due to inconsistencies in gold layer. -----	98
Figure 3.9 – DPV responses of SimpleStat and PalmSens PS4 potentiostat on one electrochemical cell. -----	99
Figure 3.10 – Schematic of different electrochemical detection methods on carbon electrodes.-----	103
Figure 3.11 – Diagram of solid-phase RPA. -----	104
Figure 3.12 – DPV response to PCR amplicon target concentrations on carbon SPEs.-----	106
Figure 3.13 – EIS and DPV examples for RPA detection on carbon SPEs. -----	107
Figure 3.14 – Bode plot of phase vs frequency for RPA detection on carbon SPEs. -----	107
Figure 3.15 – DPV Fe(CN) ₆ ^{3-/4-} peak ΔI response following positive or negative RPA reaction addition to carbon SPE. -----	108
Figure 3.16 – SWV response of 10 μM methylene blue on carbon SPEs. -----	110
Figure 3.17 – Methylene blue SWV peak current response to 10 μM dsDNA incubation.-	111
Figure 3.18 – Methylene blue SWV peak response to PCR and RPA amplicon on unmodified electrodes.-----	112
Figure 3.19 – Methylene blue SWV peak current change during real-time RPA measurement. -----	113

Figure 3.20 – Methylene blue SWV peak current one two electrodes during real time solid-phase RPA measurement. -----	115
Figure 3.21 – DPV peak ΔI change in response to Oxa RPA amplicon or blank RPA reaction mix. -----	120
Figure 3.22 – Comparison of DPV responses from electrodes functionalised using overnight or 2-hour SAM formation protocol. -----	121
Figure 3.23 – Image of 2% agarose gel electrophoresis results for solid-phase RPA performed on polycrystalline gold electrodes. -----	122
Figure 4.1 – Reversible oxidation of TMB. -----	125
Figure 4.2 – Schematic of solid-phase amplification with HRP-dTTP. -----	128
Figure 4.3 – TMB electrochemistry responses on unmodified gold SPEs. -----	132
Figure 4.4 – TMB diagnostic electrochemical responses on BT SPEs. -----	133
Figure 4.5 – Electrochemical response of HRP-dTTP oxidised TMB solutions on AT SPEs.-	134
Figure 4.6 – DNA yield from solution-phase RPA reactions containing reduced dNTP concentrations. -----	135
Figure 4.7 – Chronoamperometric detection of plasmid DNA amplified by solid-phase RPA using HRP-TMB system on AT SPEs. -----	136
Figure 4.8 – Chronoamperometric detection of DNA amplified by solid-phase RPA using HRP-TMB system on AT SPEs following washing with 1xPBS + 0.05% Tween. -----	138
Figure 4.9 – Image of 2% agarose gel of OXA-1 RPA amplification from washed bacterial culture. -----	139
Figure 4.10 – Chronoamperometry results of DNA amplified by solid-phase RPA from washed bacterial culture on AT SPEs. -----	142
Figure 4.11 – Image of 2% agarose gel electrophoresis of liquid-phase RPA on unwashed bacterial lysate. -----	143
Figure 4.12 – TMB reduction current from solid-phase amplification of unwashed bacterial lysate with low density SAM formation. -----	144
Figure 4.13 – TMB reduction current from solid-phase amplification of unwashed bacterial lysate. -----	145
Figure 4.14 – Image of 2% agarose gel electrophoresis on RPA exploratory panel. -----	146
Figure 4.15 – Degradation of Silver reference electrode through HRP reduction of peroxide. -----	148

Figure 4.16 – Mean TMB chronoamperometry current from solid-phase RPA on unwashed bacterial lysate using overnight-backfill SAM formation method. -----	149
Figure 4.17 – Comparison of TMB reduction current for 2-hour and overnight SAM formation protocols. -----	151
Figure 4.18 – Mean TMB chronoamperometry reduction current following HRP-dTTP solid-phase RPA and incubation with H ₂ O ₂ + TMB solution on 416 CFU unwashed E. coli or S. aureus.-----	153
Figure 4.19 – Dose response curve of E. coli detected using TMB reduction current following HRP-dTTP solid-phase RPA and incubation with H ₂ O ₂ + TMB solution. -----	154
Figure 5.1 – Summary of research contributions arising from this thesis. -----	161

iii. List of Tables

Table 1.1 – Overall antibiotic resistance levels against common antibiotics for <i>E. coli</i> and <i>Acinetobacter</i> species isolates reported in Europe/European Economic Area countries in 2019/20.	11
Table 1.2 – Peak antibiotic resistance levels against common antibiotics for <i>E. coli</i> and <i>Acinetobacter</i> species isolates reported in Europe/European Economic Area countries in 2019/20.	13
Table 1.3 – World Health Organisation ASSURED criteria for effective point-of-care diagnostic devices	15
Table 2.1 – DNA sequences used in initial gold electrode preparation.....	56
Table 2.2 – DNA sequences used for comparison of carbon and gold functionalisation.	66
Table 2.3 – Genes selected for bespoke plasmid development, and their associated antibiotic resistances.....	76
Table 2.4 – Primers used for traditional PCR amplification of each gene segment.	79
Table 2.5 – Primers used for isothermal amplification of the <i>bla</i> _{OXA-1} gene segment.	81
Table 3.1 – DNA probe sequence used for PCR amplicon.	86
Table 3.2 – OXA-1 Probe for RPA detection on carbon electrodes.	102
Table 3.3 – Isothermal OXA-1 Primer / Probe for solid-phase amplification on carbon.	104
Table 3.4 – OXA-1 Probe for RPA detection on gold electrodes.....	118
Table 3.5 – Isothermal OXA-1 Primer / Probe for solid-phase amplification on gold.	119
Table 4.1 – Solid-phase RPA with HRP-dTTP preparation.....	127
Table 4.2 – DNA yield from solid-phase RPA on SPEs with different electrode blocking protocols.	136
Table 4.3 – Chronoamperometry current at different time points following 1xPBS wash or 1xPBS with Tween-20.....	139
Table 4.4 – Mean CFU loaded to each RPA reaction for bacterial culture amplification. ...	140
Table 4.5 – Mean CFU loaded to each solid-phase RPA reaction for bacterial culture amplification.....	141
Table 4.6 – Summary of RPA exploratory reaction panel.....	146
Table 4.7 – Mean CFU loaded into each solid-phase RPA reaction.	152
Table 4.8 – Detection schemes and target thresholds for solid-phase RPA nucleic acid biosensors.	155

1 Introduction

1.1 Microbiology and Antimicrobial Resistance

Bacteria are a critical part of every ecosystem on earth and can be found even under the most extreme conditions. The bacteria kingdom contains highly numerous and varied species, a small number of which cause disease under certain circumstances. This variety means the shape, structure and function of the bacterial cell can change significantly between species, producing diverse morphologies and characteristics.

Bacteria are broadly categorised into Gram-positive and Gram-negative groups based upon the structure of their cellular membrane (Baron, 1996). Gram-positive bacteria have a thick layer of peptidoglycan covering the cell membrane, which is anchored by long and complex molecules of lipoteichoic acid. The inner membrane contains proteins which control the movement of molecules into and out of the cytoplasm. In contrast to this, Gram-negative bacteria have a double membrane structure, with a thin layer of peptidoglycan in the space between the two. Both the inner and outer membranes contain proteins, which gives Gram-negative organisms more control over the molecules moving into and out of the cell.

Like all living organisms, the functioning of the bacterial cell is controlled by the DNA within it. Bacterial DNA is unique from its eukaryotic counterpart in that it is a free molecule within the cell. The DNA is not contained within a nucleus, instead existing as a single large chromosome rather than the numerous chromosomes of eukaryotic organisms. Cells may also contain shorter DNA sequences such as plasmids which can replicate independently of the chromosome and may be shared readily between cells. These discrete extrachromosomal nucleic acids typically carry genes which provide a selective advantage to the host cell (Baron, 1996).

Both Gram-positive and Gram-negative organisms can cause disease, and the first line of treatment for bacterial infections is the administration of antibiotics. Identification of the specific organism causing an infection can be critical when choosing the correct antibiotic to provide effective treatment.

1.1.1 Gram-negative Pathogens

Infections caused by Gram-negative bacteria are becoming more common worldwide, overtaking those caused by Gram-positive pathogens in some settings (Kaye and Pogue,

2015; Vincent et al., 2009). Some Gram-negative bacteria are commensal and live harmlessly within the body or in the environment, but there are some which can cause severe illness such as intra-abdominal infections, ventilator-associated pneumonia, surgical site infection, urinary tract infections and bacteraemia (Esteve-Palau et al., 2015; Kaye and Pogue, 2015; Leistner et al., 2014; Munoz-Price and Weinstein, 2008). The most common pathogenic Gram-negative organisms observed in hospitals today are the *Enterobacteriaceae* family, *Acinetobacter* species (the *A. baumannii* group in particular), and *Pseudomonas aeruginosa* (Kaye and Pogue, 2015; Vincent et al., 2009). *E. coli*, of the *Enterobacteriaceae* family, currently accounts for 65% of all Gram-negative infections encountered in UK hospitals, and was projected to cost the NHS £2.3 billion in 2018 (Department of Health, 2016). These costs arise from 3.87 excess bed days compared to non-infected patients, an increased risk of developing nosocomial (hospital acquired) infections or bacteraemia which requires more intensive treatment and patient support, and the cost of potent antibiotic treatments which may be required for Gram-negative infections (de Kraker et al., 2011; Naylor et al., 2019; Thaden et al., 2017). Since 2012, cases of *E. coli* bacteraemia have increased from 60.4 per 100,000 to 77.3 per 100,000 in the UK alone, with UTIs being the major source of *E. coli* bacteraemia (Public Health England, 2020).

Many Gram-negative organisms are able to survive for long period on surfaces and under harsh conditions, and can be difficult to eradicate once established in a particular setting (European Centre for Disease Prevention and Control, 2016). For example, *A. baumannii* is capable of surviving for long periods of time on dry surfaces and is resistant to disinfectants (Peleg et al., 2008), resulting in it being easily spread between patients and wards within a hospital, and even to surfaces beyond the hospital environment (Rose et al., 2014). Another Gram-negative bacterium, *P. aeruginosa*, is resistant to the action of detergents and disinfectants and can survive despite long-term immersion in these solutions (Lanini et al., 2011; Shimono et al., 2008). All Gram-negative organisms also display some innate resistance to the action of detergents and disinfectants as a result of their double membrane structure (Nixdorff et al., 1978), which also provides some resistance to antibiotic drugs. These factors complicate treatment and make Gram-negative pathogens difficult to control, increasing the risk of spreading and the rates of infection.

1.1.2 Antibiotics and Antimicrobial Resistance

Antibiotics have been the primary defence against bacterial infection since their discovery in 1928 and their introduction to clinical practice in the 1930s (Davies and Davies, 2010). Antibiotics work by selectively disrupting cellular functions, targeting systems which bacterial cells rely upon for survival. These mechanisms include disruption of cell wall synthesis (beta-lactams and glycopeptides), inhibition of DNA replication by blocking folate synthesis (sulfonamides) or critical enzyme function (quinolones), and preventing protein synthesis (aminoglycosides, amphenicols, macrolides and tetracyclines) (Fair and Tor, 2014). Some processes are common to both the bacterial cell and mammalian cells, such as DNA and protein synthesis and transcription. In these cases, the antibiotics target enzymes or stages which have diverged between the different cells to allow selective disruption of the bacteria with minimal toxicity to the host cells.

Antimicrobial resistance (AMR) has been a growing problem since the earliest days of antimicrobial use (Davies and Davies, 2010). Antimicrobial resistance is the development of mechanisms through which microorganisms (bacteria, fungi, viruses and parasites) survive exposure to agents which would be expected to kill them or inhibit their growth and proliferation (O'Neill, 2016). In the case of bacteria, AMR arises as bacterial cells develop resistance to the antibiotics used in their treatment. This can result in the organisms which are resistant growing and spreading due to a lack of competition from other strains, and can make treatment of these organisms challenging.

The treatment of bacterial infections with antibiotics is such a routine and integral healthcare process that loss of this treatment option would have devastating effects on global health and economies. Estimates suggest that by 2050, AMR could be responsible for over 10 million deaths per year, cost up to 100 trillion USD in lost economic output annually, and result in 28 million people falling into extreme poverty (O'Neill, 2016; United Nations, 2021; World Bank Group, 2017). These deaths and costs come not only from exposure to AMR organisms, but from the increased risks associated with other procedures dependent on antibiotics; chemotherapy, organ transplant and invasive surgeries. Antimicrobial resistance will drive inequality worldwide and threatens to make current healthcare standards unsustainable within a few decades.

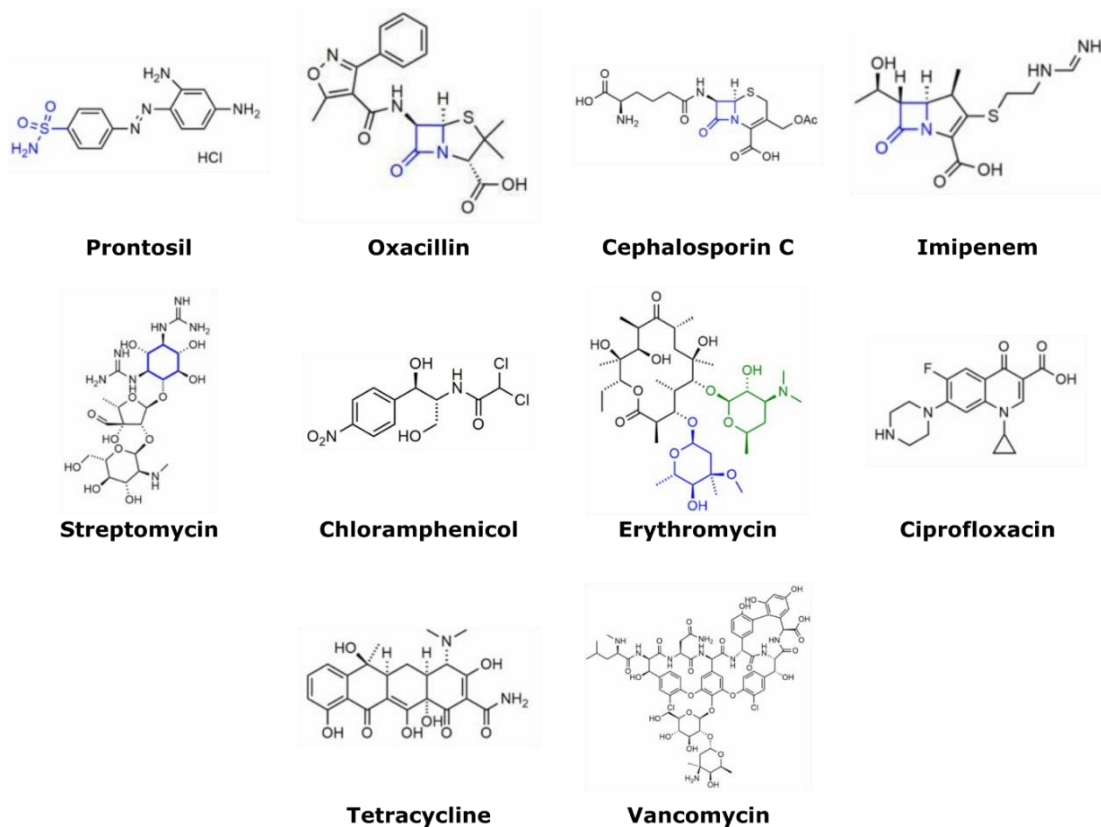


Figure 1.1 – Example structures of antibiotics of different classes. Adapted from Fair and Tor (2014) under Creative Commons Non-Commercial Attribution (CC BY-NC 3.0).

As the use of antibiotics has become more widespread, cheaper, and diverse, the potential for mismanagement and overuse has increased. In the case of many early antibiotics, misuse has led to them being essentially ineffective in modern medicine against clinically relevant organisms, and resistance to these agents is also widely present in the environment (Davies and Davies, 2010; Martinez, 2014; Williams et al., 2016). Misuse and overuse of antibiotics has produced significant selection pressure worldwide, which has led to initially small populations of resistant bacteria growing significantly compared to the susceptible strains. These are now becoming the dominant population within a species with significant consequences for treatment efficacy globally (Figure 1.2) (Davies and Davies, 2010; Fair and Tor, 2014).

Some key drivers of antibiotic pressure have been the misuse of antibiotics when treating disease, and the extreme use of antibiotics in livestock farming to improve yields (Fair and Tor, 2014). In the case of farming use, antibiotics are given to livestock in their feed to prevent infections which would reduce the growth of the animal. This results in a moderate

concentration of antibiotic being released into the environment from animal waste, which is concentrated enough to produce selection pressure in the local bacteria. This accelerates the development and spread of antibiotic resistance in the population and can lead to infections which are increasingly difficult to treat if people become exposed to these bacteria.

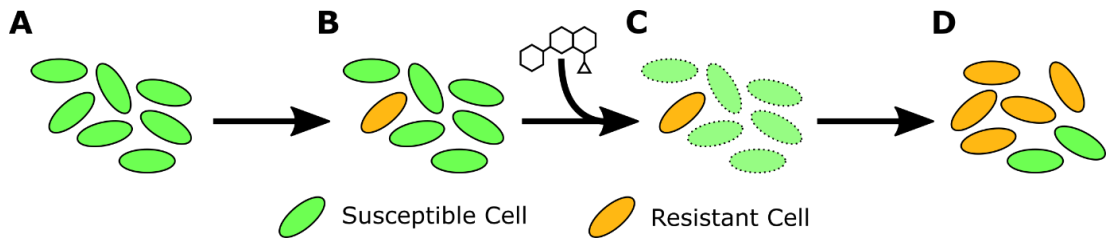


Figure 1.2 – Diagram of how antibiotic resistance can arise within a susceptible population. (A) A population of antibiotic susceptible cells are widespread in an environment. (B) A small number of cells may acquire resistance through mutation or gene transfer. (C) An antibiotic introduced to the environment gives resistant cells an advantage over susceptible cells. (D) With reduced competition and increased selection pressure, resistant cells become more prevalent in the population.

Perhaps the most well-known antibiotic resistant organism is the Gram-positive organism Methicillin-resistant *Staphylococcus aureus* (MRSA) (Davies and Davies, 2010). *S. aureus* is typically a commensal bacteria which is commonly found in the nose, with an estimated 20% of people permanently colonised (Cogen et al., 2008). *S. aureus* can cause a range of infections such as impetigo, meningitis, septicaemia, and pneumonia, which would typically be treated with antibiotics. However, with the increasing resistance of many MRSA strains to available antibiotics, what was once a routine treatment becomes increasingly ineffective. While MRSA infection rates in Europe have begun to decline in recent years due to improved infection control measures and antibiotic stewardship, this pathogen is still a threat to public health due to its antimicrobial resistance. The example of MRSA is however a good indication that with improved management and stewardship of antibiotics the problem of AMR can be managed and reduced over time (European Centre for Disease Prevention and Control, 2018).

1.1.3 Gram-negative Bacteria and Antibiotic Resistance

In 2008, Rice compiled a list of organisms (with updates suggested by Peterson in 2009) which cause the majority of hospital acquired infections worldwide and represent a major threat to public health as a result of rapidly developing pathogenesis, transmission and resistance

mechanisms. The organisms on this list are known as the ESCAPE pathogens, and consist of *Enterococcus faecium*, *Staphylococcus aureus*, *Clostridium difficile*, *Acinetobacter baumannii*, *Pseudomonas aeruginosa* and the *Enterobacteriaceae* family (Peterson, 2009; Rice, 2008). Of these six groups, four are Gram-negative organisms, including the *Enterobacteriaceae* family. The prevalence of Gram-negative pathogens on this list is largely due to the rapid increase in antimicrobial resistance observed in this group in recent years (Blair et al., 2014; Miller, 2016).

In 2017 the World Health Organisation compiled a list of priority pathogens for the development of new antimicrobial agents (World Health Organisation, 2017a). All three of the organisms identified as critical antibiotic development targets have a Gram-negative cell wall structure, and the *Enterobacteriaceae* family is again included. This demand for new antibiotic development highlights the continuing issue posed by Gram-negative antimicrobial resistance. The fact that these organisms are so often listed as critical threats to worldwide health indicates just how prevalent and varied antimicrobial resistance is within these populations.

1.1.3.1 *Methods of Antibiotic Resistance*

Bacteria have developed many methods by which antibiotics can be made ineffective upon a cell. Bacterial cells have intrinsic mechanisms which naturally protect them from antibiotics. The presentation of certain molecules in the bacterial membrane may allow or prevent the action of specific antibiotics. For example, polymyxin antibiotics do not affect Gram-positive organisms due to the lack of exposed lipopolysaccharide in the membrane (Srinivas and Rivard, 2017). The outer membrane of the Gram-negative cell presents a barrier through which many antibiotics cannot pass due to the reduced permeability of the membrane compared to Gram-positive bacteria. Hydrophilic antibiotics can pass through the membrane using proteinaceous channels such as porins which provide access to the intermembrane space. By reducing the expression of these pores at the surface, the cell can reduce the influx of antibiotic molecules. In addition, the cell may be able to increase the expression of efflux proteins, increasing the rate at which antibiotics are actively transported out of the cell and preventing them reaching a critical concentration for efficacy (Blair et al., 2014; Miller, 2016; Santajit and Indrawattana, 2016).

Alternatively, the target of the antibiotic may be modified to prevent binding. A change to the antibiotic binding site on a target protein may inhibit the action of the antibiotic while

allowing the protein to function normally, resulting in the cell surviving the presence of the antibiotic molecule. This resistance may result from a change to the amino acid sequence of the protein, or methylation of target nucleic acid sequences such as ribosomal RNA (Blair et al., 2014; Santajit and Indrawattana, 2016). Protective proteins may also be produced which bind to the target of the antibiotic and prevent it from binding.

The bacterial cell may also produce proteins which can inactivate the antibiotic before it reaches its target. The earliest antibiotics, such as penicillin, are commonly hydrolysed by beta-lactamase enzymes which are now widespread in bacterial populations and provide effective protection against many antibiotics based on the beta-lactam structure (Davies and Davies, 2010). The inactivation of antibiotics by the addition of chemical groups is also common, with aminoglycosides particularly susceptible to inactivation by the action of acetyltransferases, phosphotransferases, and nucleotidyltransferases (Blair et al., 2014).

These mechanisms can be generated spontaneously within a bacterial cell or can be acquired by the transfer of nucleic acids between bacteria. The acquisition of these diverse antimicrobial resistance mechanisms occurs primarily through mutation and horizontal gene transfer (Martinez, 2014; Ruppé et al., 2015).

1.1.3.2 Mutation as a Source of Antibiotic Resistance

Bacterial chromosomes contain the genes for all the routine processes of the organism, producing proteins, enzymes and other molecules which are vital within the cell. Many antibiotics target key proteins or enzymes and prevent their normal function, leading to cell death. Others may bind to the cell membrane and disrupt the barrier it provides, leading to the contents of the cell leaking. If binding of the antibiotic molecule is prevented, then it is unable to perform its function and the cell survives.

Figure 1.3 shows how mutation can result in resistant organisms developing. Mutation is a random process by which individual bases in the DNA sequence are swapped from their original nucleotide to a new one, without being repaired by cellular mechanisms. These mutations may cause an amino acid in the resulting protein to be substituted for a different one, determined by the new sequence created by the mutation (Figure 1.3B). Occasionally, an amino acid substitution will result in a change to the protein, such as changes to the physical structure, binding site, or activity. These changes can result in proteins which are better or worse at their function, have a different function altogether, or may even kill the

cell outright (Figure 1.3C). Mutation is a vital part of evolution for all organisms, and has played a key role in the development of antibiotic resistance (Hershberg, 2015).

Should a protein or enzyme which is the target of an antibiotic be altered through mutation, the antibiotic may no longer bind and will be unable to kill the organism. For example, fluoroquinolone resistance is commonly caused by mutations in the genes for the target proteins, the type-II topoisomerases (Mathers et al., 2015; Redgrave et al., 2014; Shin and Park, 2017). Topoisomerases regulate how tightly wound the chromosomal DNA is, preventing excessive twisting which would limit the cells ability to transcribe DNA into RNA. Fluoroquinolones bind to the topoisomerases and inactivate them, leading to the eventual death of the cell as new DNA transcripts can no longer be made for protein synthesis. Mutations in the topoisomerase proteins resist fluoroquinolone binding, allowing the cell to function normally. In the presence of fluoroquinolones, these cells survive and pass this beneficial mutation on to subsequent generations (Hooper, 2000).

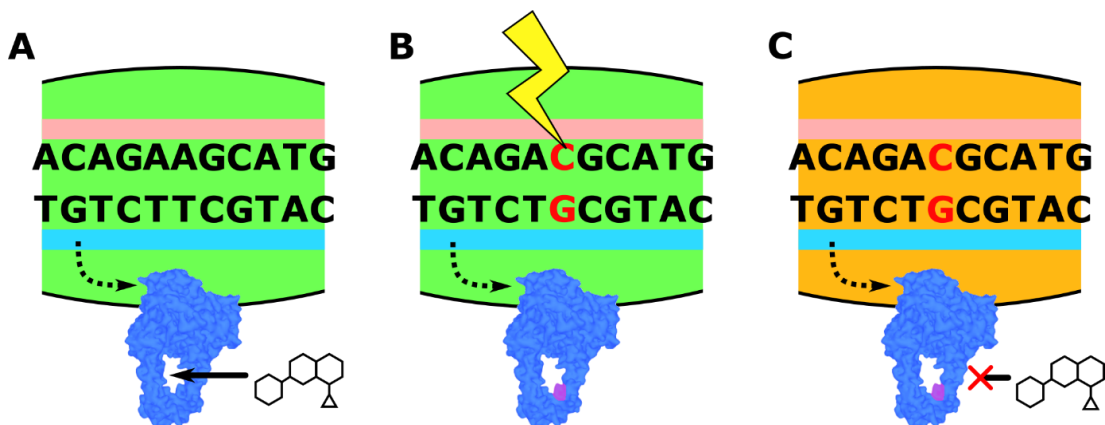


Figure 1.3 – Development of antimicrobial resistance through mutation. (A) The bacterial cell produces a critical protein which is a target for an antibiotic. (B) A random mutation may result in the protein structure changing. (C) If this change inhibits the action of an antibiotic, the cell has become resistant to that antibiotic. Protein image from The UniProt Consortium (2019).

1.1.3.3 Horizontal Gene Transfer as a Source of Antibiotic Resistance

As well as the bacterial chromosome, many bacterial cells contain smaller lengths of DNA. These smaller segments, such as plasmids, hold genes which are typically useful for survival in specific situations, and are not vital to the normal function of the cell. Plasmids are activated when required to help the cell survive adverse conditions. Plasmids which confer

no immediate benefit – those for which no selective pressure exists – are likely to be lost in the population due to genetic drift. However, plasmids which benefit the cell and are frequently transcribed, such as those conferring antibiotic resistance genes in an environment with high antibiotic concentrations, become “fixed” in the population due to the survival and reproduction of cells hosting the genes. Future transfer of these plasmids is therefore more likely as they are much more widespread in the population.

Horizontal gene transfer (HGT) allows bacteria to pass these small lengths of DNA between one-another. By acquiring free DNA from the environment (Figure 1.4), conjugating with another cell containing a plasmid (Figure 1.5), or being infected by a phage containing bacterial antimicrobial resistance genes (transduction, Figure 1.6), these sequences are transferred between cells. HGT is the most common method by which bacteria acquire new resistance genes as beneficial plasmids are readily transferred between cells (Bennett, 2008; Perry and Wright, 2014). Not all cells can incorporate environmental DNA, a process called transformation. Cells which have this capacity are known as competent cells. However, conjugation and transduction do not require the host cell to be competent, and transduction does not even require proximity of the two cells to transfer genetic material.

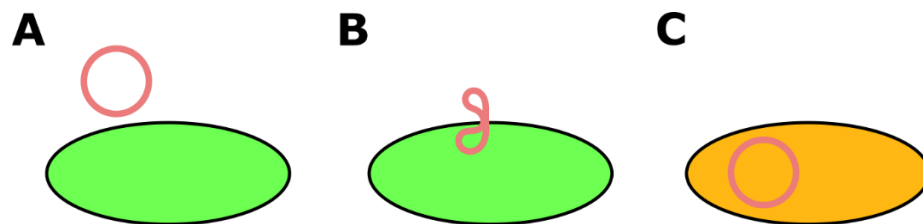


Figure 1.4 – Schematic of plasmid uptake from the environment. (A) An antibiotic susceptible competent cell encounters an environmental AMR plasmid. (B) Under certain conditions the cell may take up the plasmid. (C) Expression of AMR genes in the plasmid protects the cell from an antibiotic.

For resistance genes to be available for transfer by HGT, there must be an organism with the gene present initially. The environment is believed to be a key reservoir for most antibiotic resistance genes, with both clinically important and currently unknown genes being widespread (Williams et al., 2016). Many antibiotics are derived from antimicrobial molecules produced by the *Streptomyces* genus (Forsberg et al., 2012; Perry and Wright, 2014). These organisms are widespread in soil and undoubtedly contain resistance mechanisms against their own antimicrobials. Bacteria sharing a similar niche who are

regularly exposed to *Streptomyces* antimicrobial molecules may also have developed resistance independently. However, for a resistance mechanism to be clinically relevant, it must migrate into clinically important organisms.

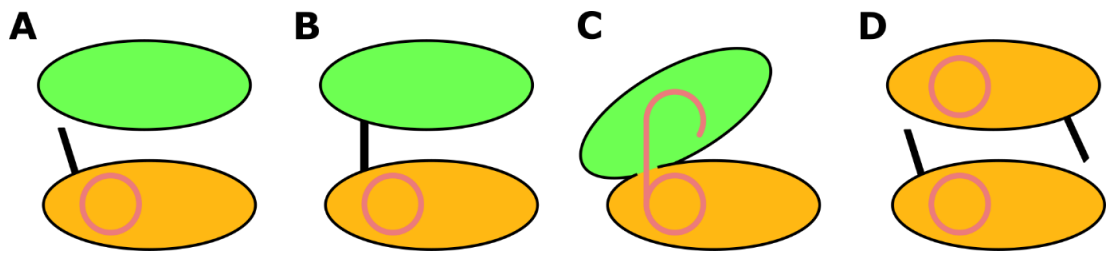


Figure 1.5 – Schematic of plasmid transfer through conjugation. (A) An antibiotic resistant bacterium capable of horizontal gene transfer meets a susceptible recipient. (B) The cells conjugate through a structure known as the pilus which draws the cells together. (C) The cell membranes fuse and the plasmid is copied to the recipient cell. (D) The cells separate, each with a copy of the original plasmid.

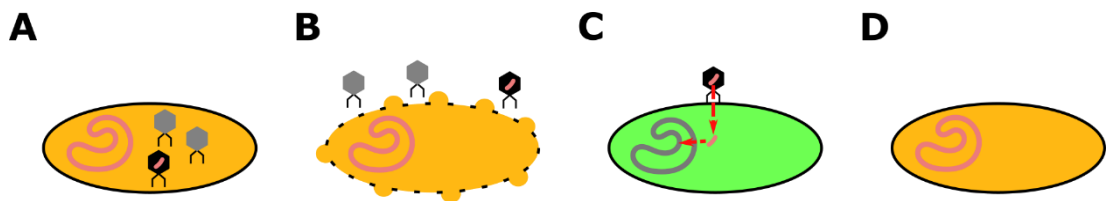


Figure 1.6 – Schematic of transduction for horizontal gene transfer. (A) A bacteriophage packages a portion of bacterial DNA, containing an antibiotic resistance sequence, during assembly. (B) The viral particles are released from the host cell. (C) Infection of a new cell can incorporate the bacterial gene into the new host chromosome. (D) The newly infected cell can express the resistance gene.

The niches of environmental and clinical organisms may rarely overlap, so direct transfer can be unlikely (Forsberg et al., 2012). However, environmental and intestinal organisms may have regular interactions, especially in livestock populations. Given that there is evidence for significant horizontal gene transfer in the colon (Shoemaker et al., 2001), combined with the historical overuse of antibiotics in livestock, it is likely that feed animals have provided a stepping stone for some current resistance genes moving between environmental and clinical organisms.

As the development and spread of antimicrobial resistance is so multifaceted and involves environmental, livestock and clinical elements, a “One Health” approach to the management of antibiotics has been established (McEwen and Collignon, 2018; World Health Organisation, 2017b). This approach acknowledges that in order to manage and reduce antimicrobial resistance in the clinic, efforts to improve antibiotic use and monitoring must be extended into environmental and agricultural settings as well. Through a combined effort by experts in each sector, the impact and spread of antimicrobial resistance can be minimised much more effectively.

1.1.4 Antibiotic Resistance in Clinically Important Bacteria

As a result of these transfers of resistance genes, many clinically important Gram-negative bacteria now exhibit some resistance to most of the antibiotics available to treat them. Table 1.1 shows the total reported resistance levels of two clinically important Gram-negative bacteria in Europe in 2019. In this table, the Fully Susceptible data details bacteria which were fully susceptible to the antibiotics classes currently used in treatment, not to all antibiotic classes. This is noteworthy regarding *Acinetobacter* resistance as treatment options are limited to fluoroquinolones, aminoglycosides and carbapenems (with polymyxin and tigecycline as a last resort) due to widespread resistance to cephalosporins and aminopenicillins, which can still be effective against *E. coli* isolates (Fournier et al., 2006; Manchanda et al., 2010; Van Looveren and Goossens, 2004).

Table 1.1 – Overall antibiotic resistance levels against common antibiotics for E. coli and Acinetobacter species isolates reported in Europe/European Economic Area countries in 2019/20. Data obtained from European Centre for Disease Prevention and Control (2020).

Antibiotic Resistances	<i>Escherichia coli</i>	<i>Acinetobacter</i>
	Resistance	Resistance
	% of all reported isolates	
Fully Susceptible	42.9	46.6
Resistant to one antibiotic class	34.8	4.8
Resistant to two antibiotic classes	10.5	5.0
Resistant to three antibiotic classes	7.3	43.6
Resistant to four antibiotic classes	4.5	----
Resistant to five antibiotic classes	0.06	----

Extra-intestinal pathogenic *E. coli* is the most common cause of bacteraemia and urinary tract infections, and is one of the most common organisms in food-borne infections worldwide (Pitout and DeVinney, 2017; Public Health England, 2020; World Health Organisation, 2014). In the UK, infections with *E. coli* account for 65% of all Gram-negative infections reported (Department of Health, 2016), and is increasing in incidence year on year (Department of Health, 2016; Public Health England, 2017).

Resistance rates in European isolates of *E. coli* have remained relatively stable in the period since 2015 (European Centre for Disease Prevention and Control, 2020, 2017). However, the already high resistance rates to some antibiotic classes means that reserved antibiotics are recommended for first line treatment of severe infections suspected to be caused by *E. coli*. This has consequences for the development of further resistance against these medicines and increased treatment costs (World Health Organisation, 2014). For example, in the period 2015 – 2019, only carbapenem resistance in *E. coli* showed a significantly increasing trend, a worrying indicator that resistance to our most potent antibiotics is spreading. Combined with the high incidence of these infections worldwide, many infections will be caused by resistant bacteria which may require tailored treatment to effectively control.

While *A. baumannii* does not cause infections to the same extent as *E. coli*, it is the 11th most reported organism in hospital-acquired infections in Europe, responsible for 3.6% of hospital acquired infections (HAIs) (European Centre for Disease Prevention and Control, 2016). The rates of resistance reported in these organisms are also much higher than those in *E. coli*. *A. baumannii* resistance rates in Europe routinely exceeded those of *E. coli* against every tested antibiotic. *A. baumannii* also exhibits much higher rates of multiple resistances, with 43.6% of reported isolates showing resistance to fluoroquinolones, aminoglycosides and carbapenems. Such infections need last line antibiotics such as polymyxins to treat, increasing the cost of treatment and the risk of resistance developing.

Table 1.2 shows the peak resistance level to each antibiotic recorded in EEA countries for the 2019/20 period. This data shows a much poorer picture for the fight against AMR, with some countries reporting over 90% resistance to certain antibiotic classes in *Acinetobacter* species, and over 90% of isolates with combined resistance to all the monitored antibiotics. For *E. coli*, peak resistance rates are high for all antibiotics other than the carbapenems. These data suggest that AMR may already be out of control in certain countries, and reserved antibiotics must now be used as first in line treatments for some bacteria. For patients in countries

reporting these high resistance rates, effective treatment options are becoming severely limited.

Table 1.2 – Peak antibiotic resistance levels against common antibiotics for E. coli and Acinetobacter species isolates reported in Europe/European Economic Area countries in 2019/20. Data obtained from European Centre for Disease Prevention and Control (2020).

#	Antibiotic Resistances	<i>Escherichia coli</i>	<i>Acinetobacter</i>
		Resistance	Resistance
		Peak Resistance Rate Reported / %	
1	Aminopenicillin	71.7	----
2	3 rd Gen Cephalosporin	38.6	----
3	Carbapenem	1.6	92.3
4	Fluoroquinolone	43.5	95.8
5	Aminoglycoside	24.4	92.1
6	Combined 2, 4 and 5	19.0	----
7	Combined 3, 4 and 5	----	91.4

1.1.5 Strategies Against Antimicrobial Resistance

In 2015 the WHO released a document outlining the steps required to improve the control, monitoring and awareness of antimicrobial resistance (World Health Organisation, 2015), which has parallels to many AMR strategies proposed by individual governments . These documents largely agree on the steps needed to manage antimicrobial resistance, which include the following:

- Improve public and professional awareness of AMR through education and communication.
- Improve surveillance, focus research efforts, and increase collaboration.
- Improve infection prevention and control practices.
- Improve management of antimicrobial stock in humans and animals.
- Develop new medicines, diagnostics, and vaccines.

Many of these steps require changes at a management or governmental level to increase awareness of antibiotic resistance and improve training and usage of these treatments. Some will benefit from new drug discoveries and vaccination strategies which could reduce the

infection rate and expand our available range of antibiotics. However, the journey to take new drugs from the laboratory to the clinic is long and difficult, with many failing to reach the patients. Until the number of available antibiotics increases, maintenance of our current stocks is vital.

Improved diagnostic processes can facilitate maintenance of our antimicrobial stockpile. By rapidly informing clinicians of the AMR present in an infection, effective treatment can be more rapidly administered. This will help improve management of antimicrobials as well as informing surveillance efforts. Rapid diagnostics also improve outcomes for patients by reducing the lag time before tailored treatment is administered, reducing time spent in care and improving adherence to medication regimes. This in turn reduces the cost burden of AMR to healthcare facilities and helps limit the spread of AMR organisms overall (Gialamas et al., 2009; Price, 2001).

1.2 Biosensors

Biosensors are devices which incorporate a biological element into a sensing system in order to identify a specific target. Typically, the recognition element of the system will be biological, taking advantage of interaction specificity offered by biological molecules to produce a signal. This signal is received by a transducer and processed into a result (Gruhl et al., 2011). Biosensors can detect the presence of cells, DNA, protein, ions and many other molecules depending upon the recognition element selected, and are therefore a versatile option when examining biological samples (Goode et al., 2015; Mehrotra, 2016). Combining a suitable recognition element and transducer system can produce sensitive and specific biosensors which rival benchtop-based tests.

Biosensors offer an attractive platform for the execution of rapid tests in a clinical environment. Many current diagnostic techniques for disease biomarkers require significant skill, time and space in a dedicated laboratory to be performed (Gruhl et al., 2011). Biosensors can produce rapid and sensitive results which are cheap to obtain and require little operator skill (Andreescu and Sadik, 2009). When moving testing outside of the lab to the point-of-care (PoC) or the field, these devices also need to be compact and portable. The requirements of an effective PoC diagnostic device were laid out by the World Health Organisation (Kettler et al., 2004) as the ASSURED criteria (Table 1.3).

Table 1.3 – World Health Organisation ASSURED criteria for effective point-of-care diagnostic devices (Kettler et al., 2004).

- A Affordable
- S Sensitive
- S Specific
- U User-friendly
- R Robust and Reliable
- E Equipment Free
- D Delivered to those who need it

The most successful and widespread biosensors developed to date include the blood glucose monitor and the pregnancy test (Hughes, 2009; Lee, 2008; Yoo and Lee, 2010). These devices have been particularly successful as they meet the ideal requirements for point-of-care diagnostics; the user doesn't need significant skill to operate the device, it is portable,

provides rapid results and is highly sensitive. The commercial success of these biosensors reveals the demand for low-cost, rapid, and reliable monitoring of conditions and disease states to alleviate load on hospital laboratories and improve patient monitoring. Biosensors have been examined for the diagnosis or monitoring of many other conditions, but none have achieved the global success of glucose and pregnancy test systems. The majority of medical testing remains confined to a laboratory setting but taking diagnostics to the point of care has clear advantages for patient health, healthcare budgets and laboratory workflows.

1.2.1 DNA Detection

DNA is the molecule which encodes the genetic information for all life. Its sequence is unique to a species, and in most cases unique to an individual. By examining the DNA of an organism, it is possible to identify the proteins that organism is capable of producing and infer characteristics of the individual as a result. As previously discussed, many antimicrobial resistance mechanisms originate from changes to a bacterial cells' DNA. By searching the DNA for sequences associated with antimicrobial resistance, it is possible to identify which antibiotics a cell may be resistant to.

Most DNA technologies rely upon the sequence specific interactions between DNA molecules. DNA will bind most strongly to another strand with a fully complementary sequence, and as the sequences become less complementary this binding efficiency decreases. This interaction can be used to capture DNA with a specific sequence of interest for amplification, detection or storage. The specificity of this DNA binding can be increased or decreased by changing variables such as the temperature or the ionic strength of solution. Reducing the binding specificity may be desirable under certain circumstances, but typically DNA detection methods use high specificity interactions to capture a target of interest.

Any number of DNA targets can be detected on one system using DNA hybridisation by changing the sequence of the capture probe. The use of sensor arrays and the development of a detection scheme for multiple target sequences is therefore relatively simple using DNA. This modularity is similar to antibody-based sensors where the capture antibody can be interchanged to detect different targets and would allow a single DNA sensing system to be rapidly adapted to meet changing diagnostic needs and emerging targets.

DNA detection has been widely used in fields such as industrial optimisation (Binder et al., 2012), environmental monitoring (Jung et al., 2014; Palchetti and Mascini, 2008), detection of food contaminants (Nordin et al., 2017; Peltomaa et al., 2016) and medical diagnostics

(Maffert et al., 2017; Wang, 2006). As previously described, rapid and sensitive detection of pathogens and their relevant characteristics in an infection allows the clinician to provide effective treatment more quickly and helps prevent the spread of infection to others. Biosensors containing DNA recognition elements offer the flexibility and specificity required for sensitive detection of many targets, which make them an ideal candidate for development of clinical test platforms.

1.2.1.1 DNA Amplification

As DNA can be present in very low concentrations in a solution – from 10^{-17} to 10^{-9} molar for bacterial infections (Kelley, 2017) – an amplification process is often performed to reach the limit of detection for a particular assay. The polymerase chain reaction (PCR) described by Mullis and Faloona (1987) has been the workhorse DNA amplification technique for many years, and can amplify single copies of a target into billions of copies in 40 to 60 minutes (New England BioLabs, 2017; ThermoFisher Scientific, 2017).

In a PCR reaction, a thermostable polymerase enzyme extends a primer sequence (which is hybridised to the target DNA) by the addition of free nucleotides to the 3' end of the sequence (Figure 1.7). Primer sequences are designed to specifically complement a target section of the DNA sequence. Symmetrical PCR reactions containing primer pairs at equal concentration are the most common format. This allows recognition of the complementary strand once it has been produced and leads to exponential amplification of both strands of the original target. Asymmetrical PCR reactions which have one primer at a higher concentration than the other can be used to amplify one strand of the target sequence preferentially, but are more difficult to optimise (Heiat et al., 2017). Such reactions are useful when a library of single stranded DNA is required.

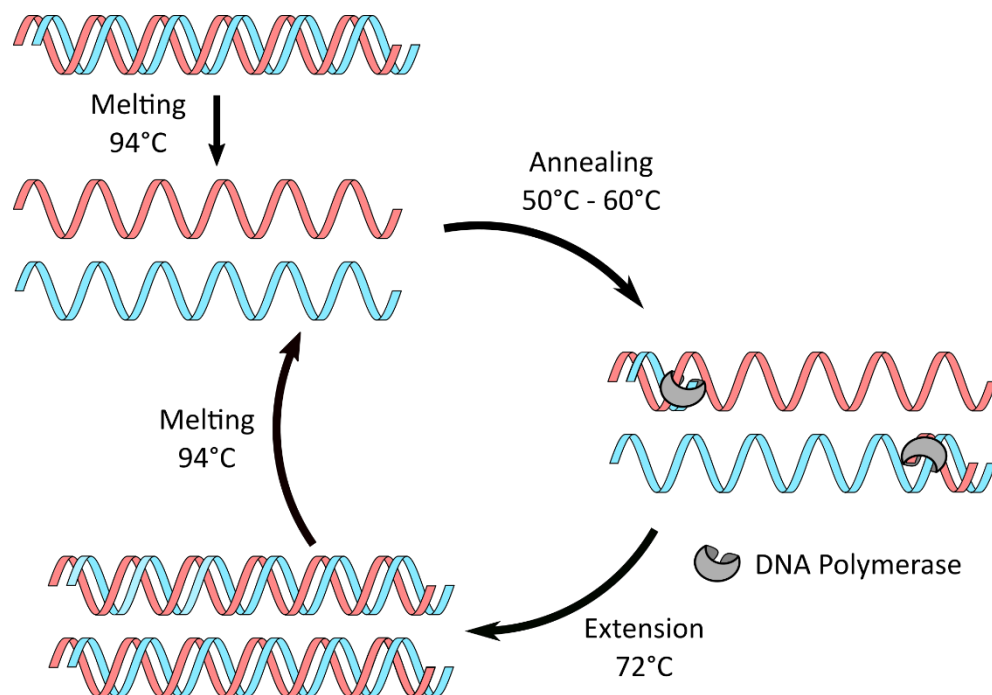


Figure 1.7 – Diagram of a typical Polymerase Chain Reaction.

Traditional PCR reactions require rapid and large changes in temperature, usually up to 95°C, which is performed by dedicated benchtop thermocycling equipment. These conditions can be challenging to reproduce in a low-cost point-of-care sensor due to the significant power requirements and control measures needed. A number of isothermal techniques which run at a single lower temperature have been developed recently, and are more suited to DNA amplification on a biosensor platform (Zhao et al., 2015). Isothermal techniques typically use polymerase enzymes with strand displacement activity, or enzymes which can separate the double stranded DNA amplicon (Li and Macdonald, 2015). These techniques often have more complex primer design and performance requirements than traditional PCR and may not produce exponential amplification on their own (such is the case with Rolling Circle Amplification) or could be less specific. Some isothermal amplification protocols such as Loop-mediated Isothermal Amplification (LAMP), Recombinase Polymerase Amplification (RPA) and Exponential Rolling Circle Amplification (E-RCA) show high levels of amplification after a similar reaction duration to traditional PCR. Several of these techniques have been successfully incorporated into DNA detecting biosensor platforms (Cheng et al., 2014; del Río et al., 2017; Hashimoto et al., 2017; Khater et al., 2019; Luo et al., 2014; Martin et al., 2016; Tsaloglou et al., 2018).

1.2.1.2 DNA Detection on Biosensor Platforms

The detection of DNA provides significant opportunities to diagnose disease, identify organisms and monitor nucleic acid biomarkers. These tests are typically confined to laboratory settings, but at-home, in-field and point-of-care diagnostics and monitoring could be achieved through the development of portable biosensor systems for DNA. There are numerous studies describing DNA biosensors in the literature, with large variety in the design of these systems.

One variable element in DNA biosensors is the capture probe design. DNA biosensors have been developed with a number of capture mechanisms, including single-stranded DNA (ssDNA), peptide nucleic acid (PNA), ribonucleic acid (RNA) and morpholino based DNA analogues (Cai et al., 2014; Cheng et al., 2014; Hu et al., 2015; Kongpeth et al., 2016; McVey et al., 2017; Wang et al., 2017). ssDNA is the most popular option due to the ease of probe design, low cost of production and the well understood interactions of the molecule. Other newer probe designs have advantages over DNA such as an uncharged backbone (which reduces the charge screening required when hybridising a DNA target), resistance to degradation by cellular enzymes and improved sequence specificity (Bala and Górski, 2016). These newer sequences are often much more expensive to produce than ssDNA probes.

Detecting hybridisation between the probe and target can also be achieved in many ways. This detection is typically done through a signal transduction system which translates the molecular interaction of the hybridisation event into a measurable or visible change in the transducer. Fluorescent or naked-eye techniques, where the binding of a target to the probe produces an optical signal, and acoustic methods, where mass changes on the sensor surface are detected, are common transduction principles. Magnetic and thermal transduction options are also available, although less common due to issues with miniaturisation, processing complexity and susceptibility of the sensor to external influence (Gruhl et al., 2011).

Electrochemical transduction methods are highly researched and well represented for DNA biosensing in the literature (Cheng et al., 2014; Cui et al., 2015; Hsieh et al., 2010; Manzano et al., 2018; Matsishin et al., 2016; Teymourian et al., 2017; Wang et al., 2017; Widaningrum et al., 2017). Electrochemical techniques are popular due to the ease of miniaturisation of electronics and ability to analyse small volumes with rapid measurements (Grieshaber et al., 2008; Gruhl et al., 2011). Research on these systems focuses on improving sensitivity and

specificity, with a wide range of transduction methods described to enhance both of these parameters. These methods generally rely on either a labelled or label-free approach.

1.2.1.3 Label-Based Electrochemical DNA Detection

Label-based electrochemical techniques rely upon the interaction of an electrochemically active intermediate to report the presence of the target DNA to an electrode. Some schematic examples of label-based methods are provided in Figure 1.8. Target binding may result in a label being accumulated near the electrode (Figure 1.8, centre), a label being displaced from the surface (Figure 1.8, right), or a change in the electrochemical signal generated by the label molecule. These systems allow for signal amplification by having a single binding event interact with multiple label molecules and can be resistant to non-specific signal due to the independent signal generated by the label. However, these systems may cost more to produce than label-free methods and could require more user interaction and more complex storage.

The use of labelled primers or secondary probes is another common method by which captured DNA is labelled. Cheng et al. (2014) describe a system where DNA target hybridisation exposes a binding site for a labelled primer. Extension of this primer using isothermal PCR releases the original target DNA for further interactions through displacement by the polymerase. Through a multi-stage amplification reaction, the signal from a single DNA binding event is enhanced multiple times, with each labelled primer acting as the nucleus for further exponential amplification reactions. These downstream reactions interact with an enzymatically labelled detection probe to generate a large electrochemical signal (Figure 1.8, left). This system is involved and complex but represents an interesting combination of labelled primers and probes for significant signal amplification.

Such label-based techniques typically report limits of detection in the femtomolar range (Cui et al., 2015; del Río et al., 2017; Fernandes et al., 2015a; Sánchez-Salcedo et al., 2019), with detection limits as low as the attomolar range occasionally reported (Widaningrum et al., 2017). Label-based protocols achieve detection limits within the clinically relevant range for most bacterial infections (nanomolar to attomolar concentration depending on the infected tissue, Kelley, 2017) and are often more specific and sensitive than label-free methods. However, the optimal time to result can be long, on the order of several hours, due to the multiple incubations and washing steps which are often required. These methods rely more heavily on user interaction, increasing the skill required by the user and the cost per test.

Automation would also result in an increased cost per device and may have little impact on the time to result. These limitations are common among many label-based methods which require precise addition of reagents, washing, or removal of part of the sensor to prevent fouling (Cui et al., 2015; Fernandes et al., 2015b; Widaningrum et al., 2017; Xu et al., 2018).

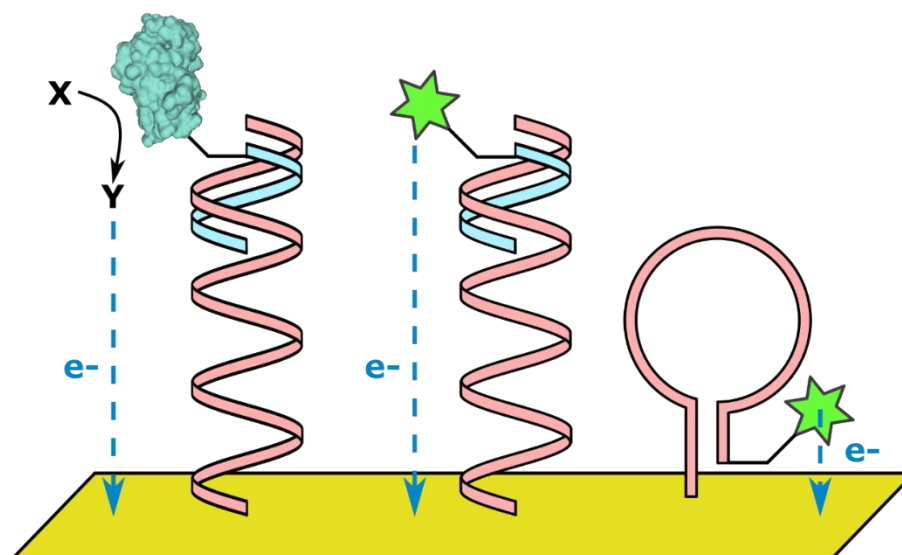


Figure 1.8 – Overview of some common label-based electrochemical methods for DNA detection. From left to right – Enzyme tagged probes produce a redox active product which can be detected at the electrode (del Río et al., 2017); probes labelled with redox active molecules can be detected when captured by their target (Levine et al., 2009); redox tagged DNA probe structures which change when the target binds, moving the active label away from the electrode surface (Hüsken et al., 2010; Xiao et al., 2007).

1.2.1.4 Label Free Electrochemical DNA Detection

Label free electrochemical detection regimes use the physical presence of a target at the sensor surface to change the electrochemical response of the system. Some example schemes of label-free detection strategies are given in Figure 1.9. Electrochemical techniques which are sensitive to changes in molecular access to the sensor surface or to disruption of the electric double layer can identify changes brought about by target binding without the use of additional labels. Label free systems typically require less user interaction than labelled systems, but can be more susceptible to non-specific signal increases, especially when samples are present in complex media. Additionally, there are fewer opportunities for signal amplification using label-free methods, as the electrochemical signal of a single binding event

cannot be enhanced in the same manner as labelled methods, which can limit the sensitivity of these systems.

One of the most basic forms of label-free detection is described by Keighley et al. (2008b). In this article, electrodes were modified with a single-stranded DNA probe and alkanethiol blocking layer. A redox reporter molecule was then added, and electrochemical impedance spectroscopy performed (Figure 1.9, left). A change in the impedance characteristics of the surface was observed following DNA hybridisation, which was attributed to an increase in charge interactions and surface blocking (steric hindrance) at the electrode surface by the complementary DNA (Figure 1.9, centre). 1 μM complementary DNA produced a signal increase of 69% using this straightforward method. Using a similar system with a protein blocking layer rather than alkanethiol, Manzano et al. (2018) achieved detection of 0.65pM of viral DNA. These results show that simple label-free protocols can achieve sensitive detection with a similar magnitude to labelled methods.

More advanced protocols are widespread but are based upon the same principles. For example, Teymourian et al. (2017) use a much more complex surface chemistry to enhance hybridisation detection and identify small mismatches in the DNA sequences. The steric hindrance and increased charge density when target DNA binds limits interaction between solution phosphate and surface bound nanoparticles, reducing the electrochemical signal. This more complex system allows a broad detection range up to nanomolar concentrations. This system is highly sensitive to nucleotide sequence mismatches allowing the discrimination of fully complementary and single-mismatched DNA targets.

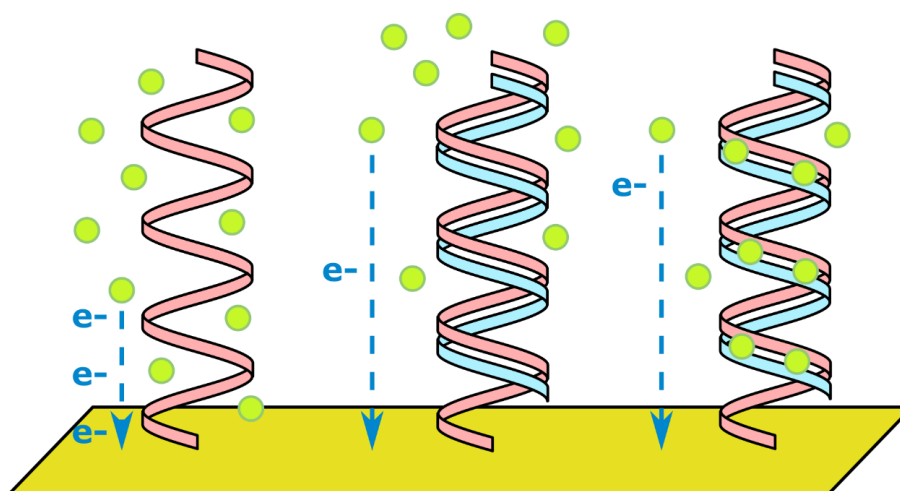


Figure 1.9 – Overview of some common label-free electrochemical methods for DNA detection. From left to right – Free redox mediator interacts strongly with electrode surface; DNA hybridisation displaces mediator from the surface; DNA hybridisation accumulates mediator, preventing / enhancing electron transfer.

DNA detection without a redox mediator in solution are also possible. Wang et al. (2017) used a microelectrode to detect DNA hybridisation using capacitance. Capacitive measurements were performed on the electrodes after modification with a DNA probe and alkanethiol blocking layer and compared to measurements performed after hybridisation with target DNA. This setup could detect low concentrations of target DNA compared to a non-complementary control without complex surface modifications or signal enhancement strategies.

Field-effect transistor based systems also offer a method of performing label-free DNA detection. Cai et al. (2014) produced a graphene oxide biosensor upon which PNA probes were immobilised. This biosensor was attached to the gate terminal of a transistor. As the gate voltage is varied, the current flow between the drain and source changes. Binding of target DNA to the electrode surface causes a change in the gate potential, producing a detectable change in the flow of current between the source and drain. Such systems have achieved limits of detection in the femtomolar level for DNA targets (Cai et al., 2014; Gao et al., 2011).

Reporter molecules which interact with double-stranded DNA preferentially over single-stranded DNA can also be used for label free measurement. These include redox-active molecules such as methylene blue (Niu et al., 2017; Patterson et al., 2013), modified

naphthalene diimides (Gaiji et al., 2017), Hoechst 33258 (Kerman et al., 2009) and ruthenium hexamine (Ahmed et al., 2013; Hashimoto et al., 2017). These molecules typically bind between the DNA bases (intercalation), in the grooves formed within the double strand, or are attracted to the negative charge of the DNA backbone (Figure 1.9, right). The greater interaction with double-stranded DNA can result in these molecules becoming concentrated at the electrode surface upon hybridisation, increasing the signal response. Alternatively, incorporation of these molecules into the DNA double strand can reduce their availability, causing a reduction in the signal upon hybridisation. Protocols based on these methods can also achieve femtomolar detection limits, which is within the typical range for DNA concentrations in many bacterial infections.

Both label-based and label-free electrochemical techniques show excellent characteristics for potential integration into DNA detection platforms, with sensitivity and specificity suitable for low concentrations of target DNA in a mixed solution and a wide variety of protocols reported for each. Each transduction system has advantages and disadvantages, and both have been studied for DNA biosensing. The use of electrochemical techniques can be advantageous over other sensing methods due to their ease of miniaturisation and sensitivity if suitable transduction methods are employed

1.2.2 Integrated Protocols for DNA Amplification and Electrochemical Detection

Combining DNA amplification with biosensing allows for signal amplification of the specific target prior to detection. This can be used together with both labelled and label free systems to enhance the signal generated from a low concentration of initial target, compounding with any signal amplification methods used during signal transduction. DNA amplification through PCR is a complex process which is typically performed off the electrode. Combining amplification and detection into a single detection scheme has become an area of interest in the move towards truly mobile diagnostics platforms, and there are several examples of systems which integrate the DNA amplification and detection reactions onto a single chip. Many of these designs offer methods by which the sensor could be multiplexed and allow for characterisation of mixed samples without initial purification, which can be problematic in low-resource or point-of-care settings.

One example of an integrated amplification and detection system is provided by Yeung et al. (2006). In this report, sample preparation, amplification and detection are performed in a single reaction chamber. Bacterial samples are thermally lysed and their DNA amplified. Gold

nanoparticles act as a label through which the hybridisation of the target DNA to the electrode surface is measured. This work shows promise for multiplexing, as *E. coli* and *B. subtilis* targets could be recognised in the same chamber due to the use of multiple working electrodes with different surface modifications. This protocol employs a single chamber to achieve detection of around 100 cells / μL , but there are still requirements for user interaction to perform washing and reagent addition throughout the protocol.

Ferguson et al. (2009) produced an integrated biosensor platform using a traditional thermocycle PCR. This protocol used methylene blue as a redox indicator, which was conjugated to a hairpin probe. Upon target hybridisation the indicator is displaced from the surface, reducing the current observed when voltammetry is performed. The use of a symmetrical PCR reaction improves the amplification efficiency compared to the asymmetrical technique used by Yeung et al., lowering the detection limit by around 2 orders of magnitude, which the authors believe could be improved further through PCR optimisation. While not demonstrated in this work, the authors suggest the chip could be multiplexed by including more electrodes and with electrode specific modifications.

To avoid the high power and design requirements of the thermal cycle process used by PCR, several groups have now included isothermal amplification steps into integrated biosensor platforms. Isothermal amplification reactions require a single, lower temperature than PCR and are therefore much more easily integrated into point-of-care detection systems. Patterson et al. (2013) described a LAMP isothermal amplification to enhance a conserved section of *Salmonella* species DNA, and were able to detect bacteria in whole blood samples at clinically relevant concentrations using square wave voltammetry.

Other groups such as Luo et al. (2014) and Tien et al. (2017) have shown LAMP reactions to be effective for isothermal amplification of pathogen DNA in a biochip system. Rolling circle amplification (Cheng et al., 2014), recombinase polymerase amplification (del Río et al., 2017; Kersting et al., 2014) and exponential amplification (Nie et al., 2014) have also been successfully integrated with an electrochemical detection method.

For performing integrated amplification and detection, a method to control the movement of solutions through the device may be required. Microfluidics systems, which consist of small channels which direct the flow of microlitre volumes of solution, have been used to perform amplification and detection on a single platform. Microfluidics can be used to perform multiple stages of a process sequentially without user interaction. These types of

devices have been used in several integrated DNA amplification and detection systems and are promising candidates for future commercial biosensors.

The integrated PCR chip described by Han et al. (2013) uses a microfluidic system to drive a sample through a PCR reaction and eventually onto a sensor where the amplicon can be detected through impedance spectroscopy. This system can amplify DNA through a standard PCR reaction without thermal cycling the chip due to the path of the microfluidic channels above a set of three heating elements.

Ben-Yoav et al. (2015) created a microfluidic biochip in which air pressure changes can cause a set of diaphragm valves to open or close, directing fluid onto a specific working electrode. This allows different surface modifications to be applied to the electrodes as well as allowing samples to be directed through the chip to control process flow. Earlier work by Liu et al. (2004), who avoided diaphragm valves due to difficulties in miniaturisation down to microfluidic levels at the time, utilised paraffin wax valves to withhold reagents until they were required. This design also used a number of air pumps to move fluid through the system, and both the valves and pumps were controlled by heating elements embedded in the chip. Such designs largely remove the need for operator interaction in the device, as an on-board computer system could control the movement of the sample.

The use of a target amplification step can be critical for successful detection of a DNA sequence. A diagnostic sample may contain the target bacteria at a low concentration, and some method of DNA target amplification is often required to detect the target if bacterial culture is to be avoided. Combining an isothermal amplification reaction and detection method in one system would enhance portability and minimise the requirement for user interaction, improving usability of the sensor at the point-of-care compared to PCR or multi-step reaction formats. There are several examples of integrated amplification and detection protocols presented here which provide a foundation for point-of-care DNA biosensing.

1.2.3 Detection of Antimicrobial Resistance using Electrochemical Techniques

Currently, electrochemical biosensors designed against antimicrobial resistance typically perform an antimicrobial susceptibility test. These may involve growth of the bacteria on the sensor surface or sampling of a culture, with the application of an antibiotic to the system at some stage. The change in the electrochemical response of the system as bacteria are killed or in stasis informs the user that the tested antibiotic is effective.

Webster et al. (2015) applied an antibiotic to *Pseudomonas aeruginosa* growing on an electrode surface and detected changes in the production of an electroactive metabolite. Halford et al. (2013) and Liu et al. (2014) examined RNA hybridisation to a DNA probe from lysed bacterial samples. While such methods are effective for providing information about the phenotypic resistance of an organism, they require growth of the organism and subsequent dilution and exposure to antibiotics, a time-consuming process which is not conducive to rapid point-of-care diagnosis. For slow growing organisms, an antibiotic susceptibility test may only produce results after days or weeks of incubation. These techniques are also resource intensive as each antibiotic must be tested against a live population of bacteria in isolation. These strategies have been combined with biosensors to measure biomarker or RNA quantities, which change more rapidly in response to antibiotic action and can produce a result more quickly than culture methods (Altobelli et al., 2017). However, these protocols require lysis, inactivation and purification of a sample making miniaturisation and automation of the process challenging. Such procedures are therefore not easily translated into point-of-care diagnostics.

Alternatively, more rapid susceptibility testing methods have been developed. Hannah et al. (2019) used antibiotic impregnated gels cast over a screen-printed electrode to detect the growth of antibiotic resistant *S. aureus*. Changes to the impedimetric characteristics of the gel occurred in response to bacterial growth, with clinically relevant concentrations of antibiotics providing an approximate minimum inhibitory concentration. Responses on this device were obtained within 45 minutes following inoculation. While still requiring individual gels for each antibiotic, the rapid time to result and simple procedure used here shows that antibiotic susceptibility testing through electrochemical means can be highly sensitive without complex sample preparation or culturing.

The direct detection of AMR gene sequences gives the possibility to identify antimicrobial resistance in even shorter time frames. Huang et al. (2015) use an impedimetric biosensor to detect the presence of the *bla_{NDM}* gene on a bacterial plasmid, which produces an extended spectrum beta-lactamase conferring resistance to a wide range of beta-lactams and related compounds. This group have also previously used impedance techniques to identify the *mecA* gene in MRSA, which confers resistance to beta-lactam antibiotics (Corrigan et al., 2012). The time to result in each case was much lower than those required for traditional culture methods, with potential for further optimisation. The methods used are also much more

transferrable to PoC platforms than culture-based methods as a simple lysis and amplification can be used directly on the sample with no outgrowth required.

Kara et al. (2009) used differential pulse voltammetry to electrochemically examine the development of Rifampin resistance in *M. tuberculosis*. They designed five capture probes to target an 81 base-pair region of the *rpoB* gene which commonly undergoes point mutations in Rifampin resistance. This system used the oxidation of guanine bases in the DNA to detect target binding. With this method, mutations associated with developing Rifampin resistance were detected directly, offering a cost effective and simple method for identification of potentially resistant TB strains. Such methods can be especially useful against bacteria like *M. tuberculosis* which are notoriously slow and difficult to culture (Wang et al., 2014).

The DNA detection protocols discussed here could be used to identify further antimicrobial resistance genes with the correct selection of probes, primers, and targets. Multiplexing these tests to detect multiple gene targets simultaneously could be as simple as modifying each electrode surface with a unique capture probe. However direct detection of AMR genes will not necessarily determine if the organism will be resistant. In some cases, there may be inactive genes or compensatory mechanisms, resulting in an organism which is phenotypically susceptible but genetically resistant. Such cases would produce a false positive response for a genetic test. Antibiotic susceptibility tests have the advantage of informing of resistance regardless of the mechanism involved, something which genetic testing has not yet addressed. However, genetic testing could provide an early warning of which antibiotics an organism may be resistant to, and effective treatment could be provided while confirmatory testing is undertaken.

The rising rates of antimicrobial resistance around the world presents a clear challenge for modern healthcare. Increasing treatment costs and poorer patient outcomes can be alleviated by the rapid administration of effective treatment. Direct antimicrobial resistance testing using biosensors would reduce the workload of centralised healthcare laboratories and accelerate the antibiotic administration process, particularly for slow growing or difficult to culture organisms where information regarding its antibiotic susceptibility may be unavailable for days. There is a clear need for rapid AMR testing to inform treatment plans earlier in the disease process, a need which could be met by the development of a biosensor system for AMR genes.

1.3 Electrochemistry Basics

Electrochemistry is the study of chemical reactions which involve the transfer of electrons. An electrode in solution which is connected to an external circuit can accept or donate electrons to an electrochemical reaction, causing a current to flow through the circuit which can be measured. Reactions can also be initiated by changing the potential at the electrode surface. The interaction between electrodes and the reaction occurring in solution can be used to discover information about the nature of the reaction, the reaction components, the electrodes, and the interface between the two.

Experimentally, electrochemical reactions do not occur at an interface in isolation, as there is no circuit through which electron transfer can occur. An electrochemical cell, consisting of two or more electrodes in solution, is used to allow this transfer of current and to measure and drive the electrochemical reactions. Figure 1.10 shows an image of a 3-electrode cell and a circuit schematic. The 3-electrode cell shown consists of a working, counter, and reference electrode, controlled by a potentiostat. The working electrode is the electrode whose potential is controlled during the experiment and is the location of the reaction of interest. The potentiostat applies potential changes to the electrochemical cell and measures the response from the working electrode. Changing the current passing through the counter electrode allows the potential at the working electrode to be fixed at the desired value. The counter electrode also closes the circuit, allowing electrons to move to and from the solution freely in response to current flow induced by changes at the working electrode. If an oxidation occurs at the working electrode, reduction occurs at the counter electrode, where the same current magnitude is passed. The reference electrode acts as a fixed potential against which to measure the potential at the working electrode. This allows the potentiostat to maintain the applied potential accurately during the measurement. The solution phase of the electrochemical cell may contain molecules of interest, as well as a concentrated background electrolyte (such as the salt KCl) to ensure that the solution is conductive (Pletcher, 2009). Solutions with low conductivity may exhibit a drop in the potential between the working and reference electrode if the electrodes are not placed in close proximity, resulting in an incorrect potential being applied at the working electrode.

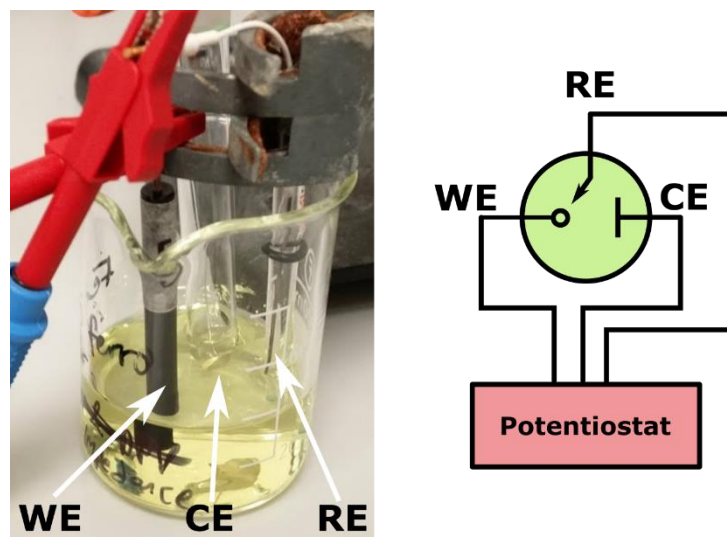


Figure 1.10 – Image and schematic for 3-electrode cell for electrochemical measurements.

WE – working electrode, RE – reference electrode, CE – counter electrode.

The electrochemical cell is used to measure the flow of electrons between species within the solution and the working electrode. Molecules which can undergo these oxidation and reduction processes are known as redox active molecules. Applying a positive potential can oxidise a species by removing electrons, whereas a negative potential may reduce a species by adding electrons to it. The magnitude of the applied potential required for oxidation or reduction depends on the molecule being examined. This process can be reversible, where the kinetics of the reaction facilitate a rapid return to the molecules original state, or irreversible, where slow reaction kinetics limit the rate at which an oxidation or reduction process can be reversed.

Applying specific potential changes to an electrochemical cell in which a redox molecule is present can interrogate properties of the redox reaction, the electrochemical cell itself and the interface between the electrode and the electrolyte. The effects of the applied potential are concentrated at the electrode surface, with the electric field rapidly decaying as distance from the electrode surface is increased. The oxidation and reduction of solution species therefore occurs primarily at the interface between the electrode and the solution.

1.3.1 Electrode-Solution Interface

The interface between an electrode and a solution is the point where electron transfer occurs and understanding how this interface behaves informs our interpretation of electrochemical responses. When an electrode is immersed into a solution, an electric double layer will form

at the surface, as shown in Figure 1.11. This double layer results from a counterbalancing of the charge at the electrode surface with ions from solution. Ions may interact with the electrode surface through specific adsorption, where a chemical bond between the ion and the electrode surface forms. This requires desolvation of the ion, where the outer layer of solvent molecules are dispersed, a process which is more common for anions than cations (Compton and Banks, 2011). The distance to the centre of these specifically adsorbed ions from the electrode surface is known as the Inner Helmholtz Plane (IHP). Within this layer there will also be polar solvent molecules which are aligned with the electric field, and which will compete with ions for space at the surface.

Solvated ions can also approach the surface, but due to the outer layer of solvent cannot approach as closely as specifically adsorbed ions. These ions are non-specifically adsorbed, and the distance to their centres from the electrode surface creates the Outer Helmholtz Plane (OHP). Beyond the Helmholtz region is the diffuse layer. In this area surrounding the electrode, the concentration of cations and anions is greater as they are influenced by the applied electric field. Moving further from the electrode this electric field strength is reduced, and at a certain distance has essentially no effect on the distribution of ions. These ions will be in the same concentrations as the bulk solution (Bard and Faulkner, 2001; Pletcher, 2009).

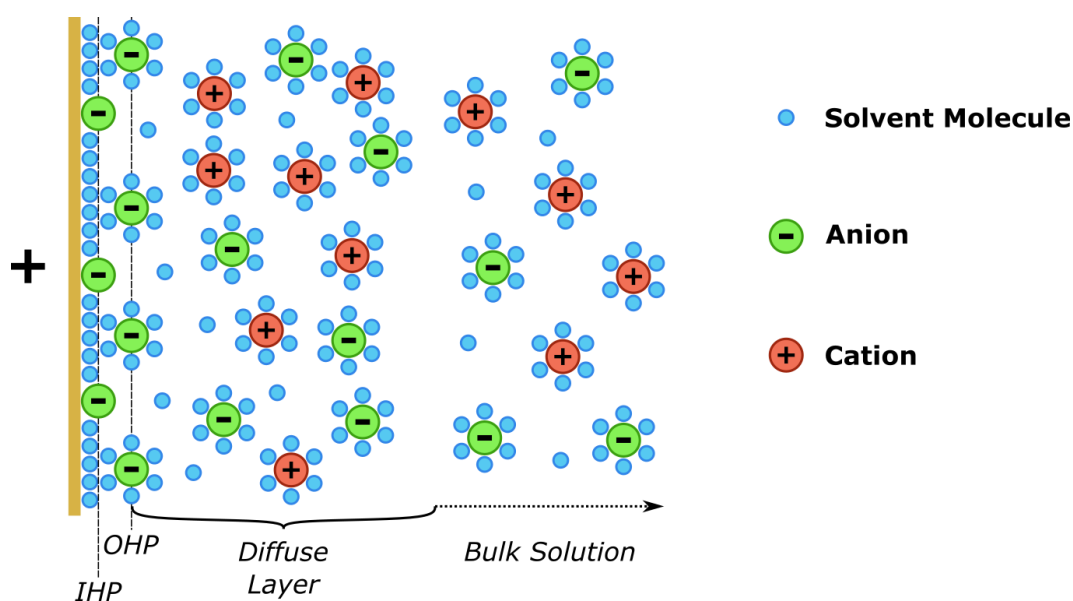


Figure 1.11 – Formation of different ion layers at an electrode solution interface. IHP / OHP – Inner / Outer Helmholtz Plane.

Upon immersion of an electrode into a solution, ions will move to counterbalance the charge within the electrode. Applying or changing the potential at the electrode changes the electric field strength, and so results in a redistribution of the ion layers. As these layers reorganise, electrons move to or from the electrode surface as the charge balance at the electrode surface changes. This current rapidly decays as the layer become more stable, and when no more net changes to the layer occur this current flow stops. In this way, the ion layer and electrode surface act like a capacitor, producing a charging current while the layer reorganises which is superimposed over the current of any oxidation and reduction reactions occurring at the interface over short time scales.

The thickness of the layer produced by the movement of ions is defined by the Debye length, κ^{-1} , through Equation 1.1;

$$\kappa^{-1} = \sqrt{\frac{\epsilon_r \epsilon_0 k_B T}{2 N_A e^2 I}} \quad (1.1)$$

where ϵ_r is the relative permittivity of the solution, ϵ_0 is the permittivity of vacuum, k_B is the Boltzmann constant, T is the temperature in Kelvin, N_A is the Avogadro constant, e is the elementary charge and I is the ionic strength of solution. The electric field strength decreases exponentially over the Debye length as the charge within the electrode is balanced by charges in the diffuse layer. By packing the electrode surface with hydrophobic molecules of a similar length to the Debye length, a significant reduction in the field strength can be achieved where the diffuse layer meets the OHP, as the OHP is now moved further from the electrode by the hydrophobic insulating layer. Self-assembly of molecules such as alkanethiols can be used to achieve such an effect on gold electrodes, effectively decreasing the capacitive effect of the electric double layer (Bard and Faulkner, 2001; Pletcher, 2009).

1.3.2 Self-Assembled Monolayers and Surface Passivation

Self-assembled monolayers (SAMs) are a well-ordered layer of molecules which spontaneously attach to a substrate in an organised manner. This spontaneous organisation can be used to modify electrode surfaces to change the electrochemical properties and resist fouling, but primarily offer a convenient method by which organic molecules can be attached to an inorganic substrate. For example, when using gold electrodes, thiol groups (consisting of sulphur and hydrogen) can be used to semi-covalently attach other molecules to the electrode surface. Alkanethiols are particularly common as the interactions of the

hydrocarbon chains allow close packing of the SAM molecules for surface blocking and further functionalisation, and the formation of these layers is energetically favourable due to low solubility (Chen et al., 2017). Initial binding of the SAM molecule to the substrate occurs over short periods of time (on the order of a few seconds to minutes). There is then a period of several hours where the SAM layer becomes more consistent through a combination of further adsorption, lateral movement to fill defects and expulsion of surface contaminants and solvent (Bain et al., 1989). This process can result in a highly uniform SAM layer with few defects (Figure 1.12).

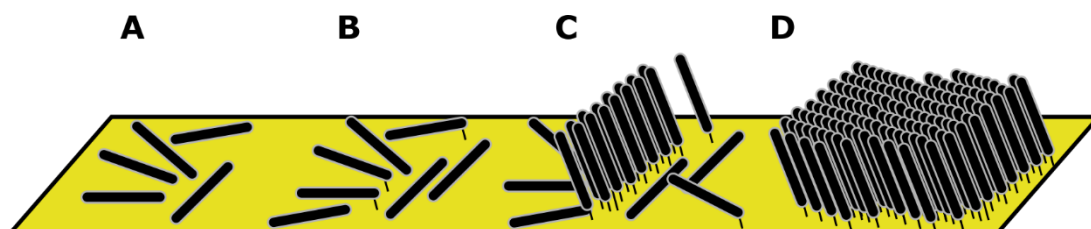


Figure 1.12 – Schematic for the formation of a confluent alkanethiol SAM on gold. (A) SAM molecules physisorb to a surface. (B) Gold-thiol bonds form, chemically attaching SAM molecules to the surface. (C) Molecules in proximity begin to interact, transitioning to an upright configuration. (D) Molecules continue to bind and rearrange, forming a confluent barrier at the surface.

Herne and Tarlov (1997) described the binding of DNA molecules to a gold surface using the gold-thiol interaction. The binding of a DNA probe to an electrode surface allows the sensor to specifically capture complementary sequences of DNA for analysis by electrochemistry. DNA SAMs formed through the gold-thiol interaction are the primary means by which gold electrodes are functionalised with nucleic acids for biosensing. Typically, one of two methods are used. The thiol-DNA may be incubated with the gold surface, and then a separate backfill step with a blocking molecule such as an alkanethiol can be used. Alternatively, a co-immobilisation of the thiol-DNA with alkanethiol can be used. This second method allows the ratio of alkanethiol to DNA to determine the packing density of the DNA on the surface which can be advantageous for sensing performance. The use of a thiolated molecule to block the electrode surface improves the orientation of the DNA by preventing non-specific interactions with the gold. Increasing the surface density of the alkanethiol through backfilling also facilitates transition of the thiol from a “lying down” to “standing up” phase. As a result of these effects, the DNA takes on a more upright configuration which improves

hybridisation efficiency with the specific target (Gebala and Schuhmann, 2010; Herne and Tarlov, 1997; Keighley et al., 2008b; Vericat et al., 2010).

In addition to their use in surface functionalisation, SAM layers can be used to block a surface from undesirable interactions with solution components. Biological molecules, especially proteins, will rapidly foul a sensor surface regardless of the properties of the sensor (Blum, 1991). This fouling can lead to non-specific signal interactions due to disruption of the double-layer, and through charge interactions and steric hindrance of redox molecules. When performing electrochemical measurements on a biosensor, it is vital that non-specific interactions occurring at the electrode surface which could interfere with detection of the analyte are minimised. SAM molecules can be selected to provide an effective barrier to surface fouling and reduce these non-specific interactions (Chapman et al., 2000; Dong and Li, 1997; Li and Ye, 2015; Mrksich and Whitesides, 1996).

Not only do SAMs passivate the surface against adsorption of biomolecules, but they also act to reduce the capacitance of the electrode. Solvated ions are unable to penetrate through a uniform SAM to the electrode so their minimum distance from the surface (and therefore the distance to the outer Helmholtz plane) is increased by the thickness of the layer (Bard and Faulkner, 2001). As capacitance is inversely proportional to the distance between the electrode surface and the counter-ion layer, longer SAM molecules will reduce the capacitance further. However, uniformity of the SAM layer is important. Pinhole or edge defects can allow access of the electroactive species to the electrode, increasing background current. In the case of a sensor system, this would result in reduced signal to noise ratio and a poorer limit of detection. Large enough defects may also limit the effectiveness of the SAM layer when resisting non-specific surface fouling.

1.3.3 Electrochemical Tests

Electrochemical tests can take advantage of the interactions between the measurement solution, the electrode surface and the target analyte to produce signal readouts in response to a variety of effects. Binding at the surface and changes to the solution properties can be measured with a variety of electrochemical techniques, allowing detection of a wide variety of biomolecules and examination of system parameters.

1.3.3.1 Cyclic Voltammetry

Cyclic voltammetry (CV) is a common technique for qualitative analysis of the response of an electrochemical system (Bard and Faulkner, 2001). When performing cyclic voltammetry, the

applied voltage is swept between two values at a fixed rate and the current response is recorded. These two values are chosen so as to cover an oxidation or reduction process of interest. As the voltage changes the energy required to drive these oxidation and reduction reactions will be exceeded and a current will flow. This current is plotted against the potential to produce a voltammogram, the shape and location of which depends on a number of factors including the rate of the electrochemical reaction, the formal potential of the reaction, the diffusion of the species in solution, and the sweep rate of the measurement. The profile of the voltammogram can be used to calculate a number of key parameters of the electrochemical system, some of which will be detailed here.

For a reversible reaction, one in which the kinetics of the redox process are rapid compared to the rate of mass transport, the equilibrium of the oxidised and reduced form of a species is related to the potential of the system as described by the Nernst equation (Equation 1.2). The potential E is dependent on the formal potential of the redox species E^0 , the temperature T in Kelvin, the universal gas constant R , the Faraday constant F , the number of electrons transferred in the reaction n , and the concentration of the reduced and oxidised species, for a system where the concentration of each species is a good approximation for its activity (Compton and Banks, 2011; Elgrishi et al., 2018).

$$E = E^0 - 2.3026 \frac{RT}{nF} \log_{10} \frac{[Red]}{[Ox]} \quad (1.2)$$

Using a defined temperature ($T = 298^{\circ}\text{K}$) and applying the constant terms, the Nernst equation simplifies to the form shown in Equation 1.3. The Nernst equation predicts that for a potential E applied to the electrochemical cell where $E = E^0$, the redox reaction will be driven towards equilibrium such that $[Red] = [Ox]$. The inverse of this is also true, such that for an equal concentration of reduced and oxidised species in a system, the potential E measured across the cell will be equal to the formal potential of the redox couple E^0 .

$$E = E^0 - \frac{0.05913}{n} \log_{10} \frac{[Red]}{[Ox]} \quad (1.3)$$

This form of the Nernst equation describes some of the behaviour expected on a cyclic voltammetry plot. An ideal single electron transfer reaction should exhibit a peak-to-peak separation (ΔE_p) of 0.05913 V, or 59 mV. Any defects or contamination present at the electrode surface will cause this separation to increase as the electron transfer deviates from the ideal conditions assumed by the equation. Peak separations close to 59 mV therefore

indicate that electron transfer between the electrode and electrolyte is rapid and relatively unimpeded as expected for a reversible reaction. As electron transfer becomes less efficient, the peak separation increases as the species concentrations at the electrode surface begin to deviate from the values predicted by the Nernst equation for a certain applied potential. This may also occur if the generated species is unstable, resulting in the formation of other products which would change the concentration ratio of the species being examined.

The ratio of the peak currents can also be informative when examining the reversibility of a reaction. Under ideal conditions, the ratio between the anodic and cathodic peak currents will be 1 when examined from their respective baselines. Deviation from this ratio may indicate again that there are inefficiencies in the electron transfer process, such as formation of intermediate species or slow electron transfer between electrode and solution. Figure 1.13A shows a typical CV response from $\text{Fe}(\text{CN})_6^{3-/4-}$ on a thoroughly cleaned gold disc electrode which was polished to a mirror shine. In this example, the peak current ratio $I_{p_a} / I_{p_c} = 0.978$, and the peak-to-peak separation $\Delta E_p = 73$ mV, showing the setup exhibits good electron transfer kinetics with minimal deviation from Nernstian behaviour.

Further parameters regarding the electrochemical reaction can be identified through the Randles-Sevcik equation shown in Equation 1.4 (Bard and Faulkner, 2001; Elgrishi et al., 2018). In addition to the variables described for the Nernst equation, A is the area of the electrode in cm^2 , C is the bulk concentration of redox species in mol/cm^3 , ν is the scan rate in V/s and D is the diffusion coefficient of the redox species in cm^2/s .

$$i_p = 0.4463nFAC \left(\frac{nF\nu D}{RT} \right)^{\frac{1}{2}} \quad (1.4)$$

This equation describes how the peak current i_p relates to the scan rate ν of the measurement and can be used to calculate diffusion coefficients or the real surface area of an electrode. For a fully reversible reaction, the graph of i_p against $\nu^{\frac{1}{2}}$ should be linear and intercept $i_p = 0$ at $\nu^{\frac{1}{2}} = 0$. This figure can also give an indication if the species are in solution or adsorbed to the electrode surface. An example of such a plot is shown in Figure 1.13B.

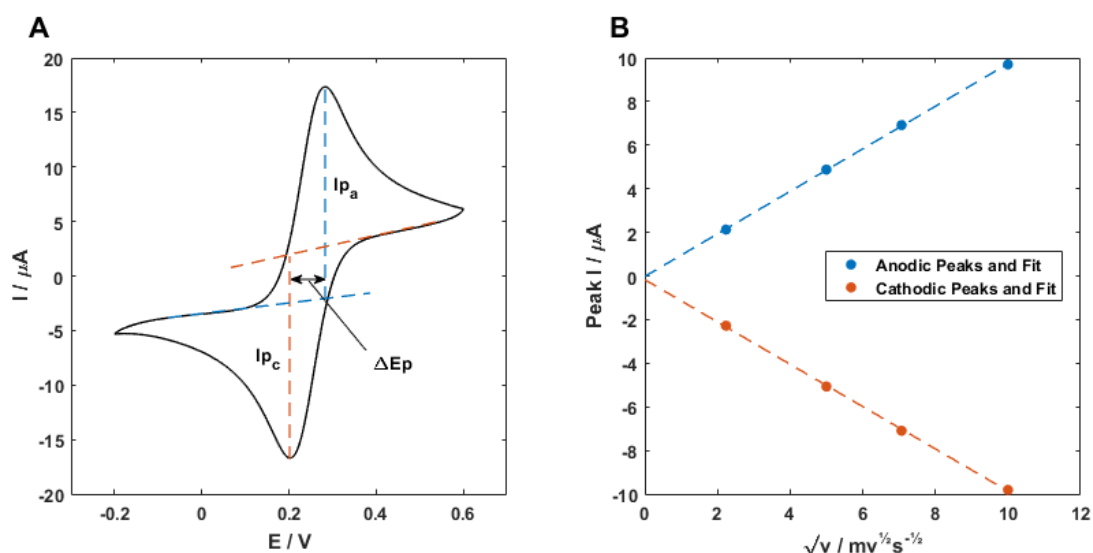


Figure 1.13 – Cyclic voltammetry plots for 2 mM $\text{Fe}(\text{CN})_6^{3-/4-}$ over a gold disc electrode. (A) Raw cyclic voltammogram. I_{p_a} and I_{p_c} indicate the anodic and cathodic peak currents respectively, and ΔE_p indicates the peak-to-peak separation. (B) Plot of I against the square root of scan rate showing a highly reversible non-adsorbed electron transfer reaction.

Cyclic voltammetry is a powerful technique for qualitative examination of a system, but there is less value in using this method analytically. The peak current always consists of a non-faradaic charging current overlaid with the reduction or oxidation (faradaic) currents, which cannot be easily isolated from one another. The magnitude of these peak currents also depends upon the real surface area of the electrode, which can be difficult to determine accurately. However, cyclic voltammetry proves an effective method for preliminary examination of a system.

1.3.3.2 Electrochemical Impedance Spectroscopy

In order to probe the characteristics of the electrode-electrolyte interface electrochemical impedance spectroscopy (EIS) can be used. EIS applies a small alternating potential perturbation to the electrochemical cell being examined and measures the response at different frequencies. These responses provide information about different characteristics of the system as the frequency is changed.

The impedance of a system is a generalised term which includes both typical electrical resistance and changes to the current phase through capacitive and inductive elements (Bard and Faulkner, 2001). The impedance at one frequency is given the symbol Z , and can be described by Equation 1.5.

$$Z(\omega) = Z_{Re} - jZ_{Im} \quad (1.5)$$

Z_{Re} (or Z') is the real component of the impedance, comprised of the purely resistive elements. Z_{Im} (or Z'') is the non-real component which is comprised of the capacitive and inductive effects within the circuit. The inclusion of the imaginary term j simplifies the display of these terms graphically, but both parts are real and measurable in an experimental environment. For the purposes of the impedance in a typical electrochemical cell the inductive effects can be considered negligible, and the equation can be rewritten to Equation 1.6, where R is the resistance, ω is the angular frequency of the applied potential (equal to $2\pi \times f$), and C is the capacitance. The magnitude of the impedance, $|Z|$, is the total impedance these resistive and capacitive effects produce and can be calculated from Equation 1.7. These parameters are shown graphically in Figure 1.14.

$$Z(\omega) = R - j\frac{1}{\omega C} \quad (1.6)$$

$$|Z| = \sqrt{R^2 + \left(\frac{1}{\omega C}\right)^2} \quad (1.7)$$

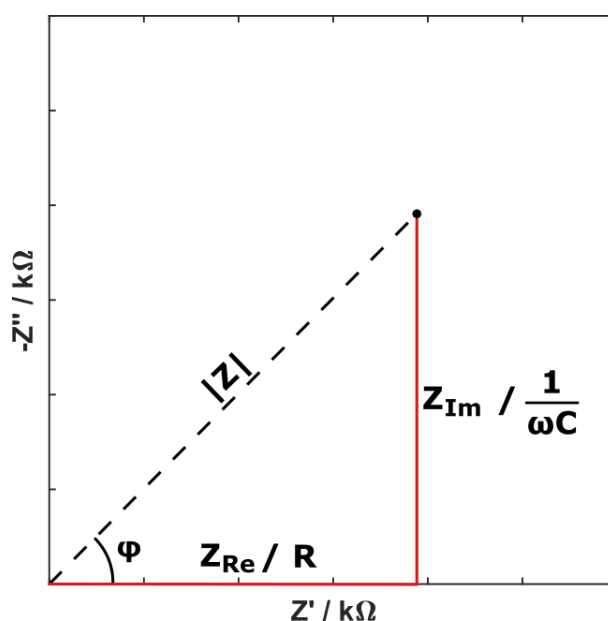


Figure 1.14 – Impedance magnitude of a single point in the Nyquist plot. The point is a distance $|Z|$ from the origin, creating a phase angle ϕ with the axis. The real and imaginary components of $|Z|$ are shown in red.

A typical impedance spectrum of a reversible reduction / oxidation reaction in solution is shown in Figure 1.15A. At high frequencies the impedance of the system is under kinetic control, where the rate of electron transfer and the reaction kinetics are significant. Diffusion to the surface is negligible, as the time the alternating potential remains at either side of the formal potential of the system is not sufficient to deplete the electroactive species surrounding the electrode surface. As the frequency falls the system is exposed to the potential perturbation for a much longer duration. The species at the electrode surface are exhausted during this time and more are attracted to the electrode, creating a diffusion layer above the electrode. The diffusion layer grows larger at lower frequencies, resulting in increasing impedance in the mass-transfer controlled region (red area) as species must diffuse over a greater distance to reach the surface.

Several important parameters can be obtained from the impedance spectrum of a system, typically calculated by circuit fitting. The elements of the electrochemical system (the electrodes, solutions, and interfaces) can be approximated using basic resistors, capacitors, and constant phase elements to produce the same impedimetric response as observed experimentally. Producing an equivalent circuit which reflects the elements present in the system and fitting it to the experimental data allows quantitative analysis of the system.

The intersection of the semi-circular region with the x-axis (where $Z_{Im} = 0$) in the high frequency region gives the resistance of the electrolyte solution, abbreviated R_s . Extension of the semicircle at its low frequency end to intersect with the x-axis can identify the charge transfer resistance. The x-intercept of this projected semicircle at the low frequency range is the sum of the solution resistance and the charge transfer resistance. The charge transfer resistance (R_{CT}) is dependent on the condition of the electrode-solution interface and any changes which interfere with the interaction of charge carriers and the electrode will cause this to increase. Charge transfer resistance is extensively used in biosensing applications to detect the binding of an analyte at the electrode.

Capacitive information can also be gained from analysis of the Nyquist plot. The C_{DL} circuit element reports the capacitance of the electrode-solution interface. This element is often replaced by a constant-phase element (Q) to improve fitting by accounting for the interfaces' deviation from a perfect capacitor.

The Warburg (W) element of the circuit represents the mass-transport controlled regime and is essentially a constant-phase element with the phase fixed at 45° . After reducing the

frequency enough to pass beyond the kinetically controlled region, the Warburg response dominates and produces the angled straight-line tail observed at low frequencies.

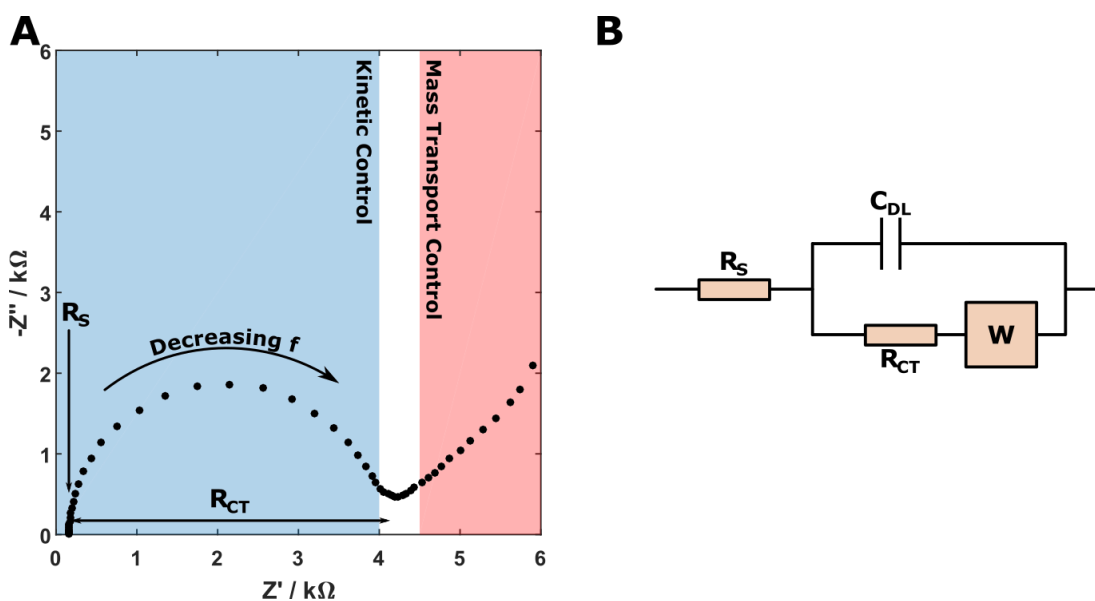


Figure 1.15 – Example EIS response. (A) Nyquist plot showing an impedance response in 2 mM $Fe(CN)_6^{3-/4-}$ following SAM formation on a gold SPE. The blue shaded area is under kinetic control, and the red shaded area is under mass transport control. (B) The Randles equivalent circuit which can be used to fit data from a Nyquist plot.

EIS is very sensitive to changes at the electrode surface which could change the kinetics of the reaction. If electron transfer between the electrode and the solution is slowed, then R_{CT} will increase to reflect this. Changes to the surface which affect the double layer charging will produce a rotation of the kinetically controlled region of the plot as the phase difference between voltage and current changes. Equivalent circuits such as the Randles equivalent circuit shown in Figure 1.15B (Randles, 1947) allow the extraction of the associated values through the use of specialised software for fitting and modelling the circuit response.

1.3.3.3 Differential Pulse Voltammetry

Voltammetric techniques using pulsatile or regular waves can also be used to interrogate the electrode-solution interface. These techniques gain increased sensitivity over other voltammetric techniques by allowing non-faradaic currents to decay before measuring. With careful choice of the pulse timing and duration, non-faradaic currents can be effectively eliminated from the measurement and only the faradaic response of the analyte in solution is recorded. This allows changes in the interface to be observed as a change in the faradaic current recorded. These measurements require less complex instrumentation than

impedimetric techniques and avoid the use of circuit fitting software for analysis, while recording less detailed information about the system. These techniques may therefore be advantageous for point-of-care testing, where low-cost instrumentation and a simple, rapid readout are critical for device manufacture and usability.

Differential pulse voltammetry (DPV) is a voltammetric technique which uses the application of voltage pulses to probe the interfacial characteristics of the electrode. Figure 1.16A shows the potential waveform typical for a DPV measurement. A pulsatile wave is superimposed upon a voltage step to produce a steadily increasing potential which pulses immediately before each step increase. Current measurements are taken immediately before the pulse (M1) and at the end of the pulse (M2), and the difference between the currents (ΔI) is recorded.

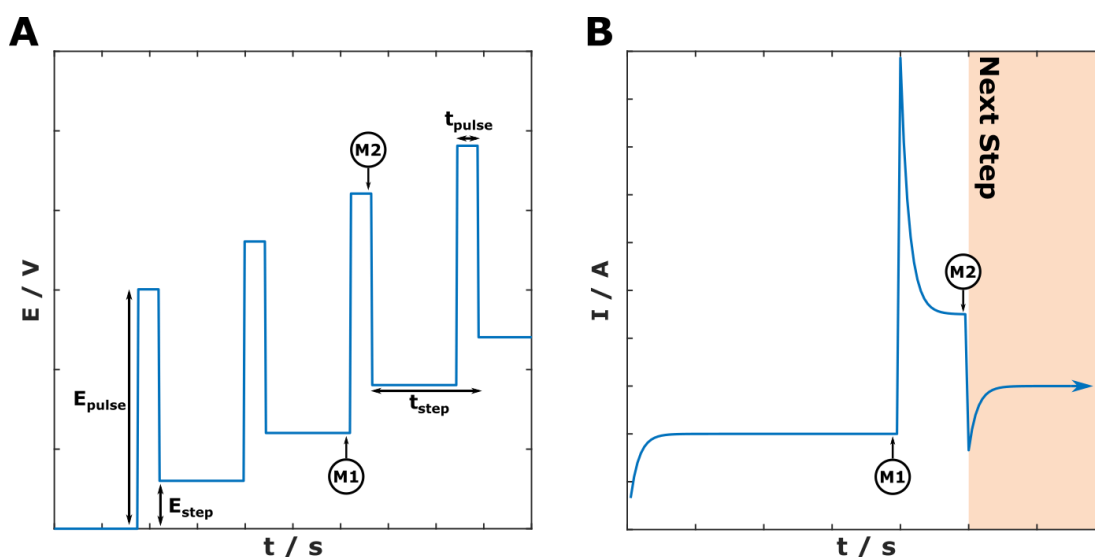


Figure 1.16 – DPV potential waveform (A) and current response (B). Current measurement points (circled) and measurement parameters are indicated.

This potential waveform results in currents such as those shown in Figure 1.16B. Upon application of the pulse a large current will flow as the electric double layer at the electrode-solution interface is charged. This capacitive current decays much more rapidly than the faradaic current. At the time of the second measurement, if the duration t_{PULSE} is optimal, little capacitive current will remain and the recorded current will be the result of faradaic processes.

Typically, t_{PULSE} is tenfold lower than t_{STEP} , allowing the baseline current to stabilise before the first measurement of each pair is taken (Compton and Banks, 2011). If t_{PULSE} is too short, the

capacitive current will not have decayed before the second measurement is taken. If t_{PULSE} is too long, the faradaic current will also decrease and convection within the solution could influence the measurement.

The difference between the two measurements is plotted against the step potential and produces a peak similar to the example shown in Figure 1.17. In the example given there is likely to be a small amount of capacitive current still present, indicating a suboptimal t_{PULSE} , as evidenced by the baseline of the measurement being greater than $\Delta I = 0$.

Changes at the electrode surface which affect the movement of ions or the efficiency of electron transfer appear as a change in the faradaic current which can be detected by DPV. Proteins and DNA can impede the movement of ions to the surface, and passivation with a SAM layer could reduce electron transfer efficiency. These effects will be seen as a change in the current recorded at M2 compared to the measurement before the surface was modified, which is reflected in the E vs ΔI plot.

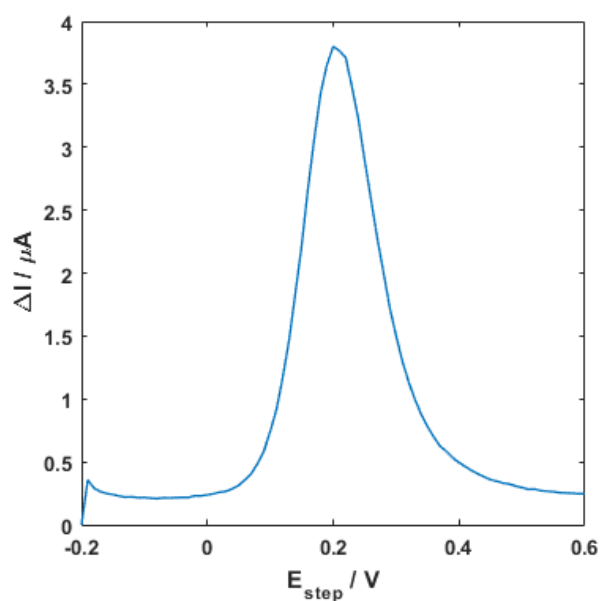


Figure 1.17 – Example DPV plot for $\text{Fe}(\text{CN})_6^{3-/4-}$.

1.3.3.4 Square Wave Voltammetry

Square wave voltammetry (SWV) shares many similarities with DPV. Figure 1.18A shows an example SWV potential waveform. SWV uses a similar potential wave to DPV but the t_{PULSE} value is equal to half the total t_{STEP} . This produces a wave with equal duration forward and reverse pulses. The current step potential is found at the midpoint of the positive and negative pulses and increases by E_{STEP} with each cycle. As with DPV, measurements are taken

at the end of each pulse and the difference between the currents is recorded. As the potential difference between these two points is relatively small, the capacitance of the interface is approximately constant and so the charging effects are eliminated when calculating ΔI . This allows SWV to run at a higher scan rate and with shorter pulse wait times than DPV, and so measurements are faster and can achieve higher sensitivity (Compton and Banks, 2011).

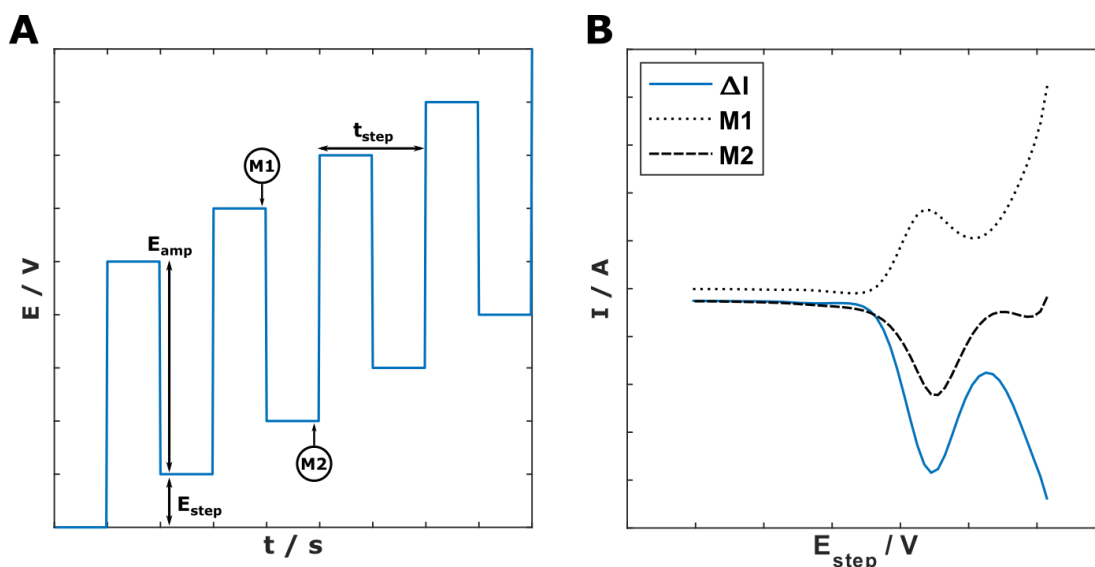


Figure 1.18 – SWV potential waveform (A) and example SWV plot (B).

Figure 1.18B shows how the components of the SWV measurement form the output response. Current values for both M1 and M2 are recorded against the step potential. These can be plotted during the measurement, but typically only the ΔI trace is output. As with DPV, changes at the surface result in a change to the ΔI value between the measurement points M1 and M2. When two SWV traces are compared a change to the peak height resulting from surface modification or target binding may be observed.

1.3.3.5 Chronoamperometry

Chronoamperometric measurements record the changing current over time, usually in response to an applied potential. The principles of chronoamperometry are used in the voltammetric measurements described above, where applying a potential step results in a current-time transient which can be sampled at a specific time point to extract certain information. Chronoamperometry records this current-time transient rather than applying transformations or calculations to the data, or sampling at a specific time.

The application of a potential step to a solution containing a redox active species can result in the species being oxidised or reduced at the electrode. Figure 1.19 gives a schematic of the effect of this potential step on the solution. While $t < 0$, the species is inert and no net current flows between the electrode and solution. Upon application of a large potential step ($t = 0$), species at the electrode surface are immediately depleted, producing a large current. Species further out in solution now move towards the electrode, following the concentration gradient produced by the depletion of species at the surface ($t > 0$). While the potential is maintained, more species surrounding the electrode are depleted and this diffusion layer grows. This causes the current to decrease as the flux of species to the electrode is reduced (sections 4 and 5). As t becomes much larger than 0 ($t \gg 0$), the diffusion layer around the electrode grows significantly and the current continues to decrease. The bulk solution may still have almost the original concentration of the electroactive species, but the region surrounding the electrode is largely depleted and continued current draw relies on the diffusion through this large depletion layer to the electrode surface.

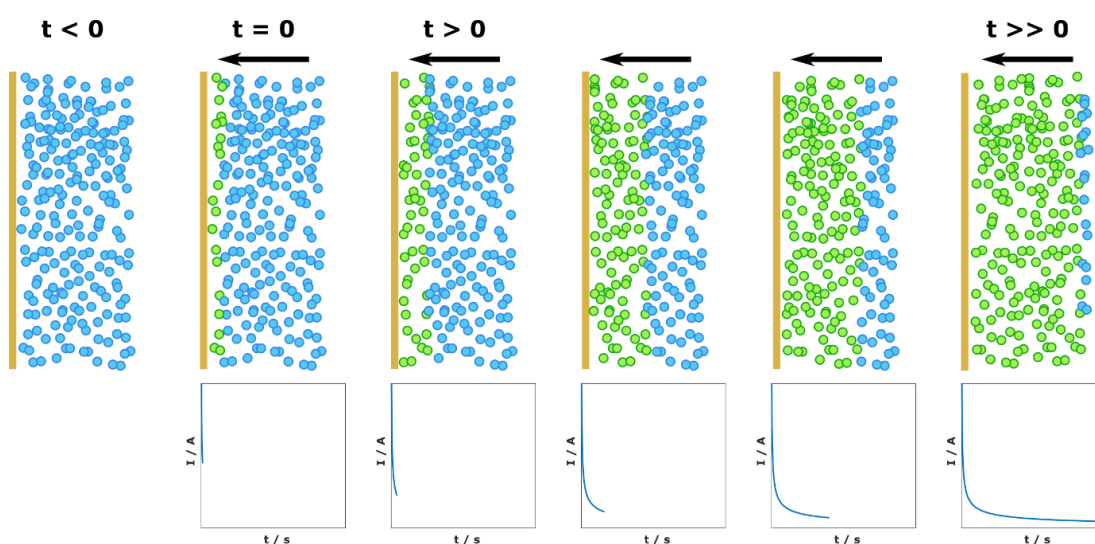


Figure 1.19 – Schematic of redox species depletion following application of a potential step, and its effect on the current response. Black arrows indicate the direction of diffusion towards the (gold) electrode surface. Blue – original species, Green – reacted / depleted species.

The current response of the system is governed by the rate of diffusion, species concentration and the time since the initial perturbation of the system, which is described by the Cottrell equation;

$$I = \frac{nFAC^*\sqrt{D}}{\sqrt{\pi t}} \quad (1.8)$$

where I is the current, n is the number of electrons transferred, F is the Faraday constant, A is the electrode area, C^* is the bulk solution concentration, D is the diffusion coefficient of the species and t is the time passed. For a redox reaction of a species which does not result in a change to the electrode surface area, the current is proportional to $t^{-\frac{1}{2}}$. This results in the exponential decay of the current as the measurement continues.

As with any change in potential, at very short time periods there will be an additional current contributed by the charging of the electric double layer where the Cottrell equation will not hold true. Additionally, as t becomes very large and assuming the solution volume is almost infinite compared to the volume of the depletion zone surrounding the electrode, the current will not tend towards zero as predicted by the Cottrell equation. Instead, due to the large solution volume and convective mixing effects, there will always be unreacted species outside of the diffusion zone which will diffuse towards the electrode. The current will therefore tend to some value other than zero as long as the bulk concentration of the reactive species (C^*) is maintained.

1.4 Scope of the Thesis

As discussed here, there is significant need for rapid, specific determination of the resistance profile of bacteria to improve treatment accuracy, enhance patient outcomes and slow the spread of antimicrobial resistance. Electrochemical techniques are an appealing option for rapid detection of nucleic acid sequences and are well established in the literature. The combination of electrochemical sensing and target amplification designed with point-of-care use in mind will allow target enrichment and selection to achieve sensitive detection of nucleic acid sequences with a low-cost assay. A focus on low time-to-result and reduced reliance on user interaction also increase the feasibility of using such devices at the bedside or in the field.

This thesis describes the production of an electrochemical sensor system with integrated isothermal DNA amplification to detect common antimicrobial resistance genes on a biosensor platform, providing information about the spectrum of resistance an organism exhibits in a short time. The development of a sensitive and specific system which can directly and rapidly detect the presence of antimicrobial resistance genes would allow for more rapid delivery of treatment without the need to identify the causative organism, removing the need for bacterial culture before effective treatment can be provided. This would supplement current diagnostic methods by providing early data to tailor treatment, which can then be confirmed or adjusted as required by results from traditional diagnostic means. If the assay is sensitive, selective, and accurate enough, it could replace current diagnostic methods and provide the primary means by which antimicrobial therapy is determined. If successful, rapid treatment facilitated by such an assay would improve patient safety, reduce reliance on hospital laboratories and help to limit further development of antimicrobial resistant organisms. I hypothesise that the detection of antimicrobial resistance genes from clinically relevant bacteria, at realistic concentrations, is possible using electrochemical sensing on low-cost substrates. A focus on rapid time-to-result and usability with is maintained, and it is anticipated that challenges associated with this focus will not prevent successful detection of resistance sequences.

Chapter 2 discusses the initial identification and testing of a number of gold and carbon electrode systems. Electrochemical performance of various low-cost electrodes for DNA detection is examined prior to the introduction of more complex AMR target sequences and background media. These electrodes are characterised using electrochemical and physical

techniques to assess their performance for general electrochemistry. The electrodes are then functionalised, and synthetic DNA oligonucleotides are detected on each format giving an indication of the sensitivity and reproducibility of each substrate for DNA biosensing.

Chapter 2 also outlines the development of a synthetic AMR plasmid to allow detection of a realistic DNA target without using resistant organisms. Amplification reactions for targets on this plasmid are also developed for both standard polymerase chain reaction and isothermal recombinase polymerase amplification. These amplification reactions will help concentrate the target DNA from low bacterial loads to improve the detection threshold for the system.

Chapter 3 combines these separate aspects of DNA detection – biosensing and target amplification – by detecting amplified PCR and RPA products on each electrode format from Chapter 2. Sensitivity of each electrode type to the same amplified DNA target indicates which electrodes show promise for further development. Several detection schemes are tested on carbon and gold electrodes, and methods to directly amplify DNA at the electrode surface are explored. These methods directly test my hypothesis with various low-cost electrodes being used to detect a clinically relevant AMR gene sequence.

Chapter 4 further builds upon the developed system to enhance sensitivity and specificity for a clinically relevant sequence and organism, while improving usability and simplifying the measurement scheme. This is achieved by combining labelled nucleotides with surface-based amplification for direct amplicon tagging. These nucleotides are shown to be accepted by an isothermal amplification reaction and are used to discriminate between bacteria containing AMR gene sequences and those without with high sensitivity and specificity. Simple electrochemical detection using surface-based amplification is demonstrated using the techniques developed throughout the thesis.

A summary of the aims of this work is provided below:

- Develop a sensitive electrochemical assay for antimicrobial resistance genes.
- Minimise electrode cost and maximise assay usability.
- Ensure specific detection of the target sequence against off-target nucleic acids.
- Achieve detection in cellular populations with minimal pre-processing.

2 Developing an Electrochemical Sensor and Amplification System for DNA Detection

Electrode selection for point-of-care biosensing is a critical process if high specificity and sensitivity are required. Numerous low-cost electrode formats are available with a wide variety of surface characteristics, interface methods and intended uses. The effect of electrode type on the performance of the resulting sensor is significant, and the benefits and drawbacks of each electrode type must be weighed against their performance as a biosensor. Furthermore suitable cleaning, pre-treatment, washing and measurement conditions are vital to maximise the sensitivity and specificity of the electrode (Creager et al., 1992; Gebala and Schuhmann, 2010; Ishida et al., 1997; Tsai and Lin, 2001; Yang et al., 1995).

This chapter discusses the process of identifying suitable electrodes and methods to be used when detecting the presence of a DNA target (Butterworth et al., 2019a). The following work was performed to identify suitable preparation methods and measurement protocols to obtain repeatable results with a strong signal response. There are numerous reported biosensor preparation methods described in the literature, and so several distinct protocols were tested to identify promising systems for sensor development on a variety of low-cost electrodes.

2.1 Selection and Characterisation of Gold Electrodes for Biosensing

2.1.1 Low-Cost Electrodes for Biosensing

Electrode material is an important factor influencing the choice of protocol and the responses observed during testing. Some electrode materials will have interfering electrochemical reactions at the potentials to be applied during measurement, such as oxygen or hydrogen evolution from solution, owing to the nature of the electrode material. The options available for cleaning electrodes are also a factor to consider. Gold electrodes can be modified by the simple addition of a thiolated molecule in solution, and do not exhibit any redox processes within the potential window defined by the $\text{Fe}(\text{CN})_6^{3-/4-}$ redox couple. This allows for straightforward surface functionalisation and produces electrochemical signals which are only influenced by the interaction of the redox couple with the electrode surface.

Gold electrodes are available in a variety of forms, with no one form appearing as an obvious choice for a diagnostic platform (Figure 2.1). Polycrystalline gold electrodes (PGEs) have a

pure, solid gold surface, which can be mechanically, chemically and electrochemically polished to obtain a pristine substrate for SAM formation and electrochemical detection (Carvalho et al., 2004). However, these electrodes are bulky and expensive, which makes them inappropriate for use in a low cost PoC test. Experiments were performed on these electrodes to validate methods and to offer a baseline from which to judge the performance of other electrode types. PGEs used here were obtained from IJ Cambria Scientific (Llanelli, UK).

Screen-printed electrodes (SPEs) were also examined as a sensor as they are much more suited to PoC testing than PGEs. Two electrode types were obtained from Dropsens (Oviedo, Spain); high temperature cured (AT) and low temperature cured (BT) surfaces. Both electrodes are produced by a screen-printing process in which the gold particles are mixed with solvents, binding agents and other substances to produce an ink, which is then printed onto the substrate. Depending on the ink formulation and curing process, each electrode type will exhibit different crystal faces and roughness characteristics which will affect their performance. These electrodes are small, low cost, and have inbuilt reference and counter electrodes which facilitate their use in a PoC environment. Use of these electrode systems to detect a range of biomarkers is also widely reported in the literature (Cardoso et al., 2016; Henihan et al., 2016; Li et al., 2012; Mousavisani et al., 2018; Ribeiro et al., 2018). However, the options for cleaning their surfaces are limited as the surface can be damaged by more aggressive cleaning methods such as mechanical polishing.

The final electrode type investigated consists of thin film gold electrodes (TFGEs). These electrodes were produced by sputter coating, where a thin layer of gold was deposited over a flexible plastic substrate. This is achieved by applying a high potential between a target electrode and a donor electrode, causing material to be ejected from the donor. The potential difference drives the transfer of material from the donor towards the target, depositing a thin, strongly bonded layer of material over surfaces at the target electrode.

TFGEs were obtained from FlexMedical Solutions (Livingstone, Scotland). The gold film is partially covered by a dielectric which defines the shape and size of the working electrode. These electrodes are again small and low cost but have a pure conductive surface with no proprietary compounds added as in the screen-printed systems. However, these electrodes are more delicate than the screen-printed chips, and their thin conductive layer (10 – 20 nm)

prevents harsh cleaning methods from being employed. They also do not contain in-built reference and counter electrodes.



Figure 2.1 – Gold electrodes examined as a potential biosensor platform. From left to right; AT SPE, BT SPE, PGE, TFGE.

2.1.2 Electrode Surface Characterisation

It is well known that the topology of a surface can have a significant impact on the formation of a SAM layer (Guo et al., 1994; Jiang et al., 2015; Love et al., 2005; Yuan et al., 2014). Substrate consistency is critical to the formation of a uniform and low-defect SAM layer. Polycrystalline gold electrodes, which can be polished mechanically to a mirror finish, provide the best surface for SAM formation with low surface roughness characteristics achievable. However, low-cost electrodes have been successfully demonstrated as biosensor platforms in the literature indicating that a highly uniform surface is not critical for biosensing, and rougher substrates can be effectively functionalised. The surfaces of each electrode type were examined by scanning electron microscopy and atomic force microscopy to assess the inherent level of roughness for each substrate.

Figure 2.2 shows scanning electron microscopy (SEM) images of the different electrode types described above. The surface topographies of each of these electrodes are quite different. AT SPEs (Figure 2.2A) exhibit crystalline surfaces which appear quite uniform but have some small pits and protruding formations across the surface. BT SPEs (Figure 2.2B) are much more multifaceted, with deep pits and channels numerous across the face. These formations arise due to the lower curing temperature and different ink formulation employed and produce a surface with significant roughness. The flexible electrode exhibited in Figure 2.2C is the smoothest surface of the three, with only small features such as shallow pits visible at this scale. This is to be expected as the sputter coating technique creates a layer of gold which conforms to the underlying smooth substrate.

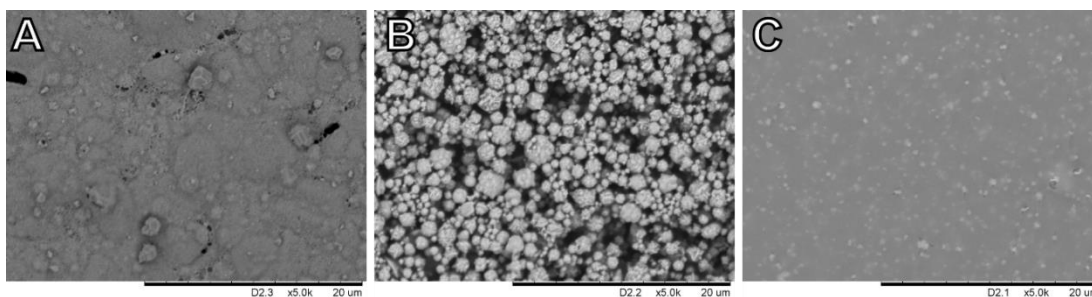


Figure 2.2 – SEM images of different electrode surfaces examined in this section (5000x magnification). (A) AT SPE, (B) BT SPE, (C) thin-film gold electrode.

Further to this data, atomic force microscopy (AFM) was also performed to quantify the microscopic surface roughness of the electrodes. AT SPEs and sputtered gold electrodes were examined by AFM; the surface of the BT SPE was believed to be too rough to accurately characterise due to the limited vertical movement of the AFM cantilever.

AFM was performed over 90 x 90 μm areas upon clean electrodes. Each electrode was randomly sampled five times with no overlap, and the root-mean-squared roughness (R_{RMS}) of each sample calculated. Figure 2.3 shows the sampled location with the median roughness from each electrode. The median R_{RMS} of AT SPEs was 712.4nm, and of sputtered gold was 186.5nm. Visually, the sputtered gold surface is much smoother than the screen-printed ink. Lower surface roughness is expected to improve SAM consistency which would increase the performance of measurements taken on these electrodes.

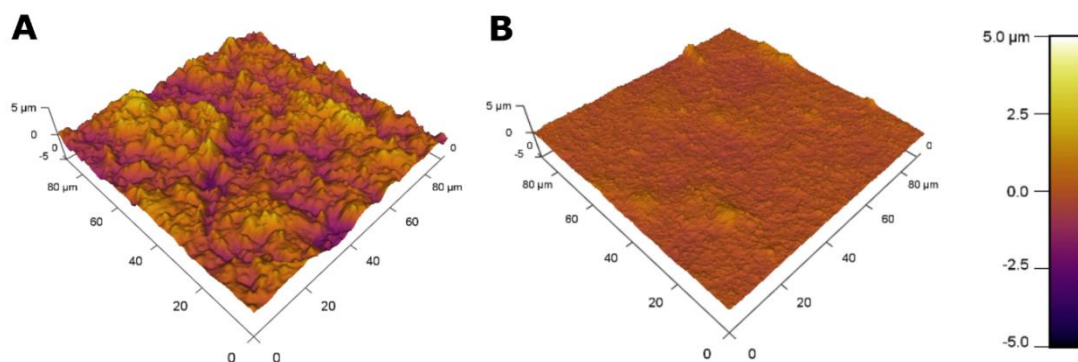


Figure 2.3 – AFM images of (A) AT SPE and (B) thin-film gold electrode.

Despite each electrode having a unique surface structure, microscopy provides no information about the performance of these devices following DNA SAM formation. The SAM quality, while being affected by substrate roughness, is also highly dependent upon surface cleanliness and immobilisation methodology. Further experiments were therefore

performed to identify effective cleaning and SAM formation protocols which could be employed on each electrode type.

2.2 Electrode Cleaning and Electrochemical Characterisation of Gold

Electrode cleaning is a vital step for the formation of a uniform SAM layer and reproducible results. Contaminants on an electrode surface can prevent DNA probes and SAM molecules from binding, which may lead to gaps in the blocking layer and variable DNA probe densities. Such defects reduce the sensitivity of the system and can introduce electrochemical processes which interfere with the measurement. Effective removal of any unwanted molecules from the gold electrode surface prior to SAM formation is therefore a key step in achieving a sensitive and specific detection protocol.

2.2.1 Methods

PGEs were cleaned first by immersion in Piranha solution consisting of a 3:1 ratio of concentrated H_2SO_4 and H_2O_2 . This solution is an aggressive oxidiser, and immersion of the electrodes for 10 minutes will remove most organic contaminants from the surface. The electrodes were thoroughly rinsed in deionised water and then mechanically polished in $0.05\mu\text{m}$ aluminium oxide slurry, followed by sonication for several minutes in deionised water to dislodge any remaining alumina particles. Electrodes were then immersed in a 0.1M H_2SO_4 solution with a platinum counter electrode and Ag/AgCl reference electrode and electrochemically cleaned. Cyclic voltammetry (CV) was performed between 0V and $+1.7\text{V}$ at 0.1V/s for 30 cycles. This process repeatedly forms and degrades a layer of gold oxide across the surface, removing organic contaminants and reducing surface roughness (Fischer et al., 2009; Tkac and Davis, 2008). The potential window was chosen to fully cover the gold oxide formation and reduction peaks and include a small amount of oxygen evolution. 30 cycles allowed the gold oxide reduction peak to stabilise, indicating a complete gold oxide layer is formed and reduced within a single cycle.

Cleaning protocols were examined for the SPEs to try and produce a uniform SAM which gave consistent responses when a DNA target was bound. As these electrodes cannot be mechanically polished or aggressively cleaned with chemicals, these protocols focussed on electrochemical cleaning methods. Both SPE types were initially cleaned by CV in 0.1M H_2SO_4 at 0.1V/s between -0.2V and a potential just before the oxygen evolution peak. This potential was typically around 1.2V for AT SPEs and 1.5V for BT SPEs vs the on-board silver

reference electrode. CV was continued for 30 cycles, or until the gold oxide reduction peak no longer increased in size.

For the TFGEs, a similar cleaning process was used. These electrodes were cleaned by CV cycling between -0.2V and +1.7V under 0.1M H₂SO₄ for 30 cycles, or until the gold oxide reduction peak no longer increased in size. This process was sufficient to produce Fe(CN)₆^{3-/4-} responses with a peak to peak separation and charge density similar to those shown on a clean PGE.

2.2.2 Results & Discussion

Figure 2.4 shows the H₂SO₄ cleaning CV for each gold electrode examined. Each electrode type shows the typical shape for a gold CV under H₂SO₄. Clear oxidation and reduction peaks are visible on each electrode type. AT and BT SPEs exhibit different oxide formation and reduction profiles, which could be attributed to different crystal faces being present on each electrode type (Štrbac et al., 1988).

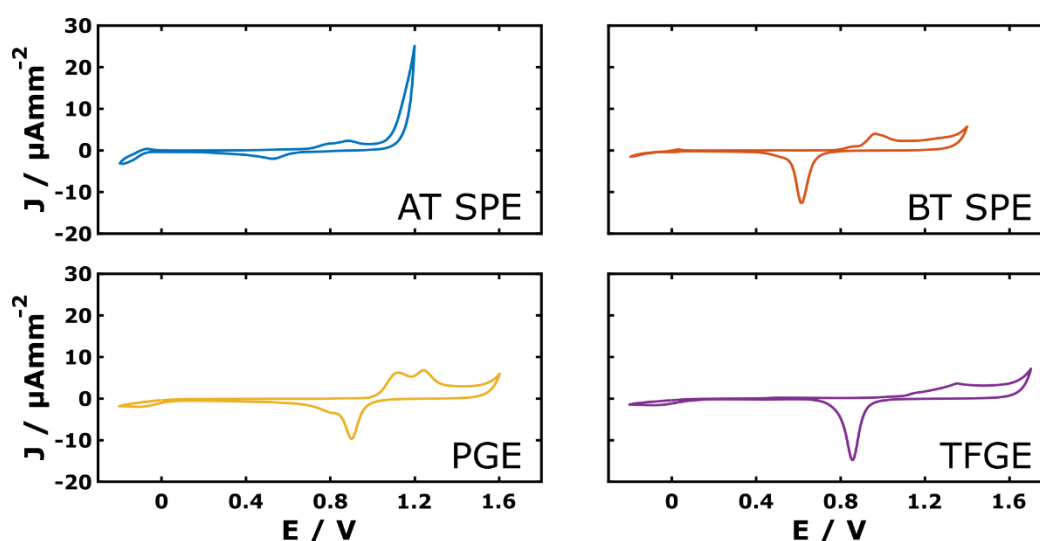


Figure 2.4 – Voltammograms of 0.1M H₂SO₄ cleaning CV for different electrode types. SPE – screen-printed electrode, PGE – polycrystalline gold electrode, TFGE – thin-film gold electrode.

Characterisation of the electrodes was performed with 2 mM Fe(CN)₆^{3-/4-} in 50 mM Phosphate Buffer + 200 mM KCl. This characterisation consisted of cyclic voltammetry at a sweep rate of 0.1 V/s between -0.2 and +0.6 V vs the associated reference electrode. EIS was also performed between 100 kHz and 0.1 Hz, with an alternating current amplitude of 10 mV

and a direct current bias equal to the open circuit potential (OCP) determined immediately before the measurement.

Figure 2.5 shows the $\text{Fe}(\text{CN})_6^{3-/4-}$ CV responses of each electrode type after cleaning using their optimum method as described above. The use of the on-board silver reference electrode for the SPEs results in their responses being shifted relative to the Ag/AgCl reference electrode used for the gold disc and flexible electrodes. All CV and EIS responses have been corrected for differences in the real surface area of the electrode.

All the electrodes tested exhibited a similar current density indicating that each electrode has pure gold exposed at the surface. The AT SPE had a slightly reduced current density relative to the other electrode types, but all electrodes exhibited a typical CV response for the $\text{Fe}(\text{CN})_6^{3-/4-}$ redox couple in solution. The peak-to-peak separation (ΔE_p) of CV cleaned AT SPEs was approximately 70 mV, whereas for BT SPEs this was typically 75 mV. The TFGEs showed a ΔE_p of around 90 mV, and the PGEs presented with 73 mV. The ΔE_p of the SPEs and PGEs are close to the ideal peak separation of 59 mV at 298°K as defined by the Nernst equation, indicating these systems have high reversibility. The TFGE exhibits a slightly greater ΔE_p than the other electrode substrates.

The CV data correlates well with the EIS responses of the electrodes under the same solution (Figure 2.6). SPEs exhibit rapid kinetics; the Warburg impedance dominates the plot even at high frequencies, and the shape of the curve indicates a high rate of electron transfer. Both the PGEs and the TFGEs show a small charge transfer resistance feature in their Nyquist plots. This is larger on the TFGEs due to the thin gold layer (10 – 20 nm), resulting in a higher internal resistance when compared with the other electrode types.

Based upon the surface imaging as well as electrochemical characterisation of each electrode, all electrode types showed promise for DNA biosensing applications at this stage. All sensors show highly reversible electrochemical behaviour with relatively low baseline impedance, and all produced responses which were similar to the existing standard, the PGE. Each electrode was therefore considered as a potential sensor substrate and tested as a platform for biosensor development.

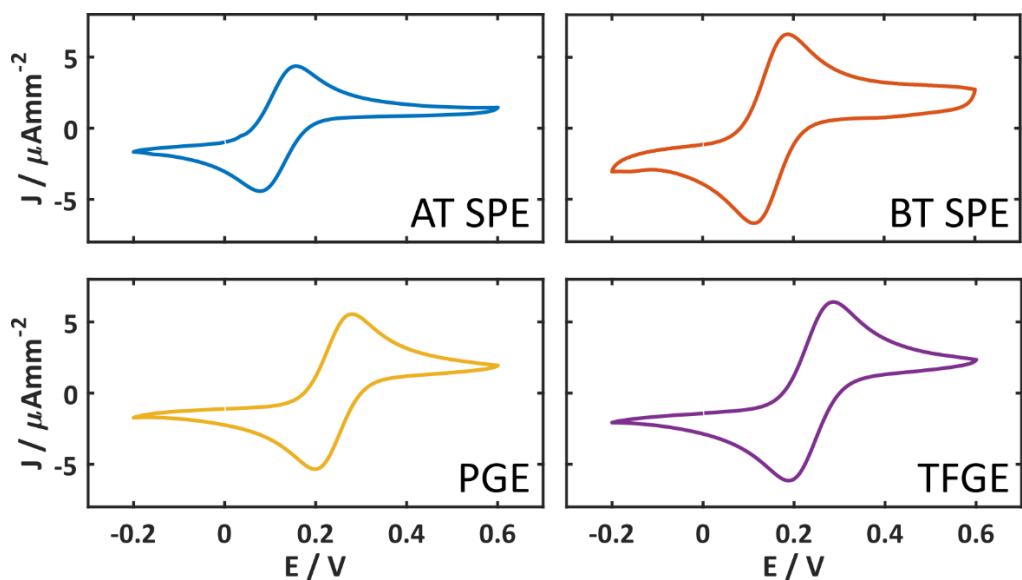


Figure 2.5 – Voltammograms of 2mM $\text{Fe}(\text{CN})_6^{3-/4-}$ CV responses of different electrode types after cleaning. All electrodes were cleaned by CV cycling under 0.1M H_2SO_4 . SPE – screen-printed electrode, PGE – polycrystalline gold electrode, TFGE – thin-film gold electrode.

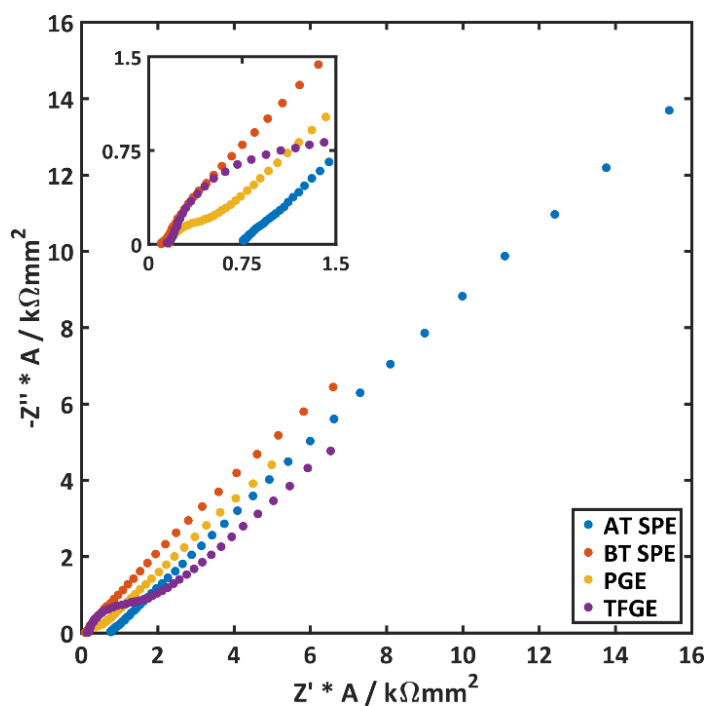


Figure 2.6 – Nyquist plot of 2mM $\text{Fe}(\text{CN})_6^{3-/4-}$ electrochemical impedance spectroscopy on different electrode types after cleaning. SPE – screen-printed electrode, PGE – polycrystalline gold electrode, TFGE – thin-film gold electrode. Inset – Magnified high frequency range.

2.3 DNA Biosensing on Gold Electrodes

As each electrode examined showed similar electrochemical properties, all electrodes were tested for their suitability as a biosensor platform. Each electrode type was modified with a specific DNA capture probe terminated with a short carbon chain and thiol group at the 5' end. The presence of the 5' thiol allows the DNA probe to be bound to the surface through the strong interaction between gold and sulphur (Bain and Whitesides, 1988; Nuzzo and Allara, 1983). In order to space these probes and passivate the unbound gold, the DNA was mixed with a short chain alkanethiol, either 6-mercapto-1-hexanol (MCH) or 3-mercapto-1-propanol (MCP) which binds to gold through the same interaction. This alkanethiol layer reduces non-specific signal and provides a barrier to electron transfer. MCH produces a thicker barrier layer than MCP and inhibits electron transfer more effectively. These two passivation molecules were compared to evaluate which layer provided the greatest signal changes when challenged with complementary DNA. The addition of a reducing agent to the mixture to break any dithiol bonds was also investigated.

2.3.1 Methods

Synthetic DNA oligonucleotides (Sigma, UK) were used as the probe and target sequences within the following methods. The DNA probe consisted of a 14 base pair DNA strand covalently attached to a 6 repeat carbon chain, which was terminated with a thiol group. The target was a fully complementary sequence with no terminal modifications present. DNA sequences are provided in Table 2.1.

Table 2.1 – DNA sequences used in initial gold electrode preparation. Sequences presented 5' to 3'.

Sequence Name	Base Sequence and Modifications
DNA Probe	SH- (CH ₂) ₆ -GATAGCTACTAGAG
DNA Target	CTCTAGTAGCTATC

The method used for initial biosensor development was based upon the protocol described by Keighley et al. (2008b). This work showed that the probe density at the electrode surface could be controlled by simultaneous immobilisation of the probe with the SAM layer and reported good responses to DNA binding. After cleaning the electrodes, a mixed solution of 3 µM probe DNA and 30 µM SAM molecule was prepared in immobilisation buffer consisting

of 0.4 M Phosphate Buffer (PB) + 1 M NaCl + 5 mM MgCl₂ + 1 mM ethylenediaminetetraacetic acid (EDTA). This solution was added to the electrode surface and allowed to incubate at 4°C overnight. Following this incubation, electrodes were rinsed sequentially in immobilisation buffer, 200 mM PB, 10 mM PB and finally 10 mM PB + 10 mM EDTA. The surface was then backfilled with the SAM molecule at a concentration of 1 mM in diH₂O for 1 hour at room temperature. Electrodes were again rinsed with diH₂O following this step.

When investigating the effect of reducing agent, 5 mM tris(2-carboxyethyl)phosphine (TCEP) was added to the immobilisation buffer and SAM backfill solutions, which were pre-reduced for 30 minutes at room temperature prior to adding the solution to each electrode.

Following backfilling, baseline measurements for each electrode were taken. Electrodes were held in 2 mM Fe(CN)₆^{3-/4-} in 50 mM PB + 200 mM KCl for 10 minutes – to allow the solution and SAM film to equilibrate – before CV and EIS were performed. Electrodes were then rinsed with 200 mM PB + 800 mM KCl, and then 1 μM target DNA in 200 mM PB + 800 mM KCl was added to the surface. Electrodes were incubated in a humidified container at room temperature for 1 hour. Each electrode was then rinsed in 200 mM PB + 800 mM KCl and 50 mM PB + 200 mM KCl, before final CV and EIS measurements with Fe(CN)₆^{3-/4-}.

Alternative cleaning methods for each SPE type were also investigated. AT SPEs were immersed in 0.1M H₂SO₄ for 10 minutes, which was chosen to attempt to minimise disruption of the relatively smooth surface which may occur after extended CV cycling. BT SPEs were also cleaned by holding at +1.5V for 100 seconds before undergoing 3 CV cycles from -0.2 to +1.5V. Basic characterisation responses from BT electrodes were at times found to be inconsistent, and this cleaning procedure was designed to maximise the oxidation of the surface to clear contaminants. Data from SAMs formed using these cleaning procedures is presented alongside CV cleaned responses.

2.3.2 Results and Discussion

2.3.2.1 DNA Detection on PGE

Figure 2.7 shows an example EIS spectrum change in response to the formation of an overnight SAM layer, backfilling, and DNA hybridisation. As expected, the impedance response shows an increasing trend at each stage as the surface becomes increasingly blocked. These results are representative of the changes observed in the impedance response when blocking gold electrodes using this protocol. Occasionally, the backfilling

process may result in a decrease in the impedance of the system. Such responses are attributed to the flexible single-stranded DNA probe “standing up” at the surface as the concentrated backfill molecule fills vacancies within the SAM layer. Orientation of the DNA probe into an upright configuration may allow improved access of the redox couple compared to DNA which rests closer to the electrode surface (Gebala and Schuhmann, 2010). SAMs which exhibit either behaviour can produce the same hybridisation induced changes to the electrochemical response and performed similarly in these experiments.

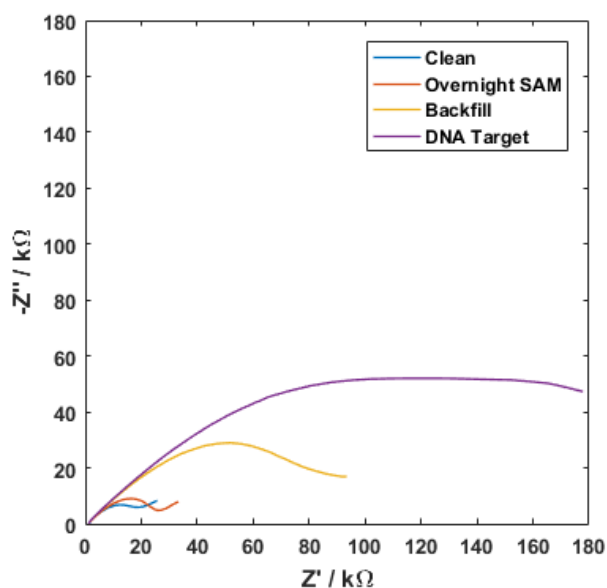


Figure 2.7 – Example $2\text{mM Fe(CN)}_6^{3-/4-}$ impedance response changes on AT screen-printed electrode as SAM formation and DNA detection process progresses.

Figure 2.8 shows the changes in charge transfer resistance (R_{CT}) in response to DNA binding on polycrystalline gold electrodes (PGEs). When electrodes are first incubated with probe, followed by backfilling with alkanethiol (Figure 2.8, Sequential Immobilise) a mean 20% R_{CT} increase is observed with MCH ($n = 2$). Immobilising with MCP as the backfill thiol resulted in a 185% R_{CT} signal increase ($n = 3$), with much poorer electrode consistency. The MCH response is much smaller, which is consistent with the higher initial impedance of the MCH-probe layer. This is a result of the longer MCH chain producing a thicker SAM, reducing the efficiency of electron transfer between the solution and the electrode (Bard and Faulkner, 2001; B. Liu et al., 2004). The binding of DNA to the layer produces a much smaller change relative to the initial impedance on MCH than MCP, giving a smaller percentage change in R_{CT} .

Improving sensitivity by reducing the initial impedance of the sensing layer has been reported in the literature through the use of PNA (Keighley et al., 2008a) or morpholino (Corrigan et al., 2013) based DNA analogues. The use of a shorter alkanethiol blocking molecule allows a similar reduction in the initial R_{CT} to be achieved at lower cost. However, this method has other limitations, primarily the reduced stability of short-chain alkanethiols due to fewer inter-molecular interactions within the film resulting in a SAM layer with more defects (Cecchet et al., 2006; Love et al., 2005). This lower SAM stability can also result in desorption or ageing of the layer when washing or regenerating the sensor (Kafka et al., 2008; Riedel et al., 2014). A combination of these effects likely resulted in the higher standard deviation seen on the MCP layers on PGEs.

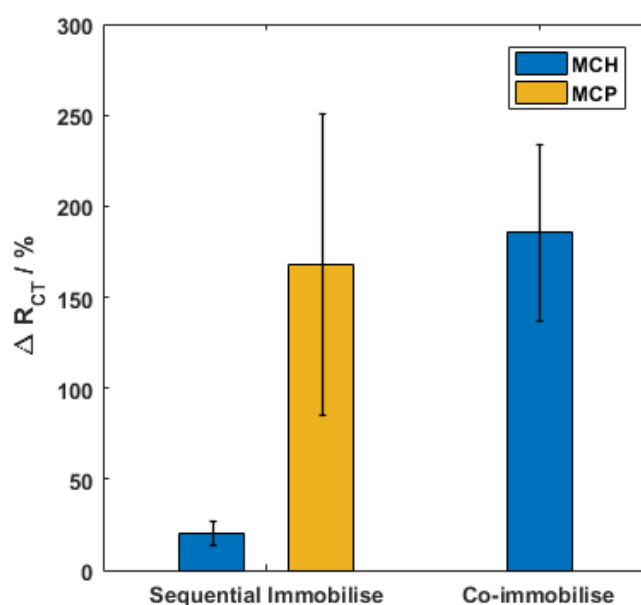


Figure 2.8 – Mean electrochemical impedance spectroscopy R_{CT} change for $2\text{mM Fe(CN)}_6^{3-/4-}$ on polycrystalline gold electrodes following DNA target binding. Electrodes were prepared with DNA probe and 6-mercapto-1-hexanol (MCH) or 3-mercapto-1-propanol (MCP) through a sequential or co-immobilisation approach. Error bars = SD, $n = 3$.

When MCH and the DNA probe were co-immobilised, a significant increase in the EIS signal change was observed. This is attributed to increased spacing between the DNA probes by controlling the mole fraction of DNA : MCH (Keighley et al., 2008b). Increasing the space between probes improves the hybridisation efficiency but reduces the charge screening effect of the duplex. Keighley found that a 20% DNA mole fraction produced the greatest change in R_{CT} upon target binding, which correlates to the results obtained here. Co-

immobilisation of the DNA probe and thiol also improved the relative standard deviation of the measurement, from 32% with the sequential protocol down to 26%. The co-immobilisation strategy was used in most cases going forward as a result of these findings.

Methods to improve the variability in the signal response were examined at this stage. Thiolated molecules, including alkanethiols and the DNA probe sequences used here, form dithiol bonds when in solution. The cleavage of these dithiol bonds prior to incubation on a gold surface is common practice to achieve the desired concentration of thiol species in a solution. Reducing agents such as dithiothreitol or TCEP can be used to cleave dithiol bonds. As dithiothreitol contains two thiol groups which may be capable of co-immobilising to gold alongside the desired alkanethiol and DNA probe, the reducing agent TCEP was chosen for immobilisation solution pre-reduction.

Figure 2.9 shows the effect of TCEP pre-reduction on the sensor's response to DNA hybridisation. The addition of TCEP to the process gives little change in the mean signal change, but significantly improves the signal variability. The relative standard deviation of the measurement decreased from 50% to 16%, greatly improving the detection capability of the sensor. For future measurements, a pre-reduction step with TCEP was included to take advantage of the improved sensor consistency observed here.

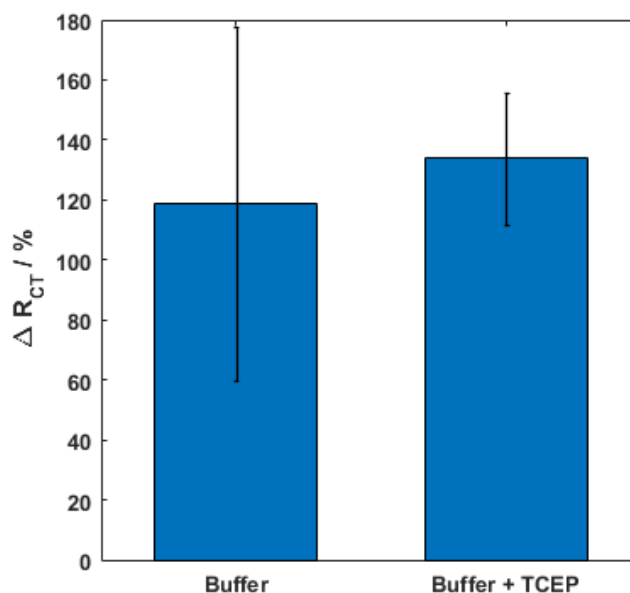


Figure 2.9 – Mean electrochemical impedance spectroscopy R_{CT} change for 2mM $Fe(CN)_6^{3-/4-}$ on PGEs with and without TCEP pre-reduction of the MCH SAM. Error bars = SD, $n = 3$.

2.3.2.2 DNA Detection on Screen-Printed Electrodes

Figure 2.10 shows the changes in charge transfer resistance in response to DNA binding on AT electrodes. Two cleaning methods were examined, a simple H₂SO₄ immersion and a standard CV cycle under H₂SO₄. Initial tests with immersion cleaning (Figure 2.10A) produced a SAM layer whose R_{CT} decreased in response to DNA binding. There was also no difference between MCH or MCP response, which indicated that the immersion cleaning method had not effectively prepared the electrode. A second trial with this method (Figure 2.10B) produced a response in the expected direction, with a small difference between the MCH and MCP SAM layers.

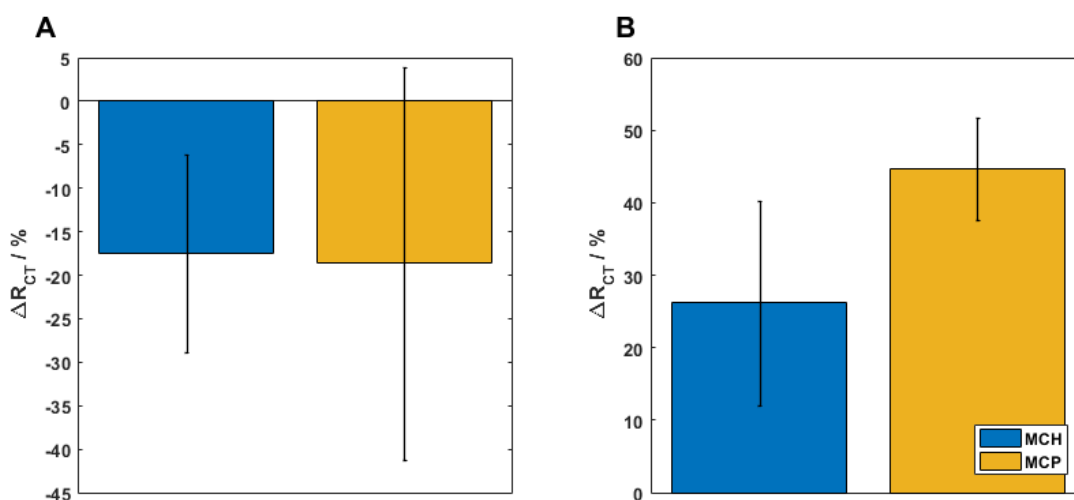


Figure 2.10 – Mean electrochemical impedance spectroscopy R_{CT} change for 2mM $Fe(CN)_6^{3-/4-}$ on immersion cleaned AT screen-printed electrodes following DNA target binding. Electrodes were prepared with DNA probe and 6-mercapto-1-hexanol (MCH) or 3-mercapto-1-propanol (MCP). Error bars = SD, $n = 3$.

Cleaning by traditional cyclic voltammetry was also performed as a comparison (Figure 2.11). The response magnitude and variability of the MCH SAM remained similar to immersion cleaned electrodes, but the response of the MCP SAM increased and became more like those seen on PGEs. The relative variability of the MCP SAM remained consistent with immersion-based cleaning. This data indicated that CV cleaning was a much more effective method than immersion, with no apparent deleterious effects on the sensor surface. As these responses were obtained in parallel to immersion cleaned electrodes, it was decided that further testing with immersion cleaning was not necessary considering the improvements which were seen using the active cleaning process.

In contrast to the PGE data, MCP SAM variability was similar or reduced compared to MCH SAMs on AT SPEs. This may be attributed to the shorter chain MCP packing more effectively around the many defects in the SPE surface than MCH, thereby producing a more consistent SAM layer.

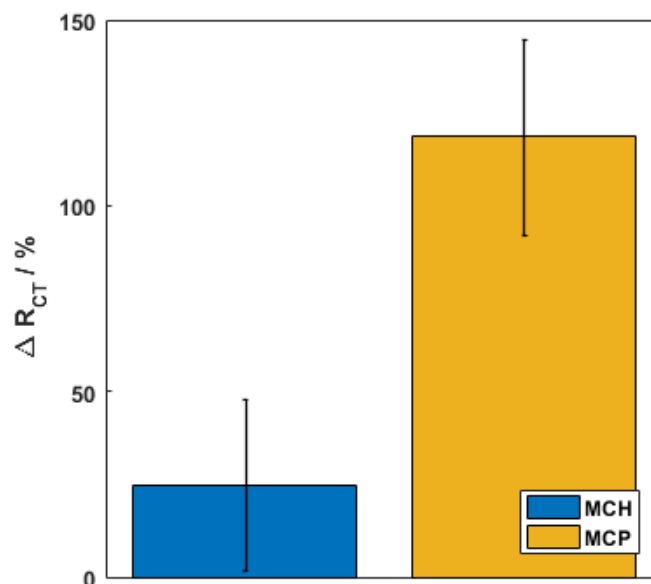


Figure 2.11 – Mean electrochemical impedance spectroscopy R_{CT} change for 2mM $Fe(CN)_6^{3-/4-}$ on CV cleaned AT screen-printed electrodes following DNA target binding. Electrodes were prepared with DNA probe and 6-mercapto-1-hexanol (MCH) or 3-mercapto-1-propanol (MCP). Error bars = SD, $n = 3$.

Figure 2.12 details the responses observed on BT SPEs. As previously, MCH produced a lower response magnitude than MCP on these electrodes. An MCH SAM without TCEP pre-incubation (Figure 2.12A) again showed a high response variability. The inclusion of a TCEP pre-reduction step produced a similar mean signal increase with significantly improved consistency. The R_{CT} increase for MCH on BT SPEs are much higher than for AT SPEs, despite the initial impedance of the electrode being greater. However, SAM formation consistency between experiments was poor. The large R_{CT} increase with MCP was due to very low initial R_{CT} (122 Ω mean on 3 electrodes) which was seen to occur in several different experiments. This suggests that SAM formation may not have occurred as expected, possibly leaving non-functionalised regions within the complex surface geometry of the electrode. This may have led to non-specific interaction of the DNA target with the surface producing a large signal response.

Unlike on AT SPEs, variability within the MCP SAM was higher than the MCH SAM when using TCEP. This variability is associated with small differences in the impedance response and not to any structural or SAM formation issues at the surface. In absolute terms, the impedance increases were quite consistent, but owing to the low initial impedance and the magnitude of change, a difference of a few tens of Ohms results in a large change in the signal increase percentage, giving rise to greater standard deviations.

The use of the voltage hold and CV cleaning technique produced a decrease in the EIS response to DNA target. While oxidation of the gold is effective at removing contaminants, SAM formation is adversely affected on highly oxidised surfaces. It is likely that the CV cycling following the oxidative hold was insufficient to fully remove the gold oxide layer, possibly leading to the results observed here through a decrease in SAM density and quality.

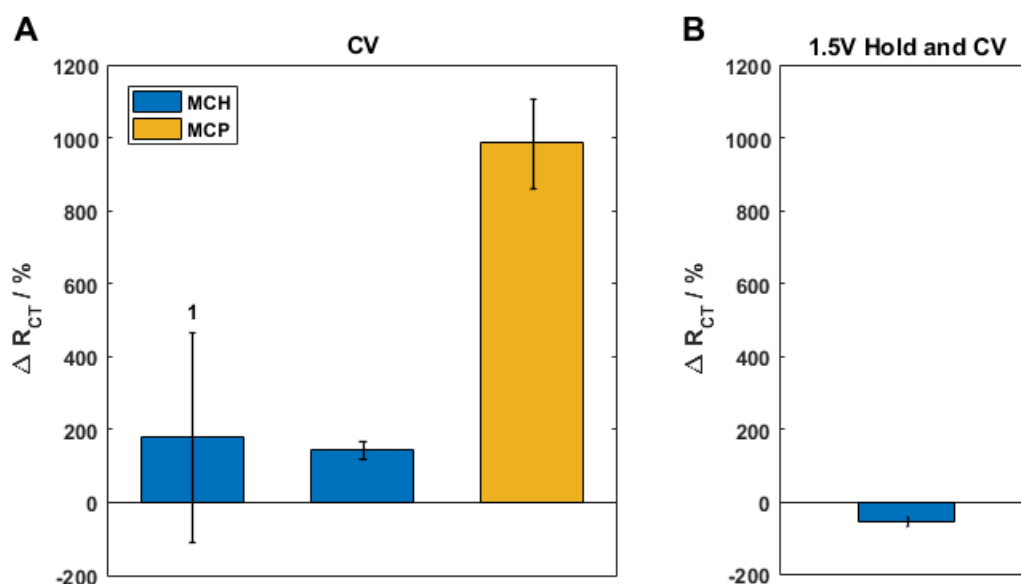


Figure 2.12 – Mean electrochemical impedance spectroscopy R_{CT} change for 2mM $Fe(CN)_6^{3-/4-}$ on BT screen-printed electrodes following DNA target binding. Electrodes cleaned by (A) cyclic voltammetry or (B) voltage hold and CV. ¹No TCEP pre-incubation. Error bars = SD, $n = 3$.

Figure 2.13 shows the results of MCP SAM formation on TFGEs. As MCP had consistently been giving greater signal responses, MCH measurements were not pursued on these electrodes at this time. Two different electrode sizes were used, either a 0.54- or 1.09-mm diameter system. While the 0.54 mm electrode gave a greater mean response change, no significant difference was observed between the two. The EIS signal change on these electrodes with

MCP was lower than other electrode types tested, largely due to the high initial impedance of the SAM layer formed on these surfaces. This is not unexpected, as the TFGE surface most closely resembled the expected PGE surface when examined under SEM and AFM, so a densely packed SAM with fewer defects than on other electrodes is likely. This is exacerbated by the thin film exhibiting a naturally high R_{CT} compared to the other electrode formats.

These electrodes showed large variability in R_{CT} response magnitude, despite appearing to have an excellent surface for SAM formation. The outcome of CV cleaning for these electrodes could be quite variable, with some responding well to the process while others showed only minor improvements in $Fe(CN)_6^{3-/4-}$ CV responses afterwards. For this experiment all electrodes were used, but in future only electrodes which showed good improvement in CV responses following H_2SO_4 cleaning were used.

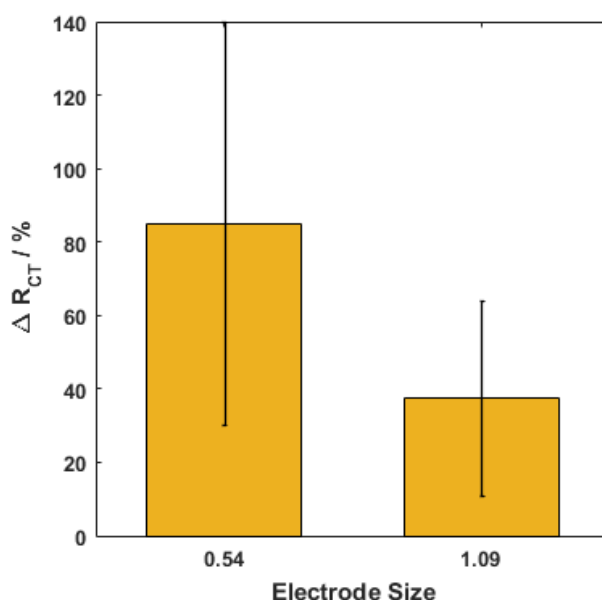


Figure 2.13 – Mean electrochemical impedance spectroscopy R_{CT} change for 2mM $Fe(CN)_6^{3-/4-}$ on thin-film gold electrodes (TFGEs) following DNA target binding. Error bars = SD, $n = 3$.

Compared to the screen-printed electrode formats, TFGEs would be expected to give a more consistent response due to the more uniform electrode surface. With SPEs, the surface morphology will result in highly variable real surface areas between each electrode which will affect the baseline R_{CT} and therefore the analytical performance. The high response variability observed here may have been due to residual manufacturing contaminants on the

electrode surface which were not removed by CV cycling, as indicated by some electrodes exhibiting poor $\text{Fe}(\text{CN})_6^{3-/4-}$ response improvements.

2.3.3 Conclusions

General characterisation of different SAM layers on each electrode type suggested that any electrode format may be suitable for DNA biosensor development once optimised cleaning protocols had been developed. Thinner SAM layers (those based on MCP) typically showed a greater signal change following DNA target binding which was largely attributed to a lower initial R_{CT} . This increased signal response was generally contrasted by greater variability between electrodes than seen on the thicker and more stable MCH layers.

All electrode types showed reasonable sensitivity with a basic SAM formation protocol and minimal optimisation of formation, incubation or hybridisation conditions. These tests also used a short DNA target sequence in buffer, and the sensitivity of different electrodes is likely to change further when longer sequences and more complex background solutions are tested. Each electrode format was taken forward into future experiments based on the responses observed in these tests.

2.4 Characterisation and Sensing on Carbon Electrodes

Electrochemical detection of DNA sequences on gold electrodes relies upon the formation of an alkanethiol SAM containing a specific capture probe. This process, while having facilitated successful detection of the target sequence herein, is error prone due to the inherently irreproducible nature of the SAM formation process. Defects within the SAM layer from substrate roughness, inefficient packing or multilayer formation can result in poor levels of detection, high background signals or non-specific interactions. SAM layers can also be unstable, desorbing over time if left in solution. This could reduce the shelf-life of a point-of-care sensor considerably and make distribution more complex.

Electrodes which can be modified with covalently bonded recognition elements could allow for a more uniform DNA probe layer and better control over the surface properties. Carbon electrodes allow such control and electrochemical modification with an amine-terminated probe is a well-established process (Jampasa et al., 2014; Lucarelli et al., 2004; Obaje et al., 2016; Saby et al., 1997). An investigation into the electrochemical characteristics of carbon electrodes was therefore performed to observe whether carbon offered a suitable substrate for DNA detection, and to identify whether the covalent attachment chemistry available on

carbon electrodes exhibited superior sensing performance to the self-assembly of alkanethiols on gold.

2.4.1 Methods

2.4.1.1 Cleaning and Characterisation of Carbon Electrodes

Glassy carbon electrodes were sourced from IJ Cambria Scientific (Llanelli, UK). Screen-printed carbon electrodes (8W110) were obtained from Dropsens (Llanera, Spain). Glassy carbon electrodes were polished with 0.05 μm alumina slurry and rinsed with dH_2O prior to electrochemical cleaning. Both screen-printed and glassy carbon electrodes were cleaned by performing cyclic voltammetry (CV) in 20 mM NaCl between 0 and +1.4V at 100 mV/s for 10 scans.

Carbon electrode functionalisation was then performed following the method outlined by Obaje et al. (2016). Aminobenzoic acid (PABA) was grafted to the electrode surface by CV from +0.4 to -0.6 V, at 100 mV/s for 3 scans under a 1:1:1 ratio of 2 mM PABA : 2 mM NaNO_2 : 0.5 M HCl before rinsing in 1xPBS (pH 7.4). N-hydroxysuccinimide (NHS) and 1-Ethyl-3-(3-dimethylaminopropyl) carbodiimide hydrochloride (EDC) in (2-N-morpholino) ethane sulfonic acid (MES) buffer at pH 5.0 was added for 1 hour to activate the surface to bind the DNA probe. After rinsing with MES buffer, electrodes were incubated with 1 μM DNA probe for 1 hour (Table 2.2). The surface was then rinsed with 1xPBS and blocked with 1% ethanolamine in 1xPBS for 30 minutes.

Table 2.2 – DNA sequences used for comparison of carbon and gold functionalisation. PEG6 – spacer molecule consisting of a 6-unit polyethylene glycol chain connecting the DNA to the anchor group.

Sequence Name	Base Sequence and Modifications
DNA Probe (Carbon)	$\text{NH}_2 - (\text{CH}_2)_6 - [\text{PEG6}] - \text{AACAGAAGCATGGCTCGAAA}$
DNA Probe (Gold)	$\text{SH} - (\text{CH}_2)_6 - [\text{PEG6}] - \text{AACAGAAGCATGGCTCGAAA}$
DNA Target	TTTCGAGCCATGCTTCTGTT

2.4.1.2 Comparison of DNA Detection on Carbon and Gold Electrodes

When comparing gold and glassy carbon electrodes, PGEs were prepared with a DNA-MCP SAM following the protocol described previously. Washes in various PBS buffers were replaced with an extended wash in 1xPBS to match the carbon electrode functionalisation process more closely.

Electrodes were incubated with 500 nM 120 base pair synthetic DNA target. EIS and DPV measurements were performed with 1 mM $\text{Fe}(\text{CN})_6^{3-/4-}$ in 1xPBS after electrode functionalisation, and then again following a 30-minute incubation with the DNA target at 39°C and rinsing in 1xPBS.

2.4.1.3 DNA Detection on Screen-Printed Carbon

For detection of DNA on screen-printed carbon, differential pulse voltammetry (DPV) was performed on 8W110 electrodes. Measurements were performed on functionalised electrodes using $\text{Fe}(\text{CN})_6^{3-/4-}$ in 1xPBS, with sufficient volume to cover all electrodes on the chip. DPV was swept from -0.2 to 0.6 V with a step potential of 5 mV, pulse potential 25 mV, pulse time 50 ms and a scan rate of 10 mV/s. Following this baseline DPV, each working electrode was isolated from all others using a custom jig design and incubated with 20 μL target DNA solution for 30 minutes at 50°C. Solution was then removed from each electrode to prevent cross-contamination and electrodes were rinsed in 0.05xPBS and 1xPBS. The electrodes were then immersed again in $\text{Fe}(\text{CN})_6^{3-/4-}$ solution and measurements repeated.

2.4.2 Results and Discussion

2.4.2.1 Cleaning and Characterisation of Carbon Electrodes

Cleaning and functionalisation of glassy carbon electrodes is shown in Figure 2.14. The cleaning CV in Figure 2.14A shows the expected response, with an oxygen evolution peak present at the higher potentials, and no other redox activity observed. This response was typical of all the glassy carbon electrodes tested. Figure 2.14B shows the electrografting response of these electrodes. These results show a small reductive peak in the 0 to -0.2V range, which is indicative of PABA grafting onto the carbon surface. The overall current and the magnitude of this peak decrease with successive scans, showing progressively greater functionalisation of the surface with PABA.

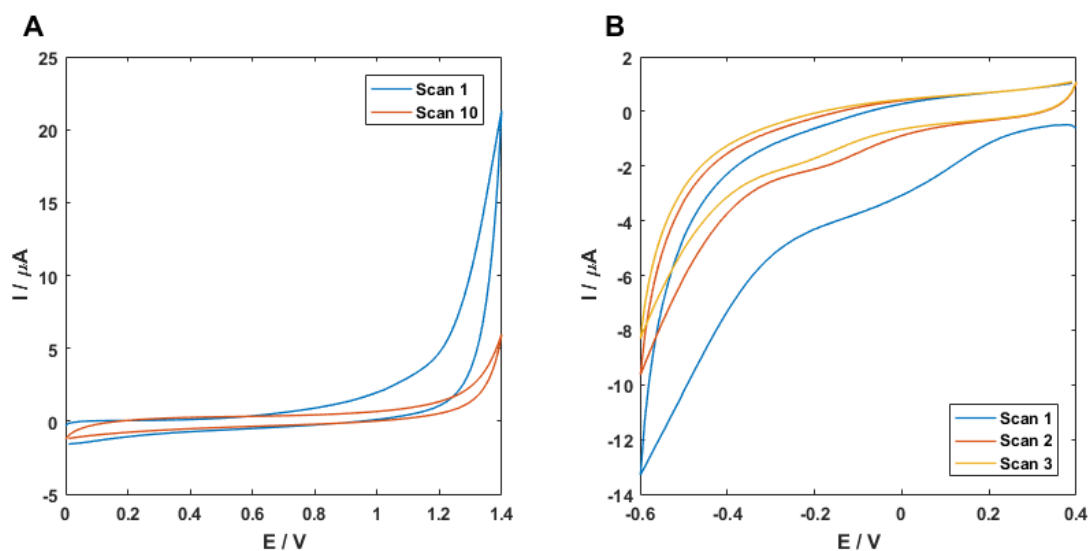


Figure 2.14 – Cleaning and electrografting voltammograms for carbon surface preparation on glassy carbon electrodes. (A) NaCl cleaning cyclic voltammetry sweeps and (B) Aminobenzoic acid electrografting cyclic voltammetry sweeps.

Following immobilisation of the DNA probe on the electrode surface, EIS and DPV baseline measurements were taken on the three glassy carbon electrodes. Figure 2.15A shows the EIS trace of one of these electrodes. This trace fits well to the modified Randles equivalent circuit giving an R_{CT} of 2019 Ω . The DPVs in Figure 2.15B show good consistency across all electrodes, with a mean peak height of 3.491 μA with a relative standard deviation of 2%. Despite these electrodes being larger than the PGEs and not being blocked with an alkanethiol SAM, the baseline R_{CT} is higher and the DPV peaks are lower. This is due to the rate constant of the electron transfer between $\text{Fe}(\text{CN})_6^{3-/4-}$ and the electrode being lower on carbon compared to gold (Ganesh et al., 2006; McCreery, 2008; Saby et al., 1997). This characterisation data suggested that carbon could be a good candidate for biosensor development.

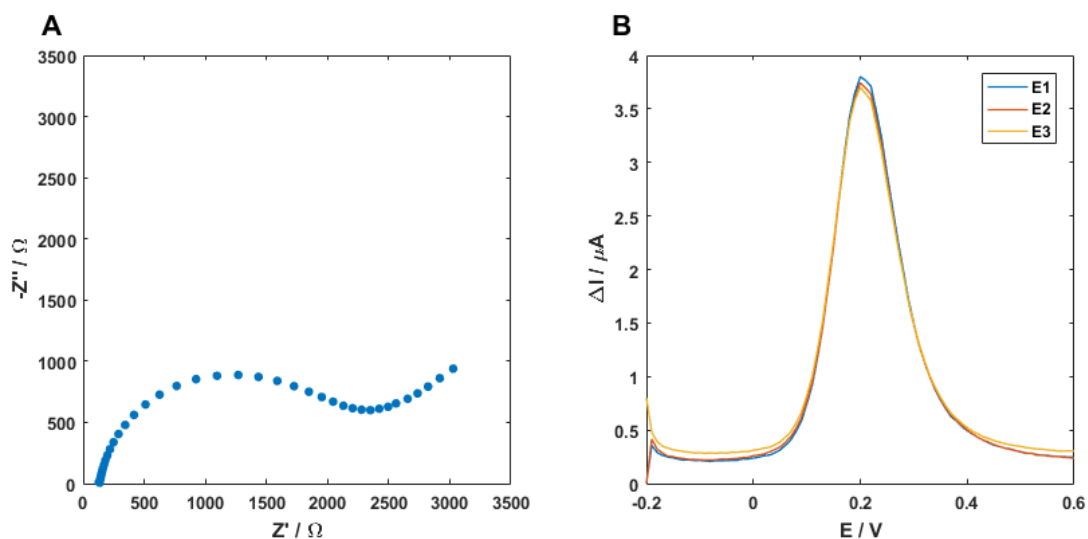


Figure 2.15 – Example $1\text{mM Fe(CN)}_6^{3-/4-}$ measurements on glassy carbon electrodes functionalised with DNA probe and blocked with 1% ethanolamine. (A) EIS and (B) DPV responses.

Screen-printed carbon electrodes were also used as a means of multiplexing measurements. Both an 8-electrode chip and a 96-well plate format were tested. Figure 2.16 shows typical NaCl cleaning CVs and PABA electrografting CVs for screen-printed electrodes. The currents observed for the cleaning CV are significantly higher than those seen on the glassy carbon electrodes, likely due to a combination of a highly electrochemically active ink and the increased surface roughness of the screen-printed electrode producing a much greater surface area. The overall current during electrografting was no larger on screen-printed electrodes, although the reduction peak indicative of PABA binding was much more pronounced. This indicates a greater background current was present on the glassy carbon electrodes.

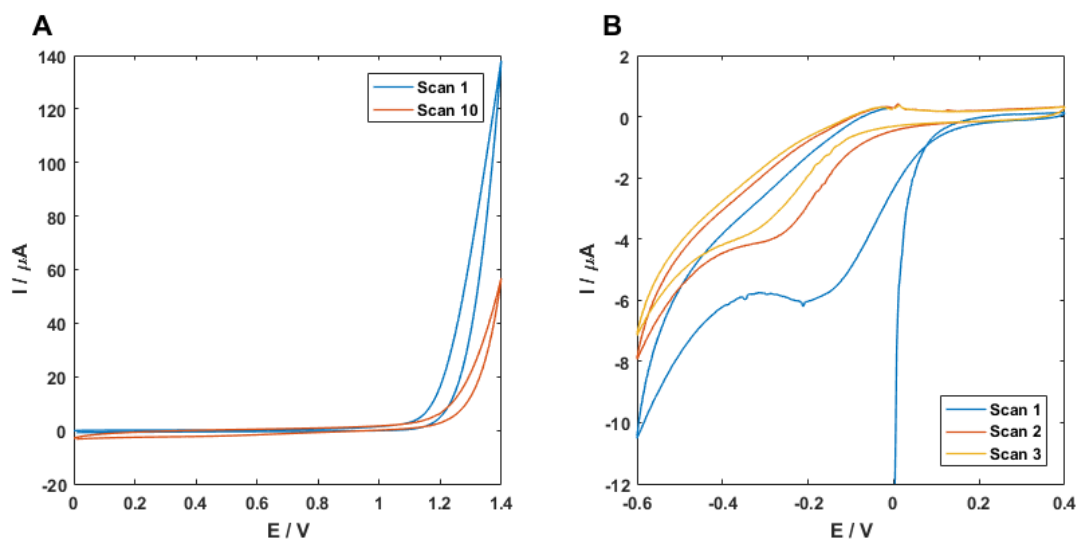


Figure 2.16 – Cleaning and electrografting voltammograms for carbon surface preparation on screen printed carbon electrodes. (A) NaCl cleaning cyclic voltammetry sweeps and (B) Aminobenzoic acid electrografting cyclic voltammetry sweeps.

Figure 2.17 shows 1 mM $\text{Fe}(\text{CN})_6^{3-/4-}$ DPVs performed on the 8 electrodes of a single modified carbon chip. The peak ΔI values are similar to those seen on the glassy carbon electrodes. DPV peak height consistency is poorer than the glassy carbon electrodes due to the greater variability in the screen-printing manufacture process and the more limited cleaning methods available, producing a relative standard deviation of 11.3%. Despite this increased variability in the baseline measurements, it was expected that screen-printed carbon could prove to be effective for DNA sensing. A shift in the DPV peak potential is observed compared to the glassy carbon system as a result of using the on-board silver reference electrode rather than an external reference electrode.

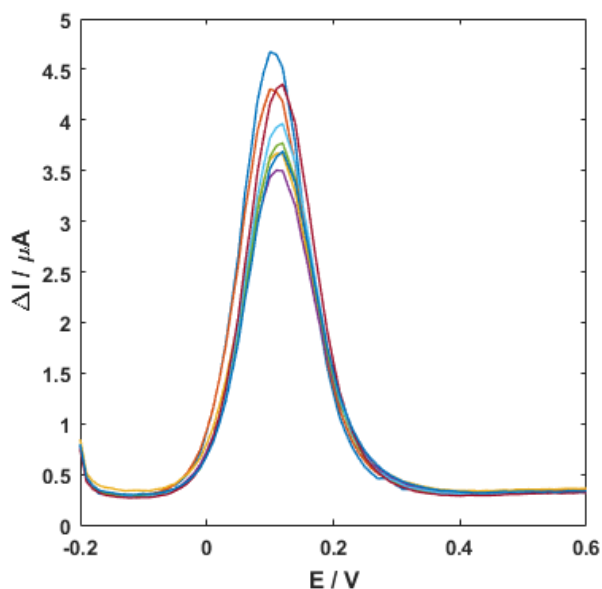


Figure 2.17 $-1\text{mM Fe(CN)}_6^{3-/4-}$ DPVs following surface modification on screen-printed carbon electrodes.

2.4.2.2 Comparison of DNA Detection on Carbon and Gold Electrodes

Detection of a synthetic DNA sequence was performed on both gold and carbon macroelectrode systems to compare the performance of each electrode and functionalisation method without complex background solutions. Figure 2.18 shows the EIS and DPV signal changes on gold and glassy carbon electrodes following incubation with target.

For EIS measurements, gold electrodes showed superior performance with a 104% signal increase compared to the 73% signal increase observed on carbon, with both electrode sets showing comparable variability. However, the reverse is true for DPV measurements, with the carbon electrode producing a 38% signal decrease compared to only 24% on the gold. Variability within the carbon DPV responses was greater than in the gold. Both signal decreases were significantly different from a 0% change (1-sample t-test, $p < 0.05$) but were not statistically different from one another.

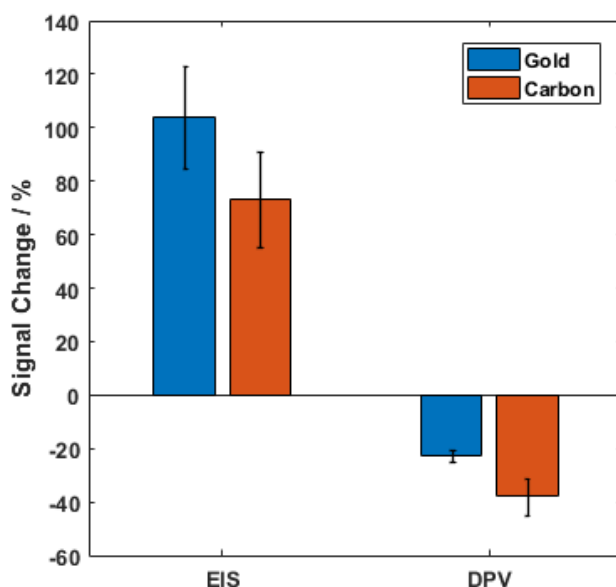


Figure 2.18 – Mean EIS (ΔR_{CT}) & DPV ($\Delta Peak I$) signal change on polycrystalline gold and glassy carbon electrodes, functionalised with their respective protocols, when detecting complementary DNA target. Error bar = SD, $n = 3$.

This discrepancy in response between the DPV and EIS results is attributed to the different initial electrochemical responses. The functionalised R_{CT} on the gold electrodes averaged 804 Ω , and showed a mean increase of 826 Ω . The carbon electrodes started with a mean R_{CT} of 2021 Ω , showing good consistency with previously characterised electrodes, and increased by 1484 Ω on average. Despite the carbon electrodes showing a greater response magnitude, the high initial impedance reduces the signal ratio. In the case of the DPV responses, the carbon electrode has a lower initial peak current (3.49 μA vs 4.54 μA for gold) and shows a greater magnitude change (-1.32 μA vs -1.03 μA). These responses may be related to the lower rate of electron transfer to $Fe(CN)_6^{3-/4-}$ on a carbon electrode, which is exacerbated by the presence of double stranded DNA. The larger initial impedance of the carbon electrode could mask this effect when converting into a signal ratio. As carbon electrodes showed better signal responses with DPV rather than EIS, EIS measurements were excluded from future measurement on carbon electrodes.

Considering the responses of the glassy carbon electrode were comparable to gold, synthetic DNA was then captured at low-cost screen-printed carbon electrodes. The 8W110 format electrodes were chosen as these electrodes allow for multiplexing up to 8 working electrodes on one chip. A dose response curve for expected electrochemical response was constructed and is shown in Figure 2.19. Figure 2.19A shows typical DPV responses for these electrodes

in 1 mM $\text{Fe}(\text{CN})_6^{3-/4-}$ before and after the hybridisation of DNA target at different concentrations. As expected, the DPV peak current decreases with the addition of target DNA, with the change in response to 100 nM DNA target greater than the change in response to 0.1 nM DNA. Figure 2.19B shows the signal change for DNA concentrations in the range 0.1 nM to 100 nM. Increasing DNA concentration results in a larger decrease in the mean DPV peak height, with a small change of -1.65% at 0.1 nM increasing to -24.56% with 100 nM target. This experiment utilised the electrode jig to isolate different DNA concentrations across the chip, so 4 concentrations could be tested in duplicate on a single chip, eliminating any effect from differences between platforms.

Carbon electrodes showed a change from baseline at a concentration as low as 100 pM. While this difference is not significant (1-sample t-test, hypothesised mean difference = 0, $p = 0.11$) owing to the low repeat number, a greater number of repeats may have facilitated detection of 100 pM DNA. This data provided a crude baseline response for the detection of DNA on carbon against which future experiments could be compared.

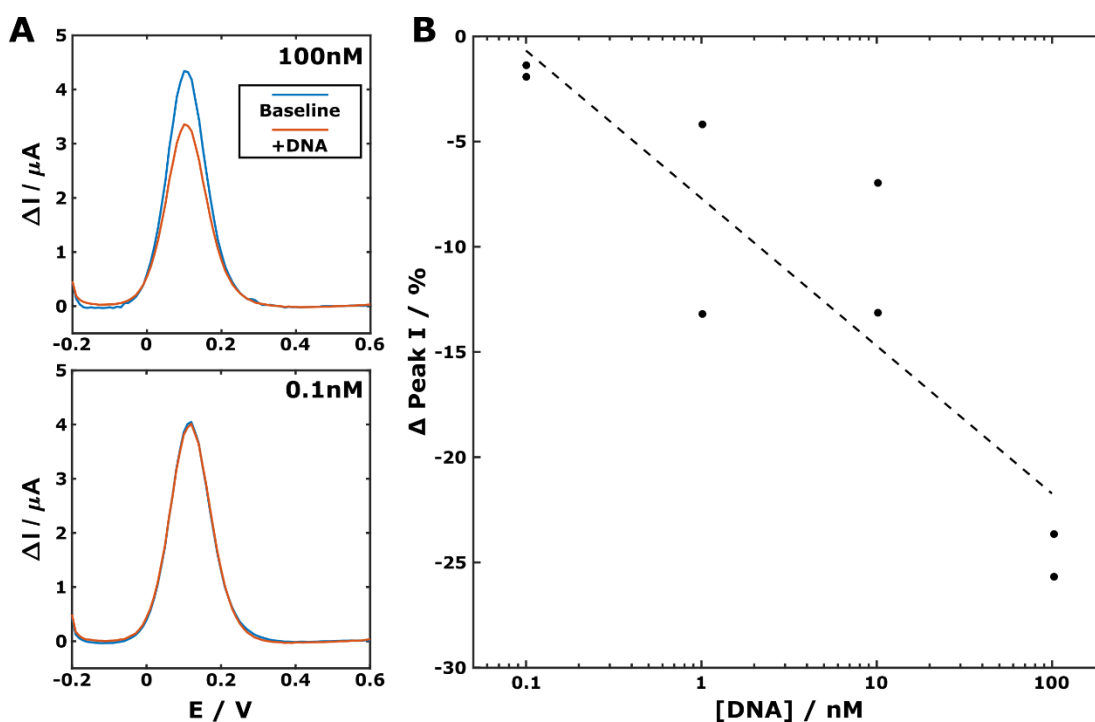


Figure 2.19 – Example 1mM $\text{Fe}(\text{CN})_6^{3-/4-}$ DPV responses and dose response curve of synthetic DNA target on carbon SPE. (A) Representative DPV responses to 100nM and 0.1nM complementary target DNA addition. (B) DPV peak ΔI change in response to DNA target concentrations between 0.1nM to 100nM. Dashed line shows linear regression approximating the trend.

2.4.3 Conclusions

The initial responses from carbon electrodes show promise for DNA detection. Similarly, to gold, the expensive glassy carbon electrodes showed low variability in characterisation response once cleaned. The lower cost screen-printed carbon surfaces were more variable but with a similar response magnitude when functionalised, indicating these surfaces could be suitable for DNA detection.

Comparison of PGE and glassy carbon electrodes showed parity between the performance of each material. Gold electrodes produced a greater signal change than carbon to the binding of a synthetic oligonucleotide when measured by EIS, but carbon was more sensitive when DPV measurements were performed. The comparative performance between carbon and gold electrode at this stage indicated that neither the covalent nor the self-assembly surface modification process was clearly best for DNA detection. These results prompted the testing of DNA detection on the low-cost screen-printed carbon electrode.

Screen-printed carbon showed high sensitivity to the hybridisation of DNA oligonucleotide. A change in the response was observed at the lowest DNA concentration tested (100 pM), although this was not statistically significant. These results suggested that low-cost carbon may also be a suitable substrate for DNA biosensor development, with a greater ability to multiplex measurement or run high throughput compared to the low-cost gold electrodes previously tested.

2.5 Methods for Design & Amplification of a Synthetic DNA Template

Many bacterial AMR genes are hosted in plasmid DNA within the cell, rather than on the chromosome, facilitating horizontal gene transfer between bacteria. In practical use, a biosensor for AMR sequences will be required to detect plasmid borne genes. A plasmid based antimicrobial resistance sequence was therefore designed to allow testing of the biosensors described here against sequences which better represented those likely to be encountered in a real sample. Several different plasmid and antibiotic resistance gene sequences were evaluated as candidates for electrochemical testing, and this section describes the work performed to prepare these targets for detection on the biosensor.

In order to detect the specific sequence of interest, an amplification step is often required to yield high quantities of the desired target. Bacterial DNA can be highly dilute in a sample depending on the organism and the infected tissue (Kelley, 2017). Amplification can increase

the quantity of detectable DNA whilst also enriching the target strand relative to non-target sequences. All antibiotic resistance that is genetically mediated, through chromosomal DNA or AMR bearing plasmids, could be enriched using such a reaction. The development of thermal and isothermal amplification reactions for several key AMR sequences is also described in this section.

2.5.1 Selection of Antibiotic Resistance Genes

E. coli was selected as the Gram-negative organism from which antibiotic resistance genes were taken. A literature search was then performed to identify existing plasmids in resistant strains of *E. coli* which contained numerous different AMR genes. Several plasmids were identified, and of these plasmid pEK499 was chosen based on its resistance profile and the organism it was isolated from (Woodford et al., 2009). This plasmid contains 10 individual resistance elements which resist against 8 different classes of antibiotic. It was isolated in the UK from an internationally disseminated clone – O25:H4-ST131 – which expresses significant antibiotic resistance, including extended spectrum beta-lactamase (ESBL) production (Nicolas-Chanoine et al., 2008, 2014). These factors mean that such a plasmid is highly relevant to the evolving AMR landscape as broad spectrum and widespread resistance elements like this pose a significant threat to worldwide public health.

From this plasmid, individual resistance genes were chosen to cover several different antibiotics. The genes *bla_{OXA-1}*, *bla_{CTX-M-15}*, *tet(A)*, and *aacA4* were selected to cover a range of resistance mechanisms and antibiotic classes. Table 2.3 describes the antibiotic resistances associated with each gene.

Table 2.3 – Genes selected for bespoke plasmid development, and their associated antibiotic resistances. (Coque et al., 2008; Frasson et al., 2011; Sugumar et al., 2014; Woodford et al., 2009)

Gene	Antibiotic Resistance Association
<i>bla_{OXA-1}</i>	Hydrolysis of aminopenicillins, ureidopenicillins, broad and narrow spectrum cephalosporins (low activity), often associated with ESBL producing genes.
<i>bla_{CTX-M-15}</i>	Extended spectrum β -lactamase with increased activity against cephalosporins. Most widely distributed CTX-M enzyme. Hydrolyses target antibiotics.
<i>tet(A)</i>	Tetracycline resistance through drug efflux.
<i>aacA4</i>	Aminoglycoside resistance through acetyltransferase activity.

2.5.2 Design of an Artificial Plasmid Containing Antibiotic Resistance Genes

In order to best reflect the form which antibiotic resistance genes would be found in a sample of resistant bacteria, the selected genes were incorporated into an artificial plasmid. This allows the biosensor to be challenged with DNA which is representative of the sequences found in real-world use and facilitates amplification of the genetic material through bacterial transformation and PCR. Ethical approval was obtained prior to plasmid purchase and generation of the genetically modified organism.

Figure 2.20 shows a diagram of the bespoke AMR plasmid designed for these experiments. The basic structure of this plasmid was provided by GeneArt (ThermoFisher Scientific, Paisley, UK), which included an *E. coli* origin of replication (pBR322) as well as two genes for confirmation of plasmid transformation: the *lacZ* alpha gene and the AmpR cassette. The *lacZ* alpha gene also contains restriction sites which allow restriction endonuclease enzymes to cleave the DNA and can be used to create a linear form of the plasmid if required.

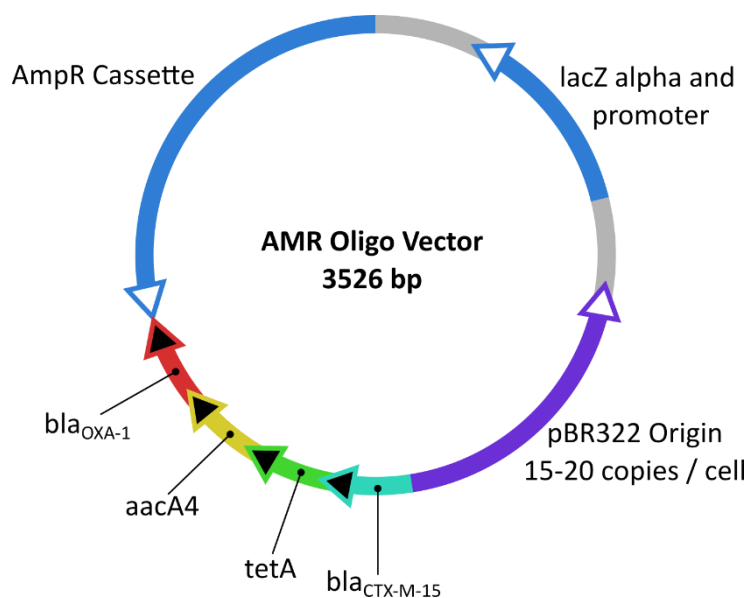


Figure 2.20 – Diagram of the artificial plasmid created to hold antibiotic resistance gene segments. Blue – Template gene sequences, Purple – Origin of replication, Grey – non-coding sequences. Antibiotic resistance sequences are labelled and coloured individually.

The antibiotic resistance genes sequences were inserted as 200 base pair segments to prevent the host bacteria from gaining functional resistance to multiple antibiotics once transformed with this plasmid. The short segments were identified by performing a Primer-BLAST search (Altschul et al., 1990) for standard PCR primers on each gene individually, with a product limit of 200 base pairs, and then selecting the 200 base pair region which contained the greatest number of suggested amplicons. These segments were then inserted into the GeneArt vector in the reverse direction to the origin of replication and the *lacZ* and AmpR promoter regions to further minimise the risk of transcription of these sequences. Finally, 10 base pair repeat sequences of stuffer DNA, each containing an *E. coli* stop codon, were included between the gene segments. This was again to reduce the likelihood of transcription of these sequences, but also to provide a buffer between each gene segment for future processing.

2.5.3 Transformation of Competent *E. coli* with Plasmid DNA

The artificial plasmid was introduced into competent *E. coli* cells to allow amplification of the plasmid DNA through bacterial culture, as well as for long term storage. NEB 10-beta competent *E. coli* cells (New England BioLabs, Hitchin, UK) were used as host cells. Powdered LB medium (SigmaAldrich, UK) was used for both liquid culture and agar plates. Competent cells were thawed on ice and then 10 ng pure plasmid DNA was introduced, and the mixture

held on ice for 30 minutes. The bacteria were then “heat shocked” by heating to 42°C in a water bath for 30 seconds, then returned to ice for 2 minutes. This suspension was then mixed with 250 µL SOC outgrowth medium (NEB, Hitchin, UK) which was preheated to 37°C. This mixture was incubated at 37°C with shaking at 250 rpm for 1 hour. Aliquots of this broth (1 µL, 10 µL and 100 µL) were spread on LB agar plates which contained 100 µg/mL Carbenicillin and incubated at 37°C overnight.

Transformed *E. coli* cells were maintained on LB agar plates containing 100 µg/mL ampicillin (SigmaAldrich, UK) at 4°C for up to four weeks. A glycerol stock was also prepared for long term storage. Glycerol was added to LB media (20% v/v) containing transformed cells which had been grown overnight to a final density of 3×10^9 CFU/mL. This stock was frozen at -80°C.

Extraction and preparation of concentrated pure plasmid was performed with the use of a GeneJET Plasmid Midiprep Kit (Thermo Scientific, Vilnius, Lithuania). 50 mL of overnight culture in LB media was centrifuged to pellet cells, which were then treated following the protocol provided with the kit. Extracted plasmid was quantified using a Qubit4 Fluorometer (ThermoFisher Scientific, Loughburgh UK) and double-stranded DNA assay kit.

2.5.4 Growth and Maintenance of *E. coli* Cultures

E. coli cultures were grown and maintained under a standard set of conditions every 4 weeks to maintain the cultures. All work with bacterial plates or culture was performed under a high Bunsen burner flame to maintain sterility of the overnight cultures and plates. Single colonies were selected from a plate and inoculated into 50 mL of autoclaved sterile LB media (25 g / L) containing 100 µg/mL ampicillin. This media was incubated overnight at 37°C on a shaking incubator.

When producing new agar plates for storage, 1.2g agar was added to 80 mL of LB media and sterilised by autoclaving. Three vials containing 9.9 mL 1xPBS were also autoclaved at this time. When slightly cooled, ampicillin was added to the agar to a final concentration of 100 µg/mL and plates were poured in triplicate under sterile conditions. These plates were kept in an incubator at 37°C overnight before use. Overnight bacterial culture was serially diluted by a factor of 10^{-2} three times, in 100µL volumes, to achieve a final 10^{-6} dilution. 100 µL of this final dilution was then transferred onto each agar plate and spread evenly using disposable spreaders. Plates were incubated overnight at 37°C before colony counting and storage at 4°C.

2.5.5 Production of DNA Targets from a Synthetic Plasmid

The artificial plasmid was used to produce DNA targets which could be detected on the biosensor platform. In a clinical sample, the plasmids containing the genes of interest could be present in low numbers and may not be at high concentration in solution once the bacteria are lysed. Some method to enhance the binding signal is often required to enable detection. This can be achieved by direct amplification of the target molecule, by downstream signal amplification through positive feedback mechanisms, or through a combination of these methods. DNA target amplification by PCR is a relatively simple and widely employed process and has been used here to produce numerous copies of a specific target gene sequence for detection.

2.5.5.1 Benchtop PCR

PCR was performed using a HotStarTaq DNA polymerase and dNTP mix (Qiagen, Hilden, Germany), and a mini8 benchtop thermocycler (miniPCR, Boston, USA). 10 μ L of PCR buffer, 2 μ L dNTP mixture and 0.5 μ L HotStarTaq Plus DNA polymerase were added to each reaction tube and mixed thoroughly.

0.25 μ L of each primer (for final concentration of 0.25 μ M) flanking the sequence to be amplified were added next. Table 2.4 shows the primer sequences used to amplify each gene segment, as well as the resulting product length. These primer pairs were selected from the list generated when identifying the 200 base pair gene segments to be included in the synthetic plasmid. Primers with a low self-complementarity at the 3' end, and those with similar melting temperatures, were prioritised to optimise the efficiency of the PCR reaction.

Table 2.4 – Primers used for traditional PCR amplification of each gene segment.

Gene	Primer (5' to 3')	Tm / °C	Length / bp
OXA-1	AACAGAAGCATGGCTCGAAA	58.1	116
	TGGTGTTTTCTATGGCTGAGTT	57.9	
tetA	GCATGATGAAGAAGACCGCCA	61.0	121
	GAGTCGCACAAAGGCGAAC	59.8	
CTX-M-15	TGTCGCCCAATGCTTTACCC	61.0	112
	ACCGAGCCGACGTTAAACAC	61.0	
aacA4	AGCAACGATTCCGTCACT	60.0	65
	AGCCACTCATAGAGCATCGC	60.0	

Following the addition of primers, molecular biology grade water and DNA template were added. The volume of DNA template was such that there was less than 1 μg of template DNA per reaction. Distilled water was added to bring the total reaction volume to 100 μL .

Once prepared, the reaction took place in the mini8 benchtop thermocycler. All reactions began with a 5-minute enzyme activation step at 95°C. Temperature cycling then proceeded for 30 cycles, with 94°C denaturing, annealing at 5°C below the melting temperature of the primers, and primer extension at 72°C. A final extension at 72°C for 10 minutes allowed all primer extensions to complete. The amplified product was frozen for future use.

2.5.5.2 Isothermal Amplification

As previously discussed, thermal PCR is difficult to implement in a point-of-care setting due to the power requirements and the long time-to-result of typical reactions. There are several PCR techniques which can run at a single temperature and can produce amplicon much more rapidly, which are attractive features for diagnostic biosensing. In this work recombinase polymerase amplification (RPA) was selected as it has several advantageous characteristics; the primer design requirements are relatively simple; the assay can produce detectable DNA levels in as little as 10 minutes and runs to completion in only 40 minutes, and the polymerase is effective around physiological temperature (TwistDx Ltd, 2020). These factors make working with RPA simple and would help to lower the cost and complexity of the final biosensor compared to some other isothermal PCR methods which require complex primer design or higher temperatures.

RPA kits were obtained from TwistDx (Maidenhead, UK) in the Liquid Basic format, with all reagents already in solution. RPA was prepared according to the instructions supplied with the kit, unless otherwise described. 25 μL reaction buffer, 9 μL dNTPs (for final concentration of 1.8 mM as recommended), 0.2 μL molecular biology grade water, 5 μL Basic E-mix, and 2.4 μL 10 μM each primer were combined in a tube for each reaction and mixed. 2.5 μL core reaction mix (containing polymerase, recombinase, and single-stranded DNA binding proteins) was then added and the reaction mixed once more. 1 μL template DNA and 2.5 μL Magnesium acetate were finally added to the reaction tube lid, and the tube was centrifuged to initiate the reaction. Tubes were gently agitated to mix, centrifuged once more and then incubated at 39°C for up to 40 minutes. Primer sequences used for these isothermal reactions are given in Table 5.3. Completed reactions were frozen for future use.

Table 2.5 – Primers used for isothermal amplification of the *bla_{OXA-1}* gene segment.

Gene	Primer (5' to 3')	Direction	Product Length / bp
OXA-1	AACAGAAGCATGGCTCGAAAGTAGCTTAAAAAT	Forward	115
	GGTGTTTTCTATGGCTGAGTTTTTAACTGGGAG	Reverse	

Figure 2.21 gives an overview of the RPA reaction process. Accessory proteins present in the RPA mixture allow this reaction to proceed without the thermal cycling required for PCR. Initially, a primer-recombinase filament (formed during the reaction preparation) seeks a complementary sequence in the target DNA (Figure 2.21A). Upon locating a complementary sequence, the primer hybridises to the target, displacing the homologous strand (Figure 2.21B). This displaced strand is stabilised by single-stranded binding proteins, and a polymerase binds the 3' end of the primer. The polymerase then elongates the bound primer, further displacing the homologous DNA strand (Figure 2.21C). This results in the formation of a new DNA duplex (Figure 2.21D). The reverse primer extension reaction can occur simultaneously, exponentially amplifying the original template sequence.

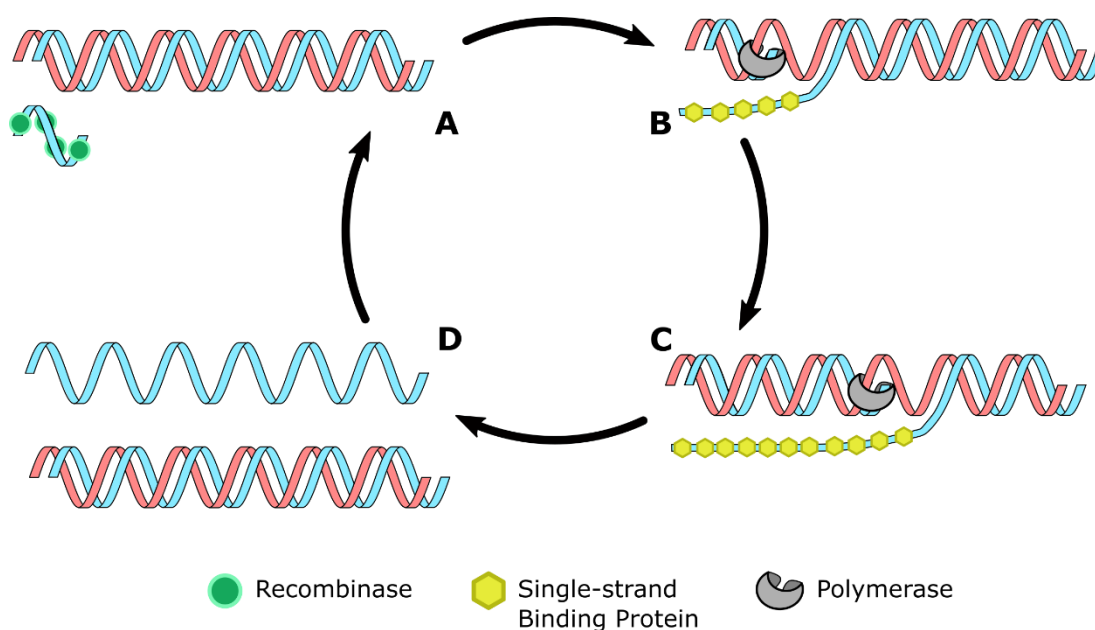


Figure 2.21 – Diagram of a typical RPA reaction showing elongation of one primer. (A) Primer-recombinase filaments seek complementary sequences on a target DNA strand. (B) Recombinase inserts the primer, displacing the homologous strand. (C) The polymerase

extends the inserted primer, displacing further DNA which is stabilised by single-strand binding proteins. (D) A new duplex is formed.

2.5.5.3 Validation of Amplified Product

PCR product formation was quantified on the Qubit4 fluorometer using the double stranded DNA assay, and an agarose gel was used for qualitative examination. This was performed in a blueGel portable DNA electrophoresis machine (miniPCR, Boston, USA). A 2% Agarose gel was cast with 1x Tris-Borate-EDTA (TBE) buffer and 1x GelGreen nucleic acid stain (miniPCR, Boston, USA) or SybrSafe stain (ThermoFisher). A HyperLadder 50bp molecular weight marker (Bioline, London, UK) was used as a reference and 1 μ L of the included DNA loading buffer was used to load 4 μ L of PCR product into the gel.

Figure 2.22 shows the results of a thermal PCR amplification on each of the AMR gene sequences. Each band appears at the correct height relative to the molecular marker, indicating that the expected product has been amplified successfully. The lanes containing CTX were run on a separate gel as production of a successful PCR reaction for CTX took longer than for other amplicons, and this reaction was validated at a later date.

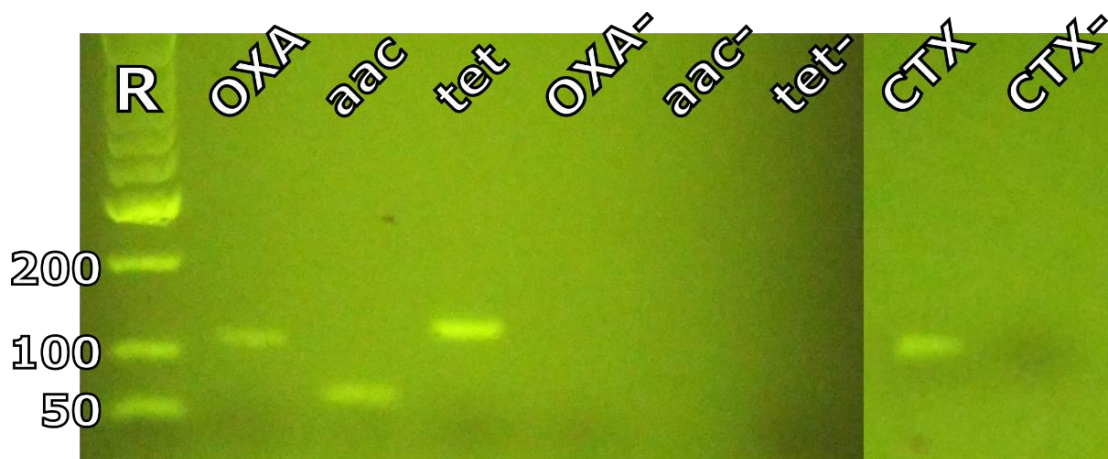


Figure 2.22 – Image of 2% agarose gel containing PCR amplicons of different plasmid gene segments (identified at top). No template controls are included as a negative control (indicated by “-” following the gene name). CTX was run on a separate gel and the reference lanes aligned to place the amplicon at the correct height relative to the other lanes. R – Hyperladder 50bp molecular weight marker (Bioline). Stained with GelGreen DNA stain.

Isothermal PCR product was also run on an agarose gel as shown in Figure 2.23. With PCR primers (Figure 2.23A) no amplification product was produced. This is not unexpected considering RPA typically requires longer primer sequences and the reaction was not optimised for use with shorter primers. A clear band at the expected height is present in the reaction containing RPA primers (Figure 2.23B). No bands equivalent to the OXA-1 gene are visible in the positive or negative control reactions.

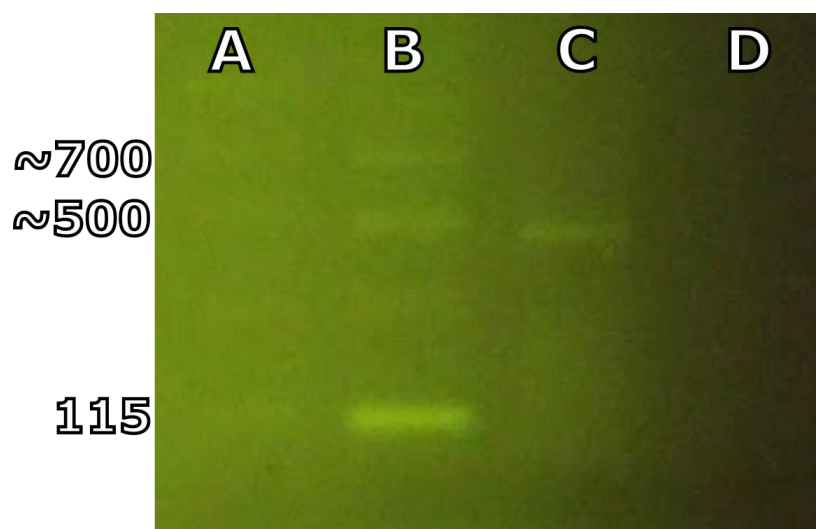


Figure 2.23 – Image of 2% agarose gel isothermal PCR amplicons of the *bla_{OXA-1}* gene. Approximate fraction length indicated on left (reference marker excluded due to distortion). A – RPA with PCR primers. B – RPA with RPA primers. C – RPA positive control. D – No template control. Stained with GelGreen DNA stain.

2.6 Conclusions

Characterisation of a variety of electrode systems was performed to determine which low-cost electrode format showed the greatest suitability for DNA biosensing. Following a comparison of each electrode type when clean, both screen-printed and sputter coated gold electrodes showed electrochemical responses consistent with those observed on the “gold standard” polycrystalline gold electrode.

Application of a DNA SAM layer to these electrodes allowed the detection of a DNA target in solution on each electrode type. Different cleaning procedures for each electrode type were examined, with a standard sulphuric acid CV cycling process, typical for gold electrodes, found to be optimal for the electrodes tested.

In response to DNA target binding, a large signal increase was observed on polycrystalline gold electrodes. Signal increases were similarly observed on all electrode types tested, with BT SPEs producing the greatest EIS signal response. Different SAM layers consisting of either a 6-carbon or 3-carbon alkanethiol were also tested. Shorter chain alkanethiols produced greater signal responses to DNA target binding on all electrode types, although with an increase in response variability. Based on this data, each electrode type was included in future experiments for testing of DNA amplicons in more complex background solutions.

Glassy carbon and screen-printed carbon electrodes were also tested for their performance as a DNA biosensor. As with the gold substrate, the low-cost screen-printed carbon exhibited electrochemical responses similar to the benchtop glassy carbon electrode format. Covalent modification of this surface by electrografting, NHS/EDC couple and DNA probe incubation produced signal changes in response to DNA binding comparable to those of the PGE. A smaller signal change was observed on screen-printed carbon.

A synthetic AMR plasmid system was also developed to provide a realistic DNA target for nucleic acid detection on these electrode systems. PCR and isothermal RPA amplification reactions were developed for a number of different AMR genes which were represented on the plasmid. These reactions showed high specificity and minimal cross-reactivity between the different gene sequences within the plasmid.

These results provide a foundation for the development of a DNA biosensor for antimicrobial resistance gene sequences. The combination of a specific amplification reaction and a sensitive detection scheme on a low-cost system could provide a route to point-of-care genetic testing for complex bacterial samples. The next chapter details further work to combine these two distinct elements onto a single sensing platform.

3 Electrochemical Detection of Antimicrobial Resistance Genes

Based on the promising results obtained with DNA oligonucleotides on gold electrodes, further experiments to detect PCR amplicon and reduce signal variability were undertaken. In this chapter, PCR amplicons of clinically relevant antimicrobial resistance genes were detected on a variety of gold and carbon electrodes. The use of a low cost potentiostat with on-board gold electrodes was explored, which would facilitate cost-effective and portable detection of antimicrobial resistance genes. Electrochemical detection of AMR genes amplified through RPA was also performed, moving away from time-consuming benchtop PCR reactions to the more portable and rapid isothermal format. These experiments lead to a system which is more suitable for point-of-care testing than previous detection schemes described here.

3.1 Detecting a Clinically Relevant AMR Gene Sequence on Gold Electrodes

Once a surface functionalisation method for DNA detection had been identified, and an amplification reaction for the target sequence designed and validated, experiments to test electrode response to PCR amplicons were performed. All electrode types from the previous chapter were prepared using a consistent protocol and challenged with amplicons of the bla_{OXA-1} (OXA-1) gene at a fixed concentration. Following on from this, PGEs and the most promising low-cost electrode format were tested for specificity by applying a complementary PCR amplicon and non-complementary oligonucleotide or amplicon. These experiments aimed to show specific detection of clinically relevant AMR gene sequences and demonstrate specificity of the sensing surface to only the amplicon of interest.

3.1.1 Methods

3.1.1.1 Amplicon Detection on Different Electrode Formats

All electrode types were cleaned according to the most favourable cleaning method identified in the previously presented DNA detection work, which typically consisted of CV cycling under 0.1M H_2SO_4 . Electrodes were then incubated using the co-immobilisation method as this proved the best method for the PGE which served as a benchmark for this test. 3 μ M OXA-1 Probe (Table 3.1) and 30 μ M MCH or MCP were pre-reduced in immobilisation buffer containing excess TCEP before incubating on the electrodes overnight at room temperature. Following incubation, electrodes were rinsed as previously described and backfilled for 1 hour in MCH or MCP, also pre-reduced in excess TCEP.

Table 3.1 – DNA probe sequence used for PCR amplicon. Sequences presented 5' to 3'.

OXA-1 Probe	SH- (CH ₂) ₆ - AACAGAAGCATGGCTCGAAA
-------------	--

Electrodes were rinsed in diH₂O and held in measurement buffer for 10 minutes prior to baseline measurements. PCR amplicons were heated to 95°C prior to addition to the electrodes. Each electrode was incubated for 1 hour with 0.74 μM OXA-1 amplicon, rinsed in the buffers described in Section 2.3.1, and held again in measurement solution before hybridisation measurements were recorded.

3.1.1.2 Specificity Testing on PGEs and TFGEs

PCR mixture represents a more complex background solution than the PBS buffers due to the high concentration of PCR proteins and other reaction components. Tests comparing the detection of a complementary PCR amplicon to a non-complementary oligonucleotide sequence in PBS, and then the discrimination of complementary and non-complementary PCR amplicons were performed.

For specificity testing on PGEs, the above functionalisation protocol was used with an MCP SAM. At the stage where PCR amplicon was applied, electrodes received either 0.74 μM OXA-1 amplicon (positive) or 0.74 μM non-complementary oligo in PBS (negative).

TFGEs were CV cleaned for 15 cycles in 0.1M H₂SO₄ before incubation with 20 μL probe solution overnight. They were otherwise treated in the same manner as the PGEs throughout the experiment. These electrodes were incubated with 0.74 μM OXA-1 amplicon (positive) or 0.74 μM non-complementary tetA amplicon (negative).

3.1.2 Results & Discussion

3.1.2.1 Amplicon Detection on Different Electrode Formats

Figure 3.1 shows the mean change in R_{CT} following hybridisation with complementary PCR amplicon on MCH and MCP based DNA SAMs. As previously observed, MCP SAMs produced a greater signal change than MCH SAMs which is consistent across all electrodes. PGEs with both MCH and MCP SAMs showed good response consistency and, using the co-immobilisation method, achieved a signal change with the MCP SAM greater than those observed for short DNA oligo targets. The MCH signal change was reduced compared to short oligonucleotide targets.

AT SPEs showed a poor response to DNA hybridisation, with MCH based SAMs giving a mean decrease in signal. This could suggest that the SAM formed atypically, as previous results with CV cleaning produced increases in signal consistently. These results more closely resemble the initial immersion cleaning results, indicating the electrode may not have been adequately cleaned. A similar MCH response is observed on the TFGEs, which showed the poorest $\text{Fe}(\text{CN})_6^{3-/4-}$ responses following cleaning with CV, supporting this hypothesis. The AT MCP response shows very a small mean change, again likely due to cleaning issues on these electrodes causing improper formation of the DNA SAM. Both the MCH and MCP responses of AT SPEs had a high R_{CT} prior to hybridisation, and the MCP initial impedance was high compared to prior experiments. There may have been some isolated effect from the surface roughness, ink composition or interaction with the partially cleaned areas on the electrode that led to an unexpectedly dense monolayer forming, or some surface fouling which was not effectively removed by CV cleaning in this case.

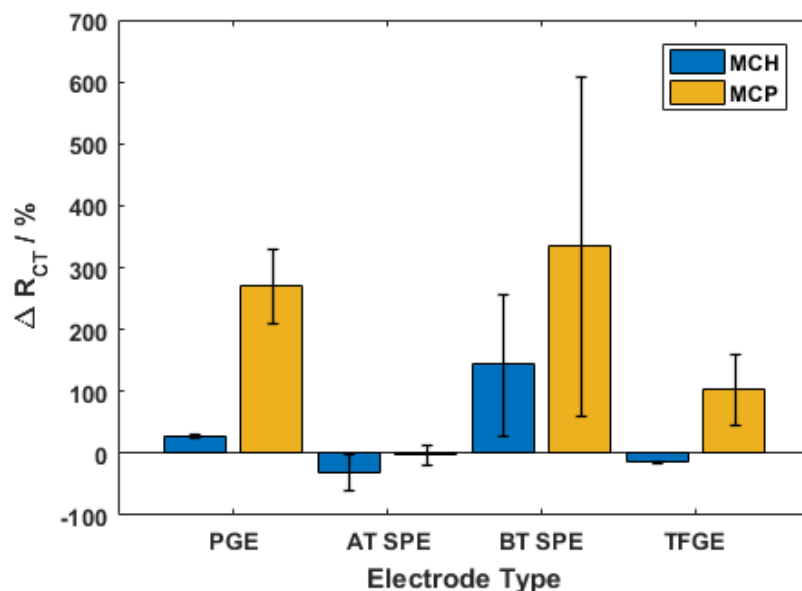


Figure 3.1 – Mean electrochemical impedance spectroscopy R_{CT} change for 2mM $\text{Fe}(\text{CN})_6^{3-/4-}$ on different electrode types, modified with 6-mercapto-1-hexanol (MCH) or 6-mercapto-1-propanol (MCP), in response to PCR amplicon binding. SPE – screen-printed electrode, PGE – polycrystalline gold electrode, TFGE – thin-film gold electrode. Error bars = SD, $n = 3$. BT SPEs showed high response changes which appear typical of these electrodes. However, on both MCH and MCP SAMs the response variability was large. It is likely that proteins from the complex PCR background solution can become trapped within the globular surface structure of the BT SPE, where washing might be unable to dislodge them. Proteins, which

are much larger than DNA, trapped at the surface could present a large barrier to charge transfer which contributes to these large responses. Variability would be expected to relate to the amount of protein trapped at the surface which is likely to differ significantly between each electrode.

TFGEs showed a similar response to AT SPEs when incubated with an MCH SAM, as previously discussed. The MCP response of TFGEs was encouraging, with a moderate signal increase and less relative standard deviation than the other low-cost electrodes examined. TFGEs were therefore determined to be the most suitable candidate for further testing in this sensing format.

3.1.2.2 Specificity Testing on PGEs and TFGEs

PGEs and TFGEs were also tested with a negative control DNA sequence, which consisted of the tetA gene segment from the AMR resistance plasmid. Figure 3.2 shows the DPV and EIS results with PGEs, where the negative control consisted of a purified oligonucleotide with the tetA gene sequence diluted in PBS. Oligonucleotide was used at this stage as a PCR reaction for tetA had not yet been developed. As expected, based on previous results, an increase in impedance (and a corresponding decrease in the DPV peak height) was observed. A significant difference was observed between the positive and negative electrodes (2-sample T-test, $p = 0.005$,) with a large signal increase on the positive. Some signal was generated on the negative, which is due to non-specific interaction of the DNA oligo with the surface. Further reduction of this signal could be achieved with the use of a more stringent wash buffer. However, this background signal was small compared to the positive and had low variability, indicating good screening of non-specific interactions from positive DNA target binding with an MCP SAM.

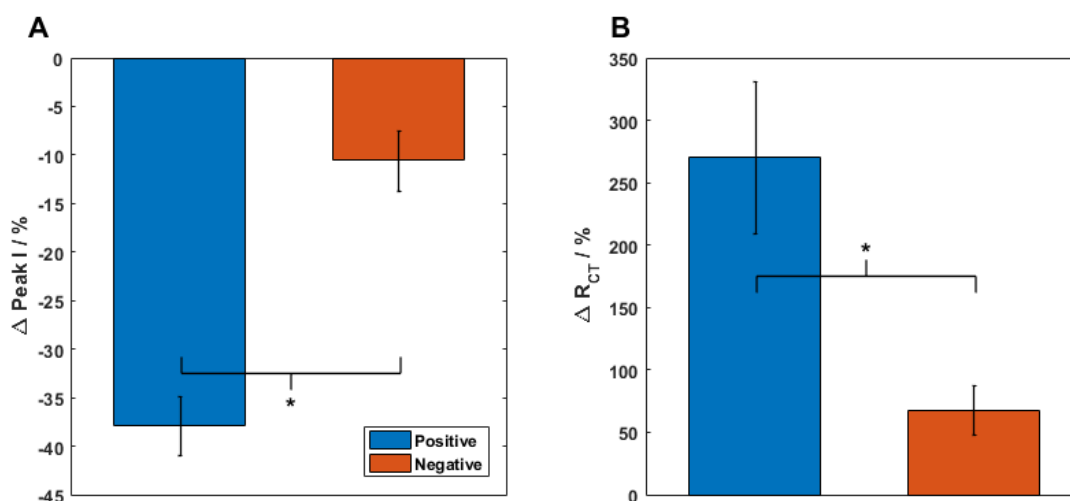


Figure 3.2 – PCR amplicon detection and sequence specificity testing on PGEs. (A) DPV and (B) EIS $\text{Fe}(\text{CN})_6^{3-/4-}$ response changes. Positive consists of Oxa PCR amplicon while negative is non-complementary tetA oligonucleotide. Error bars = SD, $n = 3$. * indicates 2-sample T-test p -value < 0.05.

On the TFGEs, a similar experiment was performed to see if the MCP SAM could effectively block the lower cost electrodes from non-specific DNA binding. The negative target used was a tetA PCR amplicon from the AMR plasmid, to test the specificity of the surface against PCR protein fouling in addition to DNA interactions. In a point-of-care device, a negative result would consist of a PCR which had not amplified any target DNA, so discrimination of negative or blank PCR from a positive reaction is also critical for accurate detection.

Figure 3.3 shows the response of TFGEs to PCR amplified DNA targets. As previously observed the response size is smaller than on the PGE, but a difference between the positive and negative mean response is clear. Variability in the positive response is at typical levels for TFGEs, but there is also high variability in the negative response. This is believed to be due to interactions between the PCR proteins and the SAM surface, which could be mitigated through enhanced washing procedures. Purification of the DNA from the PCR background is possible, but would add time, cost and complexity to a point-of-care assay and so was avoided whenever possible. Improved blocking of the electrode through the use of MCH or an alternative SAM molecule could also reduce response variability, although MCH responses on TFGEs were previously poor. These results were encouraging that discrimination of PCR product could be performed on low-cost gold electrodes with further optimisation.

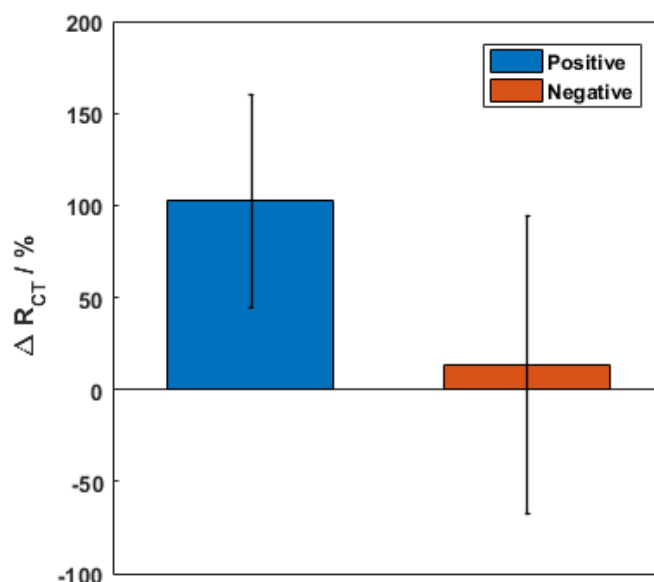


Figure 3.3 – PCR amplicon detection on TFGEs. Positive and negative consist of Oxa PCR amplicon and tetA PCR amplicon respectively. Error bars = SD, $n = 3$.

3.1.3 Conclusions

Based upon these findings, it appeared that TFGEs provided the best surface for electrochemical detection of DNA. BT SPEs showed good response magnitudes but proved too inconsistent during the SAM formation and incubation processes which resulted in high variability. In some instances, electrodes within one experiment showed both increases and decreases in signal on both AT and BT SPEs. These results suggest that forming a uniform SAM layer on screen-printed electrodes is challenging due to the rough nature of the electrode and the combined carbon / gold composition. Such issues were not observed on TFGEs with an MCP SAM, where the addition of DNA target reliably produced an increase in R_{CT} . TFGEs with an MCH SAM layer performed more poorly, and so MCP was pursued for further testing. Statistical discrimination of PCR amplicons was not possible but a large difference between the mean responses was clearly observed. Further investigations into low-cost sensor systems for PCR amplicon detection were planned to build upon the results obtained here.

3.2 Electrochemical Detection of PCR Product Using a Low Cost Potentiostat

In addition to the challenges of miniaturising an assay and electrode to detect DNA, the electronics required for electrochemical measurements can also be too bulky for a point-of-care test. Portable potentiostat systems could facilitate point-of-care testing without the use of external computer or measurement hardware, enabling more effective disease monitoring in the field, the clinic or at home. A number of portable systems designed to meet this need have been developed. The CheapStat (Rowe et al., 2011) was developed as an open source do-it-yourself potentiostat for educational use and can perform a variety of voltammetric measurements. This device was demonstrated on $\text{Fe}(\text{CN})_6^{3-/4-}$, ascorbic acid and N-acetyl-para-aminophenol, and has since been used to detect the presence of lead in drinking water (Lama and Tarrillo, 2018). Improvements upon the CheapStat came with devices such as the uMED (Nemiroski et al., 2014) and the DStat (Dryden and Wheeler, 2015), which have lower cost and better sensitivity respectively. Both devices also expanded the available measurement routines and showed much greater comparability to commercial potentiostats. Since these early designs, many low-cost potentiostat systems have been developed to improve sensitivity, reduce costs and integrate better with commercial electrodes and wearable sensors (Ahmadraji et al., 2017; Ainla et al., 2018; Aznar-Poveda et al., 2018; Bezuidenhout et al., 2018; Glasscott et al., 2020; Hoilett et al., 2020; Li et al., 2018; Lopin and Lopin, 2018; Meloni, 2016; Yokus et al., 2020). For example, such devices have been used as part of low-cost scanning electrochemical microscopes (Guver et al., 2019; Meloni, 2017) or to detect protein binding through impedance changes at a biotinylated SAM (Jiang et al., 2017).

Despite these advances and the numerous designs available, there are a limited number of reports where low-cost potentiostats have been used for diagnostic tests. Tests for malaria (Nemiroski et al., 2014), cortisol (Cruz et al., 2014), tumour necrosis factor α (Pruna et al., 2018), horseradish peroxidase (Montes-Cebrián et al., 2019), blood alcohol concentration (Aymerich et al., 2018), cocaine (Hoilett et al., 2020) and inflammation biomarkers in urine (C.-Y. Huang et al., 2015) have all been performed using low-cost devices, showing these systems are capable of detecting a wide range of analytes. However, DNA biosensing is an area not widely investigated using these low-cost systems. This may be due to the lack of more complex surface sensitive measurements being implemented on these devices, although some sensors with the capability to perform these measurements do exist (Jiang et al., 2017; Pruna et al., 2018). The CheapStat was used to identify a 200 nM synthetic DNA

target in PCR mixture using square wave voltammetry but has not been applied against clinically relevant sequences since. Another low-cost and portable potentiostat system based on CMOS technology was used to detect hybridisation of 60 nM DNA (Levine et al., 2009). The BDTminiSTAT100, a commercial portable potentiostat, has been used in the detection of RNA when coupled to a reverse-transcription isothermal amplification reaction (Nagatani et al., 2011). Further use of low-cost devices for DNA biosensing could support development of such systems into diagnostic tools and encourage their use for other relevant analytes.

In this section, the use of a newly developed SimpleStat system for DNA detection is examined (Butterworth et al., 2019b). The SimpleStat is a PCB potentiostat designed with as few components as possible to minimise complexity and cost. These devices could be mass produced at less than £3.50 per board and support on-board testing or connection to an external electrochemical cell, with integrated readout onto the board in the form of an LED which illuminates upon detection of the target. Electrochemical behaviour of the on-board gold electrodes is shown, followed by detection of PCR product binding on these electrodes using a commercial potentiostat system. Comparisons between the performance of the SimpleStat and a commercial potentiostat are made to determine if there is any performance loss from moving to a lower cost format.

3.2.1 SimpleStat Design Overview

Figure 3.4 shows the layout of the SimpleStat PCB and a circuit schematic of the device. Highlighted in orange is an ATtiny412 microcontroller (Microchip Technology Inc.) which performs circuit control and conversion of the output data. This microcontroller is low cost (<\$1) and contains analogue to digital (ADC) and digital to analogue conversion (DAC) functions as well as a built-in oscillator crystal for timekeeping. The chip is also easy to solder due to having a low number of pins making fabrication of the device more accessible. This microcontroller is connected to an LED (also highlighted orange) which can be used for simple positive / negative data readout without connecting additional hardware.

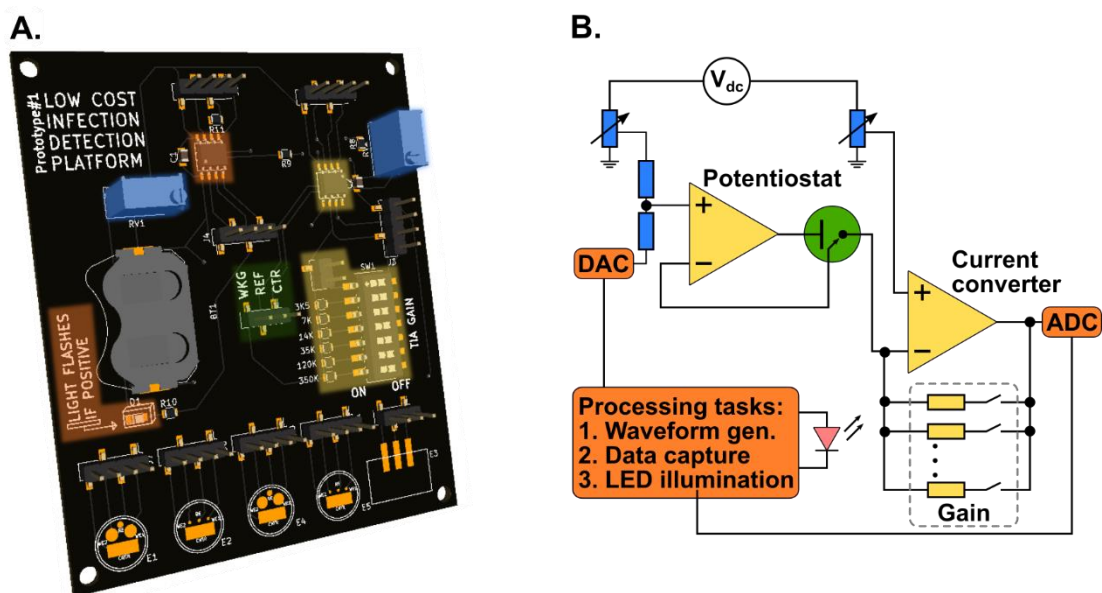


Figure 3.4 – SimpleStat PCB and circuit diagram. (A) 7 cm x 8 cm PCB layout with key components highlighted. (B) Circuit diagram showing microcontroller functions (orange), calibration resistors (blue), the measurement circuit (yellow) and the electrochemical cell (green).

Highlighted in yellow are the measurement circuit and gain resistors. The operational amplifiers which perform the measurement are biased to 1.25 V vs ground using a resistor network, allowing a measurement to be performed in the potential range -0.6 V to 0.6 V. This bias can be adjusted using the two trim potentiometers (blue highlight) to calibrate the circuit before measurements. The gain resistors allow the measurement circuit to be calibrated for different current ranges and are manually adjusted using a DIP switch. These additions reduce circuit complexity and allow a degree of flexibility in measurement conditions without introducing more complicated control systems.

Highlighted in green is the electrochemical cell. On the PCB this consists of three pins which can be attached to the working, reference and counter electrodes of one of the on-board electrode arrays, to a three-pin connector for use with commercial electrode systems, or to a standard benchtop electrochemical setup. The on-board electrodes consist of a pair of electrodes, either 2 mm or 0.5 mm diameter, which are coated in gold at the PCB manufacture stage. This gold coating is widely available as a standard protective layer for the underlying copper but is not designed for electrochemical measurement. Each electrode pair has an associated gold reference and counter electrode. In order to reduce noise in the

results, the SimpleStat firmware performs DPV measurements in triplicate which are then averaged to produce the final signal.

3.2.2 Methods

Electrode characterisation was performed using an Autolab PGSTAT204 commercial potentiostat connected to the SimpleStat on-board working, reference and counter electrodes. All measurements were performed in 2 mM $\text{Fe}(\text{CN})_6^{3-/4-}$ in 50 mM PB + 200 mM KCl.

CV measurements were performed from -0.3 V to +0.3 V with a scan rate of 0.1 V/s. DPV was performed from -0.4 V to +0.4 V at a scan rate of 0.1 V/s. A step potential of 5 mV, pulse potential of 25 mV and pulse time of 50 ms were used. For EIS measurement, the frequency range of 100 kHz to 0.1 Hz was examined, with 10 frequencies per decade and an amplitude of 10 mV applied to the OCP. Electrodes were characterised before cleaning, and then again following an immersion in 0.1M H_2SO_4 for one hour.

For DNA detection on PCB electrodes, measurements were performed using a PalmSens PS4 potentiostat and functionalisation followed the protocol developed by Keighley et al. (2008b). Electrodes were incubated overnight at 30°C with 3 μM OXA probe and 30 μM MCP in PBS + TCEP solution, then rinsed with 200 mM PB, 10 mM PB and 10 mM PB + 10 mM EDTA. Electrodes were then backfilled with 1 mM MCP pre-reduced in PBS + TCEP before rinsing in diH_2O . Each electrode was then incubated with 3 μL heated PCR product, either containing OXA (5.4 ng/ μL) or tetA (15.1 ng/ μL) amplicon. Electrodes were incubated for one hour, then rinsed with 200 mM PB + 800 mM KCl and 50 mM PB + 200 mM KCl before performing second measurements.

When comparing the SimpleStat and PalmSens potentiostats, three polycrystalline gold electrodes were functionalised as described above. Baseline measurements with both potentiostats were taken with electrodes immersed in 2 mM or 0.1 mM $\text{Fe}(\text{CN})_6^{3-/4-}$ solutions. Previously prepared PCR reactions were then heated to 95°C for 5 minutes to denature the DNA amplicon. Each electrode was incubated with 20 μL PCR mixture for one hour at 30°C, before rinsing as described above and measurements repeated.

3.2.3 Results and Discussion

3.2.3.1 Testing On-Board PCB Electrodes

Figure 3.5 shows the CV data for $\text{Fe}(\text{CN})_6^{3-/4-}$ measured over the on-board 2 mm gold electrodes. The raw CV responses (Fig 6.3A) show a classic redox response with a peak-to-peak separation of 83 mV, indicating the surface is suitably clean for measurements. These CV scans are centred around 0 V due to the reference electrode also being gold. Using the Randles-Sevcik equation the electrode area was calculated to be between 0.046 and 0.052 cm². This is 45% to 65% larger than the geometric area of the electrode indicating a relatively rough surface. For the 0.5 mm electrodes, a peak separation of 83 mV and a similar scan rate response was also observed. Calculating the electrode area using the Randles-Sevcik equation produced an area approximately 0.0027 cm², which is 66% lower than the expected geometric area of 0.0079 cm². As these electrodes are small this could be due to a higher percentage coverage by manufacturing contaminants blocking much more of the surface.

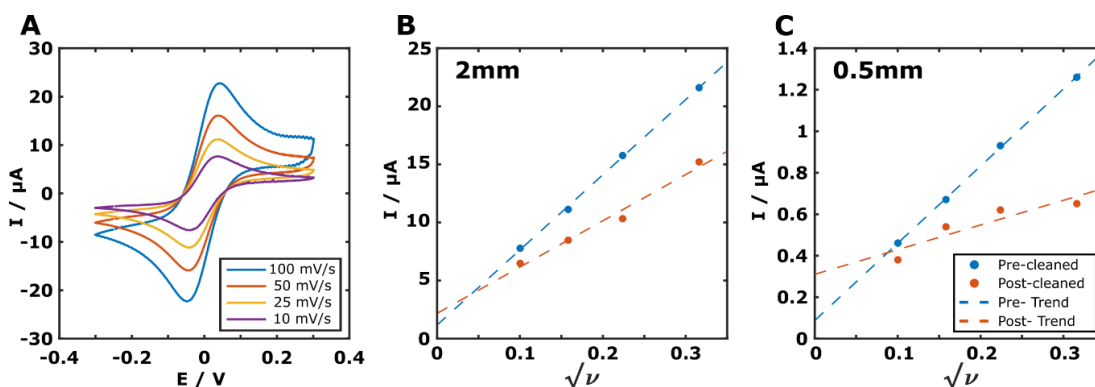


Figure 3.5 – Voltammetric characterisation of SimpleStat on-board gold electrodes using 2mM $\text{Fe}(\text{CN})_6^{3-/4-}$. (A) Typical CV responses of 2 mm electrode at 10, 25, 50 and 100mV/s scan rates (ν). (B), (C) Peak current vs $\sqrt{\nu}$ for 2 mm and 0.5 mm electrodes before and after H_2SO_4 cleaning.

Figure 3.5B and C show the CV peak currents plotted against the square-root of the scan rate on both the 2 mm and 0.5 mm diameter electrodes. Prior to cleaning, both electrode sizes showed excellent linearity (2 mm: $R^2 = 0.9989$, 0.5 mm: $R^2 = 0.9995$) and approached $I = 0$ as the scan rate tended to 0. There was also minimal shift in E_p as the scan rate was increased. These factors show that the measurement is under diffusion control and the $\text{Fe}(\text{CN})_6^{3-/4-}$ redox reaction is readily reversible (Bard and Faulkner, 2001). After immersing the electrodes

under 0.1M H₂SO₄ for 1 hour the R² reduced and the y-intercept of the linear fit increased. The CV peak currents also decreased and ΔE_p increased. This indicates that the reversibility of the reaction is reduced following cleaning, possibly due to loss of gold area at the surface and exposure of any underlying adhesion layers or the PCB itself. There may also be deposition of the coating material onto the electrodes as this was partially immersed as well. Electrodes cleaned by CV cycling showed increasing background current with each successive scan, believed to be related to exposure of the underlying copper layer. This method of cleaning was not pursued further. Based on this data future on-board measurements would be performed on uncleaned electrodes, provided the initial CV responses appeared similar. The larger electrode format was also chosen as the smaller electrodes had a low relative electrode area and exhibited signal noise when not used within a Faraday cage.

Figure 3.6 shows the impedance and DPV response of the 2 mm electrodes without any cleaning process. Fitting the impedance to the Randles equivalent circuit gives an R_{CT} of 233 Ω showing there is rapid electron transfer between the electrode and the Fe(CN)₆^{3-/4-} in solution. The DPV shows a large ΔI around 0V as expected.

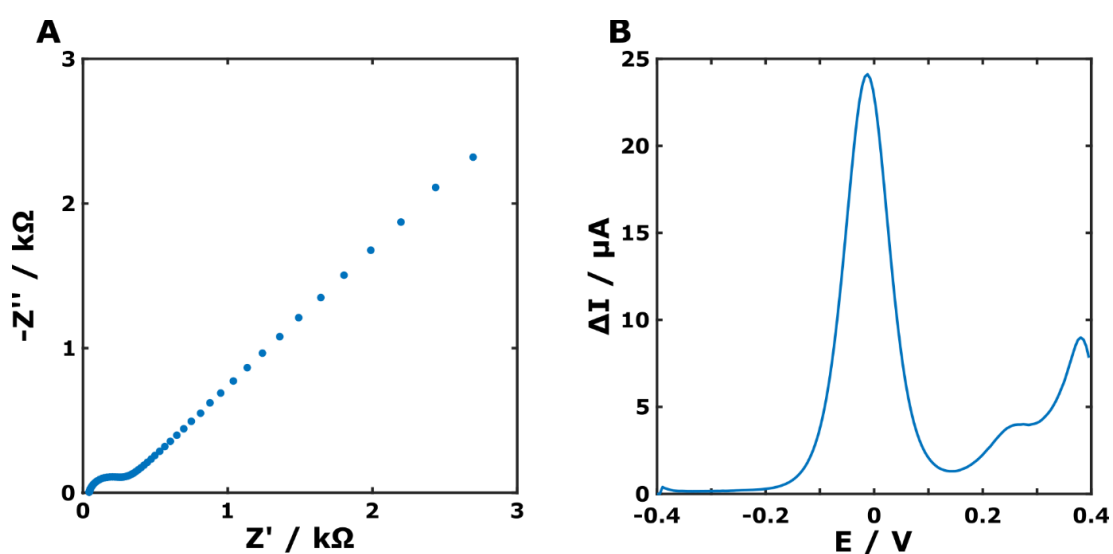


Figure 3.6 – Further characterisation of SimpleStat on-board electrodes. (A) EIS and (B) DPV Fe(CN)₆^{3-/4-} measurements from 2 mm electrodes.

Following characterisation, on-board electrodes were used to discriminate between PCR amplicon. Figure 3.7 shows the DPV traces and R_{CT} change for DNA probe modified electrodes challenged with complementary OXA or non-complementary tetA PCR product. Negative

shift of the $\text{Fe}(\text{CN})_6^{3-/4-}$ peak is associated with the application of the DNA-SAM to the working electrodes only, changing the potential between the working electrode and reference.

With the addition of complementary PCR product, the DPV peak fell by 43%, compared to negligible change when incubated with non-complementary target. The SAM layer DPV peaks between the two responses are different, possibly owing to differences in layer formation between electrodes. The DPV response is mirrored in the EIS, with the positive OXA electrode showing a greater increase in R_{CT} compared to the negative tetA. The signal changes are of similar size to those observed previously using this protocol on other electrode types, particularly the TFGEs. However, this performance is lower than other PCB electrodes in the literature. For example, a PCB electrode developed by Jolly et al. (2019) showed an increase in R_{CT} of 300 – 400% following incubation of a target oligo of a similar concentration to here. This study used a PNA probe and used a custom fabrication process for the PCB, both of which would improve the sensitivity of the electrode.

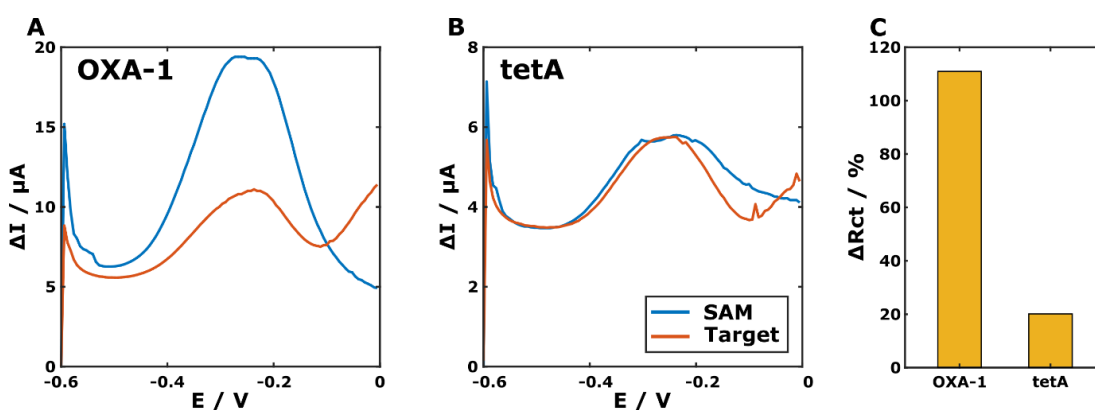


Figure 3.7 – Detection of PCR amplicon on SimpleStat on-board gold electrodes. (A) DPV response with OXA-1 complementary target. (B) DPV response with tetA non-complementary target. (C) EIS responses with OXA-1 complementary and tetA non-complementary targets.

Due to inconsistencies in the gold layer across multiple PCBs, duplicate measurements on this system were not possible. The classical $\text{Fe}(\text{CN})_6^{3-/4-}$ CV responses and the expected DPV peaks were not obtainable on all electrodes and running a measurement on these caused changes at the surface which affected future measurements (Figure 3.8). This is likely due to stripping of the gold to reveal underlying copper resulting in increasing currents on the

reverse sweep of the CV. The results shown above represent measurement on only a single pair of electrodes. With improved consistency in the gold layer it may be possible to validate these results statistically through further experimentation. However, these initial results show promise for detection of DNA using a basic gold plating process available as part of PCB manufacture.

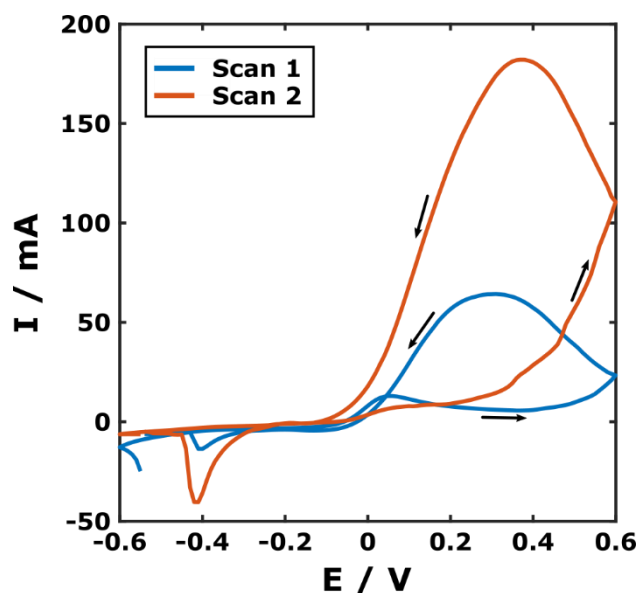


Figure 3.8 – Atypical $\text{Fe}(\text{CN})_6^{3-/4-}$ CV responses on SimpleStat on-board electrodes due to inconsistencies in gold layer. Arrows indicate the “direction” of the current trace with changing potential. Significant increases in anodic current are observed as the potential is reduced during the scan.

3.2.3.2 Comparing the SimpleStat to a Commercial Potentiostat

DNA detection experiments were also performed on polycrystalline gold electrodes to compare the analytical performance of the SimpleStat and the commercially available PS4 potentiostat manufactured by PalmSens. Figure 3.9 shows the DPV responses from these measurements.

The typical traces in Figure 3.9A and C show differences between the SimpleStat and PalmSens devices. Using 2 mM $\text{Fe}(\text{CN})_6^{3-/4-}$ in the measurement buffer (Fig 6.7A) a smooth mean trace is observed with the SimpleStat, which records a higher current than the PalmSens. There is also a slight potential shift in the DPV peak which could be due to drifting potentials across the SimpleStat board as the on-board battery is drained. Measurements following incubation with target DNA resulted in a decrease in the peak measured on both

devices; 33% on the SimpleStat vs 49% on the PalmSens, with no significant difference between these two measurements (2-sample T-test, $p = 0.17$). However, variability in the responses recorded on the SimpleStat is greater than on the PalmSens, which will make detection of a target more difficult when combined with the lower signal change.

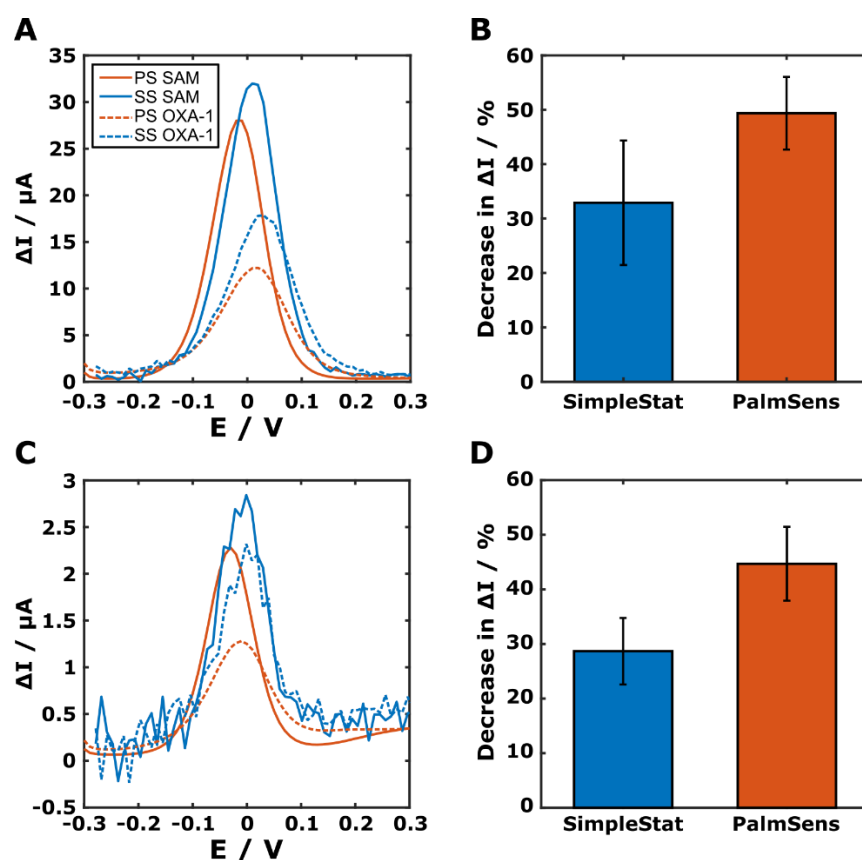


Figure 3.9 – DPV responses of SimpleStat and PalmSens PS4 potentiostat on one electrochemical cell. (A) Raw DPV traces of SimpleStat and PalmSens before and after complementary DNA binding in 2 mM $\text{Fe}(\text{CN})_6^{3-/4-}$. (B) Mean percentage decrease in ΔI for each device with 2 mM $\text{Fe}(\text{CN})_6^{3-/4-}$. (C) Raw DPV traces of SimpleStat and PalmSens before and after complementary DNA binding in 0.1 mM $\text{Fe}(\text{CN})_6^{3-/4-}$. (D) Mean percentage decrease in ΔI for each device with 0.1 mM $\text{Fe}(\text{CN})_6^{3-/4-}$. Error bars = SD, $n = 3$.

Measurements were also performed in a lower concentration of $\text{Fe}(\text{CN})_6^{3-/4-}$, as lower concentrations have the potential to be more responsive to DNA hybridisation. Reducing the $\text{Fe}(\text{CN})_6^{3-/4-}$ concentration to 0.1 mM resulted in a signal with much more noise from the SimpleStat, even following an averaging of the three repeat scans (Figure 3.9C). Similar noise is present within the low current range of the higher concentration measurement indicating this could be environmental or, more likely, generated within the measurement circuit. The

signal decrease on both instruments is also reduced at 0.1mM, with the SimpleStat recording a 29% decrease compared to a 45% decrease on the PalmSens. No significant difference was observed (p -value = 0.056) and the standard deviation between the two measurements is more similar than with the higher $\text{Fe}(\text{CN})_6^{3-/4-}$ concentration.

These results show that sensitivity is lost when using the SimpleStat measurement system, with the low-cost device recording a signal change around 35% lower than that given by the PalmSens. However, considering this device costs significantly less to build, can be manufactured at home or on site from few components and has electrodes built into the board, there are several advantages to this platform that could outweigh the reduction in sensitivity, depending on the analyte being examined. Additionally, with more work the sensing performance of the SimpleStat instrument can be significantly improved.

3.2.4 Conclusions

Results with the SimpleStat showed good parity to a traditional potentiostat system. SAM formation and electrochemical responses on the on-board gold electrodes were inconsistent, which was likely due to the use of the standard protective gold coating on the electrodes, rather than a layer which was prepared specifically for sensing. Despite this, these electrodes were used to successfully distinguish between a complementary AMR PCR amplicon and a non-complementary AMR amplicon from the same plasmid source. These results are promising for future development of the system as a fully integrated sensor and measurement platform.

When compared with a higher cost potentiostat system, the SimpleStat circuit produced similar response sizes for the detection of AMR PCR amplicons. While not significantly different, the mean response of the SimpleStat was lower than the PalmSens independent of the redox mediator concentration used. This would reduce the limit of detection of a system based on the SimpleStat compared to the PalmSens and may require an increase in the cost of the SimpleStat to overcome. Considering the SimpleStat was designed to be as low cost as possible, signal response sizes comparable to those of an expensive commercial potentiostat are highly promising.

3.3 Detecting a Clinically Relevant AMR Gene Sequence on Carbon Electrodes

Detection of AMR plasmid amplicons was performed on carbon electrodes, to build upon the promising results shown on carbon and take advantage of the greater flexibility to multiplex measurements. With DNA oligonucleotides, carbon electrodes showed good consistency with the responses on gold electrodes. When detecting PCR amplicon on gold, each low-cost electrode format exhibited poor reproducibility compared to the PGE system, which was attributed to inconsistent SAM formation and interactions between the PCR proteins, the SAM layer, and the unmodified regions of the electrode.

Carbon electrodes, which can be modified covalently by an electrografting process, may be used to overcome issues with inconsistent layer formation. Carbon also exhibits a greater inherent resistance to biofouling which may reduce non-specific interactions between the background media and the electrode, reducing both signal variability and background signal levels to enhance detection of the specific target.

This section detailed the detection of PCR and isothermal RPA amplicons on carbon electrodes using the established $\text{Fe}(\text{CN})_6^{3-/4-}$ detection scheme and a functionalisation free methylene blue intercalation method.

3.3.1 Methods

3.3.1.1 *Electrochemical Detection of PCR and RPA Amplicon*

All synthetic DNA sequences were obtained from Merck (Darmstadt, Germany). Primer sequences are the same as previously described. Polymerase chain reaction (PCR) was performed according to the instructions supplied with the polymerase (see Section 2.5.5.1), with 10 μL (30.4 ng) of purified plasmid template. No template controls were included for each reaction.

Recombinase polymerase amplification (RPA) was performed according to the manufacturer's instructions (see Section 2.5.5.2). Reactions were started by the simultaneous addition of 1 μL (3 ng) purified plasmid template and 2.5 μL Magnesium acetate and incubated at 39°C for 40 minutes. Where noted, some negative reactions did not undergo this activation step to examine the effect of RPA proteins on the electrodes without interference from DNA amplification.

PCR and RPA reactions were quantified by fluorometry using a Qubit 4 Fluorometer and a dsDNA Assay Kit (Fisher Scientific, Loughburgh, UK). Assessment of reaction specificity was

performed using a 2% Agarose Gel containing SybrSafe DNA stain run on a BlueGel electrophoresis system (Ampylus, Cambridge, US) and looking for the expected PCR product length against a 50 base pair reference ladder. Amplicons were not purified and reaction proteins were not inactivated prior to quantification and electrochemical detection.

8W110 electrodes were prepared and functionalised as previously described in Section 2.4.1, using the probe sequence shown in Table 2.2 for the detection of PCR amplicon. For RPA amplicon, an extended probe sequence was used with the sequence shown in Table 3.2.

Table 3.2 – OXA-1 Probe for RPA detection on carbon electrodes.

OXA-1 Probe	NH ₂ -(CH ₂) ₆ -AACAGAAGCATGGCTCGAAAGTAGCTTAAAAAT
-------------	---

The electrochemical detection for both PCR and RPA amplicon is the same as that described for DNA oligonucleotide. Prior to incubation on the electrode surface, the PCR or RPA mixture was denatured at 95°C for 10 minutes to produce single stranded DNA amplicons for capture by the surface bound probe.

3.3.1.2 Electrochemical Detection of PCR and RPA Amplicon using Methylene Blue

For detection based on methylene blue (MB), square wave voltammetry (SWV) was performed on a 96X110 electrode system. As these tests were used simply to assess an alternative redox system, there was no electrode functionalisation procedure used other than initial cleaning in NaCl. Wells were filled with 90 µL MB solution at various concentrations, all prepared in 1xPBS. SWV was performed from -0.5 to +0.4 V at various frequencies, with a 10 mV step potential and 100 mV amplitude. 10 µL concentrated synthetic DNA (10 µM final concentration) was then added to the well and measured after 10 minutes at room temperature.

For detection of PCR and RPA amplicons with methylene blue, the above process was followed with the inoculation of 10 µL unpurified PCR or RPA amplicon instead of synthetic oligonucleotide. Measurements were taken every ten minutes over a 30-minute period. Figure 3.10 gives a diagrammatic overview of both the Fe(CN)₆^{3-/4-} and the methylene blue detection protocols used here.

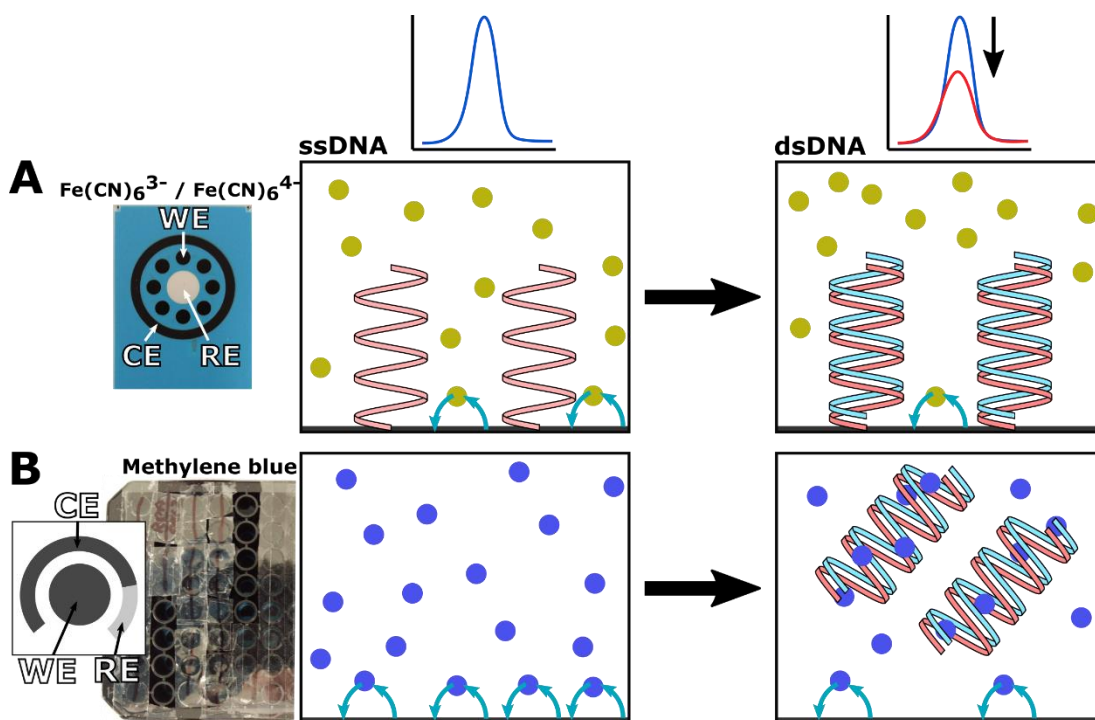


Figure 3.10 – Schematic of different electrochemical detection methods on carbon electrodes. (A) $\text{Fe}(\text{CN})_6^{3-/4-}$ detection scheme on 8W110 electrode format. (B) Methylene blue detection scheme on 96X110 electrode format. Electrode diagram also provided for each system.

3.3.1.3 Real-Time Measurement of RPA Reaction

For real-time monitoring of RPA, 96X110 electrodes were used. RPA reactions were prepared as described above, with the addition of methylene blue to a final concentration of 15 μM . In order to ensure no non-specific amplification occurred, the negative reaction was not initiated with Magnesium acetate and instead received 2.5 μL H_2O . SWV was performed with previously determined conditions. Intercalation of MB as the reaction progressed was measured by SWV on each electrode every 10 seconds over a duration of approximately 35 minutes. Samples of each reaction were removed, and DNA yield determined at the end of the experiment.

3.3.1.4 Solid-Phase RPA on Carbon SPEs

To remove the requirement for post-amplification denaturation and subsequent incubation on the electrode, RPA reactions were tested with a single primer bound to the electrode surface. This system allows RPA to generate double stranded DNA at the surface during the reaction rather than capturing the target amplicon after amplification concludes. As one of

the primers is fixed at the surface, this reaction is said to take place in the solid phase. A schematic of solid-phase RPA is provided in Figure 3.11.

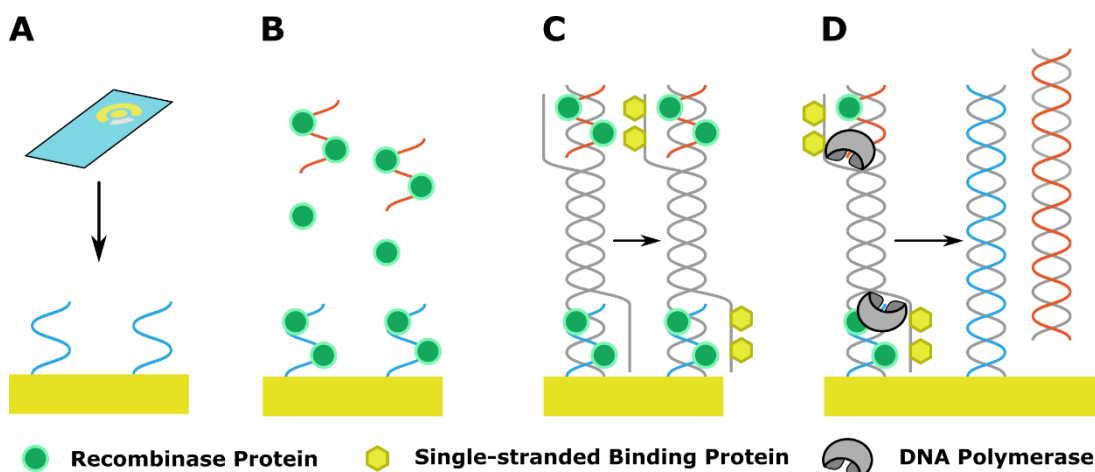


Figure 3.11 – Diagram of solid-phase RPA. (A) A primer is immobilised onto a surface. (B) The RPA reaction is added. Recombinase proteins bind the surface bound and solution phase primers. (C) Recombinase inserts primers into the template at the complementary sequence. The displaced strand is stabilised by single-stranded binding proteins. (D) Polymerase extension of the primers produces two DNA duplexes, one of which is attached to the surface.

An isothermal DNA probe / primer was designed according to work by del Río et al. (2017). This work identified a poly-15 T spacer as the optimal vertical separator between the primer and the electrode surface. This was appended to the existing OXA-1 isothermal forward primer to give the probe shown in Table 3.3.

Table 3.3 – Isothermal OXA-1 Primer / Probe for solid-phase amplification on carbon.

OXA-1 Isothermal	NH ₂ -(CH ₂) ₆ -
Probe / Primer	TTTTTTTTTTTTTTAACAGAAGCATGGCTCGAAAGTAGCTTAAAAAT

This probe was immobilised onto the carbon electrode following the previously described process. RPA reactions were prepared following the protocol described by Khater et al. (2019) for solid-phase amplification. Reaction buffer, dNTPs, molecular biology grade water, Basic E-mix, and 10 µM reverse primer were combined in a tube and mixed, following the ratios set out in the manufacturers protocol. A larger volume per reaction was required to ensure good coverage of the electrode. Methylene blue to a final concentration of 0.5 µM was included with the addition of the water. Core reaction mix was added, and the reaction

was mixed again before 70 μL was added to each well. Positive wells then received 7 μL of plasmid and 3.5 μL magnesium acetate, both being pipette mixed into solution. Negative wells received 10 μL molecular biology grade water.

Electrodes were then sealed using a standard plate seal and incubated at 39°C. SWV measurements were taken on each electrode every 10 seconds during the incubation. Following incubation for 1 hour, samples of the reaction were taken from each well and quantified using fluorometry.

3.3.2 Results & Discussion

3.3.2.1 *Electrochemical Detection of PCR and RPA Amplicon*

PCR and RPA reaction products were applied to the carbon electrodes in the same manner used for the DNA oligonucleotide. Complete PCR reactions were diluted from 62.7 nM to concentrations between 50 nM and 50 pM. Each concentration was applied to 2 electrodes of the 8-electrode array. Figure 3.12 shows the results of this assay.

When challenging carbon electrodes with amplified DNA in a complex medium rather than synthetic sequences in PBS, the expected response was not maintained. The application of diluted PCR amplicon to the electrodes caused a reversal of the expected trend observed with oligonucleotide (Figure 3.12A), with the lowest DNA concentration exhibiting the largest decrease in signal. The highest DNA concentration resulted in a 5% increase in DPV peak height which typically indicates the electrode has become more accessible to the redox system. It is expected that increasing DNA concentration would increase the negative charge and physical blocking of the surface, causing a decrease in $\text{Fe}(\text{CN})_6^{3-/4-}$ DPV signal as seen previously in this work and throughout the literature (Amouzadeh Tabrizi and Shamsipur, 2015; Butterworth et al., 2019b; Tsaloglou et al., 2018). There may be interaction between the PCR proteins and the immobilised DNA probe or biofouling of the electrodes which, at higher PCR mix concentrations, is improving access of the redox agent to the electrode. Alternatively, there could be differences in the ionic strength of the various PCR dilutions which cause the probe DNA to take on different conformations at the surface, as shown by Gebala and Schuhmann (2010), facilitating or inhibiting hybridisation with the amplicon.

In order to investigate biofouling as a potential cause of these responses, the electrodes were washed in 1xPBS containing 0.05% Tween-20 before DPV was measured again. Tween-20 is a non-ionic surfactant which is commonly used as a wash in protein binding assays to remove

non-specifically bound protein and should remove any PCR reaction proteins interacting with the electrode surface. The results following this wash are shown in Figure 3.12B. The responses changed significantly, with all electrodes exhibiting a mean increase from baseline. No specific trend is apparent, with the electrodes showing insensitivity to the concentration of DNA originally applied. Washes containing Tween-20 were avoided for measurements on carbon electrodes in light of these results.

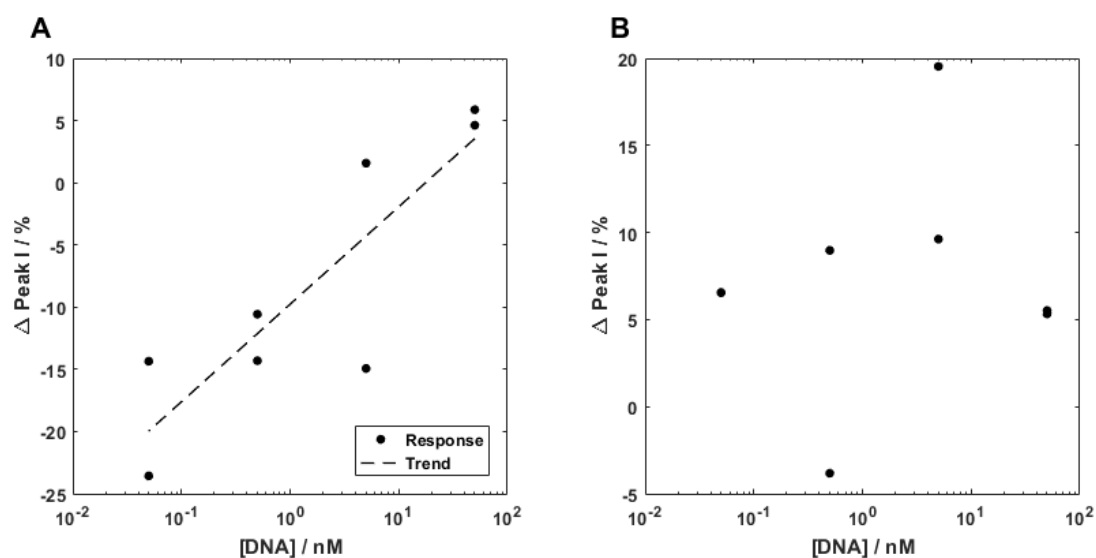


Figure 3.12 – DPV response to PCR amplicon target concentrations on carbon SPEs. (A) Signal change following washes in 1xPBS. (B) Signal change following washes with 1xPBS + 0.05% Tween-20.

Detection of isothermally amplified RPA product on carbon electrodes was also tested. In these tests, a positive RPA reaction was compared to a negative consisting of an RPA with no template and no magnesium acetate initiation, to see the effect of the RPA proteins on the detection scheme. Example EIS and DPV measurements from a positive and negative electrode are shown in Figure 3.13. There was little visible difference between the responses of the positive and negative electrode when plotted as such. The DPV showed an increase in the overall Δ I after RPA mixture addition, suggesting the decay of the capacitive charging current exceeded the pulse time of the measurement. This is supported by the bode plot of the phase recorded during EIS, shown in Figure 3.14, which showed a shift to lower frequencies indicating an increased double layer capacitance.

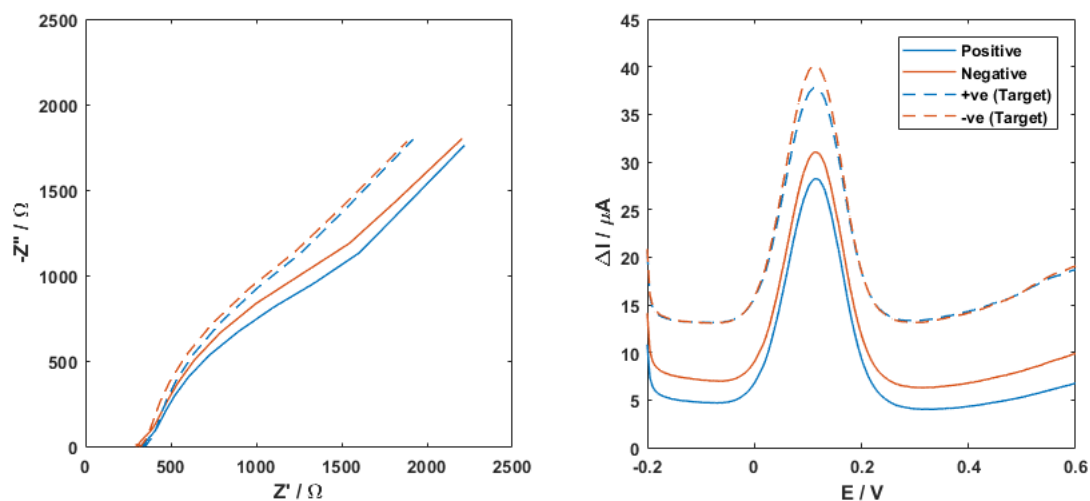


Figure 3.13 – EIS and DPV examples for RPA detection on carbon SPEs.

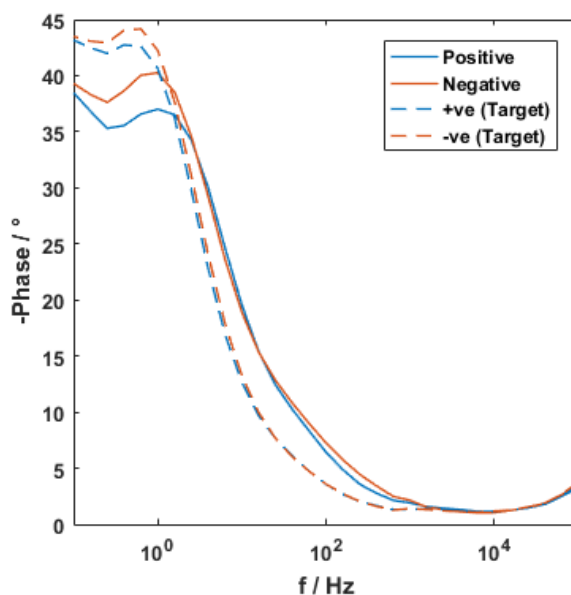


Figure 3.14 – Bode plot of phase vs frequency for RPA detection on carbon SPEs.

For this initial characterisation of RPA reaction components, EIS and DPV measurements were taken to obtain more data regarding the effect of the RPA reaction mixture. The EIS measurement provided additional data regarding the capacitive response of the system during this test. However, based on the data shown in Figure 2.18 indicating that DPV ΔI change is superior to the EIS ΔR_{CT} on carbon electrodes, DPV was selected as the primary measurement routine. DPV is less sensitive to electrode surface changes than EIS but can also be much quicker and simpler to perform which are advantageous characteristics for point-of-care sensing.

When measuring the change in DPV peak height, a difference between the positive and negative electrodes is observed. Figure 3.15 shows the DPV signal change following incubation with RPA amplicon or negative. A small increase in peak height was observed on the positive electrodes, while a significantly larger increase was present on the negatives. The RPA assay contains single-stranded binding proteins and the recombinase enzyme, which could bind to the single-stranded DNA probe at the electrode surface. These proteins may cause a conformational change in the DNA resulting in less surface blocking or have a net positive charge which attracts the $\text{Fe}(\text{CN})_6^{3-/4-}$ to the surface. There may also be components in the RPA buffer mixture which have effects on the interaction of the $\text{Fe}(\text{CN})_6^{3-/4-}$ with the electrode. These effects could cause the DPV peak to increase in response to RPA reaction mixture.

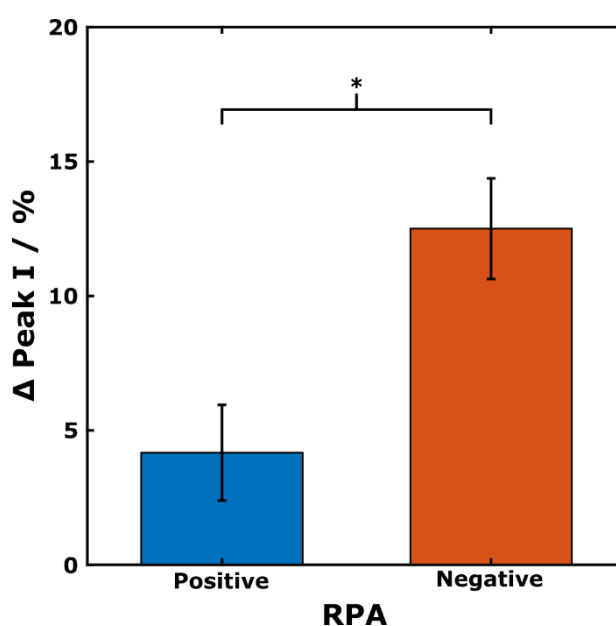


Figure 3.15 – DPV $\text{Fe}(\text{CN})_6^{3-/4-}$ peak ΔI response following positive or negative RPA reaction addition to carbon SPE. Error bar = SD, $n = 3$. * indicates 2-sample T-test p -value < 0.05 .

In the positive reaction, the high concentration amplicon may compete with these proteins or become accumulated at the surface through the activity of the recombinase, producing a signal suppression as would be expected. This effect would account for the difference between the positive and negative samples observed here. The difference between the positive and negative is not believed to be due to surface biofouling by the reaction proteins, as there should be no bias in the fouling of one electrode group over the other. Purification of the DNA from the background reaction matrix may have produced the expected response,

but would add time, cost, and complexity to a point-of-care test. Methods in which these effects could be bypassed were therefore examined next.

3.3.2.2 *Electrochemical Detection of PCR and RPA Amplicon using Methylene Blue*

An alternative detection scheme involving the intercalating dye methylene blue was used to avoid non-specific signal issues when using the $\text{Fe}(\text{CN})_6^{3-/4-}$ method. This system does not include a DNA probe at the surface, which was believed to be the cause of the signal increases observed in previous experiments. An entirely solution-phase detection system also reduces the influence of surface effects which can have a large impact on sensitivity as previously shown.

Methylene blue (MB) was measured on 96X110 electrodes, which follow the same screen-printing process as the 8W110 electrodes but come in a 96-well plate format. Square-wave voltammetry is used widely in the literature for the detection of methylene blue (Liu et al., 2010; Tran et al., 2011; Valério et al., 2008), and as such SWV was used instead of DPV in these measurements. In order to find optimal detection and measurement parameters, SWV at different frequencies was performed on solutions containing 3 different MB concentrations. 10 μM synthetic double-stranded DNA was then introduced to each solution and allowed to incubate for 10 minutes before the measurements were repeated.

Figure 3.16 shows the SWV traces at each frequency for 10 μM MB before and after the addition of dsDNA. The peak ΔI increases with frequency, producing a sharper peak at higher frequencies. The addition of dsDNA (Figure 3.16B) causes a decrease in the SWV response at all frequencies, but this is especially pronounced at higher frequencies. A shift in the peak potential is also observed with the addition of dsDNA, which has been previously reported in the literature for intercalating MB (Tani et al., 2001; Wong et al., 2004). However, the peak shift here is attributed to interaction of the dsDNA with the electrodes, as the potential shift is much larger than typically reported and is towards more positive potentials rather than more negative.

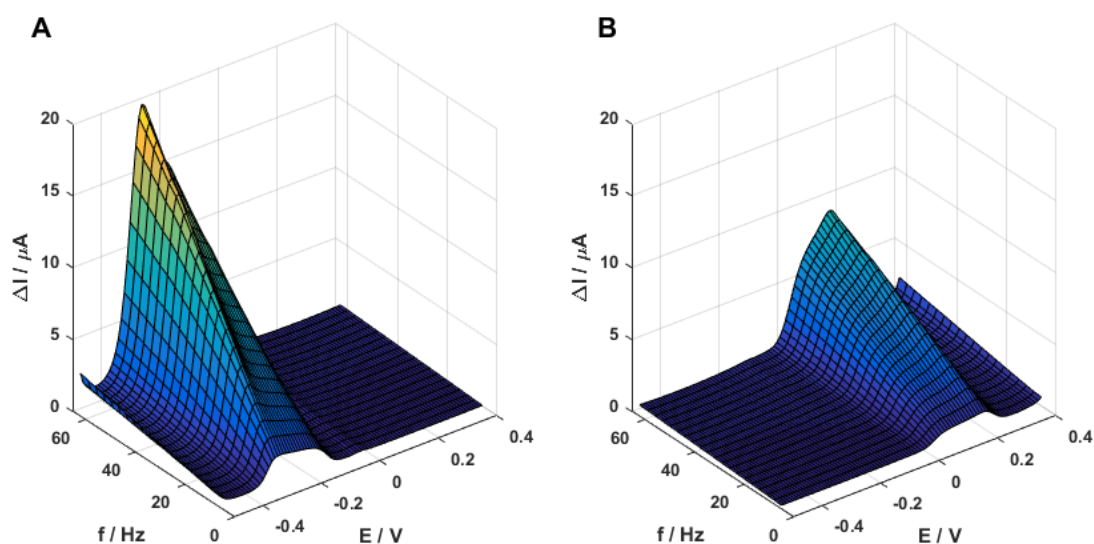


Figure 3.16 – SWV response of 10 μM methylene blue on carbon SPEs. (A) Before and (B) after addition of 10 μM double-stranded DNA.

To find the optimal SWV frequency and concentration of methylene blue, SWV peak currents at each concentration and frequency were compared before and after 10 μM dsDNA incubation. Figure 3.17A shows the SWV peak ratio between the pre-DNA and post-DNA measurements. The peak ratio;

$$\text{Peak Ratio} = \frac{\Delta I_{p_{\text{Pre-DNA}}}}{\Delta I_{p_{\text{Post-DNA}}}} \quad (3.1)$$

is used to aid in visualisation. At low frequencies the peak decrease is smallest, and in all cases the peak ratio increased as frequency rose. 15 μM MB concentration resulted in the greatest SWV response change at 60 Hz, around a 2.8-fold change, and 10 μM MB gave the lowest response change at each frequency. The signal decrease of each concentration of MB at 60 Hz SWV frequency is given in Figure 3.17B. All concentrations gave a similar signal decrease around 50% to 60% in response to 10 μM dsDNA addition.

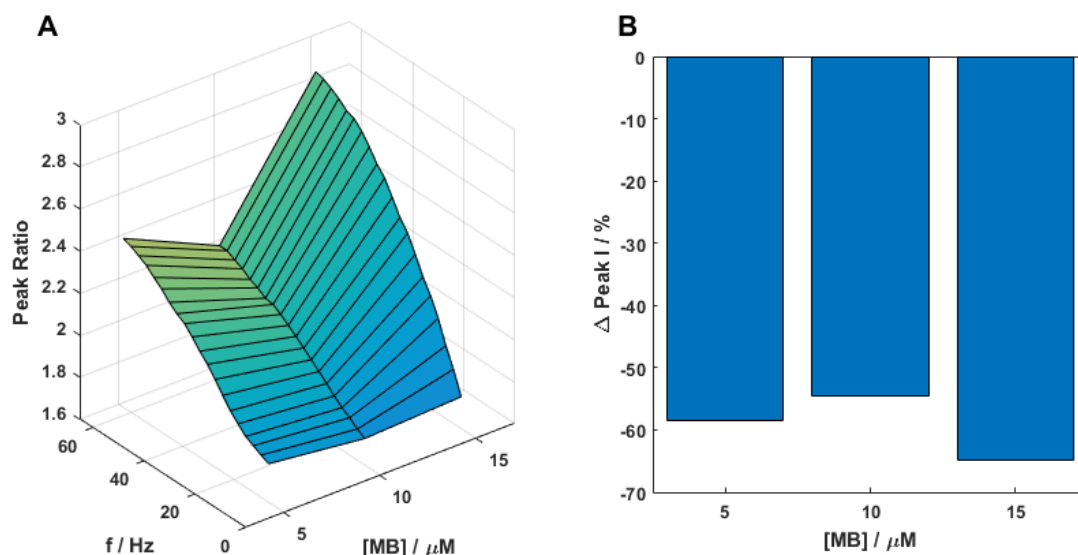


Figure 3.17 – Methylene blue SWV peak current response to 10 μ M dsDNA incubation. (A) Peak ratio at different MB concentrations and SWV frequencies. (B) Peak signal change with different MB concentrations at 60Hz SWV frequency.

This data suggested that the SWV response when spiking synthetic DNA into methylene blue solution was large enough to detect DNA. Next, these solutions were exposed to PCR or RPA amplicons to see if the response was maintained. Figure 3.18 shows the percentage change in SWV peak height following the addition of PCR and RPA. Lower concentrations of MB were used in this experiment as both the PCR and RPA amplicon concentrations are much lower than the 10 μ M synthetic DNA concentration used above. The 5 μ M MB concentration was used as the maximum to act as a benchmark between the two experiments. The experimental concentration of PCR amplicon was 13.9 nM and of RPA amplicon was 97.5 nM (both a 10-fold dilution from end-point concentration).

PCR amplicon (Figure 3.18A) produced an increase in MB signal after 10 minutes at all MB concentrations, which decayed to around 0% over the next 20 minutes of incubation. RPA amplicon (Figure 3.18B) showed the same pattern as PCR amplicon when added to 0.5 μ M MB, but at 1 and 5 μ M caused a large decrease in signal after 10 minutes incubation. This changed to a signal increase after 20 minutes, and then followed a similar trend to the PCR amplicon with a decrease in signal towards 0%. These results are not in line with similar DNA sensing systems reported in the literature, where methylene blue has been used to detect amplicons from PCR (Fang et al., 2009; Meric et al., 2002; Yamanaka et al., 2011) and

isothermal amplification methods (Cheng et al., 2014; Luo et al., 2014; Martin et al., 2016; Tien et al., 2017).

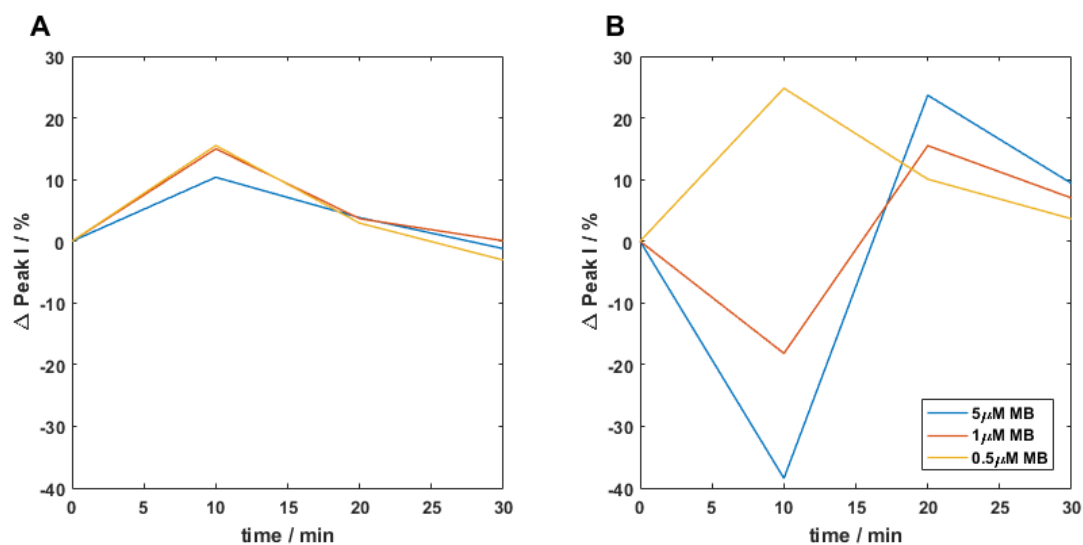


Figure 3.18 – Methylene blue SWV peak response to PCR and RPA amplicon on unmodified electrodes. SWV peak signal change with (A) PCR amplicon and (B) RPA amplicon incubation for 30 minutes.

Work by Meric et al. (2002) shows a similar response to the RPA incubation, where a decrease in MB signal recovers rapidly over the first 10 minutes of incubation, although occurring over a longer timescale here. This behaviour is attributed to an initial depletion of the MB by hybridisation. This recovers as DNA hybridises at the surface of the electrode, or as single-stranded DNA fouls the surface in a non-specific manner, resulting in a greater amount of MB at the surface when later SWV measurements are performed. It is possible that a similar process occurred in the PCR and RPA measurements here, with the first measurement at 10 minutes missing this depletion and recovery effect in the PCR. The RPA may have slowed this process through the reduced mobility of ssDNA-protein complexes enough to be captured with 10-minute measurement interval.

Additionally, work by Deféver et al. (2011) and Moreau et al., (2017) suggests that the poor DNA binding affinity of MB results in minimal signal change upon successful amplification. These articles demonstrate that more strongly intercalating compounds containing 2,20-bipyridine and dipyrido[3,2-a:20,30-c]phenazine can give a much stronger response to amplification without inhibiting the PCR reaction. The methylene blue used here may be unable to effectively intercalate the DNA when in complex media containing DNA binding

proteins and polymerases, resulting in the poor signal response and 30-minute decay observed here.

3.3.2.3 Real-Time Measurement of RPA Reaction

Real-time measurements of an ongoing RPA reaction were also performed. End-point detection requires the reaction to run to completion before being applied to the sensor. For RPA, the manufacturer claims that results are typically generated in 3 – 10 minutes (TwistDx Ltd, 2020). By monitoring the reaction as it progresses, it may therefore be possible to detect target DNA in this 3 – 10 minutes timeframe rather than the 70 – 80 minutes of previous experiments.

Figure 3.19 shows the SWV peak current change over the duration of the experiment. Within the first few seconds of the reaction the SWV peak fell rapidly due to reaction protein fouling of the electrode surface and localised depletion of the methylene blue. In both the positive and negative the signal change recovered, with a greater and more rapid response seen in the electrode containing an active RPA reaction. This data shows a similar trend to the endpoint RPA measurements, where after 10 minutes the SWV was lower than initially measured, and as the incubation time progressed this peak tended towards 0% change. The positive reaction yielded 28.7 $\mu\text{g}/\text{mL}$ dsDNA, while the negative reported only 0.8 $\mu\text{g}/\text{mL}$, as expected for a manufactured negative.

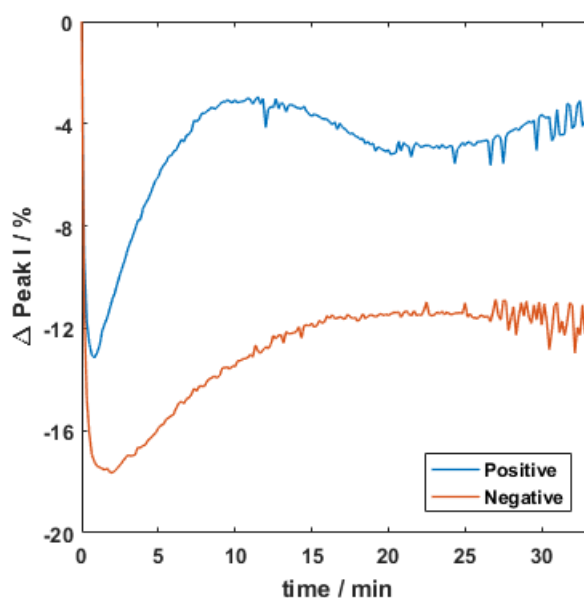


Figure 3.19 – Methylene blue SWV peak current change during real-time RPA measurement. Each electrode measured every 10 seconds as reaction progressed and normalised to $t = 0$.

The difference between the positive and negative observed here may be due to differences in the electrode surfaces, or a result of accumulating dsDNA in the ongoing reaction increasing the MB response at the surface. This contrasts with the expected result, where MB depletion from the bulk solution by intercalation into the DNA would cause a decrease in the redox peak. It has been shown that redox active intercalators, including MB, can maintain redox activity within the DNA duplex (Wong et al., 2004; Wong and Gooding, 2006), so this recovery of signal may also be associated with dsDNA accumulating at the electrode surface leading to a concentration of the MB as it intercalates into the strand. Work by Kelley et al. (1997) also shows that the redox current of methylene blue within a DNA film at the electrode surface increases when intercalated into DNA compared to when in bulk solution, which also supports the theory that DNA accumulation at the surface has contributed to the differences observed here.

3.3.2.4 Solid-Phase RPA on Carbon SPEs

Previously, in order to detect PCR or RPA amplicon, the end product of the reaction must be heated to 95°C to denature the DNA double strand, allowing the reaction product to hybridise with the probe bound to the electrode surface. In the standard protocol, the secondary incubation adds significantly to the time-to-result, the process requires a heat block and presents a cross contamination risk when opening heated amplicon solutions. By immobilising one of the RPA primers on the electrode surface and incubating the entire electrode system at 39°C, the reaction can directly generate amplicons at the sensor surface. The extension of the surface bound primer and the formation of a tethered DNA duplex during the reaction, rather than following it, allows the post-amplification denaturation stage to be removed from the protocol. This is significantly less feasible using PCR, as the rapid and precise temperature cycle could not easily be performed on a solution at an electrode surface, but is readily achievable with isothermal amplification systems (del Río et al., 2017; Khater et al., 2019; Santiago-Felipe et al., 2014).

Solid-phase RPA was tested to examine the effect of surface concentration of methylene blue through DNA hybrid formation at the electrode surface, and to produce a route to hybridisation-free $\text{Fe}(\text{CN})_6^{3-/4-}$ measurements. Initially, two 96X110 electrodes were functionalised with the solid-phase RPA primer. One well contained both the forward and reverse primer in solution to act as a control, while the other contained only the reverse primer in solution phase. From this test, samples of each reaction were taken and DNA yield

quantified. The positive control (solution-phase) reaction yielded 60.3 $\mu\text{g/mL}$ dsDNA, while the solid-phase reaction produced 38.7 $\mu\text{g/mL}$. A yield of 64% of the solution-phase reaction was acceptable considering the reduced kinetics and lower forward primer concentration limiting the reaction rate in the solid-phase.

Following the successful amplification using RPA in a solid-phase format, live monitoring of such a reaction was performed. Considering the RPA reactions typically reach DNA concentrations of up to 1 μM , real-time monitoring of solid-phase RPA used a final MB concentration of 0.5 μM . Figure 3.20 shows the SWV peak response of a positive and negative real-time reaction.

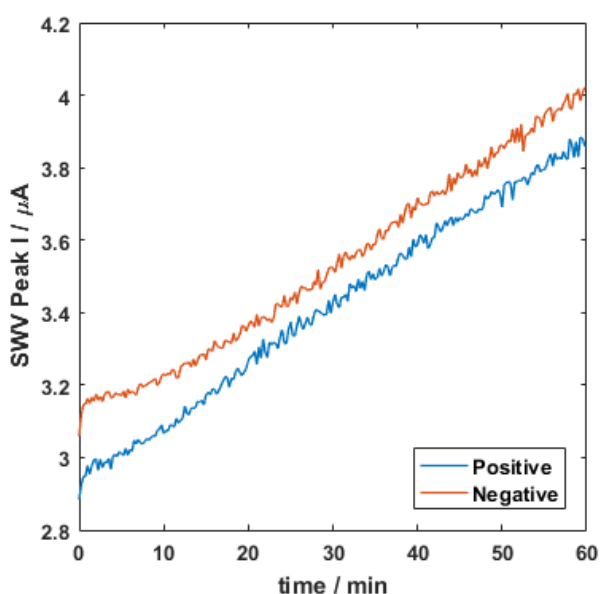


Figure 3.20 – Methylene blue SWV peak current one two electrodes during real time solid-phase RPA measurement. Each electrode measured every 10 seconds as reaction progressed.

Despite the final DNA concentration being considerably different between the two wells (77.3 $\mu\text{g/mL}$ positive vs 2.76 $\mu\text{g/mL}$ negative), both electrodes showed a similar SWV peak response. Methylene blue is known to adsorb to both carbon and gold surfaces (Wong et al., 2004; Yan et al., 2005), and these steadily increasing SWV peaks are believed to be the result of MB adsorption. There is no DNA dependent difference between the peak increases observed here. The previously observed results, which may have been due to MB accumulation in the DNA duplex at the surface, could be orientation dependent. By

amplifying in the solid-phase, and considering the persistence length of dsDNA, the majority of intercalated MB will be held away from the surface within the duplex.

Work by Kelley et al. (1997) showed that MB redox activity through the dsDNA strand can occur at a distance of around 65 Å, approximately from the end of a 15 base pair DNA strand with a 6-carbon thiol linker modification, assuming that MB is mostly bound at the solution end of the packed DNA film. Through control of the location of a G-C pair in the dsDNA sequence, later work by the same group (Kelley et al., 1999) showed that the redox intercalator daunomycin can achieve electron transfer over a distance of 10 base pairs from the electrode surface.

Experimentally, Kelley et al. also showed that MB appeared to intercalate to a density of 1.4 MB per 15 base pair DNA sequence, at a 75% surface coverage with DNA. This is much lower than the theoretical maximum of around 7 MB per 15 base pair sequence (Crothers, 1968; Kelley et al., 1997). In this work, it could therefore be assumed that only a small number of MB molecules intercalate into each of the DNA amplicons, and most would be much further from the electrode than the 15 base pair sequences tested in other work, potentially reducing the measurable effect of intercalation.

3.3.3 Conclusions

Responses with carbon electrodes initially showed promise, with reasonable signal changes, inter-electrode consistency and a nanomolar range dose response curve obtained when using synthetic DNA oligos. However, the surface modification and target capture protocol did not respond well to challenge with PCR or RPA amplicons. This was attributed to interactions between the reaction proteins and the surface altering the blocking behaviour of the DNA probe or fouling the electrode. In all cases, a reversal of the expected trend for $\text{Fe}(\text{CN})_6^{3-/4-}$ was observed and so methods avoiding DNA probes at the surface were pursued.

A solution-based detection using methylene blue again showed a strong signal change when introducing synthetic dsDNA. This response was not replicated when introducing PCR or RPA amplicons into the solution. In both cases, a 30-minute incubation resulted in little signal change from baseline, with an overall signal increase observed in the PCR at each time point and high variability in the RPA. A signal increase could be accounted for by accumulation of methylene blue in the DNA duplex at the electrode surface as previously described in the literature. However, a very minimal change after incubation was observed here for both PCR and RPA which is not conducive to DNA detection. No difference between positive and

negative reactions was observed when using a solid-phase reaction to concentrate DNA at the electrode, suggesting that methylene blue accumulation responses may depend on the free movement of the DNA duplex.

Although not successfully detected using the carbon electrode system, the solid-phase RPA reaction performed well, achieving a relatively high yield compared to the more kinetically favourable solution-phase reaction. Solid-phase RPA offered a method by which DNA capture at the electrode could be performed simultaneously with amplification, reducing the total time to result of the detection system and removing the requirement to thermally denature the DNA prior to hybridisation.

Following these investigations, it appeared that screen-printed carbon electrodes were not an optimal format for electrochemical detection of PCR or RPA products, but may be effective for other DNA solutions or with different surface modification protocols. Solid-phase RPA showed promise for lowering the total assay time, as large quantities of specific DNA target were amplified directly on the electrode surface. Pairing this amplification system with a suitable electrochemical detection scheme would allow rapid and specific target identification.

3.4 Detection of Amplified AMR Genes: A Return to Gold

Previous work on gold electrodes had shown excellent discrimination of positive PCR products from a negative reaction, alongside good sensitivity and resistance to non-specific signal when using PGEs. Solid-phase RPA was attempted on PGEs modified with an alkanethiol SAM to examine whether the interfering effects observed on carbon electrodes could be mitigated. Combination of gold electrodes with solid-phase RPA could also facilitate enhanced detection as no heat denaturation of the DNA hybrid would be required. This would keep the RPA proteins intact, reducing non-specific interactions which may be more likely with denatured protein.

3.4.1 Methods

3.4.1.1 RPA Detection on PGEs

Detection of RPA on gold followed the functionalisation protocol set out by Khater et al. (2019), but with modifications based on previous detection of PCR products on PGEs. PGEs were initially cleaned by immersion in piranha solution, alumina slurry polish and cyclic voltammetry. Probe solution consisting of 1 μ M DNA probe (Table 3.4) and 100 μ M MCH in 1xPBS with excess TCEP was prepared. A higher concentration of probe was used compared to that described in the article, as previous detection on gold had shown good signal responses with probe concentrations at this magnitude. Additionally, as this test did not use solid-phase RPA, the optimised ratio of primer to backfill used in the study was not expected to be optimal for this detection method. Each electrode was incubated with this solution at room temperature for 2 hours, before rinsing in 1x saline sodium citrate (SSC) buffer. Initial measurements were then performed in 1 mM $\text{Fe}(\text{CN})_6^{3-/4-}$ in 1xPBS.

Table 3.4 – OXA-1 Probe for RPA detection on gold electrodes.

OXA-1 Probe	SH- $(\text{CH}_2)_6$ -AACAGAAGCATGGCTCGAAAGTAGCTTAAAAAT
-------------	--

Previously completed RPA and an RPA blank (consisting of reaction buffer, core reaction mix and E-mix) were heated to 95°C for 10 minutes prior to addition to each electrode. These solutions were incubated on electrodes for 40 minutes at room temperature. Electrodes were then rinsed in 1xPBS + 0.05% Tween-20 before measurements were taken.

3.4.1.2 Solid-Phase RPA on PGEs

Solid-phase RPA was also tested on PGEs to confirm that amplification on these electrodes was possible. These reactions were not measured electrochemically due to the need for large external reference and counter electrodes, but DNA yield and product identification were performed.

Following the protocol described by Khater et al., 0.1 μM DNA probe (Table 3.5) and 100 μM MCH were applied to each electrode and incubated for 2 hours at room temperature, before rinsing in 1xPBS. DPV measurements using 2 mM $\text{Fe}(\text{CN})_6^{3-/4-}$ in 1xPBS were taken following SAM formation using this protocol and compared to an electrode prepared using the standard overnight protocol to ensure the SAM formation was effective.

An RPA reaction was then prepared in the same manner as for the carbon solid-phase amplification, with the addition of magnesium acetate to the reaction prior to incubation on the surface. 20 μL was applied to each electrode, or to the positive control tube which also contained the OXA forward primer at the same concentration the isothermal primer / probe was applied to the electrode. 5 μL (86 ng) plasmid template was added to each electrode and to the control tube to begin amplification.

Table 3.5 – Isothermal OXA-1 Primer / Probe for solid-phase amplification on gold.

OXA-1 Isothermal Probe / Primer	SH- $(\text{CH}_2)_6$ - TTTTTTTTTTTTTTTAAACAGAAGCATGGCTCGAAAGTAGCTTAAAAAT
---------------------------------------	--

Aliquots of these reactions were run on 2% agarose gels containing GelGreen or SybrSafe DNA stain, and DNA yield was quantified by Qubit fluorometry.

3.4.2 Results and Discussion

3.4.2.1 RPA Detection on PGEs

Figure 3.21 shows the DPV signal response to RPA mixture. In the positive reaction, containing all the components required for an RPA, a large decrease in the DPV signal is observed with good reproducibility between electrodes. This is significantly different from the negative, consisting of the core proteins, buffer, and E-mix of the reaction, which shows a much smaller signal drop. Due to issues with contamination in the RPA, a true negative reaction could not be achieved when these results were produced, and so a manufactured

negative was required. Despite this, these results show that an MCH based SAM using a protocol identified in the literature is capable of differentiating between an RPA containing amplified DNA and the background proteins in the reaction.

These results contrast those obtained on carbon where an increase in DPV signal was observed in both the positive and negative responses, and the signal change was small. There was no blocking molecule used on the carbon surface, only an inactivation of the carboxylic acid motifs through ethanolamine incubation. The use of an alkanethiol on gold may have prevented non-specific protein interactions which has resulted in the direction and magnitude of signal change observed here. It is unlikely that the DNA probe conformation is significantly different between the carbon and gold electrodes, suggesting that conformational changes at the carbon electrode may not have been responsible for the results observed there (e.g. Figure 3.15).

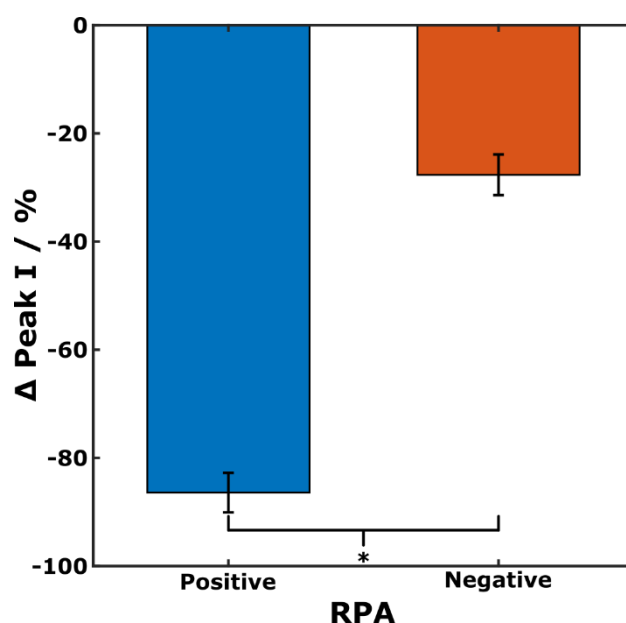


Figure 3.21 – DPV peak ΔI change in response to Oxa RPA amplicon or blank RPA reaction mix. Error bar = SD, $n = 5$. * indicates 2-sample T-test p -value < 0.05 .

3.4.2.2 Solid-Phase RPA on PGEs

Figure 3.22 shows the $\text{Fe}(\text{CN})_6^{3-/4-}$ DPV responses of 3 electrodes prepared using the 2-hour SAM formation protocol compared to electrodes produced using the overnight incubation and backfill method. The DPV response between the two groups is highly consistent indicating that the SAM formation process achieved a similar level of surface blocking with both methods. The standard deviation of the 2-hour protocol was improved compared to the

overnight protocol, suggesting that this method may create a more reproducible SAM layer which would enhance DNA detection.

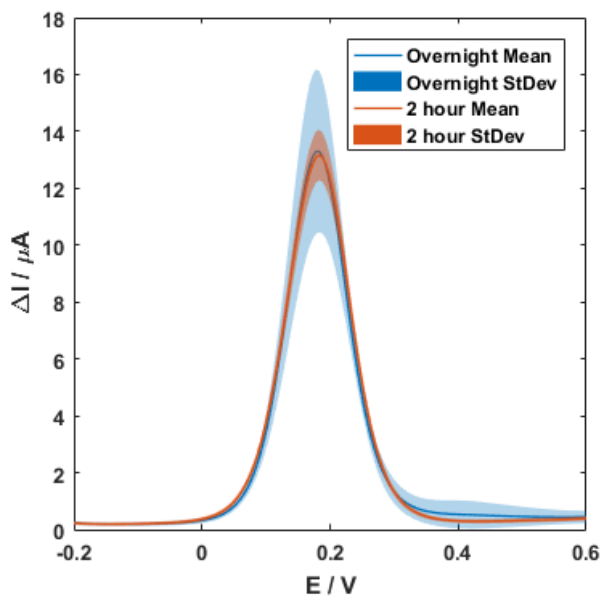


Figure 3.22 – Comparison of DPV responses from electrodes functionalised using overnight or 2-hour SAM formation protocol. N = 3.

Figure 3.23 shows the agarose gel electrophoresis results following solid-phase RPA amplification of OXA-1 on polycrystalline gold electrodes. The positive control tube produced 20.1 $\mu\text{g}/\text{mL}$, with a clear band in the gel above the 100 base pair mark as expected. For solid-phase amplifications (E1 – 3), similar bands are visible in the gel, with little non-specific amplification present. These electrodes yielded 10.5 to 16.1 $\mu\text{g}/\text{mL}$ DNA (mean 12.5 $\mu\text{g}/\text{mL}$), giving a yield around 62% of the solution phase amplification. This yield is consistent with those observed for solid-phase RPA on carbon electrodes and suggests that the amplification on gold progresses at a similar rate to that on carbon with differences in the surface chemistry having little effect on amplification efficiency.

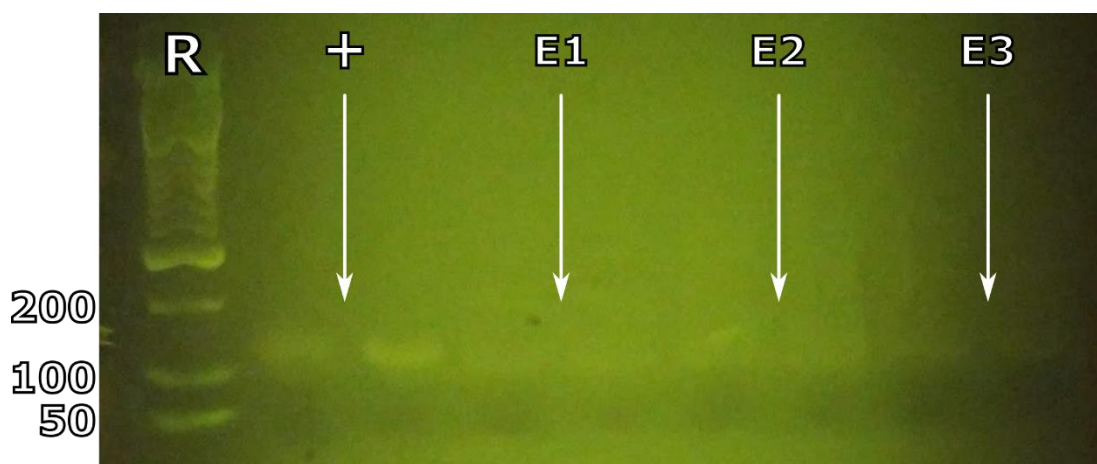


Figure 3.23 – Image of 2% agarose gel electrophoresis results for solid-phase RPA performed on polycrystalline gold electrodes. Two aliquots of surface-bound RPA reaction collected and loaded to gel. Arrows indicate height of bands for clarity. + - positive control reaction performed in a standard PCR tube rather than in solid-phase.

3.4.3 Conclusions

The detection of DNA amplicon through the use of solid-phase RPA was achieved on gold. With minimal optimisation, RPA amplicons were identified from a negative control reaction using electrochemical measurements. Additionally, solid-phase RPA performed on gold electrodes achieved a similar level of amplification compared to on carbon, suggesting that detection of solid-phase amplified DNA sequences may be achieved more readily on gold surfaces. These differences in response are attributed to the ability to block gold with an alkanethiol, reducing the impact of the highly complex RPA reaction mixture on the measurement by minimising non-specific interactions between protein and the surface. These results show promise for integrated detection strategies where solid-phase amplification can specifically anchor target amplicons at the electrode surface.

4 Detection of Amplified DNA Using Enzyme Tagged Nucleotides

To reduce the impact of SAM formation variability on a measurement system, it is possible to use a labelling method to produce a signal, rather than relying on electrochemical changes at an inconsistent interface. A labelled reaction using a signal on system can produce a redox active analyte which can be measured at the electrode. This has the advantage of requiring only a single measurement – one following target incubation – and reduces the impact of SAM layer reorganisation or desorption over the timescale of the experiment, factors which can have a large effect on label free techniques such as EIS.

As previously discussed, DNA labelling can be achieved through several methods. A labelled hybridisation probe producing a sandwich assay format is common (Fernandes et al., 2015a; Ghosh et al., 1990; Urdea et al., 1988; van Gijlswijk et al., 2000; Wang et al., 2019; Xu et al., 2018). These methods capture or amplify a DNA target at a surface, and then hybridise a labelled reporter sequence which produces the detection signal. In the case of Xu et al., each captured DNA strand binds up to 7 hybridisation probes each containing an HRP label, amplifying the signal produced by a single binding event. These methods are similar to the use of labelled primers or surface bound probes. With labelled primers amplification of each DNA double strand incorporates a single primer tag, which may produce a signal on or signal off effect based on the characteristics of the label chosen (Ahmed et al., 2020; del Río et al., 2017; Kersting et al., 2014; Toldrà et al., 2020; Tortajada-Genaro et al., 2015).

Surface bound probes may be designed such that they form a hairpin structure (Ferguson et al., 2009) or use DNA analogues such as PNA or morpholino to allow close proximity of an electroactive label to the electrode (Jampasa et al., 2014). These designs rely upon the increased persistence length of dsDNA compared to ssDNA to move the label further from the surface and reduce the rate of electron transfer. Hairpin structures can also enable labelling through a secondary reporter probe as demonstrated by Cheng et al. (2014), where target binding exposes a section of hairpin which interacts with a biotinylated primer to specifically label the opened hairpin.

Alternatively, DNA may be labelled through intercalating or associative interactions with the DNA double strand (Ahmed et al., 2013; Cui et al., 2015; Gaiji et al., 2017; H. Huang et al., 2015; Kerman et al., 2009; Sun et al., 2018; Widaningrum et al., 2017). Redox active

intercalating agents or groove binders can be used to distinguish between single and double stranded DNA, whereas molecules such as Ruthenium Hexamine interact with the DNA through the negative charge of the backbone structure. The presence of a DNA double strand results in a change in the signal these molecules produce, allowing the user to identify hybridisation events at the surface.

While these methods can all efficiently incorporate a label into a DNA detection scheme, there are drawbacks to each. Hybridisation probes require additional DNA sequences to be included and may interfere with amplification reactions if not carefully designed. Hairpin probes hold their own design challenges, and redox labelled probes typically operate on a signal-off approach which may limit detection sensitivity as the signal saturates. Intercalating or strand-binding mediators can have slow kinetics requiring a long incubation step to see a response. Certain compounds also have affinity for both single-stranded and double-stranded DNA, resulting in a high background signal prior to hybridisation (Gebala et al., 2009; Paleček and Bartošík, 2012; Rye and Glazer, 1995).

One method of signal enhancement and target labelling is using modified nucleotide bases. Bases modified with antigens or redox active labels can be incorporated into the amplification reaction (Kortli et al., 2020; Magriňá et al., 2019; Santiago-Felipe et al., 2016). Subsequent incubations with labelled antibodies, or simply measuring the attached redox molecules, reports whether the amplification was successful. These methods allow amplified signals to be generated from a single amplicon and may have little effect on the progress of the reaction, with some modified dNTPs being utilised more readily than their natural counterparts (Kielkowski et al., 2014). There are no specific primer design requirements or modified oligonucleotide sequences needed for these methods. This signal-on approach can also produce a wider linear range and detection window.

In this chapter, a novel approach to direct DNA labelling was investigated. Protein-tagged nucleotides have been shown to be well tolerated by *Taq* polymerase enzymes driving PCR reactions, even when the bound protein is of a similar size to the polymerase. Work by Welter et al. (2016) showed that HRP-conjugated dTTP is incorporated into a single-base primer extension, resulting in a product which gives bands 178 base pairs higher than expected on a polyacrylamide gel. Compared with unmodified dTTP, dT^{15HRP}TP (HRP-dTTP) exhibited only a 6-fold reduction in inclusion efficiency for the *KlenTaq* polymerase tested. This system was used to perform naked-eye detection of a complementary DNA target compared to non-

complementary and single-base mismatched DNA. Taking advantage of the enzymatic activity of the HRP, as low as 1 fmol complementary DNA could be distinguished based on a colour change of the solution from clear to red. However, this required filtering of the PCR reaction to remove unincorporated HRP-dTTP which would produce background signal.

The experiments reported in this chapter take advantage of HRP activity to report detection of a DNA target. The HRP enzyme reduces H_2O_2 , taking an electron from a donor species to do so. In this case the species used was 3,3',5,5'-Tetramethylbenzidine (TMB), which becomes oxidised as a result of this donation (Figure 4.1). Each HRP enzyme will convert H_2O_2 at a specific rate, and the overall rate of H_2O_2 reduction and TMB oxidation is therefore dependent on the concentration of HRP. Using chronoamperometry to reduce the oxidised TMB, the current response will be proportional to the concentration of TMB surrounding the electrode. By allowing the HRP to oxidise TMB for a fixed duration, this response also becomes proportional to the amount of HRP within the solution. It is this proportionality that the following experiments were designed to exploit, where the presence of a DNA target will anchor more HRP to the electrode and produce a greater current response.

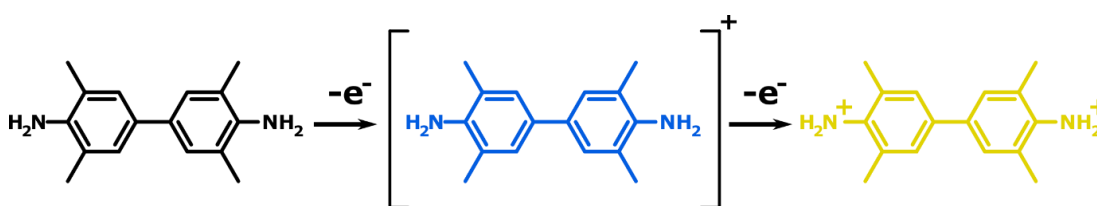


Figure 4.1 – Reversible oxidation of TMB. Colourless when reduced, the first oxidation of TMB results in a blue solution. Oxidising further produces a yellow solution. Both can be reduced to return the solution to colourless. Figure adapted from Bally and Gribnau, 1989; Josephy et al., 1982.

A detection system based on the incorporation of HRP-dTTP nucleotides into an isothermally amplified DNA sequence was examined. Using a sample of these HRP-dTTP nucleotides, oxidation of TMB was detected electrochemically on a previously tested electrode platform. Tolerance of an isothermal RPA reaction towards these modified nucleotides was then tested, as well as RPA performance using low nucleotide concentrations to enhance inclusion of the modified nucleotides. Next, solid-phase RPA reactions were performed to tether the HRP-dTTP to the electrode surface and perform electrochemical readout without extensive purification of the amplicon. Finally, these reactions were tested on bacteria bearing the synthetic AMR plasmid, working towards minimal sample preparation following overnight

culture to sensitively detect low concentrations of resistant bacteria in under an hour. When referring to plasmid in this chapter, all plasmid bearing bacteria contained the bespoke AMR plasmid designed as part of this research. No clinical plasmid isolates were tested.

4.1 Methods

4.1.1 Measurement of TMB Redox Responses on Gold SPEs

AT and BT SPEs were cleaned following previously discussed methods and then covered with 50 μL of H_2O_2 and TMB solution. CV was performed from -0.4 V to 0.8 V at 100 mV/s. Based on these CV's, chronoamperometry was performed with the following parameters; -0.4 V pre-treatment for 10 seconds to reduce oxidised TMB; 0.225 V oxidation for 2, 4, 8 or 16 seconds to simulate increasing oxidised TMB concentration; -0.15 V amperometric measurement for 20 seconds. These results are shown in Figure 4.3. The same pre-treatment and oxidation settings were used for DPV measurements on BT SPEs, with the DPV being performed from 0.2 V to -0.1 V with a 50 mV pulse, 50 ms pulse duration and 20 mV/s scan rate. The results from BT SPEs are shown in Figure 4.4.

4.1.2 Measurement of HRP Oxidation of TMB

1 μL of 39.5 μM HRP modified dTTP was added to a clean AT SPE working electrode and allowed to dry. 50 μL H_2O_2 + TMB solution was added to this electrode and to a non-exposed AT SPE. Chronoamperometry and DPV were then performed as above without any pre-treatment or pre-oxidation steps.

4.1.3 Examining RPA Reaction Efficiency with Low Concentration dNTPs

The performance of an RPA reaction with low dNTP concentrations was examined. RPA reactions were prepared as standard, with different working concentrations of dNTPs. The standard concentration of 1.8 mM dNTPs was prepared as a control, and 100 μM and 7.36 μM dNTPs were also tested. Each of these reactions was quantified on a Qubit 4 Fluorometer for yield.

4.1.4 Measurement of HRP-dTTP Inclusion into Solid-Phase RPA

Solid-phase RPA on AT SPEs was performed following the previous protocol used on gold (detailed in Section 3.4.1.2) with some modifications. A 10:1 ratio of 1 μM OXA Forward RPA primer : 1 mM MCH in 1xPBS + 5 mM TCEP was prepared and pre-reduced for one hour. 8 μL of this solution was added to the working electrode of each device and incubated for 2 hours

at room temperature. Electrodes were then rinsed with diH₂O. This concentration of OXA Forward RPA primer is higher than those used by Khater et al.

RPA reactions for the solid-phase amplification were prepared following electrode functionalisation. Table 4.1 shows the reaction components and preparation process, with the reaction prepared in a single tube by sequential addition of reagents, unless otherwise stated in the Table. 10 µL of this RPA reaction was added to each electrode, followed by AMR plasmid template or H₂O which was pipette mixed into the reaction. Electrode groups were then incubated in separate humidified chambers. Electrodes were then rinsed with 1xPBS for 20 seconds and incubated with H₂O₂ + TMB for 1 minute before amperometry was performed.

Table 4.1 – Solid-phase RPA with HRP-dTTP preparation. Notes indicate at which points the mixture is mixed or added to electrodes.

Component	Volume / µL	Preparation Notes
Reaction Buffer	25	
160 µM dNTP Mix	6	
79 µM HRP dTTP	3	
Water	2.6	
10x Basic E-mix	5	
10 µM Reverse Primer	2.4	Vortex and briefly centrifuge.
Core Reaction Mix	2.5	Vortex and briefly centrifuge.
Magnesium Acetate	2.5	Vortex, then add to electrode.
Template	X	Volume X equals half the RPA volume added to the electrodes. Pipette mix on surface.

During a second experiment, the SAM layer was formed with 10 µM OXA Forward RPA primer and 100 µM MCH in 1xPBS + 500 µM TCEP for 2 hours to produce a more probe-dense SAM film. To reduce any non-specific adsorption of the HRP-dTTP to the electrodes, the working, reference and counter electrodes were coated with this MCH SAM. The negative control electrodes in this repeat were modified with 100 µM MCH only across the entire 3-electrode cell. A reaction scheme for this process is shown in Figure 4.2.

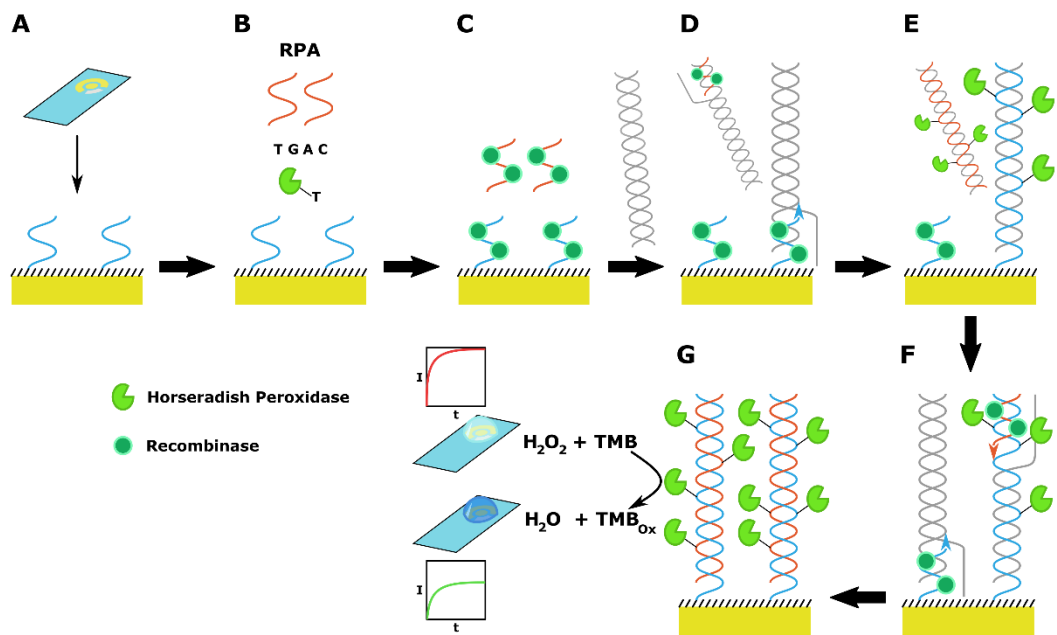


Figure 4.2 – Schematic of solid-phase amplification with HRP-dTTP. (A) Forward primer is immobilised on electrode surface with an alkanethiol monolayer. (B) An isothermal RPA reaction containing dNTPs, reverse primers and HRP-dTTP is added to the surface. (C) Recombinase proteins from reaction mix bind to solid and solution phase primers. (D) Addition of DNA template triggers recombinase insertion of primers and initiation of primer extension reaction. (E) Primer extension reactions include HRP tagged nucleotides in the extending DNA strand. (F) The reaction continues, extending further solid-phase primers and priming surface bound sequences. (G) RPA reaction is removed from the surface and replaced with peroxide and TMB solution for chronoamperometric detection of HRP mediated TMB oxidation. Polymerases and single-stranded binding proteins excluded for clarity.

4.1.5 RPA Amplification from *E. coli* Cultures

E. coli containing the AMR plasmid structure were grown overnight under standard conditions and then washed 3 times in sterile 1xPBS. These cultures were diluted in PBS to 10^{-2} , 10^{-4} and 10^{-6} . 100 μL of the 10^{-6} dilution was plated in triplicate for colony counting. 10 μL of each dilution was incubated at 95°C for 3 minutes to release the DNA from the cells. Standard liquid-phase RPA reactions were then prepared following the recommended protocol, using unmodified dNTPs. 1 μL aliquots of each dilution were used as template for a reaction; 3 reactions contained heat-treated (lysed) cells and 3 contained unheated (intact)

cells. A positive control consisting of 1 μL frozen plasmid and a negative control were also included. Following amplification, RPA amplicons were run on a 2% agarose gel for validation.

4.1.6 Detection of Plasmid Bearing *E. coli* Through HRP-dTTP Solid-Phase RPA

Next, the above protocol was tested using intact and lysed *E. coli* containing the template plasmid. *E. coli* were grown under standard conditions overnight and then washed 3 times in sterile 1xPBS. The culture was then diluted by a factor of 10^{-4} and 10^{-6} . Cells in the lysis trial were thermally lysed at this point by heating 100 μL of each dilution at 95°C for 10 minutes. 8 AT SPEs were prepared for this trial; 3 for the 10^{-4} dilution, 3 for the 10^{-6} dilution and 2 as a 1xPBS negative control. The 6 positive electrodes were modified with 10 μM OXA Forward RPA primer and 100 μM MCH. The two negative electrodes were modified with 100 μM MCH only.

The RPA reaction was prepared as in previous experiments with solid-phase RPA, with HRP-dTTP included as before. 10 μL of reaction mixture was added to each electrode. 5 μL of each bacterial dilution, or 1xPBS for the negative control, was added as the template material and electrode groups were incubated in separate humidified chambers for 40 mins. Samples of each RPA reaction were tested for DNA yield. Electrodes were washed with 1xPBS, incubated with H_2O_2 + TMB for 20 minutes before measuring. 100 μL 10^{-6} dilution of *E. coli* was plated in triplicate and incubated overnight before colony counting.

4.1.7 Discrimination of Plasmid Bearing and Non-Plasmid Bearing Bacteria

Primer sequences used in these reactions were sourced from Integrated DNA Technologies (Leuven, Belgium). For all reactions the RPA probe was used as the forward primer (Table 3.5).

4.1.7.1 RPA Discrimination of *E. coli* and *S. aureus*

A standard solution-phase RPA was first performed to determine the levels of non-specific amplification when using unwashed bacterial lysate. RPA was prepared without the addition of HRP-dTTP nucleotides. Positive *E. coli* template was grown as previously through overnight culture, and overnight culture was used without including a PBS wash. A negative control bacterium, *S. aureus* (strain NCTC 10788), was reconstituted in 1xPBS from a frozen Bioball stock (bioMérieux, UK) to produce a solution containing 1.1×10^8 CFU/mL. 100 μL of each template was then heated to 95°C for 10 minutes and diluted by a factor of 10^{-3} . 1 μL of these dilutions were added as template to the reaction mixtures. The reaction was run for 40

minutes at 39°C, before analysing on the Qubit 4 fluorometer and via agarose gel electrophoresis.

Solid-phase RPA was then tested on synthetic AMR plasmid bearing *E. coli* and plasmid free *Staphylococcus aureus*. AT SPEs were prepared, with all electrodes receiving 3 µM or 10 µM OXA Forward RPA primer and MCH (at a tenfold higher concentration) across the entire electrode array for 2 hours. The solid-phase RPA mixture was prepared with HRP-dTTP and 8 µL added to each electrode, followed by 4 µL of *E. coli* overnight lysate or *S. aureus* Bioball lysate. Templates were pipette mixed on the surface and incubated for 40 minutes at 39°C before washing in 1xPBS. Electrodes were then incubated for 15 minutes with H₂O₂ + TMB and chronoamperometry measurements performed in the solution.

4.1.7.2 Isolation of Non-Specific Amplification Sources

Solution-phase RPAs were performed using TwistAmp Liquid Basic and TwistAmp Basic RPA kits. Reactions were prepared according to the manufacturer's instructions.

4.1.7.3 Enhanced Surface Blocking for Bacterial Discrimination

AT SPE on-board reference electrodes were anodised by immersing the AT SPE into a 1M solution of NaCl. The AT SPE reference was connected as the working electrode, with external counter and reference electrodes used, and a potential of 1V was applied for 1 minute to form a layer of AgCl over the reference electrode surface.

Electrodes were modified using the gold functionalisation process used in early testing (described in Sections 2.3.1 and 3.2.2), with adjustments based upon the methods used for successful solid-phase RPA. 8 µL of 10 µM probe and 100 µM MCH, pre-reduced in 1xPBS + 500 µM TCEP, was incubated on the working electrode of each AT SPE chip overnight at room temperature. Electrodes were then rinsed in diH₂O and the entire electrode array was incubated for 1 hour with 1 mM MCH pre-reduced in PBS + 5 mM TCEP (40 µL per electrode). This was again rinsed with diH₂O.

Solid-phase RPA then proceeded as previously. As only the working electrode contained DNA probe, RPA volumes were reduced to 4 µL per electrode chip, with the addition of 2 µL of template solution which was pipette mixed into the reaction on the surface. Template consisted of heated *E. coli* overnight culture diluted in PBS, or heated *S. aureus* bioball diluted in PBS. Following amplification, electrodes were rinsed for 20 seconds in 1xPBS + 0.05% Tween and 10 seconds in 1xPBS to remove reaction proteins and non-specific amplification

products. Electrodes were then incubated for 12 minutes in H_2O_2 + TMB solution before chronoamperometry measurements taken.

4.2 Results and Discussion

4.2.1 Measurement of TMB Redox Responses on Gold SPEs

Screen-printed electrodes were chosen for this reaction due to the convenient format for small volume work. The 3-electrode cell can be completely covered with 40 μL of solution, unlike PGEs and TFGEs which have previously required large external reference and counter electrodes, increasing the required volume of measurement solution significantly. SPEs showed good response to SAM formation, and as this detection scheme was expected to rely less on the consistency of the SAM layer the issues with SAM variability would have a smaller impact on the measurement.

Figure 4.3 shows the CV and AT SPE chronoamperometry results for H_2O_2 + TMB solution. As seen in Figure 4.3A, both the AT and BT SPEs give a classic dual-peak profile for the 2-electron oxidation and reduction of TMB. The HRP enzyme performs a single electron oxidation of TMB, corresponding to the lower-potential oxidation peak. The electrochemical methods used here therefore target the lower-potential reduction peak.

Figure 4.3B shows the chronoamperometry results from an AT SPE when TMB is oxidised electrochemically to different concentrations. The potential of this oxidation (0.225V) was poised between the two oxidation peaks observed in the CV to give a single-electron oxidation of the TMB solution. A typical current-time transient for the reduction of TMB is observed at all oxidation durations, with increasing oxidation time resulting in a larger reductive current being passed. This data shows that chronoamperometry could be a suitable measurement technique for detecting the levels of oxidised TMB as a result of HRP mediated oxidation.

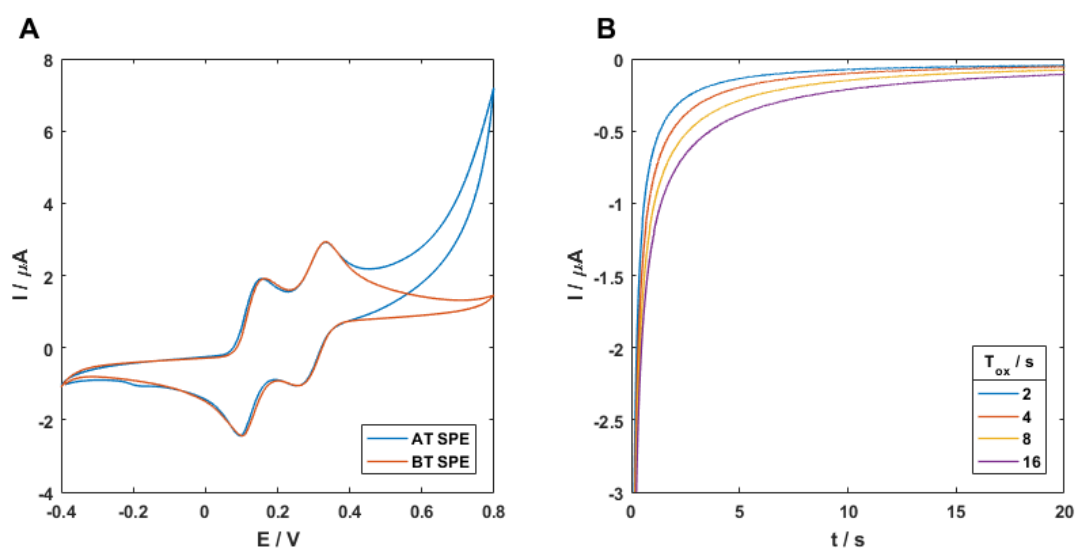


Figure 4.3 – TMB electrochemistry responses on unmodified gold SPEs. (A) CV responses of TMB + H_2O_2 solution on AT and BT screen-printed electrodes, exhibiting classic dual peak response. (B) Chronoamperometry at -0.15V with different TMB pre-treatment oxidation durations, on AT screen-printed electrode.

Following these tests, chronoamperometry and DPV were performed on BT SPEs as shown in Figure 4.4. The chronoamperometry responses of the BT electrodes were not as distinctive as those observed on the AT SPE (Figure 4.4A), with a 16 second oxidation step being more similar to the 8 second oxidation measurement. This may be due to differences in the rate of TMB oxidation on carbon vs gold, with the BT electrodes known to have much more carbon present in the electrode surface than the AT SPEs (Bernalte et al., 2013). Based on this, future detection experiments were performed on AT SPEs.

DPV measurements tested on BT SPEs (Figure 4.4B) do not show an increasing ΔI response with increasing initial oxidation; as oxidation time increases the peak ΔI decreases. This is likely due to the overlapping oxidation and reduction peaks, resulting in both processes occurring simultaneously during the DPV measurement and therefore reducing the current difference. DPV may therefore not be a suitable method for measuring the amount of HRP oxidised TMB as an inverse relationship between TMB_{ox} concentration and peak ΔI appears to exist.

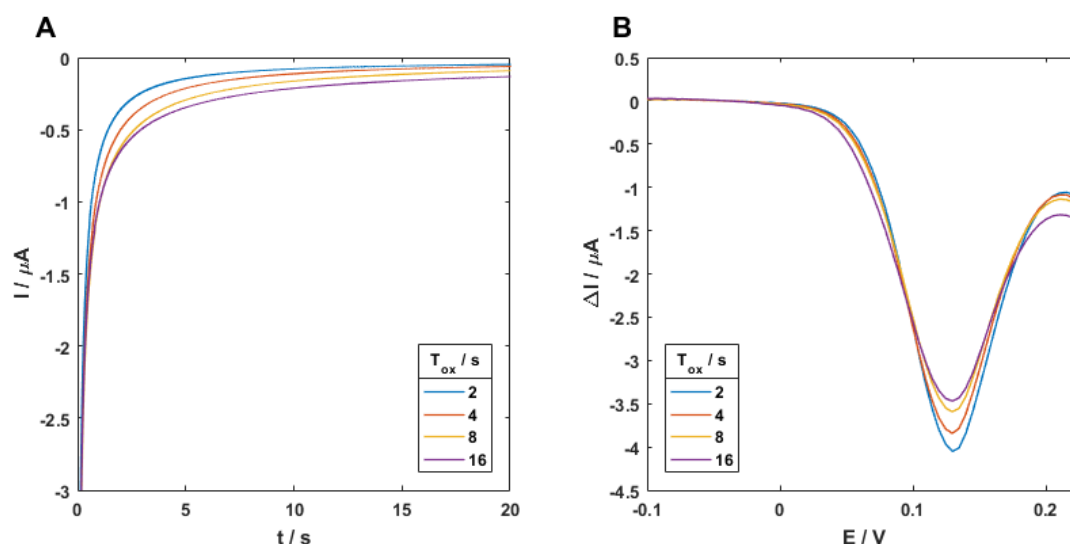


Figure 4.4 – TMB diagnostic electrochemical responses on BT SPEs. (A) Chronoamperometry with different TMB oxidation durations. (B) DPV with different TMB oxidation durations.

4.2.2 Measurement of HRP Oxidation of TMB

AT SPEs were then coated in HRP-dTTP nucleotides and the enzymatic oxidation of TMB in the presence of H_2O_2 was measured. Figure 4.5 shows chronoamperometry and DPV responses of measurements taken on an electrode with HRP-dTTP and one without.

Chronoamperometry results (Figure 4.5A) show a large increase in current when HRP-dTTP is present vs an electrode with no enzyme after 1 minute of incubation. With the concentration of HRP-dTTP applied to this electrode, total oxidation of the TMB solution was almost immediate (Figure 4.5A inset). DPV results (Figure 4.5B) were consistent with previous measurements using an electrochemical oxidation. The negative electrode exhibited much higher peak ΔI than the positive. The DPV responses show a 69% reduction in peak height between the negative and positive electrodes, despite there being large quantities of oxidised TMB present on the positive electrode and little to none on the negative. In contrast to this, the chronoamperometry results on the positive electrode show a 4636% increase at 20 seconds compared to the negative. Chronoamperometry appears to be a much more sensitive measurement for TMB oxidation by HRP than the DPV measurement used here. It also has the advantage of being a signal-on method allowing for much greater signal changes. Chronoamperometry was therefore used as the primary detection method for HRP oxidation of TMB moving forward.

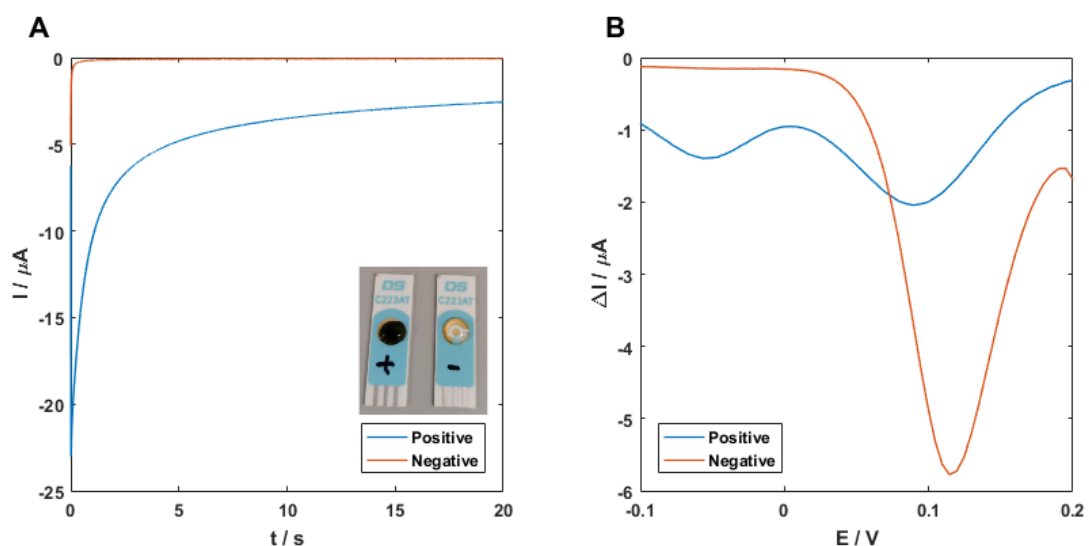


Figure 4.5 – Electrochemical response of HRP-dTTP oxidised TMB solutions on AT SPEs. (A) Chronoamperometry and (B) DPV.

4.2.3 Examining RPA Reaction Efficiency with Low Concentration dNTPs

Once the HRP-dTTP nucleotides were shown to be capable of oxidising TMB, the efficiency of RPA reactions using lower concentrations of nucleotides was examined. The DNA amplicon contains 55 thymine bases which are potential sites for HRP-dTTP inclusion, and in order to maximise HRP loading onto each amplicon a high ratio of HRP-dTTP to dTTP is required.

Due to the low concentration of HRP-dTTP, a high ratio requires lower dNTP concentrations than typically used. Two dNTP concentrations were tested alongside a standard reaction: a 100 μM working concentration and a 7.36 μM concentration. 7.36 μM was chosen as this represented a 1:1 mixture of 80 μM dNTP mixture and 79 μM HRP-dTTP solution giving an approximate 1:1 ratio of dTTP to HRP-dTTP. 100 μM was selected as an intermediate concentration for comparison.

Figure 4.6 shows the Qubit measured amplicon production for each of these reactions. The reaction containing 1.8 mM dNTP produced a dsDNA yield of 30.1 $\mu\text{g}/\text{mL}$. The 100 μM reaction yielded 31.4 $\mu\text{g}/\text{mL}$ and the 7.36 μM concentration yielded 17.3 $\mu\text{g}/\text{mL}$. Considering RPA performed with electrode-bound primers already exhibits reduced yields, a working concentration of 7.36 μM was deemed to be too low. A concentration between these two values was chosen, and a mixture of 2:1 160 μM dNTPs : 79 μM HRP-dTTP was used in future RPA reactions. This ratio could be expected to incorporate 4 - 5 HRP-dTTP nucleotides into

each OXA amplicon considering the reduced incorporation rate observed with *KlenTaq* polymerase.

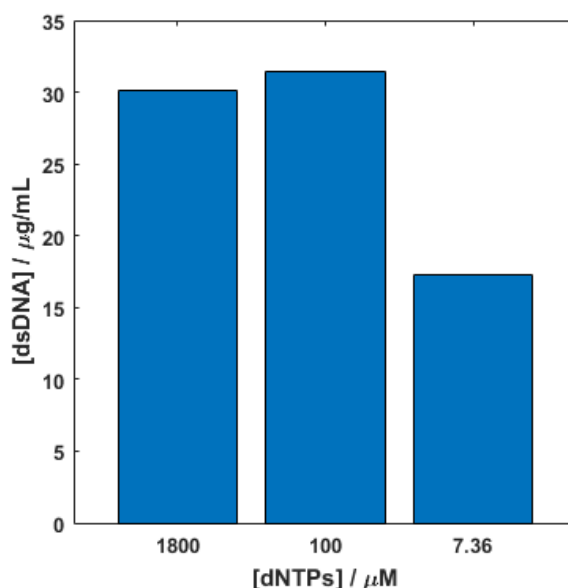


Figure 4.6 – DNA yield from solution-phase RPA reactions containing reduced dNTP concentrations. DNA quantified by Qubit 4 fluorometry after 40-minute reaction duration had elapsed.

4.2.4 Measurement of HRP-dTTP Inclusion into Solid Phase RPA

Using the previously identified ratio of nucleotides, solid-phase RPA reactions were performed on AT SPEs. Figure 4.7 shows chronoamperometry results from these experiments. Initially, only the working electrode was modified with the SAM layer (Figure 4.7A). When chronoamperometry was performed, no difference between positive and negative electrodes is observed despite there being a difference between the RPA amplicon yield (Table 4.2). The lack of distinction between the positive and negative electrodes was thought to be due to non-specific adsorption of the HRP-dTTP onto the untreated reference and counter electrodes, producing a consistent background signal across all devices.

A second experiment was performed to assess whether the background signal could be reduced. This followed the same protocol as the previous test but used a higher concentration of surface bound primer and had a negative control with no surface bound primer on the electrode to stop the RPA reaction. This experiment also coated all three electrodes in the system with a SAM layer to reduce non-specific adsorption of the HRP-dTTP. These modifications minimise RPA amplification in the negative and were made to give a

better indication of the effect blocking all three electrodes had on the non-specific signal. When the entire electrode array was incubated with SAM and primer solution (Figure 4.7B) a significant difference between the positive and negative electrodes is observed. This is largely attributed to increased primer density and primer coverage resulting in a 110% increase in RPA yield as detected by Qubit fluorometry (Table 4.2). This increase in yield led to a 4-fold increase in the measured current at 10 seconds, which was significantly different from the negative electrodes (2-sample T-test, 95% confidence).

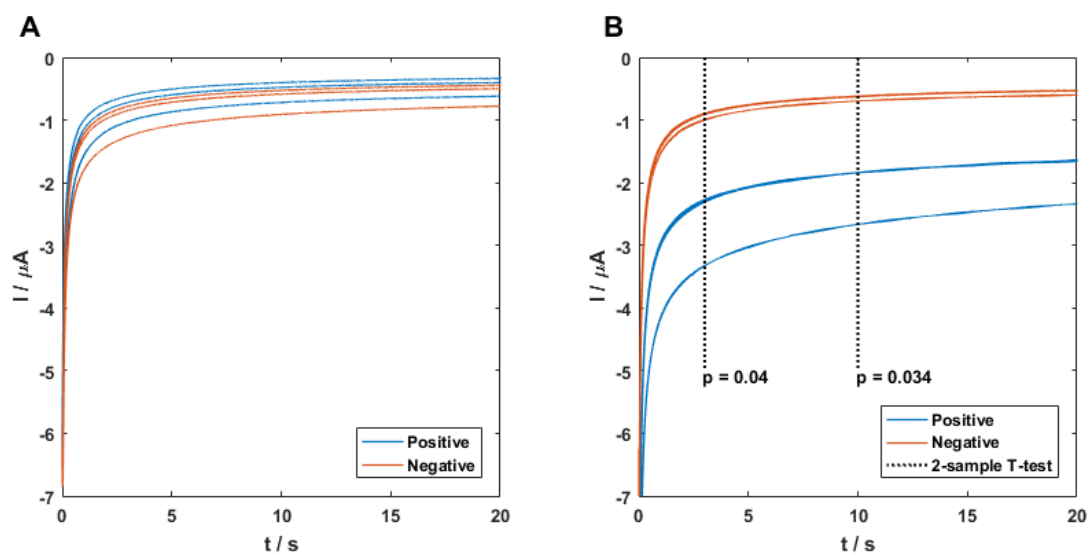


Figure 4.7 – Chronoamperometric detection of plasmid DNA amplified by solid-phase RPA using HRP-TMB system on AT SPEs. (A) Only working electrode modified with DNA probe and alkanethiol SAM layer. (B) A repeat of experiment shown in (A) with working, counter and reference electrodes modified with DNA probe and alkanethiol SAM layer.

Table 4.2 – DNA yield from solid-phase RPA on SPEs with different electrode blocking protocols.

Functionalisation	Positive Yield \pm SD (ng/ μL)	Negative Yield \pm SD (ng/ μL)
WE blocked, 3 μM Probe	1.43 \pm 0.195	0.55 \pm 0.055
All electrodes blocked, 10 μM Probe	3.00 \pm 0.397	0.49 \pm 0.055

The negative electrode shows a similar baseline current between the two experiments. This suggests that during the initial experiment either HRP wasn't adsorbing to the electrodes in significant quantities, or during the second experiment the MCH SAM was not effective at

preventing non-specific HRP adsorption at the reference and counter electrodes. MCH has been successfully used as a blocking agent in solid-phase RPA by del Río et al. (2017) and was found to produce a greater current density than other blocking agents such as a short DNA oligo or a more complex thiol. However, in these tests the SAM layer was incubated for 20 hours prior to measurements and so may have formed a much more consistent and effective barrier than the 2-hour protocol used here. There may simply have been minimal HRP fouling of the reference and counter electrodes observed in this first experiment.

Removing the surface bound forward primer from the negative control reaction had no effect on the measured current or DNA yield. This shows that there was no significant extension of the surface bound primers by the RPA reaction in the first negative controls, which could occur due to non-specific amplification or template contamination.

The relative standard deviation of the negative controls improved when incubating all three electrodes with MCH (30.9% with working electrode only, reducing to 6.2% with the entire electrochemical cell, measurement sampled at 10 seconds). This high initial standard deviation was due to a single negative electrode exhibiting a relatively high current, likely due to small amounts of HRP fouling which was prevented by blocking the whole 3-electrode cell with MCH. This blocking method had a smaller effect on the positive electrodes (30.6% reducing to 22.5% at 10 seconds).

Some interaction between the forward primer and the electrode may also be responsible for the electrode variability observed in the first test, and would explain why a larger decrease in the standard deviation was observed for the negative but not positive electrodes in the second test. AT SPEs are known to have variable carbon to gold ratios and may not have responded as well to cleaning as previously, both of which could affect surface probe density or conformation. However, the 22.5% relative standard deviation in the positive electrodes is the result of one response, which could be an outlier due to the highly variable SAM formation process on AT SPEs.

Adding surfactants such as Tween-20 to a wash buffer is a common method of reducing non-specific protein interactions. After measurements were taken, each electrode was washed with 1xPBS + 0.05% Tween for 10 seconds, before repeating the measurement process. This was used to determine if greater separation of the positive and negative signals could be achieved through removal of all HRP not anchored in the double helix.

Figure 4.8 shows the same electrodes as Figure 4.7B following a wash with PBS-Tween. Washing with PBS-Tween solution increased the mean current and the standard deviation of the measurements. These measurements are distorted by one electrode in each group. The PBS-Tween wash had little effect on the responses of electrodes 1 and 3 (positive) and 4 and 6 (negative). However, this wash caused a large change in the responses of electrodes 2 and 5. This greatly increases the mean and standard deviation of the group as a whole (shown in Table 4.3). Electrode 2 exhibited low similarity with the other positive electrodes during the first measurement, but electrode 5 showed a consistent response to the other negative electrodes. It is unknown what interactions between the wash buffer and matrix at the electrode surface caused such large increases in these two electrodes. It is interesting that washing with Tween resulted in a greater TMB oxidation signal for certain electrodes when a decrease would be expected. There may be some interaction between the hydrocarbon chain present in Tween and certain sites in the SAM layer which could allow for more efficient electron transfer by introducing defects in the blocking layer.

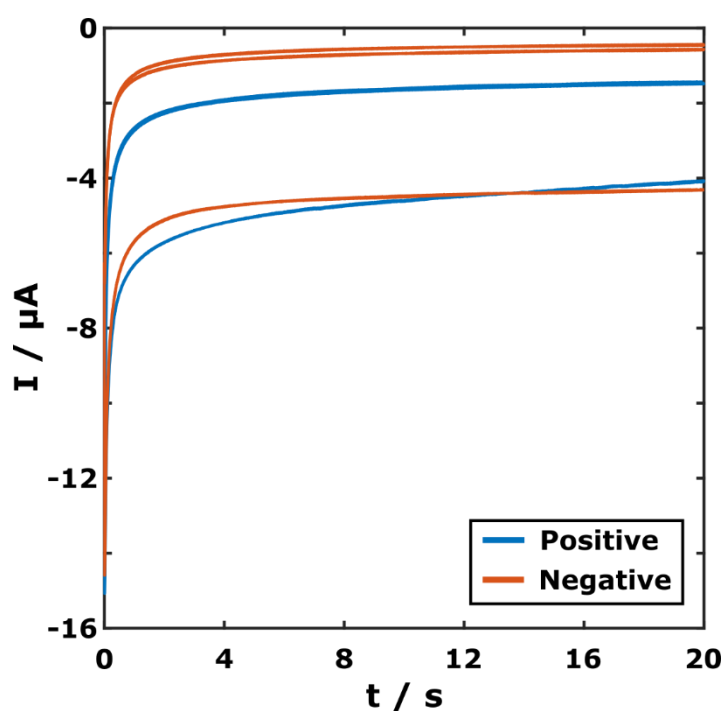


Figure 4.8 – Chronoamperometric detection of DNA amplified by solid-phase RPA using HRP-TMB system on AT SPEs following washing with 1xPBS + 0.05% Tween.

Table 4.3 – Chronoamperometry current at different time points following 1xPBS wash or 1xPBS with Tween-20.

Electrodes	Wash	I (mean ± SD) / μ A	
		Time t = 3s	Time t = 10s
Positive	1xPBS	-2.635 ± 0.600	-2.114 ± 0.476
	1xPBS + 0.05% Tween	-3.166 ± 1.936	-2.617 ± 1.712
Negative	1xPBS	-0.941 ± 0.041	-0.648 ± 0.045
	1xPBS + 0.05% Tween	-2.202 ± 2.314	-1.904 ± 2.253

4.2.5 RPA Amplification from *E. coli* Cultures

To confirm that RPA is capable of amplifying plasmid from a bacterial culture, reactions were performed using overnight *E. coli* cultures. Figure 4.9 shows the agarose gel electrophoresis results from each of these RPA reactions. Table 4.4 shows the colony counting results and equivalent CFU loaded into each reaction.

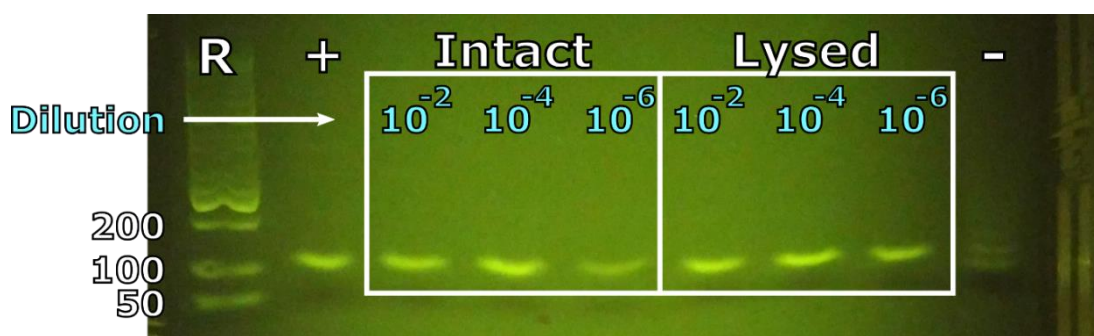


Figure 4.9 – Image of 2% agarose gel of OXA-1 RPA amplification from washed bacterial culture. R – 50bp reference ladder, + / - – positive / negative control, intact / lysed – cells heat treated (lysed) or not (intact) prior to reaction. Dilution indicates dilution factor from washed resuspended pellet. Faint bands are visible in the negative control due to slight contamination of the RPA kit. Stained with Sybr Safe DNA stain.

Table 4.4 – Mean CFU loaded to each RPA reaction for bacterial culture amplification.

Mean Colony Count (CFU / 100 μ L at a 10^{-6} dilution)	148
CFU Loaded to 10^{-2}	14767
CFU Loaded to 10^{-4}	148
CFU Loaded to 10^{-6}	1 - 2

Both intact and lysed bacterial cells exhibited good amplification of the target sequence. The positive control shows the expected position of the OXA amplicon clearly at 115bp. This is matched by the amplicon from each reaction confirming that the OXA sequence within the bacterial plasmid has amplified well. There are no additional bands which indicates that specific amplification has occurred. A small amount of amplification is present in the negative control which shows there is slight contamination in the reaction. As RPA produces high yields of DNA and is sensitive to even a single target this contamination is likely to have come from previous reactions using the same equipment.

All reactions amplified to a similar intensity as the positive control other than the 10^{-6} dilution of the intact cells. This is not unexpected considering the low number of cells loaded and the lower availability of template material with the intact cells. The washing step, performed at 4300 x g for 15 minutes, pellets bacterial cells but leaves free DNA in the supernatant to be discarded. The presence or absence of free plasmid within the bacterial pellet was not confirmed. This washing step was performed three times to minimise the abundance of plasmid in the final suspension. It is likely that in a biological sample there will be free plasmid due to immune mediated destruction or genetic transfer mechanisms which could be detected through RPA alongside the cell hosted plasmid.

4.2.6 Detection of Plasmid Bearing *E. coli* Through HRP-dTTP Solid-Phase RPA

Solid-phase RPA was then used to amplify OXA sequences from samples of *E. coli* cultures. Plasmid bearing *E. coli* were grown overnight and dilutions added to RPA reactions with or without cell lysis. Table 4.5 shows the colony counts of these overnight cultures, and the equivalent number of colony forming units added to each RPA reaction.

Table 4.5 – Mean CFU loaded to each solid-phase RPA reaction for bacterial culture amplification.

	Intact	Lysed
Mean Colony Count (CFU / 100 μ L at a 10^{-6} dilution)	160	126
CFU Loaded to 10^{-4}	800	630
CFU Loaded to 10^{-6}	8	6 - 7

Figure 4.10 shows the amperometry traces following RPA reactions loaded with *E. coli* or PBS. RPA reactions with *E. coli* present result in an increase in the chronoamperometry signal in all cases when compared with electrodes which inhibit amplification. Intact cells (Figure 4.10A) produce an increase in the measured current when 5 μ L of the 10^{-6} dilution is added to the reaction, but this is not significantly different from the negative control ($p = 0.16$). When a 100-fold higher concentration of cells are used as template, a further increase in current is observed. This is significantly different from the negative control at 3 and 10 seconds when measured by 2-sample T-test ($p = 0.04$). This concentration equates to approximately 800 cells loaded into the reaction, which gives confidence that samples with a similar concentration of cells could be detected without a lytic pre-treatment step. This concentration of cells is within the clinical range for bacterial infections of the skin or urinary tract, but above the typical range for bacterial blood infections (Kelley, 2017). Detection will depend not only on the CFU count, but also on the plasmid replicate number, so while detection of the specific bacterium may not be possible the sensor may be able to detect antimicrobial resistance genes of suspected bacterial blood infections if they are contained on high copy number plasmids.

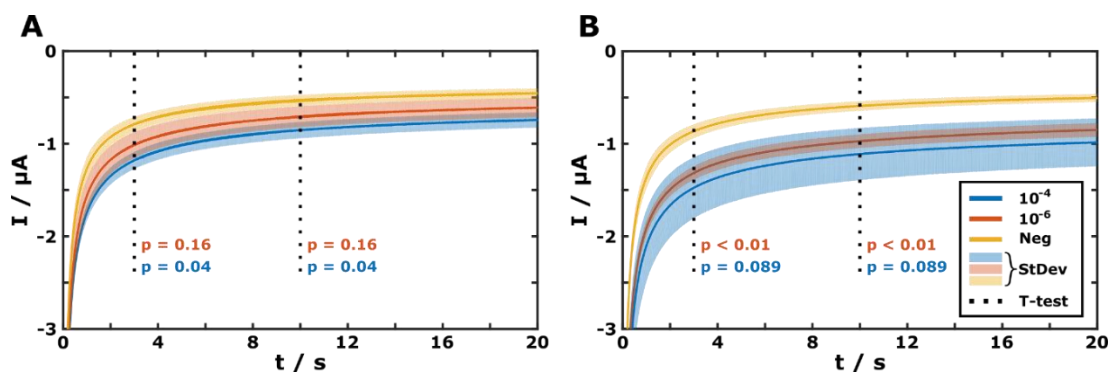


Figure 4.10 – Chronoamperometry results of DNA amplified by solid-phase RPA from washed bacterial culture on AT SPEs. Loaded cells were (A) Intact or (B) lysed prior to reaction. $n = 3$.

Figure 4.10B shows the chronoamperometry results when lysing cells prior to adding them to the electrode. Lysing cells prior to amplification results in greater differences between the positive samples and the negative control. The recorded current for the 10^{-6} dilution was significantly higher than the negative control across the measured duration. The 10^{-4} dilution produced a higher mean current than the 10^{-6} dilution as expected, but greater variability in the measured current means this is not significantly different from the negative. The response of the 10^{-6} dilution, detecting the addition of 6 – 7 CFU, is below the typical detection range for many bacterial infections.

Pre-treatment of the cells by thermal lysis increases the current measured by chronoamperometry following amplification. When loading a 10^{-6} dilution of lysed cells, the response (normalised against the negative control for each test) increased by 25% over the period 10 – 20 seconds since measurement start compared to the intact cells. The 10^{-4} dilution showed a normalised increase of 18.6% over the same period. This indicates that the lysis step is increasing the availability of plasmid for amplification, resulting in a greater amount of HRP being captured at the electrode surface.

4.2.7 Discrimination of Plasmid Bearing and Non-Plasmid Bearing Bacteria

For point-of-care testing, an electrochemical system must be able to distinguish between AMR gene bearing bacteria and bacteria without the specific target gene. Previous results have shown that this protocol can identify low numbers of bacterial cells compared to a solution containing only RPA proteins and HRP-dTTP. Tests to observe whether, with a fully

functional RPA reaction, this system could discriminate between AMR and non-AMR containing cells were undertaken next.

4.2.7.1 RPA Discrimination of *E. coli* and *S. aureus*

Initially, a standard solution-phase RPA reaction was run. Previous tests had used a PBS resuspension wash on the overnight culture to remove cellular debris and genomic DNA. This step requires a centrifuge and increases the total time from sample collection to answer. Figure 4.11 shows the gel electrophoresis result from these RPA reactions. A band above the 100 base pair reference line is clearly visible in the positive, with no amplification of this length in the negative. Fluorometry measurements of the *E. coli* and *S. aureus* loaded reactions reported a DNA yield of 76.8 and 42.8 ng/ μ L respectively. Longer DNA fragments are visible in both the positive and negative lanes of the gel. The difference between the two yields is associated with the production of the target amplicon in the positive which is absent in *S. aureus*.

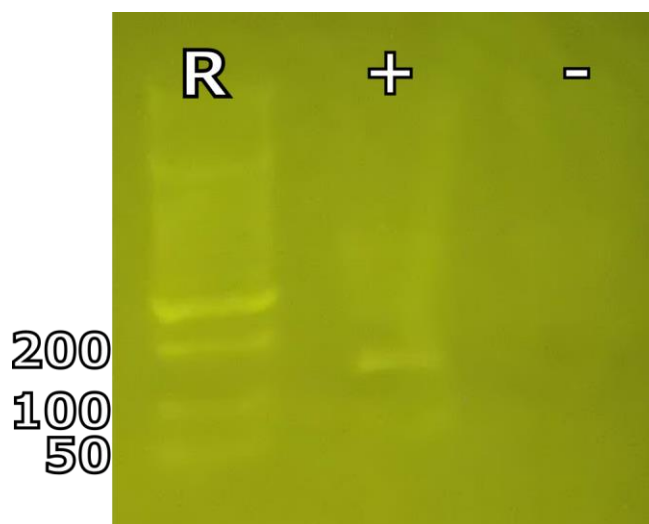


Figure 4.11 – Image of 2% agarose gel electrophoresis of liquid-phase RPA on unwashed bacterial lysate. R – reference, + – plasmid bearing *E. coli*, – – non-plasmid bearing *S. aureus*. Stained with Sybr Safe DNA stain.

This non-specific amplification may be due to complementarity between different sections of the genome (producing hairpin structures) or between the genome and other DNA sequences within the bacterial cell. However, as the RPA runs at a temperature below the natural annealing temperature of the primers there may also be non-specific interactions between the primers and the *E. coli* and *S. aureus* genomes resulting in amplification. The

quantity of specific amplicon produced in the *E. coli* indicated that electrochemical detection may still be successful, and electrodes were prepared for solid-phase detection.

AT SPEs were prepared using a concentration of 3 μM DNA Probe and 30 μM MCH. This concentration was revisited, since using 40 μL of 10 μM probe per electrode rapidly depleted probe stocks. Figure 4.12 shows the first attempt to discriminate *E. coli* and *S. aureus* using the electrochemical system. Chronoamperometry was unable to distinguish between positive and negative targets with either a PBS wash (Figure 4.12A) or PBS-Tween wash (Figure 4.12B). The noise visible in some of the traces was due to poor connection to the electrode, but the general trend of the data is clearly visible.

Washing with PBS-Tween produced the same increase in signal variability as previously observed. In these responses, both the positive and negative electrodes exhibited a high current response, greater than those observed for previous negative RPA reactions. These responses were initially attributed to poor blocking as a result of using the lower DNA and MCH concentrations.

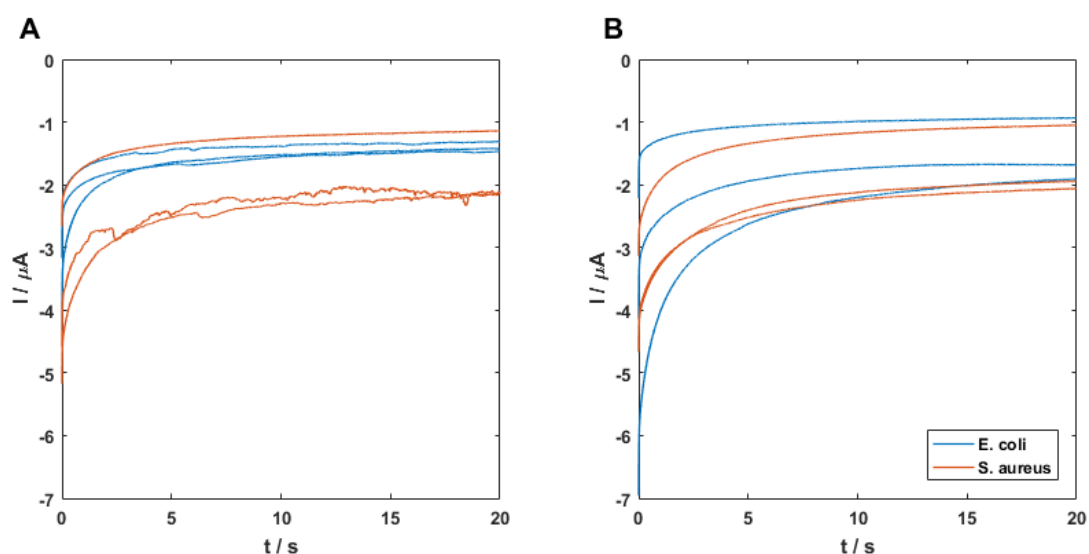


Figure 4.12 – TMB reduction current from solid-phase amplification of unwashed bacterial lysate with low density SAM formation. (A) Chronoamperometry following surface washing with 1xPBS and TMB incubation. (B) Chronoamperometry following surface washing with 1xPBS + 0.05% Tween and TMB incubation.

The more concentrated DNA SAM solution was then tested to confirm the above theory. A new set of electrodes were prepared using 10 μM DNA probe and 100 μM MCH and the

experiment repeated. Figure 4.13 shows the chronoamperometry traces following solid-phase amplification of *E. coli* and *S. aureus* on these electrodes. At both very short (Figure 4.13A) and long (Figure 4.13B) measurement durations, the electrodes loaded with *E. coli* produced a lower current response than those with *S. aureus*. Again, the current response of the negative electrodes is significantly higher than those previously observed for a negative RPA reaction containing HRP-dTTP, which typically showed 0.5 μA current after a 20 second measurement period (Figure 4.10). This suggested that the response observed here was not entirely due to fouling by the HRP-dTTP or poor surface blocking but could be linked to non-specific amplification occurring within the reaction. Further experiments were undertaken to identify the source of the suspected non-specific amplification responsible for these large current responses.

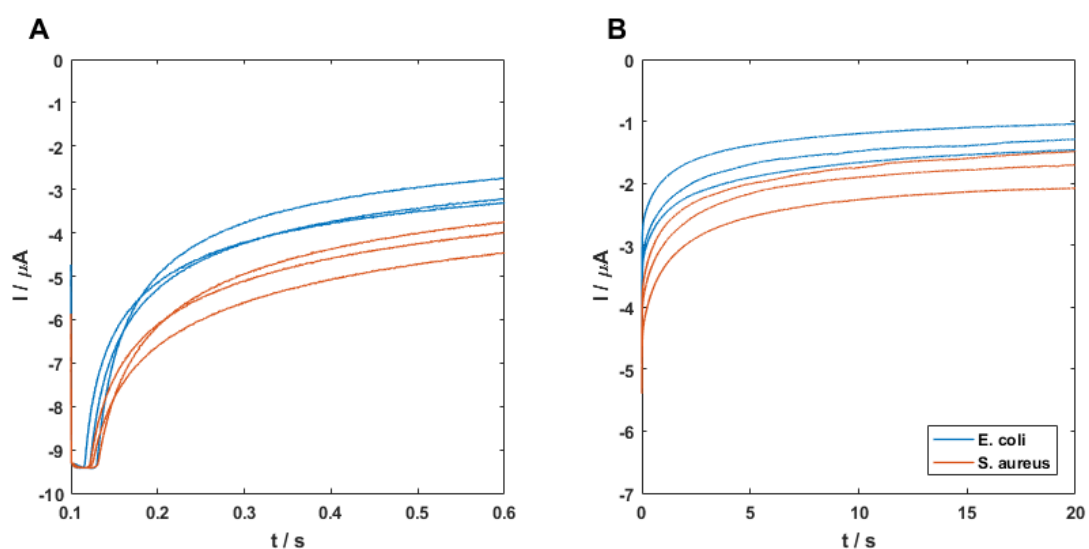


Figure 4.13 – TMB reduction current from solid-phase amplification of unwashed bacterial lysate. (A) High resolution rapid chronoamperometry measurement. (B) The following 20 seconds of measurement.

4.2.7.2 Isolation of Non-Specific Amplification Sources

Several standard solution-phase RPA reactions were performed to examine whether non-specific amplification occurs within these reactions. Four reactions were performed with the liquid basic RPA kit; one benchmark using the existing lysed *E. coli* solution at a 10^{-4} dilution, one with this solution diluted another 100-fold, one with freshly prepared *E. coli* culture using a new Ampicillin solution, and this same culture washed with 1xPBS three times as previously described. These two cultures were also diluted to 10^{-4} .

Four additional reactions were performed to identify if this was a specific issue with the Liquid Basic kit being used. Two reactions were prepared using a TwistAmp Basic kit which uses a freeze-dried reagent format, and two prepared using an older Liquid Basic kit. A reaction for a 10^{-4} diluted *E. coli* template and a 10^{-4} diluted *S. aureus* template was prepared with each kit. These reactions are summarised in Table 4.6, along with the Qubit reported dsDNA yield for each. Figure 4.14 shows the gel electrophoresis results for each of the reactions.

Table 4.6 – Summary of RPA exploratory reaction panel.

No.	1	2	3	4	5	6	7	8
Kit	Liquid Basic	Liquid Basic	Liquid Basic	Liquid Basic	Basic	Basic	Liquid Basic (Old)	Liquid Basic (Old)
Target	<i>E. coli</i>	<i>E. coli</i> (10^{-6} dilution)	New <i>E. coli</i> (LB)	New <i>E. coli</i> (PBS)	<i>E. coli</i>	<i>S. aureus</i>	<i>E. coli</i>	<i>S. aureus</i>
Yield (ng/ μ L)	40.8	22.6	35.2	27.2	47.6	36.7	26.2	29.8

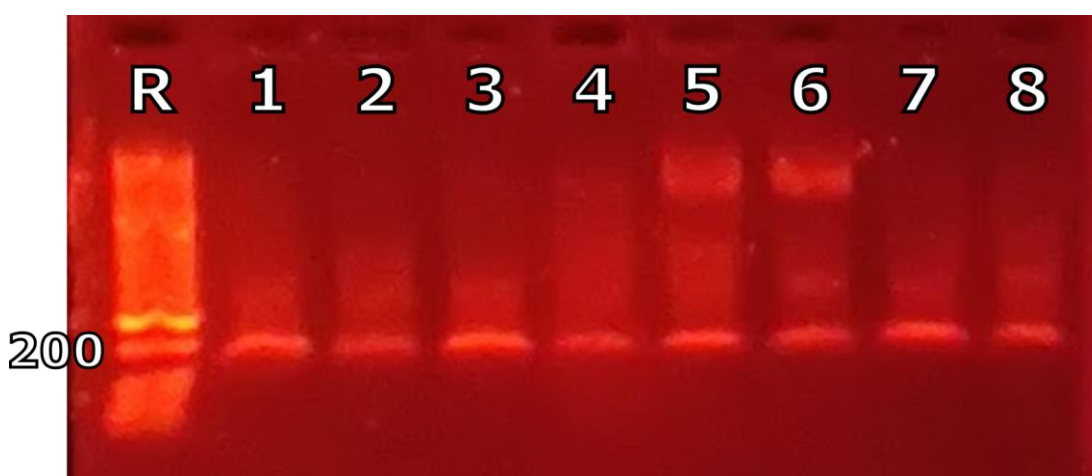


Figure 4.14 – Image of 2% agarose gel electrophoresis on RPA exploratory panel. R – reference, lane numbers correspond to reaction number in Table 4.6. Stained with Sybr Safe DNA stain. This image is red due to the use of an alternative transilluminator system to the BlueGel.

All reactions appeared to show a level of non-specific amplification. Reaction 2, containing a lower concentration of *E. coli*, indicates that these longer DNA sequences are not simply

genomic DNA fragments from the cell lysis process as the smear is of a similar intensity to that observed in reactions containing 100-fold greater *E. coli* concentrations. Reactions 3 and 4 indicate that the ampicillin concentration was not an issue, which may have led to a higher concentration of non-plasmid bearing *E. coli* or contaminant bacteria growing in the culture resulting in larger quantities of genomic DNA being observed in the gel. Reaction 4 also confirms that the PBS washing process does not resolve this issue.

Reactions 5 through 8 all show a band at the expected height for the OXA amplicon, even in the *S. aureus* reactions. These older kits were replaced due to known contamination issues so the presence of the OXA band here is expected and does not indicate contamination of the in-use Liquid Basic kit or *S. aureus* lysate. These reactions each show that the non-specificity is not limited to the new Liquid Basic kit, and therefore could not be solved by using an alternative RPA reaction kit.

Sánchez-Salcedo et al. (2019) reported issues with non-specific interaction between a fluorescently labelled primer and electrode surface. This reaction used a 6-FAM tagged primer which bound to an anti-fluorescein antibody-enzyme conjugate to produce an electrochemical signal. The report attributed non-specific signal using the liquid basic kit to unwanted interactions between the solution-phase primer and the electrode (blocked with p-aminothiophenol). By changing the concentration of core reaction mix in the final reaction, an increase in signal to noise ratio (up to the recommended concentration of CRM) and a decrease in signal magnitude was observed. A reduction in the background signal by reducing the concentration of the solution-phase primer from 480nM to 75nM was also noted.

Toldrà et al. (2020) also described high levels of background signal using unpurified RPA amplicon for electrochemical detection of target DNA. These electrodes were functionalised using an overnight probe immobilisation and backfilled with MCH. Similarly, this article reported that reducing the solution phase primer concentration below the manufacturer's recommendation improved the signal to noise ratio, but without any decrease of the positive signal (when measured through absorbance). This background signal was attributed to the formation of primer-dimers from an excess of residual primer in the reaction.

These changes to the reaction constituents resulted in a background chronoamperometry signal of 500nA, which was equivalent to the background currents observed herein for a non-amplifying RPA reaction (Figure 4.10A/B, yellow traces). Both highlighted reports performed SAM formation using an overnight protocol, in contrast to the shorter 2-hour method

described by Khater and adapted for use in the experiments reported here. Considering this similarity between results with different SAM formation protocols, improvements to the SAM layer formation process were examined before changes to the RPA reaction matrix were made.

4.2.7.3 *Enhanced Surface Blocking for Bacterial Discrimination*

Changes to the electrode preparation process were implemented to circumvent the effect of non-specific amplification on the electrochemical detection. Improvements to the blocking and pre-treatment processes were expected to limit the amount of biofouling by non-specifically amplified DNA sequences and allow a specific signal to be isolated from the background DNA amplification.

During previous experiments with HRP-dTTP on AT SPEs, it was noted that blue speckling and discolouration of the silver reference electrode occurred after longer incubation times with HRP-dTTP, H₂O₂ and TMB (Figure 4.15). These discrete sites for TMB oxidation appeared to be the result of degradation of the reference electrode, and it was believed that the reference electrode could be a source of non-specific HRP adsorption alkanethiol SAMs do not form readily on silver. The reference electrode was anodised in a solution of sodium chloride to produce an AgCl layer to prevent this degradation and reduce the amount of background signal generated. The incubation time with H₂O₂ and TMB was also reduced to 12 minutes as the previous *E. coli* and *S. aureus* SP-RPA experiment produced large chronoamperometry currents and high quantities of oxidised TMB across all electrodes with a 20-minute incubation.

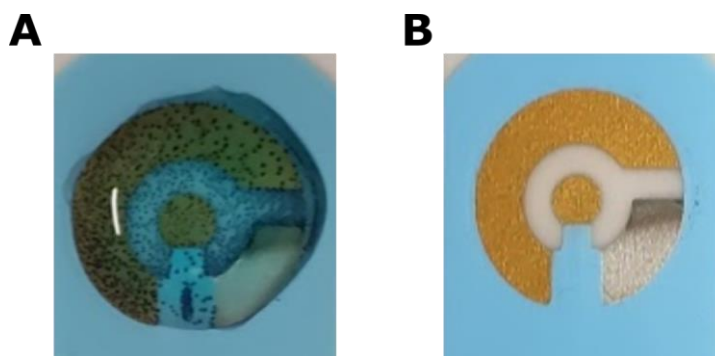


Figure 4.15 – Degradation of Silver reference electrode through HRP reduction of peroxide. (A) Localised TMB oxidation sites and discolouration of reference electrode while in H₂O₂ + TMB solution. (B) Degradation of reference electrode following incubation.

In addition to the anodisation of the reference electrode, blocking of the gold electrodes was improved. It was believed that the 2-hour SAM formation process, using moderate concentrations of MCH, was not sufficient to create a confluent SAM layer across the electrode surface. Electrodes were therefore treated using the overnight SAM formation protocol, with a concentrated backfill step across the whole electrode array to block the surface more effectively from adsorbing species.

Figure 4.16 shows the chronoamperometry results from solid-phase RPA on *E. coli* and *S. aureus* using this alternative electrode functionalisation method. The current response for electrodes loaded with plasmid bearing *E. coli* is significantly greater than for *S. aureus*. A 2-sample T-test performed on these results at 5 seconds and 10 seconds produces p-values of 0.005 and 0.006 respectively (2-sample T-test, 95% confidence).

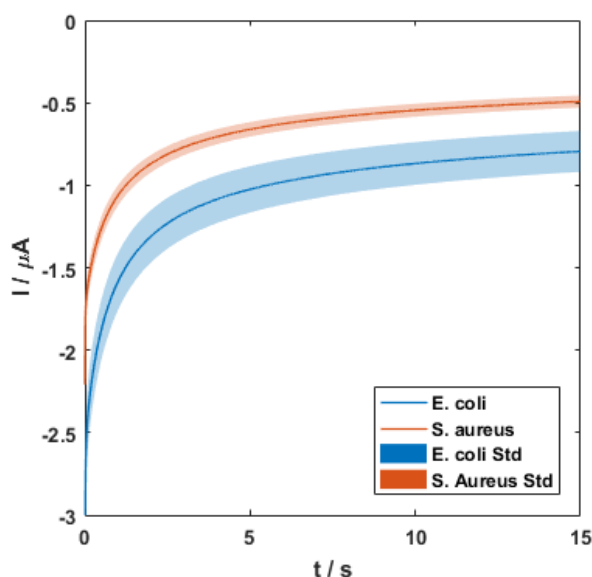


Figure 4.16 – Mean TMB chronoamperometry current from solid-phase RPA on unwashed bacterial lysate using overnight-backfill SAM formation method. Mean \pm standard deviation, $n = 5$.

Using a concentrated SAM solution to block the working and reference electrodes, as well as applying an AgCl layer to the reference electrode resulted in greatly improved detection compared to using the 2-hour SAM formation protocol for unwashed bacterial lysate. The current response from all electrodes is lower than observed for the 2-hour method, indicating either improved electrode blocking or reduced HRP concentration at the surface.

Both factors likely contribute, as the improvements to surface passivation will reduce the amount of HRP non-specifically bound to the electrode.

Figure 4.17 shows a comparison between this overnight detection scheme and the data obtained for bacterial cells or blank RPA using the 2-hour protocol as shown in Figure 4.10. The current responses of the overnight *E. coli* reactions shown in Figure 4.17A lie within the standard deviation of the 2-hour protocol responses. This result suggests that there is minimal decrease in RPA efficiency when using very low RPA volumes. Reaction volumes as low as 10 μL are often used for solid-phase amplification, with some groups reporting amplification with 6 μL reaction volumes in a small volume sealed chamber (del Río et al., 2017; Jauset-Rubio et al., 2017; Khater et al., 2019; Santiago-Felipe et al., 2016, 2014). These lower volume reactions in a simple humidity chamber have performed similarly to the higher volumes typically used in solid-phase RPA.

This overlap also shows that the RPA reaction is not significantly affected by amplification from a complex sample. *E. coli* in the 2-hour functionalisation protocol shown here were washed in 1xPBS, whereas the overnight results come from unwashed culture samples. Removal of this pre-treatment requirement simplifies and speeds up the assay without reducing performance of the reaction or sensor.

The negative current response produced by *S. aureus* is also very similar to the response observed when a non-amplifying RPA was previously used (Figure 4.17B). This data indicates that the improved blocking of the surface has successfully prevented the significant background signal that non-specific amplification was previously producing. The results obtained with *S. aureus* are equivalent to using a non-amplifying reaction containing HRP-dTTP nucleotides. This current range may be due to similar levels of HRP remaining at the surface in each case or could be related to the improved surface coverage by MCH decreasing the TMB reduction current despite higher HRP levels.

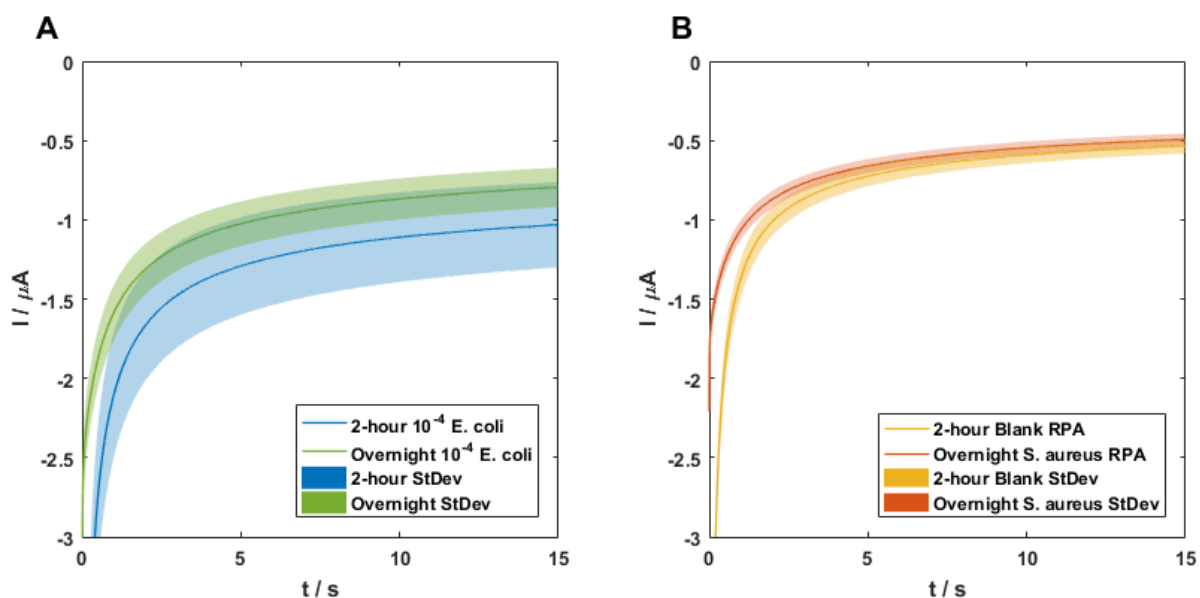


Figure 4.17 – Comparison of TMB reduction current for 2-hour and overnight SAM formation protocols. (A) RPA reactions loaded with 10^{-4} dilution of *E. coli*. (B) Blank RPA compared to *S. aureus* loaded reaction.

The relative standard deviation of the *E. coli* loaded reactions decreased from 25.6% with the 2-hour protocol to 14.9% with the overnight protocol. This reduction is greater than expected for increasing from 3 to 5 electrodes. This data supports the theory that the overnight protocol produces a more consistent SAM layer with more effective blocking, reducing the effects of RPA proteins, SAM layer defects and non-specific HRP adsorption on the resulting TMB signal.

Using the following equation;

$$C_P = \frac{N_C N_P M_P}{617.96 L_P V} \quad (4.1)$$

where C_P is the plasmid concentration, N_C is the estimated number of cells loaded to the reaction, N_P is the estimated number of plasmid copies per cell, M_P is the mass of each plasmid in grams, L_P is the length of the plasmid in base pairs, and V is the volume of solution used, an estimate of the concentration of plasmid loaded into each reaction can be made. The cultures for this reaction were not colony counted, but using the highest colony count previously observed for these cells in LB media (160 cells per $1 \mu\text{L}$ at a 10^{-4} dilution) and the highest expected number of plasmid copies (20 copies per cell), an estimated 23fg of cell-borne plasmid was loaded into each reaction, equivalent to a concentration of 5.31fM DNA

target. As the cells were not pelleted and resuspended there is likely to be free plasmid in the media also, resulting in the cell-based value being an underestimation of total target load. However, detection at and below this level using washed bacteria has been previously shown against a similar current response in the negative control.

Based on the estimated values above, this reaction was loaded with approximately 320 CFU of *E. coli* diluted in PBS directly from overnight culture. The *S. aureus* reaction was calculated to contain approximately 22 CFU, which is an order of magnitude lower than the estimated loading to the positive reaction.

A dose response curve for the discrimination of *E. coli* from *S. aureus* was then generated. An overnight culture of *E. coli* was colony counted and three dilutions of this broth were used in solid-phase RPA reactions on AT-SPEs modified using the overnight functionalisation protocol. The mean colony count for *E. coli* produced an overnight count of 2.08×10^9 CFU/mL. This was diluted by a factor of 10^{-4} , 10^{-5} and 10^{-6} for inoculation into solid-phase RPA. Table 4.7 gives the CFU loaded into each of these reactions, and their equivalent CFU/mL at the given dilution factor. *S. aureus* was diluted to the same concentration as the highest *E. coli* concentration used, loading 416 CFU of *S. aureus* into the negative control reaction.

Table 4.7 – Mean CFU loaded into each solid-phase RPA reaction.

	Actual CFU	Equivalent CFU/mL
Mean Colony Count (CFU / 100 μ L)	208	2.08×10^9
CFU Loaded to 10^{-4}	416	208×10^3
CFU Loaded to 10^{-5}	41.6	20.8×10^3
CFU Loaded to 10^{-6}	4.16	2.08×10^3

Figure 4.19 shows the chronoamperometry traces of 416 CFU *E. coli* and 416 CFU *S. aureus* amplified using HRP-dTTP solid-phase RPA on electrodes modified using the overnight functionalisation protocol. A significant difference between the two responses is observed as in previous experiments, with a p-value of 0.003 for the currents recorded at 10 seconds (2-sample T-test, 95% confidence).

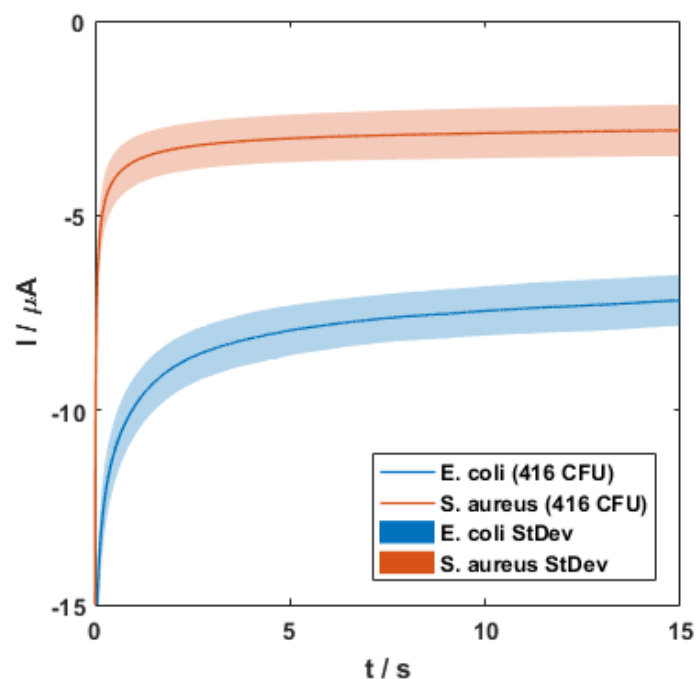


Figure 4.18 – Mean TMB chronoamperometry reduction current following HRP-dTTP solid-phase RPA and incubation with H_2O_2 + TMB solution on 416 CFU unwashed *E. coli* or *S. aureus*. Traces show mean \pm standard deviation, $n = 3$.

Issues surrounding the reproducibility of the SAM formation protocol persist, with all currents recorded in these reactions notably higher than previously. For example, whereas previous negative controls showed a consistent current response around $-0.5 \mu A$ after 15 seconds, the negative here produced a mean current of $-2.89 \mu A$. As the positive current is also high ($-7.45 \mu A$) with a similar magnitude of cell loading to previously, this effect is not believed to be the result of the higher *S. aureus* concentration in the negative reaction.

Figure 4.19 shows a dose response curve for the three concentrations of *E. coli* tested. The baseline is calculated from the *S. aureus* electrode responses using the common formula for limit-of-detection calculations;

$$\text{Baseline} = \text{Negative mean} + 3 \times SD \quad (4.2)$$

where the intersection of the fitted curve and the baseline indicates the limit-of-detection of the system.

All three concentrations tested exceed the baseline value, indicating that as few as 4.16 CFU of *E. coli* were successfully detected compared to 416 CFU *S. aureus*. High variability was present in the lowest concentration responses which is attributed to the apparent issues with

SAM formation across these electrodes. Definitive detection of 41.6 CFU of *E. coli* was achieved despite these issues, with both the mean and standard deviation of this measurement lying outside of the baseline.

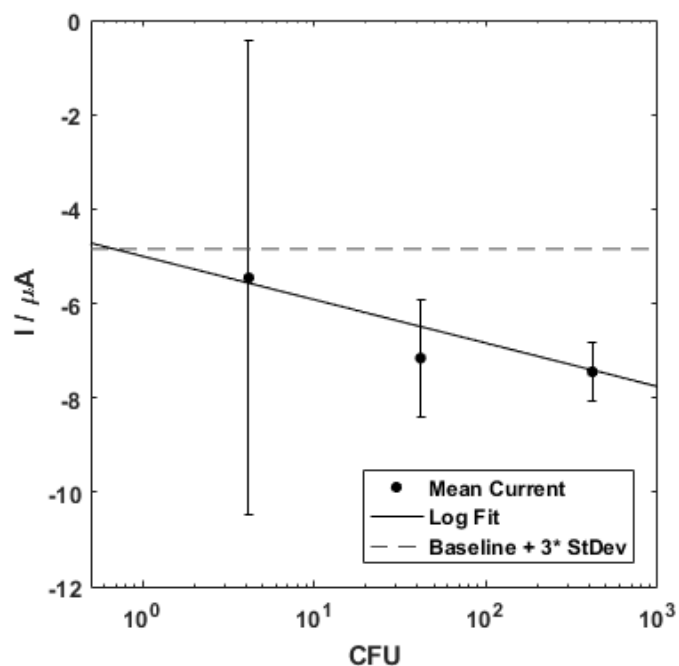


Figure 4.19 – Dose response curve of *E. coli* detected using TMB reduction current following HRP-dTTP solid-phase RPA and incubation with $\text{H}_2\text{O}_2 + \text{TMB}$ solution. 416 CFU *S. aureus* was used to produce a negative baseline response. Error bars = SD, $n = 3$.

Fitting a curve to the data allows the calculation of a limit of detection for the system. This LoD is indicative of the minimum possible CFU or DNA load the sensor could detect, although improvements to the variability in this set of experiments would allow a greater confidence in the calculated LoD. The intercept of the line of best fit and the baseline threshold occurs at a CFU value of 0.637. This value is equivalent to a bacterial concentration of 319 CFU/mL.

4.2.7.4 Comparisons with Similar Amplification-Based Biosensors

The combination of enzyme-tagged nucleotides to an electrochemical detection scheme has improved upon the detection limits previously attained using HRP-dTTP nucleotides. Welter et al. (2016) achieved naked eye detection of 0.5 μg of *E. coli* RNA when adding a single HRP-tagged nucleotide to the end of each primer strand at room temperature. The extension reaction proceeded over 15 minutes, but several centrifugation, resuspension and washing steps were required before readout could be performed. The increased sensitivity of electrochemical methods compared to naked eye optical detection, as well as the full-length

reaction product and longer reaction time, have allowed this system to detect significantly lower quantities of nucleic acid target using the same chimeric nucleotide. The total time to result of this system is around 1 hour, which is similar to the RPA amplification times of some other solid-phase electrochemical detection systems reported in the literature (del Río et al., 2017; Kersting et al., 2014; Khater et al., 2019) and the time to result of other enzyme-based solid-phase RPA systems (Mayboroda et al., 2016; Sánchez-Salcedo et al., 2019).

Table 4.8 summarises the detection schemes and limits of detection (LoD) for some solid-phase RPA based biosensor systems. The amplification and detection system described here produced an LoD of 319 CFU/mL, equivalent to 10.6 aM DNA, which is comparable or better than the limits of detection of other solid-phase RPA sensing systems.

Table 4.8 – Detection schemes and target thresholds for solid-phase RPA nucleic acid biosensors.

Detection Scheme	Measurement	LoD	Reference
HRP-labelled Primers	Chronoamperometry	1 – 500 fM	del Río et al. (2017)
Fluorescent Primers	Fluorescence	10 – 100 CFU	Kersting et al. (2014)
Redox Mediator	EIS	1000 fg / μ L	Khater et al. (2019)
Biotinylated Primer and HRP-Streptavidin	Absorbance	0.314 fM	Mayboroda et al. (2016)
Peroxidase-labelled Anti-primer Antibody	Chronoamperometry	10 ⁵ Copies	Sánchez-Salcedo et al. (2019)
DIG-labelled dNTP, Anti-DIG Antibody and HRP-labelled Antibody	Optical Intensity	50 - 900 fg DNA	Santiago-Felipe et al. (2016)
Micro-ring Resonance	Wavelength Shift	500 fg / μ L	Shin et al. (2013)
HRP-labelled Antibody and Anti-Primer Antibody	Optical Intensity	110 μ g/g	Tortajada-Genaro et al. (2015)
HRP-labelled dNTP	Chronoamperometry	319 CFU/mL (indicative)	This work

The HRP-dTTP system developed here achieved an indicative LoD for bacterial sequences lower than many other systems using peroxidase enzymes for electrochemical detection. Primer sequences labelled with HRP and systems taking advantage of antibody-antigen interactions or the streptavidin-biotin system are common choices for enzymatic detection. Directly labelled primers used by del Río et al. (2017) achieved detection of 1fM synthetic oligo target, or 500fM of bacterial DNA extracts from tissue samples. Sánchez-Salcedo et al. (2019) used a two-step process involving RPA amplification using 6-FAM labelled primers followed by incubation with HRP-labelled anti-6-FAM antibody to detect 10^5 copies of *Salmonella* genomic DNA.

Fluorescent and optical methods have also been used successfully for RPA amplicon detection. Detection of target DNA in the femtomolar range have been reported by Mayboroda et al. (2016) for the detection of *Y. pestis* DNA extracts through absorbance, as measured on a benchtop microplate reader. A wavelength shift in the resonance of a silicon micro-ring was used by Shin et al. (2013) to detect single nucleotide polymorphisms in extracted human genomic DNA, with femtogram range sensitivity. This process is simple and facilitates real-time monitoring of the reaction progress with no additional reagents necessary but requires bulky optical equipment.

A more portable system uses a standard digital versatile disc (DVD), taking advantage of DIG-labelled nucleotides to incorporate multiple HRP enzymes onto the amplicon. This system fully encloses the reaction chamber but currently performs washes by centrifuging the reaction out of the chamber which could contaminate nearby surfaces or the internals of the disc drive, leading to issues with hardware reuse. However, this system achieved a low LoD for extracted samples, and utilisation of a well-established technology could facilitate development and uptake of such a system were it produced commercially.

The approach described here improves upon these schemes in several ways. The use of labelled primers limits the maximum number of labels on each DNA strand to one when using a conventional PCR primer setup as these papers do. The inclusion of a labelled dNTP increases the potential incorporation of labels onto each double strand, up to a maximum equal to the total number of the equivalent dNTP in the double strand sequence. This could produce a significant signal enhancement effect where the amplification of only a few surface bound probes could anchor a large number of enzymes. This effect also reduces time to result, as a high enzyme count will rapidly oxidise a solution of TMB, thereby reducing the

incubation time of the H₂O₂ + TMB solution to achieve similar signal intensity. The direct labelling of the nucleotide also removes the need for subsequent incubation with antibody or streptavidin, minimising incubation steps and user interaction which simplifies device operation in a point-of-care setting.

The system presented here also facilitates simple surface-based amplification and detection with minimal complexity. The clean electrode can be prepared through a simple incubation and washing with water and following the reaction only standard PBS and PBS-Tween washes are currently required. The DNA is detectable following cell lysis without filtering, removing the need for ancillary kits to extract and purify the target from the sample, and no isolation from the reaction mixture is required as the amplicon is generated at the surface.

Additionally, the measurement performed here is straightforward. Applying a potential and measuring current is a simple process compared to the analysis and recording of EIS signals. The electronics for such a system can also be easily miniaturised as shown by the results presented herein using the SimpleStat and the work by other groups on portable potentiostats. This is advantageous compared to optical measurements requiring plate readers or other bulky equipment, and DVD based systems which require a personal computer and disc drive which could limit use at the bedside in a clinical setting. Sample preparation is also minimal, with only a short heating step required to release DNA. This could be replaced by a chemical lysis to further support point-of-care use.

One key consideration for the method presented here is that the attachment chemistry for HRP-dTTP is modular. While HRP mediated TMB oxidation is demonstrated, the binding of other redox enzymes such as glucose oxidase or alkaline phosphatase would allow the conversion of other substrates for electrochemical detection. In the case of glucose oxidase, the extensive use of this enzyme for electrochemical blood glucose monitoring means there are well established and robust reactions which could be taken advantage of to improve the sensor shelf-life and reproducibility. Appropriate enzyme chemistry can be chosen to meet the needs of different sensor and target requirements while using the same amplification and surface modification systems established herein.

The use of modified nucleotides for RPA amplification has been further reported in the literature, without the addition of a solid-phase system for electrochemical detection. Kortli et al. (2020) used biotinylated dNTPs in a PCR and RPA reaction, subsequently hybridising the reaction product to a capture probe on a microwell plate or lateral flow strip. These biotin-

dNTPs allowed the reaction to report through streptavidin-HRP or, for the lateral flow assay, streptavidin modified gold nanoparticles to produce a visual output. This system achieved detection of 0.63fg extracted *Y. pestis* genomic DNA following RPA purification, which is an order of magnitude lower than the system reported here, but with greater sample and amplicon processing required. However, detection of such low quantities of DNA in a lateral flow format supports the case for RPA deployment in a diagnostic setting.

An alternative to enzyme-labelled nucleotides is to directly label the nucleotides with a redox active species, as done by Magriñá et al. (2019). Using Ferrocene labelled nucleotides, extracted genes from *Bacillus anthracis* were detected on a gold electrode array following PCR amplicon hybridisation with a capture probe. While these nucleotides have not been tested with RPA, and the reaction is performed off-chip, the one-pot nature of the reaction allows an analyte to be tested for multiple genes simultaneously. There is also no need to incubate further with a measurement solution as the direct ferrocene electrochemistry can be measured following hybridisation. This reaction achieved a similar LoD to the HRP-dTTP system used here at 0.8 – 3.4fM depending on the DNA target. The use of redox-labelled nucleotides could be an avenue for further reductions in assay time and complexity.

4.3 Conclusions

In this chapter the incorporation of enzyme tagged nucleotides into an isothermal RPA reaction has been demonstrated for the first time. HRP-tagged nucleotides are known to be well tolerated by high-fidelity polymerases in PCR reactions, and the result presented here show that they are amenable within the more complex protein interactions required for RPA.

Electrochemical detection of TMB was initially examined, showing that screen-printed electrodes were suitable to detect changes in the level of oxidised TMB present. DPV and chronoamperometry were examined as possible measurement techniques, with chronoamperometry producing a more reliable and expected response change compared to DPV, which showed peak decreases in response to increasing TMB concentration. This behaviour was attributed to the small overlap between the oxidation and reduction potentials of TMB which the pulsatile nature of the DPV measurement interacted with.

Using HRP-tagged nucleotides and a H₂O₂ and TMB redox system, chronoamperometric responses for the solid-phase amplification of plasmid DNA were measured. Modification of the working electrode for 2-hours produced a low amplification yield which could not be

distinguished from the negative control. Removing the forward primer from the negative control reaction produced chronoamperometry traces with a similar current, suggesting that non-specific HRP adsorption was minimal. Functionalising the whole electrode system with a higher concentration of DNA SAM for the same duration produced significantly more amplification and resulted in successful detection of target DNA compared to a blank RPA reaction.

RPA amplification of *E. coli* bacterial cultures then showed that low concentrations of intact and lysed cells containing plasmid could be detected. Cells were loaded into solid-phase RPA reactions on screen-printed electrodes and as low as 6 – 7 cells could be detected compared to a blank RPA reaction following lysis, and approximately 800 cells without a lytic pre-treatment. From sample collection to result took one hour, plus the time taken washing cells to remove free plasmid in the media.

Discrimination of plasmid bearing and non-plasmid bearing bacteria was then tested. *E. coli* bearing the synthetic AMR plasmid and *S. aureus* without resistance genes were examined. Solution-phase reactions indicated that there were genomic fragments or non-specific amplification products produced for unwashed *E. coli* cell culture and *S. aureus* in PBS. Addition of these organisms as template for solid-phase RPA produced high current responses on both positive and negative electrodes, despite previous results indicating there was an appreciable difference in the DNA yield and little non-specific HRP interaction with the electrode. Further examination of the *E. coli* amplification process indicated that non-specific amplification was occurring, which could lead to high background signal.

By changing from a 2-hour protocol to the previously established overnight and backfill method, as well as anodising the reference electrode which degraded during the incubation with peroxide and TMB, the impact of non-specific amplification was reduced. This allowed the detection of around 320 CFU of *E. coli* compared to 22 *S. aureus* in the negative control, which produced a similar response to the blank RPA from previous experiments. Performing a dose response analysis using a verified concentration of *E. coli* achieved definitive detection of 41.6 CFU *E. coli* compared to 416 CFU *S. aureus*. Detection of 4.18 CFU *E. coli* also appeared successful as the mean response was greater than the baseline noise threshold. However, this measurement point showed high variability with the standard deviation intersecting with the baseline level. Fitting the data points allowed the calculation of an indicative limit of

detection. The LoD of this system was calculated to be 0.637 CFU per reaction, or 319 CFU/mL in a sample.

5 Conclusions and Future Work

5.1 Conclusions

Presented in this thesis is the development of a DNA biosensor to detect antibiotic resistance. The need for rapid, low-cost, and user-friendly diagnostics for antimicrobial resistant organisms continues to grow as antimicrobial resistant infections become more prevalent worldwide and our generation of novel antibiotics slows down. Many biosensor devices have been reported in the literature, but many have complex sample preparation requirements or intensive protocols which limit their efficacy in a point-of-care setting. In addition, systems which can be mass manufactured would be advantageous, generally requiring simpler sensor functionalisation processes. The work presented here demonstrates development of a sensitive biosensor system for AMR genes which addresses many of these challenges, focussing on low-cost electrode substrates, instrumentation, and simple test procedures. A summary of the research contributions generated in this thesis is presented in Figure 5.1.

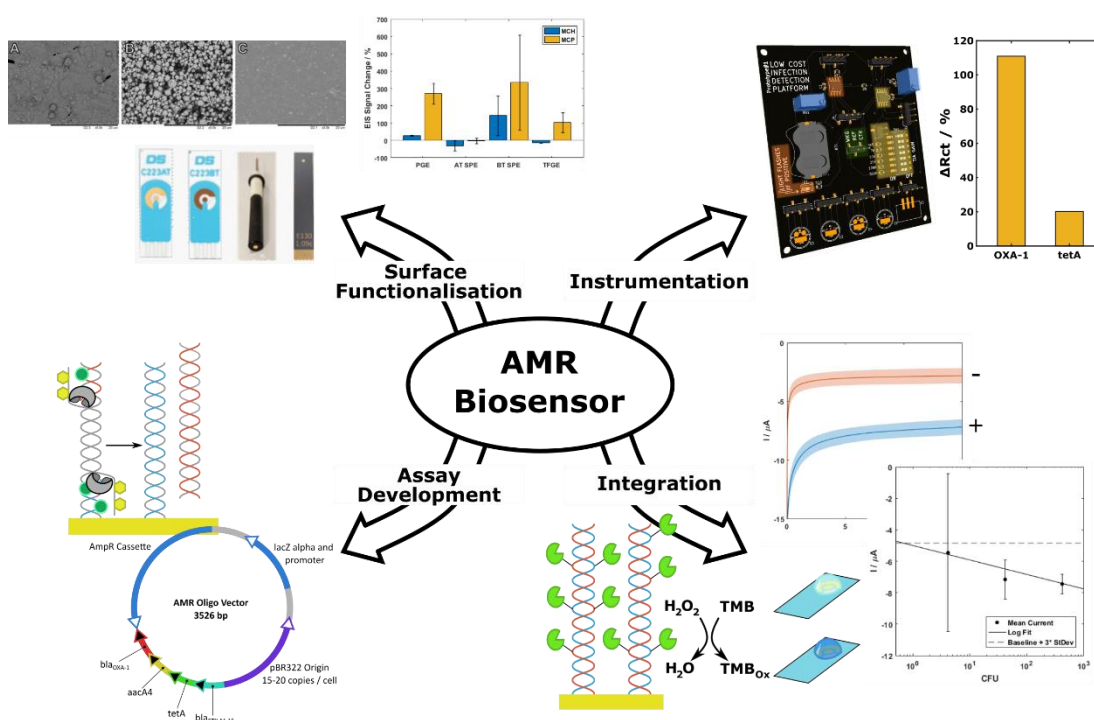


Figure 5.1 – Summary of research contributions arising from this thesis.

Initially, a variety of low-cost electrode formats were compared to the “gold standard” polycrystalline gold electrode. Characterisation of electrodes suggested that each electrode type would be a suitable substrate for DNA biosensing of AMR genes. A number of cleaning

protocols were examined, and electrodes were functionalised with a simple overnight incubation process. It has been shown that, following surface functionalisation and challenging each electrode with synthetic oligonucleotide, both screen-printed and sputter coated gold electrodes produced good signal responses. A low-cost method of enhancing signal response by using a shorter alkanethiol blocking molecule was also identified.

Carbon electrodes were also characterised using an established cleaning and functionalisation method. Carbon electrodes have advantageous characteristics compared to gold, including covalent modification options and increased biofouling resistance. These features could reduce background signal and allow more controlled functionalisation of the surface. Screen-printed electrodes showed similar response magnitudes to the more expensive glassy carbon format when challenged with DNA oligonucleotide, suggesting detection could be readily achieved on this electrode format also. A dose response for DNA oligonucleotide on carbon showed good sensitivity and response linearity.

To avoid the use of multi-antimicrobial resistant bacteria in the lab, a synthetic plasmid containing inactive AMR gene sequences was designed. This bespoke plasmid was transformed into competent *E. coli* to allow for realistic AMR target sequences to be tested with no additional risk to the researcher. This plasmid was successfully used as a proxy for clinical AMR genes in PCR and isothermal RPA reactions, both in a purified form and when obtained without purification from the lysis of bacterial cells.

When PCR amplicons were applied to electrodes, the previously impressive signal responses were lost. Instead, large variability on the screen-printed substrates was observed, with only the traditional PGE and the thin-film systems showing suitable responses. SAM layers on these electrodes produced a large response difference between positive and negative sequences, but variability on the TFGE prevented statistically significant detection. This was thought to be due to insufficient surface blocking or washing which could be overcome through optimisation of these parameters.

Detection of PCR products was next tested using a low-cost potentiostat system with inbuilt gold electrodes, the SimpleStat. The SimpleStat offered a portable potentiostat platform with 8 electrodes built onto the board for handheld electrochemical testing of samples. These on-board electrodes were characterised and appeared to be similar to other electrode formats previously tested. PCR amplified sequences were detected on these electrodes, which appeared capable of discriminating between complementary and non-complementary

sequences. However, issues with the integrity of the gold surface prevented the production of replicate data and statistical analysis.

The SimpleStat was also tested against a commercial potentiostat and had good comparability when detecting PCR amplicons. A small reduction in signal change was observed with the SimpleStat compared to the PalmSens, but this was not significant. This platform showed promise for deployment as a low-cost biosensor platform, having showed that detection of unpurified PCR amplicon was possible with the SimpleStat using either an off-chip 3-electrode cell or the on-chip gold electrodes. Issues with using the commercial gold plating, designed as a protective layer rather than a sensing substrate, reduced the usability of the on-chip electrodes, but further development of the gold plating would improve these PCB electrodes for future use.

Detection of amplification products was then tested on the carbon electrode system. The application of PCR and RPA products to screen-printed carbon electrodes showed a reversal of the trend observed with DNA oligonucleotide, with low concentrations of amplicon producing the greatest signal response. This was attributed to interactions between reaction proteins and the electrode producing a significant effect on the electrochemical response which could not be easily screened.

Alternative detection schemes involving methylene blue were pursued on carbon electrodes with similar results. Oligonucleotides produced a large change in the electrochemical response, but unpurified amplicon resulted in little signal change over the measurement period. Further real-time experiments with methylene blue produced conflicting results, where low levels of amplification could produce signals which followed the trend of the positive reaction. Electrochemical detection of DNA amplification was not achieved on carbon electrodes. However, during these tests, a surface-bound amplification reaction using RPA was identified in the literature and tested. Performance of this solid-phase isothermal RPA reaction showed promise, with high yields of DNA being produced. This reaction could be used to anchor DNA at the surface during the reaction, removing the requirement for a separate heating and hybridisation step as had been previously used for DNA detection.

This solid-phase RPA reaction was tested on gold electrodes. While the reaction yield was typically lower than on carbon, statistically significant detection of amplicon was achieved compared to a blank reaction. This was attributed to the alkanethiol SAM layer providing a better barrier to protein fouling than the functionalised carbon electrode. These results

showed promise for detection of DNA amplicons if the challenges surrounding SAM stability, background signal and variability could be addressed.

Towards this end, a labelling approach was explored. By generating the redox species as part of the reaction rather than relying on changes at the interface, an improvement to the overall sensitivity and specificity of the measurement was sought. Horseradish peroxidase is an enzyme commonly used in biosensing and has widespread use in biochemical assays. By using HRP-labelled nucleotide bases (HRP-dTTP), the enzyme could be incorporated into the elongating DNA strand. Coupling this to the solid-phase RPA allows a DNA strand to be amplified, anchoring the HRP at the surface, without the risk of enzyme denature that would come with high temperature amplification methods.

The substrates for HRP, hydrogen peroxide and tetramethylbenzidine, were initially tested on screen-printed gold electrodes. Despite earlier data favouring the thin-film electrodes, SPEs were chosen due to their convenient 3-electrode format which minimised the volume of solutions required. TMB electrochemistry was clear on these electrodes, with chronoamperometry chosen as the most appropriate measurement. HRP-dTTP rapidly oxidised TMB, producing significant current on the electrodes tested.

Alongside the electrochemical development, HRP-dTTP inclusion into RPA reactions was examined. The large enzyme attached to the dNTP could prevent effective uptake of the nucleotide by the DNA polymerase. However, amplifying AMR sequences in the solid phase effectively incorporated the HRP nucleotides. Blocking the entire 3-electrode cell with SAM molecules and using a higher density of DNA probe than previously used were critical for successful detection of AMR gene sequences.

RPA was also tested to observe if amplification of template from bacterial cells was possible. Interference from cellular components or off-target bacterial nucleic acids could inhibit the RPA reaction, and would mean samples had to be extracted and purified prior to application to the sensor. However, using washed cell pellets, high levels of amplification were observed for both intact and lysed cells in the range of 2 – 14,000 CFU per reaction. This showed that RPA could successfully amplify low concentrations of template even in the presence of cellular debris, and that sample processing requirements for this system were quite low. Further tests removing the washing process resulted in successful amplification from overnight culture, further reducing sample preparation.

Loading washed cells into a solid-phase RPA reaction containing HRP-dTTP produced significant detection of both lysed and intact cells. Cells at a 10^{-4} and 10^{-6} dilution (equivalent to 800 and 8 CFU loaded into the reaction) gave mean chronoamperometry currents higher than a blank RPA background. For intact cells, only the 10^{-4} dilution was significant. When lysing the cells, the 10^{-6} dilution produced a statistically significant detection, but the 10^{-4} dilution, while having a larger mean current, was unable to reach significance due to measurement variability.

Finally, discrimination between different bacterial cells was attempted. *E. coli* containing the synthetic plasmid was compared to *S. aureus* with no antibiotic resistance. From solution phase RPA, specific amplification of the target from the positive was achieved with no specific band in the negative. However, when using electrochemical detection, no difference between the two samples was observed. Tests indicated that this could be due to ineffective blocking of the surface allowing non-specific amplicons to trap HRP at the electrode, or that the silver reference electrode was fouled with HRP and amplicon.

Improvements to the SAM formation protocol were made, alongside anodisation of the reference electrode to silver / silver chloride. These combined changes prevented non-specific adsorption of reaction products and resulted in negative controls which has similar current responses to previously tested blank RPA reactions. With these changes, the positive current response could be distinguished from the background, achieving statistically significant detection of 320 CFU of *E. coli* compared to 22 CFU of *S. aureus*.

A dose response curve for the detection of *E. coli* was then created using the improved electrode functionalisation method. Samples containing 418 and 41.8 CFU were detected against a background of 418 CFU *S. aureus*, with the sample containing 4.18 CFU achieving a mean response greater than the background but with high variability. Fitting this data gave an indicative limit of detection of 319 CFU/mL, or 0.637 CFU per electrode. This detection range is comparable to other enzyme based electrochemical sensing systems for nucleic acids reported in the literature and is below the relevant clinical range for many bacterial infections.

Detection of plasmid borne AMR genes has been successfully demonstrated using low-cost screen-printed electrodes and a novel direct enzyme-labelling isothermal amplification reaction. Using a simple overnight SAM formation process, electrodes sensitive to clinically relevant levels of bacterial DNA were produced which could identify the presence of an AMR

gene in a bacterial lysate in under one hour. These results show promise for detection of a variety of nucleic acid targets, which can be tested using a custom AMR plasmid structure designed for this work. The low cost and rapid production of results from this system, along with early stage nucleic acid testing with a portable potentiostat, lay the framework for development of a point-of-care test for antimicrobial resistance genes which could be produced at scale to meet the growing demand for rapid diagnostics.

5.2 Future Work

The limit of detection of this system should be confirmed with a larger study using a greater number of electrodes for each dilution. The current limit of detection shows this method has high sensitivity to low concentrations of bacterial cells. However, this final experiment also exhibited higher variability than observed for measurements using the overnight SAM formation protocol for solid-phase RPA with HRP-dTTP. A higher replicate number for generation of the dose response curve would identify outlier responses and allow a more accurate limit-of-detection to be calculated.

Further work to reduce the background signal should also be performed. Several articles have described how reducing the primer concentrations in RPA reactions can reduce non-specific amplification. This has been tested for solid-phase and solution-phase RPA. Examination of whether this would have an impact on the amplification efficiency of the reactions described here, and if a resulting decrease in the background signal occurred, may allow further improvements to the sensor performance.

Currently, the HRP-dTTP system has been tested with only a single AMR gene, *bla_{OXA-1}*. The synthetic plasmid designed for this work contains four resistance gene sequences which could be detected simultaneously. In practical use, a tested bacterium may express many different AMR genes and the ability of this system to identify each individual gene would be critical for effective antibiotic selection by clinicians and treatment for the patient. As such, further testing of this system with electrode arrays, functionalised with different probe sequences, is merited.

To this end, the design of such an array would greatly facilitate multiplexed testing. While DropSens SPEs are an ideal format for testing and development owing to their compact size and single-use nature, a clinical device would need to be much simpler to use. Testing an electrode array with individually addressable electrode cells and splitting a single RPA

reaction between multiple units on an array may have consequences for RPA reaction efficiency and cross contamination. However, design of a multiplexed array of electrodes for HRP mediated DNA detection would give an indication if deployment of this system is truly feasible outside of a laboratory environment.

Stability of the SAM layer formed on these electrodes should also be investigated. Long term storage of these electrodes would require the SAM layer to remain stable, and an unstable SAM would be detrimental to the manufacture and deliverability of these devices to the point of use. Alkanethiol monolayers on gold are known to desorb over time in solution. Investigating the rate of degradation and identifying means by which the SAM layer can be maintained for a longer period would improve the manufacturability of these sensors.

Finally, this detection scheme should be tested using a low-cost potentiostat system. The SimpleStat has been developed further outside of the scope of this thesis, and chronoamperometric measurements are comparatively simple compared to the DPV measurement performed on the SimpleStat in this thesis. Successfully demonstrating equivalent levels of detection using a low-cost potentiostat would present a significant step towards highly sensitive and affordable diagnostics for routine nucleic acid testing.

6 References

- Ahmadraji, T., Gonzalez-Macia, L., Ritvonen, T., Willert, A., Ylimaula, S., Donaghy, D., Tuurala, S., Suhonen, M., Smart, D., Morrin, A., Efremov, V., Baumann, R.R., Raja, M., Kemppainen, A., Killard, A.J., 2017. Biomedical Diagnostics Enabled by Integrated Organic and Printed Electronics. *Anal. Chem.* 89, 7447–7454. <https://doi.org/10.1021/acs.analchem.7b01012>
- Ahmed, M.U., Nahar, S., Safavieh, M., Zourob, M., 2013. Real-time electrochemical detection of pathogen DNA using electrostatic interaction of a redox probe. *Analyst* 138, 907–915. <https://doi.org/10.1039/C2AN36153A>
- Ahmed, N., AL-Madhagi, S., Ortiz, M., O’Sullivan, C.K., Katakis, I., 2020. Direct electrochemical detection of enzyme labelled, isothermally amplified DNA. *Analytical Biochemistry* 598, 113705. <https://doi.org/10.1016/j.ab.2020.113705>
- Ainla, A., Mousavi, M.P.S., Tsaloglou, M.-N., Redston, J., Bell, J.G., Fernández-Abedul, M.T., Whitesides, G.M., 2018. Open-Source Potentiostat for Wireless Electrochemical Detection with Smartphones. *Anal. Chem.* 90, 6240–6246. <https://doi.org/10.1021/acs.analchem.8b00850>
- Altobelli, E., Mohan, R., Mach, K.E., Sin, M.L.Y., Anikst, V., Buscarini, M., Wong, P.K., Gau, V., Banaei, N., Liao, J.C., 2017. Integrated Biosensor Assay for Rapid Uropathogen Identification and Phenotypic Antimicrobial Susceptibility Testing. *European Urology Focus* 3, 293–299. <https://doi.org/10.1016/j.euf.2015.12.010>
- Altschul, S.F., Gish, W., Miller, W., Myers, E.W., Lipman, D.J., 1990. Basic local alignment search tool. *Journal of Molecular Biology* 215, 403–410. [https://doi.org/10.1016/S0022-2836\(05\)80360-2](https://doi.org/10.1016/S0022-2836(05)80360-2)
- Amouzadeh Tabrizi, M., Shamsipur, M., 2015. A label-free electrochemical DNA biosensor based on covalent immobilization of salmonella DNA sequences on the nanoporous glassy carbon electrode. *Biosensors and Bioelectronics* 69, 100–105. <https://doi.org/10.1016/j.bios.2015.02.024>
- Andreescu, S., Sadik, O.A., 2009. Trends and challenges in biochemical sensors for clinical and environmental monitoring. *Pure and Applied Chemistry* 76, 861–878. <https://doi.org/10.1351/pac200476040861>

- Aymerich, J., Márquez, A., Terés, L., Muñoz-Berbel, X., Jiménez, C., Domínguez, C., Serra-Graells, F., Dei, M., 2018. Cost-effective smartphone-based reconfigurable electrochemical instrument for alcohol determination in whole blood samples. *Biosensors and Bioelectronics* 117, 736–742. <https://doi.org/10.1016/j.bios.2018.06.044>
- Aznar-Poveda, J., Lopez-Pastor, J.A., Garcia-Sanchez, A.-J., Garcia-Haro, J., Otero, T.F., 2018. A COTS-Based Portable System to Conduct Accurate Substance Concentration Measurements. *Sensors* 18, 539. <https://doi.org/10.3390/s18020539>
- Bain, C.D., Troughton, E.B., Tao, Y.T., Evall, J., Whitesides, G.M., Nuzzo, R.G., 1989. Formation of monolayer films by the spontaneous assembly of organic thiols from solution onto gold. *J. Am. Chem. Soc.* 111, 321–335. <https://doi.org/10.1021/ja00183a049>
- Bain, C.D., Whitesides, G.M., 1988. Molecular-Level Control over Surface Order in Self-Assembled Monolayer Films of Thiols on Gold. *Science* 240, 62–63. <https://doi.org/10.1126/science.240.4848.62>
- Bala, A., Górski, Ł., 2016. Application of nucleic acid analogues as receptor layers for biosensors. *Analytical Methods* 8, 236–244. <https://doi.org/10.1039/C5AY02620B>
- Bally, R.W., Gribnau, T.C., 1989. Some aspects of the chromogen 3,3',5,5'-tetramethylbenzidine as hydrogen donor in a horseradish peroxidase assay. *J Clin Chem Clin Biochem* 27, 791–796. <https://doi.org/10.1515/cclm.1989.27.10.791>
- Bard, A., Faulkner, L., 2001. *Electrochemical Methods: Fundamentals and Applications*, 2nd ed. Wiley.
- Baron, S. (Ed.), 1996. *Medical Microbiology*, 4th ed. University of Texas Medical Branch at Galveston, Galveston (TX).
- Bennett, P.M., 2008. Plasmid encoded antibiotic resistance: acquisition and transfer of antibiotic resistance genes in bacteria. *Br J Pharmacol* 153, S347–S357. <https://doi.org/10.1038/sj.bjp.0707607>
- Ben-Yoav, H., Dykstra, P.H., Bentley, W.E., Ghodssi, R., 2015. A controlled microfluidic electrochemical lab-on-a-chip for label-free diffusion-restricted DNA hybridization analysis. *Biosens. Bioelectron.* 64, 579–585. <https://doi.org/10.1016/j.bios.2014.09.069>
- Bernalte, E., Marín-Sánchez, C., Pinilla-Gil, E., Brett, C.M.A., 2013. Characterisation of screen-printed gold and gold nanoparticle-modified carbon sensors by electrochemical impedance spectroscopy. *J. Electroanal. Chem.* 709, 70–76. <https://doi.org/10.1016/j.jelechem.2013.09.007>

- Bezuidenhout, P., Smith, S., Joubert, T.-H., 2018. A Low-Cost Inkjet-Printed Paper-Based Potentiostat. *Applied Sciences* 8, 968. <https://doi.org/10.3390/app8060968>
- Binder, S., Schendzielorz, G., Stäbler, N., Krumbach, K., Hoffmann, K., Bott, M., Eggeling, L., 2012. A high-throughput approach to identify genomic variants of bacterial metabolite producers at the single-cell level. *Genome Biology* 13, R40. <https://doi.org/10.1186/gb-2012-13-5-r40>
- Blair, J.M.A., Webber, M.A., Baylay, A.J., Ogbolu, D.O., Piddock, L.J.V., 2014. Molecular mechanisms of antibiotic resistance. *Nature Reviews Microbiology* 13, nrmicro3380. <https://doi.org/10.1038/nrmicro3380>
- Blum, 1991. *Biosensor Principles and Applications*. CRC Press.
- Butterworth, A., Blues, E., Williamson, P., Cardona, M., Gray, L., Corrigan, D.K., 2019a. SAM Composition and Electrode Roughness Affect Performance of a DNA Biosensor for Antibiotic Resistance. *Biosensors* 9, 22. <https://doi.org/10.3390/bios9010022>
- Butterworth, A., Corrigan, D., Ward, A.C., 2019b. Electrochemical detection of oxacillin resistance with SimpleStat: a low cost integrated potentiostat and sensor platform. *Anal. Methods* 11, 1958–1965. <https://doi.org/10.1039/C9AY00383E>
- Cai, B., Wang, S., Huang, L., Ning, Y., Zhang, Z., Zhang, G.-J., 2014. Ultrasensitive Label-Free Detection of PNA–DNA Hybridization by Reduced Graphene Oxide Field-Effect Transistor Biosensor. *ACS Nano* 8, 2632–2638. <https://doi.org/10.1021/nn4063424>
- Cardoso, A.R., Moreira, F.T.C., Fernandes, R., Sales, M.G.F., 2016. Novel and simple electrochemical biosensor monitoring attomolar levels of miRNA-155 in breast cancer. *Biosens. Bioelectron.* 80, 621–630. <https://doi.org/10.1016/j.bios.2016.02.035>
- Carvalho, R.F., Sanches Freire, R., Kubota, L.T., 2004. Polycrystalline Gold Electrodes: A Comparative Study of Pretreatment Procedures Used for Cleaning and Thiol Self-Assembly Monolayer Formation. *Electroanalysis* 17, 1251–1259. <https://doi.org/10.1002/elan.200403224>
- Cecchet, F., Marcaccio, M., Margotti, M., Paolucci, F., Rapino, S., Rudolf, P., 2006. Redox Mediation at 11-Mercaptoundecanoic Acid Self-Assembled Monolayers on Gold. *J. Phys. Chem. B* 110, 2241–2248. <https://doi.org/10.1021/jp054290n>
- Chapman, R.G., Ostuni, E., Takayama, S., Holmlin, R.E., Yan, L., Whitesides, G.M., 2000. Surveying for Surfaces that Resist the Adsorption of Proteins. *J. Am. Chem. Soc.* 122, 8303–8304. <https://doi.org/10.1021/ja000774f>

- Chen, J., Chang, B., Oyola-Reynoso, S., Wang, Z., Thuo, M., 2017. Quantifying Gauche Defects and Phase Evolution in Self-Assembled Monolayers through Sessile Drops. *ACS Omega* 2, 2072–2084. <https://doi.org/10.1021/acsomega.7b00355>
- Cheng, W., Zhang, W., Yan, Y., Shen, B., Zhu, D., Lei, P., Ding, S., 2014. A novel electrochemical biosensor for ultrasensitive and specific detection of DNA based on molecular beacon mediated circular strand displacement and rolling circle amplification. *Biosens. Bioelectron.* 62, 274–279. <https://doi.org/10.1016/j.bios.2014.06.056>
- Cogen, A.L., Nizet, V., Gallo, R.L., 2008. Skin microbiota: a source of disease or defence? *Br J Dermatol* 158, 442–455. <https://doi.org/10.1111/j.1365-2133.2008.08437.x>
- Compton, R.G., Banks, C.E., 2011. *Understanding Voltammetry*, 2nd ed. Imperial College Press.
- Coque, T.M., Novais, Â., Carattoli, A., Poirel, L., Pitout, J., Peixe, L., Baquero, F., Cantón, R., Nordmann, P., 2008. Dissemination of Clonally Related *Escherichia coli* Strains Expressing Extended-Spectrum β -Lactamase CTX-M-15. *Emerg Infect Dis* 14, 195–200. <https://doi.org/10.3201/eid1402.070350>
- Corrigan, D.K., Schulze, H., Henihan, G., Ciani, I., Giraud, G., Terry, J.G., Walton, A.J., Pethig, R., Ghazal, P., Crain, J., Campbell, C.J., Mount, A.R., Bachmann, T.T., 2012. Impedimetric detection of single-stranded PCR products derived from methicillin resistant *Staphylococcus aureus* (MRSA) isolates. *Biosens. Bioelectron.* 34, 178–184. <https://doi.org/10.1016/j.bios.2012.01.040>
- Corrigan, D.K., Schulze, H., Henihan, G., Hardie, A., Ciani, I., Giraud, G., G. Terry, J., J. Walton, A., Pethig, R., Ghazal, P., Crain, J., J. Campbell, C., E. Templeton, K., R. Mount, A., T. Bachmann, T., 2013. Development of a PCR-free electrochemical point of care test for clinical detection of methicillin resistant *Staphylococcus aureus* (MRSA). *Analyst* 138, 6997–7005. <https://doi.org/10.1039/C3AN01319G>
- Creager, S.E., Hockett, L.A., Rowe, G.K., 1992. Consequences of microscopic surface roughness for molecular self-assembly. *Langmuir* 8, 854–861. <https://doi.org/10.1021/la00039a020>
- Crothers, D.M., 1968. Calculation of binding isotherms for heterogeneous polymers. *Biopolymers* 6, 575–584. <https://doi.org/10.1002/bip.1968.360060411>
- Cruz, A.F.D., Norena, N., Kaushik, A., Bhansali, S., 2014. A low-cost miniaturized potentiostat for point-of-care diagnosis. *Biosensors and Bioelectronics* 62, 249–254. <https://doi.org/10.1016/j.bios.2014.06.053>

- Cui, H.-F., Xu, T.-B., Sun, Y.-L., Zhou, A.-W., Cui, Y.-H., Liu, W., Luong, J.H.T., 2015. Hairpin DNA as a Biobarcode Modified on Gold Nanoparticles for Electrochemical DNA Detection. *Anal. Chem.* 87, 1358–1365. <https://doi.org/10.1021/ac504206n>
- Davies, J., Davies, D., 2010. Origins and Evolution of Antibiotic Resistance. *Microbiol Mol Biol Rev* 74, 417–433. <https://doi.org/10.1128/MMBR.00016-10>
- de Kraker, M.E.A., Davey, P.G., Grundmann, H., 2011. Mortality and Hospital Stay Associated with Resistant *Staphylococcus aureus* and *Escherichia coli* Bacteremia: Estimating the Burden of Antibiotic Resistance in Europe. *PLoS Med* 8. <https://doi.org/10.1371/journal.pmed.1001104>
- Deféver, T., Druet, M., Evrard, D., Marchal, D., Limoges, B., 2011. Real-Time Electrochemical PCR with a DNA Intercalating Redox Probe. *Anal. Chem.* 83, 1815–1821. <https://doi.org/10.1021/ac1033374>
- del Río, J.S., Lobato, I.M., Mayboroda, O., Katakis, I., O’Sullivan, C.K., 2017. Enhanced solid-phase recombinase polymerase amplification and electrochemical detection. *Anal Bioanal Chem* 409, 3261–3269. <https://doi.org/10.1007/s00216-017-0269-y>
- Department of Health, 2016. Reducing infections in the NHS [WWW Document]. GOV.UK. URL <https://www.gov.uk/government/news/reducing-infections-in-the-nhs> (accessed 11.15.17).
- Dong, S., Li, J., 1997. Self-assembled monolayers of thiols on gold electrodes for bioelectrochemistry and biosensors. *Bioelectrochem. Bioenerg.* 42, 7–13. [https://doi.org/10.1016/S0302-4598\(96\)05172-0](https://doi.org/10.1016/S0302-4598(96)05172-0)
- Dryden, M.D.M., Wheeler, A.R., 2015. DStat: A Versatile, Open-Source Potentiostat for Electroanalysis and Integration. *PLOS ONE* 10, e0140349. <https://doi.org/10.1371/journal.pone.0140349>
- Elgrishi, N., Rountree, K.J., McCarthy, B.D., Rountree, E.S., Eisenhart, T.T., Dempsey, J.L., 2018. A Practical Beginner’s Guide to Cyclic Voltammetry. *J. Chem. Educ.* 95, 197–206. <https://doi.org/10.1021/acs.jchemed.7b00361>
- Esteve-Palau, E., Solande, G., Sánchez, F., Sorlí, L., Montero, M., Güerri, R., Villar, J., Grau, S., Horcajada, J.P., 2015. Clinical and economic impact of urinary tract infections caused by ESBL-producing *Escherichia coli* requiring hospitalization: A matched cohort study. *Journal of Infection* 71, 667–674. <https://doi.org/10.1016/j.jinf.2015.08.012>
- European Centre for Disease Prevention and Control, 2020. Antimicrobial resistance in the EU/EEA (EARS-Net) - Annual Epidemiological Report 2019.

- European Centre for Disease Prevention and Control, 2018. Antimicrobial resistance in the EU/EEA (EARS-Net) - Annual Epidemiological Report 2017.
- European Centre for Disease Prevention and Control, 2017. Antimicrobial resistance surveillance in Europe 2015.
- European Centre for Disease Prevention and Control, 2016. Rapid Risk Assessment: Carbapenem-resistant *Acinetobacter baumannii* in healthcare settings.
- Fair, R.J., Tor, Y., 2014. Antibiotics and Bacterial Resistance in the 21st Century. *Perspect Medicin Chem* 6, 25–64. <https://doi.org/10.4137/PMC.S14459>
- Fang, T.H., Ramalingam, N., Xian-Dui, D., Ngin, T.S., Xianting, Z., Lai Kuan, A.T., Peng Huat, E.Y., Hai-Qing, G., 2009. Real-time PCR microfluidic devices with concurrent electrochemical detection. *Biosens. Bioelectron.* 24, 2131–2136. <https://doi.org/10.1016/j.bios.2008.11.009>
- Ferguson, B.S., Buchsbaum, S.F., Swensen, J.S., Hsieh, K., Lou, X., Soh, H.T., 2009. Integrated Microfluidic Electrochemical DNA Sensor. *Anal. Chem.* 81, 6503–6508. <https://doi.org/10.1021/ac900923e>
- Fernandes, A.M., Abdalhai, M.H., Ji, J., Xi, B.-W., Xie, J., Sun, J., Noeline, R., Lee, B.H., Sun, X., 2015a. Development of highly sensitive electrochemical genosensor based on multiwalled carbon nanotubes–chitosan–bismuth and lead sulfide nanoparticles for the detection of pathogenic *Aeromonas*. *Biosens. Bioelectron.* 63, 399–406. <https://doi.org/10.1016/j.bios.2014.07.054>
- Fernandes, A.M., Abdalhai, M.H., Ji, J., Xi, B.-W., Xie, J., Sun, J., Noeline, R., Lee, B.H., Sun, X., 2015b. Development of highly sensitive electrochemical genosensor based on multiwalled carbon nanotubes–chitosan–bismuth and lead sulfide nanoparticles for the detection of pathogenic *Aeromonas*. *Biosens Bioelectron* 63, 399–406. <https://doi.org/10.1016/j.bios.2014.07.054>
- Fischer, L.M., Tenje, M., Heiskanen, A.R., Masuda, N., Castillo, J., Bentien, A., Émneus, J., Jakobsen, M.H., Boisen, A., 2009. Gold cleaning methods for electrochemical detection applications. *Microelectronic Engineering, MNE '08* 86, 1282–1285. <https://doi.org/10.1016/j.mee.2008.11.045>
- Forsberg, K.J., Reyes, A., Wang, B., Selleck, E.M., Sommer, M.O.A., Dantas, G., 2012. The Shared Antibiotic Resistome of Soil Bacteria and Human Pathogens. *Science* 337, 1107–1111. <https://doi.org/10.1126/science.1220761>

- Fournier, P.-E., Vallenet, D., Barbe, V., Audic, S., Ogata, H., Poirel, L., Richet, H., Robert, C., Mangenot, S., Abergel, C., Nordmann, P., Weissenbach, J., Raoult, D., Claverie, J.-M., 2006. Comparative Genomics of Multidrug Resistance in *Acinetobacter baumannii*. *PLoS Genet* 2. <https://doi.org/10.1371/journal.pgen.0020007>
- Frasson, I., Cavallaro, A., Bergo, C., Richter, S.N., Palù, G., 2011. Prevalence of *aac(6')*-*lb-cr* plasmid-mediated and chromosome-encoded fluoroquinolone resistance in Enterobacteriaceae in Italy. *Gut Pathog* 3, 12. <https://doi.org/10.1186/1757-4749-3-12>
- Gaiji, H., Jolly, P., Ustuner, S., Goggins, S., Abderrabba, M., Frost, C.G., Estrela, P., 2017. A Peptide Nucleic Acid (PNA)-DNA Ferrocenyl Intercalator for Electrochemical Sensing. *Electroanalysis* 29, 917–922. <https://doi.org/10.1002/elan.201600576>
- Ganesh, V., Pal, S.K., Kumar, S., Lakshminarayanan, V., 2006. Self-assembled monolayers (SAMs) of alkoxy cyanobiphenyl thiols on gold—A study of electron transfer reaction using cyclic voltammetry and electrochemical impedance spectroscopy. *Journal of Colloid and Interface Science* 296, 195–203. <https://doi.org/10.1016/j.jcis.2005.08.051>
- Gao, A., Lu, N., Dai, P., Li, T., Pei, H., Gao, X., Gong, Y., Wang, Y., Fan, C., 2011. Silicon-Nanowire-Based CMOS-Compatible Field-Effect Transistor Nanosensors for Ultrasensitive Electrical Detection of Nucleic Acids. *Nano Lett.* 11, 3974–3978. <https://doi.org/10.1021/nl202303y>
- Gebala, M., Schuhmann, W., 2010. Controlled orientation of DNA in a binary SAM as a key for the successful determination of DNA hybridization by means of electrochemical impedance spectroscopy. *Chemphyschem* 11, 2887–2895. <https://doi.org/10.1002/cphc.201000210>
- Gebala, M., Stoica, L., Neugebauer, S., Schuhmann, W., 2009. Label-Free Detection of DNA Hybridization in Presence of Intercalators Using Electrochemical Impedance Spectroscopy. *Electroanalysis* 21, 325–331. <https://doi.org/10.1002/elan.200804388>
- Ghosh, S., Kao, P., McCue, A., Chappelle, H., 1990. Use of maleimide-thiol coupling chemistry for efficient syntheses of oligonucleotide-enzyme conjugate hybridization probes. *Bioconjug Chem* 1, 71–76. <https://doi.org/10.1021/bc00001a009>
- Gialamas, A., Yelland, L.N., Ryan, P., Willson, K., Laurence, C.O., Bubner, T.K., Tideman, P., Beilby, J.J., 2009. Does point-of-care testing lead to the same or better adherence to medication? A randomised controlled trial: the PoCT in General Practice Trial. *Medical Journal of Australia* 191, 487–491. <https://doi.org/10.5694/j.1326-5377.2009.tb02910.x>

- Glasscott, M.W., Verber, M.D., Hall, J.R., Pendergast, A.D., McKinney, C.J., Dick, J.E., 2020. SweepStat: A Build-It-Yourself, Two-Electrode Potentiostat for Macroelectrode and Ultramicroelectrode Studies. *Journal of Chemical Education* 97, 265–270. <https://doi.org/10.1021/acs.jchemed.9b00893>
- Goode, J.A., Rushworth, J.V.H., Millner, P.A., 2015. Biosensor Regeneration: A Review of Common Techniques and Outcomes. *Langmuir* 31, 6267–6276. <https://doi.org/10.1021/la503533g>
- Grieshaber, D., MacKenzie, R., Vörös, J., Reimhult, E., 2008. Electrochemical Biosensors - Sensor Principles and Architectures. *Sensors (Basel)* 8, 1400–1458.
- Gruhl, F.J., Rapp, B.E., Länge, K., 2011. Biosensors for Diagnostic Applications, in: *Molecular Diagnostics, Advances in Biochemical Engineering/Biotechnology*. Springer, Berlin, Heidelberg, pp. 115–148. https://doi.org/10.1007/10_2011_130
- Guo, L.-H., Facci, J.S., McLendon, G., Mosher, R., 1994. Effect of Gold Topography and Surface Pretreatment on the Self-Assembly of Alkanethiol Monolayers. *Langmuir* 10, 4588–4593. <https://doi.org/10.1021/la00024a033>
- Guver, A., Fifita, N., Milas, P., Straker, M., Guy, M., Green, K., Yildirim, T., Unlu, I., Yigit, M.V., Ozturk, B., 2019. A low-cost and high-precision scanning electrochemical microscope built with open source tools. *HardwareX* 6, e00082. <https://doi.org/10.1016/j.ohx.2019.e00082>
- Halford, C., Gonzalez, R., Campuzano, S., Hu, B., Babbitt, J.T., Liu, J., Wang, J., Churchill, B.M., Haake, D.A., 2013. Rapid antimicrobial susceptibility testing by sensitive detection of precursor rRNA using a novel electrochemical biosensing platform. *Antimicrob. Agents Chemother.* 57, 936–943. <https://doi.org/10.1128/AAC.00615-12>
- Han, D., Chand, R., Shin, I.-S., Kim, Y.-S., 2013. Screening and electrochemical detection of an antibiotic producing gene in bacteria on an integrated microchip. *Analytical Methods* 5, 6814–6820. <https://doi.org/10.1039/C3AY41321G>
- Hannah, S., Addington, E., Alcorn, D., Shu, W., Hoskisson, P.A., Corrigan, D.K., 2019. Rapid antibiotic susceptibility testing using low-cost, commercially available screen-printed electrodes. *Biosensors and Bioelectronics* 145, 111696. <https://doi.org/10.1016/j.bios.2019.111696>
- Hashimoto, K., Inada, M., Ito, K., 2017. A novel voltammetric approach for real-time electrochemical detection of targeted nucleic acid sequences using LAMP. *Anal. Biochem.* 539, 113–117. <https://doi.org/10.1016/j.ab.2017.10.019>

- Heiat, M., Ranjbar, R., Latifi, A.M., Rasaee, M.J., Farnoosh, G., 2017. Essential strategies to optimize asymmetric PCR conditions as a reliable method to generate large amount of ssDNA aptamers. *Biotechnology and Applied Biochemistry* 64, 541–548. <https://doi.org/10.1002/bab.1507>
- Henihan, G., Schulze, H., Corrigan, D.K., Giraud, G., Terry, J.G., Hardie, A., Campbell, C.J., Walton, A.J., Crain, J., Pethig, R., Templeton, K.E., Mount, A.R., Bachmann, T.T., 2016. Label- and amplification-free electrochemical detection of bacterial ribosomal RNA. *Biosens. Bioelectron.* 81, 487–494. <https://doi.org/10.1016/j.bios.2016.03.037>
- Herne, T.M., Tarlov, M.J., 1997. Characterization of DNA Probes Immobilized on Gold Surfaces. *J. Am. Chem. Soc.* 119, 8916–8920. <https://doi.org/10.1021/ja9719586>
- Hershberg, R., 2015. Mutation--The Engine of Evolution: Studying Mutation and Its Role in the Evolution of Bacteria. *Cold Spring Harb Perspect Biol* 7, a018077. <https://doi.org/10.1101/cshperspect.a018077>
- Hoilett, O.S., Walker, J.F., Balash, B.M., Jaras, N.J., Boppana, S., Linnes, J.C., 2020. Kickstat: A coin-sized potentiostat for high-resolution electrochemical analysis. *Sensors (Switzerland)* 20. <https://doi.org/10.3390/s20082407>
- Hooper, D.C., 2000. Mechanisms of Action and Resistance of Older and Newer Fluoroquinolones. *Clin Infect Dis* 31, S24–S28. <https://doi.org/10.1086/314056>
- Hsieh, K., Xiao, Y., Soh, H.T., 2010. Electrochemical DNA Detection via Exonuclease and Target-Catalyzed Transformation of Surface-Bound Probes. *Langmuir* 26, 10392–10396. <https://doi.org/10.1021/la100227s>
- Hu, W., Ning, Y., Li, L., Kong, J., Zhang, X., 2015. Highly sensitive detection of sequence-specific DNA with morpholino-functionalized magnetic microspheres. *Analytical Methods* 7, 6712–6717. <https://doi.org/10.1039/C5AY00628G>
- Huang, C.-Y., O'Hare, D., Chao, I.-J., Wei, H.-W., Liang, Y.-F., Liu, B.-D., Lee, M.-H., Lin, H.-Y., 2015. Integrated potentiostat for electrochemical sensing of urinary 3-hydroxyanthranilic acid with molecularly imprinted poly(ethylene-co-vinyl alcohol). *Biosensors and Bioelectronics, Special Issue: BIOSENSORS 2014* 67, 208–213. <https://doi.org/10.1016/j.bios.2014.08.018>
- Huang, H., Bai, W., Dong, C., Guo, R., Liu, Z., 2015. An ultrasensitive electrochemical DNA biosensor based on graphene/Au nanorod/polythionine for human papillomavirus DNA detection. *Biosens. Bioelectron.* 68, 442–446. <https://doi.org/10.1016/j.bios.2015.01.039>

- Huang, J.M.-Y., Henihan, G., Macdonald, D., Michalowski, A., Templeton, K., Gibb, A.P., Schulze, H., Bachmann, T.T., 2015. Rapid Electrochemical Detection of New Delhi Metallo-beta-lactamase Genes To Enable Point-of-Care Testing of Carbapenem-Resistant Enterobacteriaceae. *Anal. Chem.* 87, 7738–7745. <https://doi.org/10.1021/acs.analchem.5b01270>
- Hughes, M.D., 2009. The Business of Self-Monitoring of Blood Glucose: A Market Profile. *J Diabetes Sci Technol* 3, 1219–1223.
- Hüsken, N., Gębala, M., Schuhmann, W., Metzler-Nolte, N., 2010. A Single-Electrode, Dual-Potential Ferrocene–PNA Biosensor for the Detection of DNA. *ChemBioChem* 11, 1754–1761. <https://doi.org/10.1002/cbic.200900748>
- Ishida, T., Tsuneda, S., Nishida, N., Hara, M., Sasabe, H., Knoll, W., 1997. Surface-Conditioning Effect of Gold Substrates on Octadecanethiol Self-Assembled Monolayer Growth. *Langmuir* 13, 4638–4643. <https://doi.org/10.1021/la970241t>
- Jampasa, S., Wonsawat, W., Rodthongkum, N., Siangproh, W., Yanatatsaneejit, P., Vilaivan, T., Chailapakul, O., 2014. Electrochemical detection of human papillomavirus DNA type 16 using a pyrrolidiny peptide nucleic acid probe immobilized on screen-printed carbon electrodes. *Biosens. Bioelectron.* 54, 428–434. <https://doi.org/10.1016/j.bios.2013.11.023>
- Jauset-Rubio, M., Sabaté del Río, J., Mairal, T., Svobodová, M., El-Shahawi, M.S., Bashammakh, A.S., Alyoubi, A.O., O’Sullivan, C.K., 2017. Ultrasensitive and rapid detection of β -conglutin combining aptamers and isothermal recombinase polymerase amplification. *Anal Bioanal Chem* 409, 143–149. <https://doi.org/10.1007/s00216-016-9973-2>
- Jiang, H., Sun, A., Venkatesh, A.G., Hall, D.A., 2017. An Audio Jack-Based Electrochemical Impedance Spectroscopy Sensor for Point-of-Care Diagnostics. *IEEE Sensors Journal* 17, 589–597. <https://doi.org/10.1109/JSEN.2016.2634530>
- Jiang, L., Sangeeth, C.S.S., Yuan, L., Thompson, D., Nijhuis, C.A., 2015. One-Nanometer Thin Monolayers Remove the Deleterious Effect of Substrate Defects in Molecular Tunnel Junctions. *Nano Lett.* 15, 6643–6649. <https://doi.org/10.1021/acs.nanolett.5b02481>
- Jolly, P., Rainbow, J., Regoutz, A., Estrela, P., Moschou, D., 2019. A PNA-based Lab-on-PCB diagnostic platform for rapid and high sensitivity DNA quantification. *Biosensors and Bioelectronics* 123, 244–250. <https://doi.org/10.1016/j.bios.2018.09.006>

- Josephy, P.D., Eling, T., Mason, R.P., 1982. The horseradish peroxidase-catalyzed oxidation of 3,5,3',5'-tetramethylbenzidine. Free radical and charge-transfer complex intermediates. *J Biol Chem* 257, 3669–3675.
- Jung, I., Seo, H.B., Lee, J., Kim, B.C., Gu, M.B., 2014. A dip-stick type biosensor using bioluminescent bacteria encapsulated in color-coded alginate microbeads for detection of water toxicity. *Analyst* 139, 4696–4701. <https://doi.org/10.1039/C4AN00308J>
- Kafka, J., Pänke, O., Abendroth, B., Lisdat, F., 2008. A label-free DNA sensor based on impedance spectroscopy. *Electrochim. Acta*, 7th International Symposium on Electrochemical Impedance Spectroscopy 53, 7467–7474. <https://doi.org/10.1016/j.electacta.2008.01.031>
- Kara, P., Cavusoglu, C., Cavdar, S., Ozsoz, M., 2009. Direct electrochemical genosensing for multiple point mutation detection of *Mycobacterium tuberculosis* during the development of rifampin resistance. *Biosens. Bioelectron.* 24, 1796–1800. <https://doi.org/10.1016/j.bios.2008.08.033>
- Kaye, K.S., Pogue, J.M., 2015. Infections Caused by Resistant Gram-Negative Bacteria: Epidemiology and Management. *Pharmacotherapy* 35, 949–962. <https://doi.org/10.1002/phar.1636>
- Keighley, S.D., Estrela, P., Li, P., Migliorato, P., 2008a. Optimization of label-free DNA detection with electrochemical impedance spectroscopy using PNA probes. *Biosens. Bioelectron.* 24, 906–911. <https://doi.org/10.1016/j.bios.2008.07.041>
- Keighley, S.D., Li, P., Estrela, P., Migliorato, P., 2008b. Optimization of DNA immobilization on gold electrodes for label-free detection by electrochemical impedance spectroscopy. *Biosens. Bioelectron.* 23, 1291–1297. <https://doi.org/10.1016/j.bios.2007.11.012>
- Kelley, S.O., 2017. What Are Clinically Relevant Levels of Cellular and Biomolecular Analytes? *ACS Sens.* 2, 193–197. <https://doi.org/10.1021/acssensors.6b00691>
- Kelley, S.O., Barton, J.K., Jackson, N.M., Hill, M.G., 1997. Electrochemistry of Methylene Blue Bound to a DNA-Modified Electrode. *Bioconjugate Chem.* 8, 31–37. <https://doi.org/10.1021/bc960070o>
- Kelley, S.O., Jackson, N.M., Hill, M.G., Barton, J.K., 1999. Long-Range Electron Transfer through DNA Films. *Angewandte Chemie International Edition* 38, 941–945. [https://doi.org/10.1002/\(SICI\)1521-3773\(19990401\)38:7<941::AID-ANIE941>3.0.CO;2-7](https://doi.org/10.1002/(SICI)1521-3773(19990401)38:7<941::AID-ANIE941>3.0.CO;2-7)

- Kerman, K., Vestergaard, M., Tamiya, E., 2009. Electrochemical DNA Biosensors: Protocols for Intercalator-Based Detection of Hybridization in Solution and at the Surface, in: *Biosensors and Biodetection, Methods in Molecular Biology*TM. Humana Press, pp. 99–113. https://doi.org/10.1007/978-1-60327-569-9_7
- Kersting, S., Rausch, V., Bier, F.F., Nickisch-Rosenegk, M. von, 2014. Multiplex isothermal solid-phase recombinase polymerase amplification for the specific and fast DNA-based detection of three bacterial pathogens. *Microchim Acta* 181, 1715–1723. <https://doi.org/10.1007/s00604-014-1198-5>
- Kettler, H., White, K., Hawkes, S., 2004. Mapping the landscape of diagnostics for sexually transmitted infections [WWW Document]. TDR. URL <http://www.who.int/tdr/publications/tdr-research-publications/mapping-landscape-sti/en/> (accessed 12.19.17).
- Khater, M., de la Escosura-Muñiz, A., Altet, L., Merkoçi, A., 2019. In situ plant virus nucleic acid isothermal amplification detection on gold nanoparticle-modified electrodes. *Anal. Chem.* <https://doi.org/10.1021/acs.analchem.9b00340>
- Kielkowski, P., Fanfrlík, J., Hocek, M., 2014. 7-Aryl-7-deazaadenine 2'-Deoxyribonucleoside Triphosphates (dNTPs): Better Substrates for DNA Polymerases than dATP in Competitive Incorporations. *Angewandte Chemie International Edition* 53, 7552–7555. <https://doi.org/10.1002/anie.201404742>
- Kongpeth, J., Jampasa, S., Chaumpluk, P., Chailapakul, O., Vilaivan, T., 2016. Immobilization-free electrochemical DNA detection with anthraquinone-labeled pyrrolidinyI peptide nucleic acid probe. *Talanta* 146, 318–325. <https://doi.org/10.1016/j.talanta.2015.08.059>
- Kortli, S., Jauset-Rubio, M., Tomaso, H., Abbas, M.N., Bashammakh, A.S., El-Shahawi, M.S., Alyoubi, A.O., Ben-Ali, M., O'Sullivan, C.K., 2020. *Yersinia pestis* detection using biotinylated dNTPs for signal enhancement in lateral flow assays. *Analytica Chimica Acta* 1112, 54–61. <https://doi.org/10.1016/j.aca.2020.03.059>
- Lama, F., Tarrillo, J., 2018. Remote acquisition of lead in water using Anodic Stripping Voltammetry method, in: 2018 IEEE XXV International Conference on Electronics, Electrical Engineering and Computing (INTERCON). Presented at the 2018 IEEE XXV International Conference on Electronics, Electrical Engineering and Computing (INTERCON), pp. 1–4. <https://doi.org/10.1109/INTERCON.2018.8526419>

- Lanini, S., D'Arezzo, S., Puro, V., Martini, L., Imperi, F., Piselli, P., Montanaro, M., Paoletti, S., Visca, P., Ippolito, G., 2011. Molecular Epidemiology of a *Pseudomonas aeruginosa* Hospital Outbreak Driven by a Contaminated Disinfectant-Soap Dispenser. *PLoS One* 6. <https://doi.org/10.1371/journal.pone.0017064>
- Lee, T.M.-H., 2008. Over-the-Counter Biosensors: Past, Present, and Future. *Sensors (Basel)* 8, 5535–5559. <https://doi.org/10.3390/s8095535>
- Leistner, R., Gurntke, S., Sakellariou, C., Denkel, L.A., Bloch, A., Gastmeier, P., Schwab, F., 2014. Bloodstream infection due to extended-spectrum beta-lactamase (ESBL)-positive *K. pneumoniae* and *E. coli*: an analysis of the disease burden in a large cohort. *Infection* 42, 991–997. <https://doi.org/10.1007/s15010-014-0670-9>
- Levine, P.M., Gong, P., Levicky, R., Shepard, K.L., 2009. Real-time, multiplexed electrochemical DNA detection using an active complementary metal-oxide-semiconductor biosensor array with integrated sensor electronics. *Biosens Bioelectron* 24, 1995–2001. <https://doi.org/10.1016/j.bios.2008.10.012>
- Li, B., Ye, Q., 2015. Antifouling Surfaces of Self-assembled Thin Layer, in: *Antifouling Surfaces and Materials*. Springer, Berlin, Heidelberg, pp. 31–54. https://doi.org/10.1007/978-3-662-45204-2_2
- Li, J., Macdonald, J., 2015. Advances in isothermal amplification: novel strategies inspired by biological processes. *Biosens. Bioelectron.* 64, 196–211. <https://doi.org/10.1016/j.bios.2014.08.069>
- Li, Y., Deng, L., Deng, C., Nie, Z., Yang, M., Si, S., 2012. Simple and sensitive aptasensor based on quantum dot-coated silica nanospheres and the gold screen-printed electrode. *Talanta* 99, 637–642. <https://doi.org/10.1016/j.talanta.2012.06.054>
- Li, Y.C., Melenbrink, E.L., Cordonier, G.J., Boggs, C., Khan, A., Isaac, M.K., Nkhonjera, L.K., Bahati, D., Billinge, S.J., Haile, S.M., Kreuter, R.A., Crable, R.M., Mallouk, T.E., 2018. An Easily Fabricated Low-Cost Potentiostat Coupled with User-Friendly Software for Introducing Students to Electrochemical Reactions and Electroanalytical Techniques. *J. Chem. Educ.* 95, 1658–1661. <https://doi.org/10.1021/acs.jchemed.8b00340>
- Liu, B., Bard, A.J., Mirkin, M.V., Creager, S.E., 2004. Electron Transfer at Self-Assembled Monolayers Measured by Scanning Electrochemical Microscopy. *J. Am. Chem. Soc.* 126, 1485–1492. <https://doi.org/10.1021/ja038611p>

- Liu, R.H., Yang, J., Lenigk, R., Bonanno, J., Grodzinski, P., 2004. Self-Contained, Fully Integrated Biochip for Sample Preparation, Polymerase Chain Reaction Amplification, and DNA Microarray Detection. *Anal. Chem.* 76, 1824–1831. <https://doi.org/10.1021/ac0353029>
- Liu, T., Lu, Y., Gau, V., Liao, J.C., Wong, P.K., 2014. Rapid antimicrobial susceptibility testing with electrokinetics enhanced biosensors for diagnosis of acute bacterial infections. *Ann Biomed Eng* 42, 2314–2321. <https://doi.org/10.1007/s10439-014-1040-6>
- Liu, Y., Tuleouva, N., Ramanculov, E., Revzin, A., 2010. Aptamer-Based Electrochemical Biosensor for Interferon Gamma Detection. *Anal. Chem.* 82, 8131–8136. <https://doi.org/10.1021/ac101409t>
- Lopin, P., Lopin, K.V., 2018. PSoC-Stat: A single chip open source potentiostat based on a Programmable System on a Chip. *PLOS ONE* 13, e0201353. <https://doi.org/10.1371/journal.pone.0201353>
- Love, J.C., Estroff, L.A., Kriebel, J.K., Nuzzo, R.G., Whitesides, G.M., 2005. Self-Assembled Monolayers of Thiolates on Metals as a Form of Nanotechnology. *Chem. Rev.* 105, 1103–1170. <https://doi.org/10.1021/cr0300789>
- Lucarelli, F., Marrazza, G., Turner, A.P.F., Mascini, M., 2004. Carbon and gold electrodes as electrochemical transducers for DNA hybridisation sensors. *Biosens. Bioelectron.* 19, 515–530. [https://doi.org/10.1016/S0956-5663\(03\)00256-2](https://doi.org/10.1016/S0956-5663(03)00256-2)
- Luo, J., Fang, X., Ye, D., Li, H., Chen, H., Zhang, S., Kong, J., 2014. A real-time microfluidic multiplex electrochemical loop-mediated isothermal amplification chip for differentiating bacteria. *Biosens. Bioelectron.* 60, 84–91. <https://doi.org/10.1016/j.bios.2014.03.073>
- Maffert, P., Reverchon, S., Nasser, W., Rozand, C., Abaibou, H., 2017. New nucleic acid testing devices to diagnose infectious diseases in resource-limited settings. *Eur J Clin Microbiol Infect Dis* 36, 1717–1731. <https://doi.org/10.1007/s10096-017-3013-9>
- Magriñá, I., Jauset-Rubio, M., Ortiz, M., Tomaso, H., Simonova, A., Hocek, M., O'Sullivan, C.K., 2019. Duplex Electrochemical DNA Sensor to Detect *Bacillus anthracis* CAP and PAG DNA Targets Based on the Incorporation of Tailed Primers and Ferrocene-Labeled dATP. *ACS Omega* 4, 21900–21908. <https://doi.org/10.1021/acsomega.9b02890>
- Manchanda, V., Sanchaita, S., Singh, N., 2010. Multidrug Resistant *Acinetobacter*. *J Glob Infect Dis* 2, 291–304. <https://doi.org/10.4103/0974-777X.68538>

- Manzano, M., Viezzi, S., Mazerat, S., Marks, R.S., Vidic, J., 2018. Rapid and label-free electrochemical DNA biosensor for detecting hepatitis A virus. *Biosens. Bioelectron.* 100, 89–95. <https://doi.org/10.1016/j.bios.2017.08.043>
- Martin, A., Bouffier, L., B. Grant, K., Limoges, B., Marchal, D., 2016. Real-time electrochemical LAMP: a rational comparative study of different DNA intercalating and non-intercalating redox probes. *Analyst* 141, 4196–4203. <https://doi.org/10.1039/C6AN00867D>
- Martinez, J.L., 2014. General principles of antibiotic resistance in bacteria. *Drug Discovery Today: Technologies, Drug Resistance* 11, 33–39. <https://doi.org/10.1016/j.ddtec.2014.02.001>
- Mathers, A.J., Peirano, G., Pitout, J.D.D., 2015. Chapter Four - Escherichia coli ST131: The Quintessential Example of an International Multiresistant High-Risk Clone, in: Sariaslani, S., Gadd, G.M. (Eds.), *Advances in Applied Microbiology*. Academic Press, pp. 109–154. <https://doi.org/10.1016/bs.aambs.2014.09.002>
- Matsishin, M., Rachkov, A., Errachid, A., Dzyadevych, S., Soldatkin, A., 2016. Development of impedimetric DNA biosensor for selective detection and discrimination of oligonucleotide sequences of the rpoB gene of Mycobacterium tuberculosis. *Sens. Actuators, B* 222, 1152–1158. <https://doi.org/10.1016/j.snb.2015.08.012>
- Mayboroda, O., Benito, A.G., del Rio, J.S., Svobodova, M., Julich, S., Tomaso, H., O’Sullivan, C.K., Katakis, I., 2016. Isothermal solid-phase amplification system for detection of Yersinia pestis. *Anal Bioanal Chem* 408, 671–676. <https://doi.org/10.1007/s00216-015-9177-1>
- McCreery, R.L., 2008. Advanced Carbon Electrode Materials for Molecular Electrochemistry. *Chem. Rev.* 108, 2646–2687. <https://doi.org/10.1021/cr068076m>
- McEwen, S.A., Collignon, P.J., 2018. Antimicrobial Resistance: a One Health Perspective. *Microbiol Spectr* 6. <https://doi.org/10.1128/microbiolspec.ARBA-0009-2017>
- McVey, C., Huang, F., Elliott, C., Cao, C., 2017. Endonuclease controlled aggregation of gold nanoparticles for the ultrasensitive detection of pathogenic bacterial DNA. *Biosens. Bioelectron.* 92, 502–508. <https://doi.org/10.1016/j.bios.2016.10.072>
- Mehrotra, P., 2016. Biosensors and their applications – A review. *J Oral Biol Craniofac Res* 6, 153–159. <https://doi.org/10.1016/j.jobcr.2015.12.002>
- Meloni, G.N., 2017. 3D Printed and Microcontrolled: The One Hundred Dollars Scanning Electrochemical Microscope. *Anal. Chem.* 89, 8643–8649. <https://doi.org/10.1021/acs.analchem.7b01764>

- Meloni, G.N., 2016. Building a Microcontroller Based Potentiostat: A Inexpensive and Versatile Platform for Teaching Electrochemistry and Instrumentation. *J. Chem. Educ.* 93, 1320–1322. <https://doi.org/10.1021/acs.jchemed.5b00961>
- Meric, B., Kerman, K., Ozkan, D., Kara, P., Erensoy, S., Akarca, U.S., Mascini, M., Ozsoz, M., 2002. Electrochemical DNA biosensor for the detection of TT and Hepatitis B virus from PCR amplified real samples by using methylene blue. *Talanta* 56, 837–846. [https://doi.org/10.1016/S0039-9140\(01\)00650-6](https://doi.org/10.1016/S0039-9140(01)00650-6)
- Miller, S.I., 2016. Antibiotic Resistance and Regulation of the Gram-Negative Bacterial Outer Membrane Barrier by Host Innate Immune Molecules. *mBio* 7, e01541-16. <https://doi.org/10.1128/mBio.01541-16>
- Montes-Cebrián, Y., Álvarez-Carulla, A., Ruiz-Vega, G., Colomer-Farrarons, J., Puig-Vidal, M., Baldrich, E., Miribel-Català, P.L., 2019. Competitive USB-Powered Hand-Held Potentiostat for POC Applications: An HRP Detection Case. *Sensors* 19, 5388. <https://doi.org/10.3390/s19245388>
- Moreau, M., Delile, S., Sharma, A., Fave, C., Perrier, A., Limoges, B., Marchal, D., 2017. Detection of a few DNA copies by real-time electrochemical polymerase chain reaction. *Analyst* 142, 3432–3440. <https://doi.org/10.1039/C7AN00978J>
- Mousavisani, S.Z., Raoof, J.B., Ojani, R., Bagheryan, Z., 2018. An impedimetric biosensor for DNA damage detection and study of the protective effect of deferoxamine against DNA damage. *Bioelectrochemistry* 122, 142–148. <https://doi.org/10.1016/j.bioelechem.2018.03.012>
- Mrksich, M., Whitesides, G.M., 1996. Using Self-Assembled Monolayers to Understand the Interactions of Man-made Surfaces with Proteins and Cells. *Annu. Rev. Biophys. Biomol. Struct.* 25, 55–78. <https://doi.org/10.1146/annurev.bb.25.060196.000415>
- Mullis, K.B., Faloona, F.A., 1987. Specific synthesis of DNA in vitro via a polymerase-catalyzed chain reaction, in: *Methods in Enzymology, Recombinant DNA Part F*. Academic Press, pp. 335–350. [https://doi.org/10.1016/0076-6879\(87\)55023-6](https://doi.org/10.1016/0076-6879(87)55023-6)
- Munoz-Price, L.S., Weinstein, R.A., 2008. *Acinetobacter* Infection. *New England Journal of Medicine* 358, 1271–1281. <https://doi.org/10.1056/NEJMra070741>
- Nagatani, N., Yamanaka, K., Saito, M., Koketsu, R., Sasaki, T., Ikuta, K., Miyahara, T., Tamiya, E., 2011. Semi-real time electrochemical monitoring for influenza virus RNA by reverse transcription loop-mediated isothermal amplification using a USB powered portable potentiostat. *Analyst* 136, 5143–5150. <https://doi.org/10.1039/C1AN15638A>

- Naylor, N.R., Pouwels, K.B., Hope, R., Green, N., Henderson, K.L., Knight, G.M., Atun, R., Robotham, J.V., Deeny, S.R., 2019. The health and cost burden of antibiotic resistant and susceptible *Escherichia coli* bacteraemia in the English hospital setting: A national retrospective cohort study. *PLOS ONE* 14, e0221944. <https://doi.org/10.1371/journal.pone.0221944>
- Nemiroski, A., Christodouleas, D.C., Hennek, J.W., Kumar, A.A., Maxwell, E.J., Fernández-Abedul, M.T., Whitesides, G.M., 2014. Universal mobile electrochemical detector designed for use in resource-limited applications. *Proc Natl Acad Sci U S A* 111, 11984–11989. <https://doi.org/10.1073/pnas.1405679111>
- New England BioLabs, 2017. Guidelines for PCR Optimization with Taq DNA Polymerase | NEB [WWW Document]. New England BioLabs. URL <https://www.neb.com/tools-and-resources/usage-guidelines/guidelines-for-pcr-optimization-with-taq-dna-polymerase> (accessed 11.22.17).
- Nicolas-Chanoine, M.-H., Bertrand, X., Madec, J.-Y., 2014. *Escherichia coli* ST131, an Intriguing Clonal Group. *Clin Microbiol Rev* 27, 543–574. <https://doi.org/10.1128/CMR.00125-13>
- Nicolas-Chanoine, M.-H., Blanco, J., Leflon-Guibout, V., Demarty, R., Alonso, M.P., Caniça, M.M., Park, Y.-J., Lavigne, J.-P., Pitout, J., Johnson, J.R., 2008. Intercontinental emergence of *Escherichia coli* clone O25:H4-ST131 producing CTX-M-15. *J Antimicrob Chemother* 61, 273–281. <https://doi.org/10.1093/jac/dkm464>
- Nie, J., Zhang, D.-W., Zhang, F.-T., Yuan, F., Zhou, Y.-L., Zhang, X.-X., 2014. Reporter-triggered isothermal exponential amplification strategy in ultrasensitive homogeneous label-free electrochemical nucleic acid biosensing. *Chemical Communications* 50, 6211–6213. <https://doi.org/10.1039/C4CC00475B>
- Niu, X., Zheng, W., Yin, C., Weng, W., Li, G., Sun, W., Men, Y., 2017. Electrochemical DNA biosensor based on gold nanoparticles and partially reduced graphene oxide modified electrode for the detection of *Listeria monocytogenes* hly gene sequence. *J. Electroanal. Chem.* 806, 116–122. <https://doi.org/10.1016/j.jelechem.2017.10.049>
- Nixdorff, K., Gmeiner, J., Martin, H.H., 1978. Interaction of lipopolysaccharide with detergents and its possible role in the detergent resistance of the outer membrane of gram-negative bacteria. *Biochimica et Biophysica Acta (BBA) - Biomembranes* 510, 87–98. [https://doi.org/10.1016/0005-2736\(78\)90132-3](https://doi.org/10.1016/0005-2736(78)90132-3)

- Nordin, N., Yusof, N.A., Abdullah, J., Radu, S., Hushiarian, R., 2017. A simple, portable, electrochemical biosensor to screen shellfish for *Vibrio parahaemolyticus*. *AMB Express* 7, 41. <https://doi.org/10.1186/s13568-017-0339-8>
- Nuzzo, R.G., Allara, D.L., 1983. Adsorption of bifunctional organic disulfides on gold surfaces. *J. Am. Chem. Soc.* 105, 4481–4483. <https://doi.org/10.1021/ja00351a063>
- Obaje, E.A., Cummins, G., Schulze, H., Mahmood, S., Desmulliez, M.P.Y., Bachmann, T.T., 2016. Carbon screen-printed electrodes on ceramic substrates for label-free molecular detection of antibiotic resistance. *Journal of Interdisciplinary Nanomedicine* 1, 93–109. <https://doi.org/10.1002/jin2.16>
- O’Neill, 2016. Tackling Drug-Resistant Infections Globally: Final Report and Recommendations.
- Palchetti, I., Mascini, M., 2008. Nucleic acid biosensors for environmental pollution monitoring. *Analyst* 133, 846–854. <https://doi.org/10.1039/B802920M>
- Paleček, E., Bartošík, M., 2012. Electrochemistry of Nucleic Acids. *Chem. Rev.* 112, 3427–3481. <https://doi.org/10.1021/cr200303p>
- Patterson, A.S., Heithoff, D.M., Ferguson, B.S., Soh, H.T., Mahan, M.J., Plaxco, K.W., 2013. Microfluidic Chip-Based Detection and Intraspecies Strain Discrimination of *Salmonella* Serovars Derived from Whole Blood of Septic Mice. *Appl Environ Microbiol* 79, 2302–2311. <https://doi.org/10.1128/AEM.03882-12>
- Peleg, A.Y., Seifert, H., Paterson, D.L., 2008. *Acinetobacter baumannii*: Emergence of a Successful Pathogen. *Clin Microbiol Rev* 21, 538–582. <https://doi.org/10.1128/CMR.00058-07>
- Peltomaa, R., Vaghini, S., Patiño, B., Benito-Peña, E., Moreno-Bondi, M.C., 2016. Species-specific optical genosensors for the detection of mycotoxigenic *Fusarium* fungi in food samples. *Analytica Chimica Acta* 935, 231–238. <https://doi.org/10.1016/j.aca.2016.06.009>
- Perry, J.A., Wright, G.D., 2014. Forces shaping the antibiotic resistome. *BioEssays* 36, 1179–1184. <https://doi.org/10.1002/bies.201400128>
- Peterson, L.R., 2009. Bad Bugs, No Drugs: No ESCAPE Revisited. *Clin Infect Dis* 49, 992–993. <https://doi.org/10.1086/605539>
- Pitout, J.D.D., DeVinney, R., 2017. *Escherichia coli* ST131: a multidrug-resistant clone primed for global domination. *F1000Research* 6, 195. <https://doi.org/10.12688/f1000research.10609.1>

- Pletcher, D., 2009. *A First Course in Electrode Processes*, 2nd ed. Royal Society of Chemistry.
- Price, C.P., 2001. Point of care testing. *BMJ* 322, 1285–1288. <https://doi.org/10.1136/bmj.322.7297.1285>
- Pruna, R., Palacio, F., Baraket, A., Zine, N., Streklas, A., Bausells, J., Errachid, A., López, M., 2018. A low-cost and miniaturized potentiostat for sensing of biomolecular species such as TNF- α by electrochemical impedance spectroscopy. *Biosensors and Bioelectronics* 100, 533–540. <https://doi.org/10.1016/j.bios.2017.09.049>
- Public Health England, 2020. Annual epidemiological commentary: Gram-negative bacteraemia, MRSA bacteraemia, MSSA bacteraemia and *C. difficile* infections, up to and including financial year April 2019 to March 2020.
- Public Health England, 2017. Laboratory surveillance of *Escherichia coli* bacteraemia in England, Wales and Northern Ireland: 2016.
- Randles, J.E.B., 1947. Kinetics of rapid electrode reactions. *Discuss Faraday Soc* 1, 11–19. <https://doi.org/10.1039/df9470100011>
- Redgrave, L.S., Sutton, S.B., Webber, M.A., Piddock, L.J.V., 2014. Fluoroquinolone resistance: mechanisms, impact on bacteria, and role in evolutionary success. *Trends in Microbiology* 22, 438–445. <https://doi.org/10.1016/j.tim.2014.04.007>
- Ribeiro, J.A., Pereira, C.M., Silva, A.F., Sales, M.G.F., 2018. Disposable electrochemical detection of breast cancer tumour marker CA 15-3 using poly(Toluidine Blue) as imprinted polymer receptor. *Biosens. Bioelectron.* 109, 246–254. <https://doi.org/10.1016/j.bios.2018.03.011>
- Rice, L.B., 2008. Federal Funding for the Study of Antimicrobial Resistance in Nosocomial Pathogens: No ESKAPE. *J Infect Dis* 197, 1079–1081. <https://doi.org/10.1086/533452>
- Riedel, M., Kartchemnik, J., Schöning, M.J., Lisdat, F., 2014. Impedimetric DNA Detection—Steps Forward to Sensorial Application. *Anal. Chem.* 86, 7867–7874. <https://doi.org/10.1021/ac501800q>
- Rose, M., Landman, D., Quale, J., 2014. Are community environmental surfaces near hospitals reservoirs for gram-negative nosocomial pathogens? *American Journal of Infection Control* 42, 346–348. <https://doi.org/10.1016/j.ajic.2013.12.025>
- Rowe, A.A., Bonham, A.J., White, R.J., Zimmer, M.P., Yadgar, R.J., Hobza, T.M., Honea, J.W., Ben-Yaacov, I., Plaxco, K.W., 2011. CheapStat: An Open-Source, “Do-It-Yourself” Potentiostat for Analytical and Educational Applications. *PLOS ONE* 6, e23783. <https://doi.org/10.1371/journal.pone.0023783>

- Ruppé, É., Woerther, P.-L., Barbier, F., 2015. Mechanisms of antimicrobial resistance in Gram-negative bacilli. *Ann Intensive Care* 5. <https://doi.org/10.1186/s13613-015-0061-0>
- Rye, H.S., Glazer, A.N., 1995. Interaction of dimeric intercalating dyes with single-stranded DNA. *Nucleic Acids Res* 23, 1215–1222.
- Saby, C., Ortiz, B., Champagne, G.Y., Bélanger, D., 1997. Electrochemical Modification of Glassy Carbon Electrode Using Aromatic Diazonium Salts. 1. Blocking Effect of 4-Nitrophenyl and 4-Carboxyphenyl Groups. *Langmuir* 13, 6805–6813. <https://doi.org/10.1021/la961033o>
- Sánchez-Salcedo, R., Miranda-Castro, R., de los Santos-Álvarez, N., Lobo-Castañón, M.J., 2019. On-Gold Recombinase Polymerase Primer Elongation for Electrochemical Detection of Bacterial Genome: Mechanism Insights and Influencing Factors. *ChemElectroChem* 6, 793–800. <https://doi.org/10.1002/celec.201801208>
- Santajit, S., Indrawattana, N., 2016. Mechanisms of Antimicrobial Resistance in ESKAPE Pathogens. *Biomed Res Int* 2016. <https://doi.org/10.1155/2016/2475067>
- Santiago-Felipe, S., Tortajada-Genaro, L.A., Morais, S., Puchades, R., Maquieira, Á., 2014. One-pot isothermal DNA amplification – Hybridisation and detection by a disc-based method. *Sensors and Actuators B: Chemical* 204, 273–281. <https://doi.org/10.1016/j.snb.2014.07.073>
- Santiago-Felipe, S., Tortajada-Genaro, L.A., Puchades, R., Maquieira, Á., 2016. Parallel solid-phase isothermal amplification and detection of multiple DNA targets in microliter-sized wells of a digital versatile disc. *Microchim Acta* 183, 1195–1202. <https://doi.org/10.1007/s00604-016-1745-3>
- Shimono, N., Murata, M., Kanamoto, Y., Uchida, Y., Matsumoto, H., Hayashi, J., Shimono, N., Takuma, T., Tsuchimochi, N., Shimono, N., Uchida, Y., Shiose, A., Morita, S., Murata, M., Kanamoto, Y., Hayashi, J., 2008. An outbreak of *Pseudomonas aeruginosa* infections following thoracic surgeries occurring via the contamination of bronchoscopes and an automatic endoscope reprocessor. *Journal of Infection and Chemotherapy* 14, 418–423. <https://doi.org/10.1007/s10156-008-0645-9>
- Shin, B., Park, W., 2017. Antibiotic resistance of pathogenic *Acinetobacter* species and emerging combination therapy. *J Microbiol.* 55, 837–849. <https://doi.org/10.1007/s12275-017-7288-4>

- Shin, Y., Perera, A.P., Kim, K.W., Park, M.K., 2013. Real-time, label-free isothermal solid-phase amplification/detection (ISAD) device for rapid detection of genetic alteration in cancers. *Lab Chip* 13, 2106–2114. <https://doi.org/10.1039/C3LC50129A>
- Shoemaker, N.B., Vlamakis, H., Hayes, K., Salyers, A.A., 2001. Evidence for Extensive Resistance Gene Transfer among *Bacteroides* spp. and among *Bacteroides* and Other Genera in the Human Colon. *Appl Environ Microbiol* 67, 561–568. <https://doi.org/10.1128/AEM.67.2.561-568.2001>
- Srinivas, P., Rivard, K., 2017. Polymyxin Resistance in Gram-negative Pathogens. *Current Infectious Disease Reports* 19. <https://doi.org/10.1007/s11908-017-0596-3>
- Štrbac, S., Adžić, R.R., Hamelin, A., 1988. Oxide formation on gold single crystal stepped surfaces. *J. Electroanal. Chem. Interfacial. Electrochem.* 249, 291–310. [https://doi.org/10.1016/0022-0728\(88\)80366-8](https://doi.org/10.1016/0022-0728(88)80366-8)
- Sugumar, M., Kumar, K.M., Manoharan, A., Anbarasu, A., Ramaiah, S., 2014. Detection of OXA-1 β -Lactamase Gene of *Klebsiella pneumoniae* from Blood Stream Infections (BSI) by Conventional PCR and In-Silico Analysis to Understand the Mechanism of OXA Mediated Resistance. *PLOS ONE* 9, e91800. <https://doi.org/10.1371/journal.pone.0091800>
- Sun, X., Chen, H., Wang, S., Zhang, Y., Tian, Y., Zhou, N., 2018. Electrochemical detection of sequence-specific DNA based on formation of G-quadruplex-hemin through continuous hybridization chain reaction. *Analytica Chimica Acta* 1021, 121–128. <https://doi.org/10.1016/j.aca.2018.02.076>
- Tani, A., J. Thomson, A., N. Butt, J., 2001. Methylene blue as an electrochemical discriminator of single- and double-stranded oligonucleotides immobilised on gold substrates. *Analyst* 126, 1756–1759. <https://doi.org/10.1039/B104260M>
- Teymourian, H., Salimi, A., Khezrian, S., 2017. Development of a New Label-free, Indicator-free Strategy toward Ultrasensitive Electrochemical DNA Biosensing Based on Fe₃O₄ Nanoparticles/Reduced Graphene Oxide Composite. *Electroanalysis* 29, 409–414. <https://doi.org/10.1002/elan.201600336>
- Thaden, J.T., Li, Y., Ruffin, F., Maskarinec, S.A., Hill-Rorie, J.M., Wanda, L.C., Reed, S.D., Fowler, V.G., 2017. Increased Costs Associated with Bloodstream Infections Caused by Multidrug-Resistant Gram-Negative Bacteria Are Due Primarily to Patients with Hospital-Acquired Infections. *Antimicrobial Agents and Chemotherapy* 61. <https://doi.org/10.1128/AAC.01709-16>

- The UniProt Consortium, 2019. UniProt: a worldwide hub of protein knowledge. *Nucleic Acids Research* 47, D506–D515. <https://doi.org/10.1093/nar/gky1049>
- ThermoFisher Scientific, 2017. PCR Cycling Parameters—Six Key Considerations for Success [WWW Document]. ThermoFisher Scientific. URL <https://www.thermofisher.com/uk/en/home/life-science/cloning/cloning-learning-center/invitrogen-school-of-molecular-biology/pcr-education/pcr-reagents-enzymes/pcr-cycling-considerations.html> (accessed 11.22.17).
- Tien, B.Q., Ngoc, N.T., Loc, N.T., Thu, V.T., Lam, T.D., 2017. Biochip for Real-Time Monitoring of Hepatitis B Virus (HBV) by Combined Loop-Mediated Isothermal Amplification and Solution-Phase Electrochemical Detection. *Journal of Elec Materi* 46, 3565–3571. <https://doi.org/10.1007/s11664-017-5483-z>
- Tkac, J., Davis, J.J., 2008. An optimised electrode pre-treatment for SAM formation on polycrystalline gold. *J. Electroanal. Chem.* 621, 117–120. <https://doi.org/10.1016/j.jelechem.2008.04.010>
- Toldrà, A., Furones, M.D., O’Sullivan, C.K., Campàs, M., 2020. Detection of isothermally amplified ostreid herpesvirus 1 DNA in Pacific oyster (*Crassostrea gigas*) using a miniaturised electrochemical biosensor. *Talanta* 207, 120308. <https://doi.org/10.1016/j.talanta.2019.120308>
- Tortajada-Genaro, L.A., Santiago-Felipe, S., Amasia, M., Russom, A., Maquieira, Á., 2015. Isothermal solid-phase recombinase polymerase amplification on microfluidic digital versatile discs (DVDs). *RSC Adv.* 5, 29987–29995. <https://doi.org/10.1039/C5RA02778K>
- Tran, L.D., Nguyen, B.H., Van Hieu, N., Tran, H.V., Nguyen, H.L., Nguyen, P.X., 2011. Electrochemical detection of short HIV sequences on chitosan/Fe₃O₄ nanoparticle based screen printed electrodes. *Materials Science and Engineering: C* 31, 477–485. <https://doi.org/10.1016/j.msec.2010.11.007>
- Tsai, M.-Y., Lin, J.-C., 2001. Preconditioning Gold Substrates Influences Organothiol Self-assembled Monolayer (SAM) Formation. *Journal of Colloid and Interface Science* 238, 259–266. <https://doi.org/10.1006/jcis.2001.7522>
- Tsaloglou, M.-N., Nemiroski, A., Camci-Unal, G., Christodouleas, D.C., Murray, L.P., Connelly, J.T., Whitesides, G.M., 2018. Handheld isothermal amplification and electrochemical detection of DNA in resource-limited settings. *Analytical Biochemistry* 543, 116–121. <https://doi.org/10.1016/j.ab.2017.11.025>

- TwistDx Ltd, 2020. RPA - The versatile replacement to PCR [WWW Document]. TwistDx. URL <https://www.twistdx.co.uk/en/rpa> (accessed 12.15.20).
- United Nations, 2021. High-Level Interactive Dialogue on Antimicrobial Resistance [WWW Document]. General Assembly of the United Nations. URL <https://www.un.org/pga/75/antimicrobial-resistance/> (accessed 6.29.21).
- Urdea, M.S., Warner, B.D., Running, J.A., Stempien, M., Clyne, J., Horn, T., 1988. A comparison of non-radioisotopic hybridization assay methods using fluorescent, chemiluminescent and enzyme labeled synthetic oligodeoxyribonucleotide probes. *Nucleic Acids Res* 16, 4937–4956.
- Valério, E., Abrantes, L.M., Viana, A.S., 2008. 4-Aminothiophenol Self-Assembled Monolayer for the Development of a DNA Biosensor Aiming the Detection of *Cylindrospermopsis* Producing Cyanobacteria. *Electroanalysis* 20, 2467–2474. <https://doi.org/10.1002/elan.200804350>
- van Gijlswijk, R.P.M., van de Corput, M.P.C., Bezrookove, V., Wiegant, J., Tanke, H.J., Raap, A.K., 2000. Synthesis and purification of horseradish peroxidase-labeled oligonucleotides for tyramide-based fluorescence in situ hybridization. *Histochemistry* 113, 175–180. <https://doi.org/10.1007/s004180050436>
- Van Looveren, M., Goossens, H., 2004. Antimicrobial resistance of *Acinetobacter* spp. in Europe. *Clinical Microbiology and Infection* 10, 684–704. <https://doi.org/10.1111/j.1469-0691.2004.00942.x>
- Vericat, C., E. Vela, M., Benitez, G., Carro, P., C. Salvarezza, R., 2010. Self-assembled monolayers of thiols and dithiols on gold : new challenges for a well-known system. *Chemical Society Reviews* 39, 1805–1834. <https://doi.org/10.1039/B907301A>
- Vincent, J.-L., Rello, J., Marshall, J., Silva, E., Anzueto, A., Martin, C.D., Moreno, R., Lipman, J., Gomersall, C., Sakr, Y., Reinhart, K., EPIC II Group of Investigators, 2009. International study of the prevalence and outcomes of infection in intensive care units. *JAMA* 302, 2323–2329. <https://doi.org/10.1001/jama.2009.1754>
- Wang, J., 2006. Electrochemical biosensors: Towards point-of-care cancer diagnostics. *Biosens. Bioelectron.* 21, 1887–1892. <https://doi.org/10.1016/j.bios.2005.10.027>
- Wang, L., Veselinovic, M., Yang, L., Geiss, B.J., Dandy, D.S., Chen, T., 2017. A sensitive DNA capacitive biosensor using interdigitated electrodes. *Biosens. Bioelectron.* 87, 646–653. <https://doi.org/10.1016/j.bios.2016.09.006>

- Wang, Q., Wen, Y., Li, Yan, Liang, W., Li, W., Li, Yuan, Wu, J., Zhu, H., Zhao, K., Zhang, J., Jia, N., Deng, W., Liu, G., 2019. Ultrasensitive Electrochemical Biosensor of Bacterial 16S rRNA Gene Based on polyA DNA Probes. *Anal Chem* 91, 9277–9283. <https://doi.org/10.1021/acs.analchem.9b02175>
- Wang, R.-A., Ke, Z.-Y., Liang, Y., Yang, T., Qin, J.-H., Wang, L., 2014. Why is Mycobacterium Tuberculosis Hard to Grow? The Principle of Biorelativity Explains. *Journal of Clinical & Experimental Pathology* 4. <https://doi.org/10.4172/2161-0681.1000176>
- Webster, T.A., Sismaet, H.J., Chan, I.-ping J., Goluch, E.D., 2015. Electrochemically monitoring the antibiotic susceptibility of *Pseudomonas aeruginosa* biofilms. *Analyst* 140, 7195–7201. <https://doi.org/10.1039/c5an01358e>
- Welter, M., Verga, D., Marx, A., 2016. Sequence-Specific Incorporation of Enzyme–Nucleotide Chimera by DNA Polymerases. *Angewandte Chemie International Edition* 55, 10131–10135. <https://doi.org/10.1002/anie.201604641>
- Widaningrum, T., Widyastuti, E., Pratiwi, F.W., Faidoh Fatimah, A.I., Rijiravanich, P., Somasundrum, M., Surareungchai, W., 2017. Sub-attomolar electrochemical measurement of DNA hybridization based on the detection of high coverage biobarcode latex labels at PNA-modified screen printed electrodes. *Talanta* 167, 14–20. <https://doi.org/10.1016/j.talanta.2017.01.094>
- Williams, M.R., Stedtfeld, R.D., Guo, X., Hashsham, S.A., 2016. Antimicrobial Resistance in the Environment. *Water Environment Research* 88, 1951–1967. <https://doi.org/10.2175/106143016X14696400495974>
- Wong, E.L.S., Erohkin, P., Gooding, J.J., 2004. A comparison of cationic and anionic intercalators for the electrochemical transduction of DNA hybridization via long range electron transfer. *Electrochemistry Communications* 6, 648–654. <https://doi.org/10.1016/j.elecom.2004.05.002>
- Wong, E.L.S., Gooding, J.J., 2006. Charge Transfer through DNA: A Selective Electrochemical DNA Biosensor. *Anal. Chem.* 78, 2138–2144. <https://doi.org/10.1021/ac0509096>
- Woodford, N., Carattoli, A., Karisik, E., Underwood, A., Ellington, M.J., Livermore, D.M., 2009. Complete Nucleotide Sequences of Plasmids pEK204, pEK499, and pEK516, Encoding CTX-M Enzymes in Three Major *Escherichia coli* Lineages from the United Kingdom, All Belonging to the International O25:H4-ST131 Clone. *Antimicrob Agents Chemother* 53, 4472–4482. <https://doi.org/10.1128/AAC.00688-09>
- World Bank Group, 2017. Drug Resistant Infections: A Threat to Our Economic Future.

- World Health Organisation, 2017a. Global priority list of antibiotic-resistant bacteria to guide research, discovery, and development of new antibiotics [WWW Document]. World Health Organisation. URL http://www.who.int/medicines/publications/WHO-PPL-Short_Summary_25Feb-ET_NM_WHO.pdf (accessed 11.22.17).
- World Health Organisation, 2017b. One Health [WWW Document]. World Health Organisation. URL <https://www.who.int/news-room/q-a-detail/one-health> (accessed 6.29.21).
- World Health Organisation, 2015. Global Action Plan on Antimicrobial Resistance.
- World Health Organisation, 2014. Antimicrobial Resistance: Global Report on Surveillance.
- Xiao, Y., Lai, R.Y., Plaxco, K.W., 2007. Preparation of electrode-immobilized, redox-modified oligonucleotides for electrochemical DNA and aptamer-based sensing. *Nat Protoc* 2, 2875–2880. <https://doi.org/10.1038/nprot.2007.413>
- Xu, L., Liang, W., Wen, Y., Wang, L., Yang, X., Ren, S., Jia, N., Zuo, X., Liu, G., 2018. An ultrasensitive electrochemical biosensor for the detection of *mecA* gene in methicillin-resistant *Staphylococcus aureus*. *Biosens. Bioelectron.* 99, 424–430. <https://doi.org/10.1016/j.bios.2017.08.014>
- Yamanaka, K., Saito, M., Kondoh, K., Mosharraf Hossain, M., Koketsu, R., Sasaki, T., Nagatani, N., Ikuta, K., Tamiya, E., 2011. Rapid detection for primary screening of influenza A virus: microfluidic RT-PCR chip and electrochemical DNA sensor. *Analyst* 136, 2064–2068. <https://doi.org/10.1039/C1AN15066A>
- Yan, Y., Zhang, M., Gong, K., Su, L., Guo, Z., Mao, L., 2005. Adsorption of Methylene Blue Dye onto Carbon Nanotubes: A Route to an Electrochemically Functional Nanostructure and Its Layer-by-Layer Assembled Nanocomposite. *Chem. Mater.* 17, 3457–3463. <https://doi.org/10.1021/cm0504182>
- Yang, Z., Gonzalez-Cortes, A., Jourquin, G., Viré, J.-C., Kauffmann, J.-M., Delplancke, J.-L., 1995. Analytical application of self assembled monolayers on gold electrodes: critical importance of surface pretreatment. *Biosens. Bioelectron.* 10, 789–795. [https://doi.org/10.1016/0956-5663\(95\)99217-9](https://doi.org/10.1016/0956-5663(95)99217-9)
- Yeung, S.-W., Lee, T.M.H., Cai, H., Hsing, I.-M., 2006. A DNA biochip for on-the-spot multiplexed pathogen identification. *Nucleic Acids Res* 34, e118–e118. <https://doi.org/10.1093/nar/gkl702>

- Yokus, M.A., Songkakul, T., Pozdin, V.A., Bozkurt, A., Daniele, M.A., 2020. Wearable multiplexed biosensor system toward continuous monitoring of metabolites. *Biosensors and Bioelectronics* 153, 112038. <https://doi.org/10.1016/j.bios.2020.112038>
- Yoo, E.-H., Lee, S.-Y., 2010. Glucose Biosensors: An Overview of Use in Clinical Practice. *Sensors (Basel)* 10, 4558–4576. <https://doi.org/10.3390/s100504558>
- Yuan, L., Jiang, L., Thompson, D., Nijhuis, C.A., 2014. On the Remarkable Role of Surface Topography of the Bottom Electrodes in Blocking Leakage Currents in Molecular Diodes. *J. Am. Chem. Soc.* 136, 6554–6557. <https://doi.org/10.1021/ja5007417>
- Zhao, Y., Chen, F., Li, Q., Wang, L., Fan, C., 2015. Isothermal Amplification of Nucleic Acids. *Chem. Rev.* 115, 12491–12545. <https://doi.org/10.1021/acs.chemrev.5b00428>